JAERI-Review
2003-028

JAERI TANDEM ANNUAL REPORT 2002
APRIL 1, 2002 – MARCH 31, 2003

November 2003

Department of Materials Science

日本原子力研究所
Japan Atomic Energy Research Institute

本レポートは、日本原子力研究所が不定期に公刊している研究報告書です。
入手の問合わせは、日本原子力研究所研究情報部研究情報課（〒319-1195 茨城県那珂郡東海村）あて、お申し越し下さい。なお、このほかに財団法人原子力弘済会資料センター（〒319-1195 茨城県那珂郡東海村日本原子力研究所内）で複写による実費頒布を行っております。

This report is issued irregularly.
Inquiries about availability of the reports should be addressed to Research Information Division, Department of Intellectual Resources, Japan Atomic Energy Research Institute, Tokai-mura, Naka-gun, Ibaraki-ken 〒319-1195, Japan.

編集兼発行　日本原子力研究所

JAERI－Review 2003－028

JAERI TANDEM Annual Report 2002
April 1, 2002 – March 31, 2003

Department of Materials Science*

Tokai Research Establishment
Japan Atomic Energy Research Institute
Tokai-mura, Naka-gun, Ibaraki-ken

(Received September 4, 2003)

This annual report describes research activities which have been performed with the JAERI tandem accelerator and the Van de Graaff accelerator from April 1, 2002 to March 31, 2003. Summary reports of 54 papers, and lists of publication, personnel and cooperative research with universities are contained.

Keywords: JAERI Tandem, Nuclear Structure, Nuclear Reactions, Nuclear Chemistry, Nuclear Theory, Atomic Physics, Solid State Physics, Radiation Effects in Materials, Progress Report.

Editors: Suehiro TAKEUCHI, Masumi OSHIMA, Tetsuro ISHII, Yuichiro NAGAME, Satoshi CHIBA and Masao SATAKA

JAERI－Review 2003－028

原研タンデム加速器
２００２年度年次報告

日本原子力研究所東海研究所
物質科学研究部※

（２００３年９月４日受理）

本年次報告書は、東海研究所の原研タンデム及びバンデグラフ加速器で、２００２年４月１日から２００３年３月３１日までの間に行われた研究活動をとりまとめたものである。

(1) 加速器の運転状況および開発　(2)原子核構造　(3)原子核反応　(4)核化学　(5)原子核理論 (6)原子分子物理及び固体物理 (7)材料の照射効果の 7 部門にまたがる５４編の研究報告、公表された文献、関与した職員及び大学等との協力研究のリストを収録している。

東海研究所：〒319-1195　茨城県那珂郡東海村白方白根２－４
※（編集者）竹内末広・大島真澄・石井哲朗・永目諭一郎・千葉　敏
左高正雄

Forward

This report covers research and development activities of the tandem accelerator and its superconductiong booster at JAERI, Tokai, for the period of April 1, 2002 to March 31, 2003. During this period, the tandem accelerator was operated over 4800 hours or 208 days to deliver ion beams to the experiments in the fields of nuclear structure, nuclear reactions, atomic physics, solid state physics and radiation effects in materials. The superconducting booster was utilized over 50 days for 15 experimental subjects. Thirty-two research programs have been carried out in collaboration with about 150 researchers from universities and research institutes. The following are some of the highlights in FY 2002.

Since FY2001, JAERI-Tokai and KEK-IPNS (Institute of Particle and Nuclear Studies) have been collaborating on a joint project of developing an ISOL-based radioactive-nuclear-beam (RNB) facility in the tandem accelerator laboratory. This facility utilizes an existing KEK linac system of 1 MeV/u Neutron-rich nuclei are produced by proton-induced fission of uranium. An existing neutron target room was reformed to the RNB accelerator room in FY2002 and the KEK linac will be installed in FY2003.

In the accelerator development, the acceleration tube replacement program with NEC compressed tubes was proceeding. High pressure water jet rinsing was found to have an obvious effect in improving high voltage performance as a result of carrying out a 3MV test with water-jet rinsed tubes. All the new tubes were rinsed, baked and ready for the replacement to be done in early FY2003.

In research of nuclear physics, electromagnetic properties of low-lying states in ^{66,70}Zn, ^{78}Se and ^{84}Kr isotopes were clarified utilizing a technique of projectile Coulomb excitation. The gamma-ray detector array used in this study was upgraded to GEMINI-II which was composed of seventeen BGO anti-Compton spectrometers and three LOAX detectors. A new isomer in a neutron-rich isotope ^{70}Cu was found using an isomer-scope which allowed one to identify the mass number as well as the atomic number of nuclei emitting unknown gamma rays. Reaction cross sections of ^{16}N(α, n) and ^{16}N (p,n), which are related to the α-process preceding the r-process in the "hot-bubble" of the supernova explosion, were measured for the first time. The ^{16}N-RNB was produced via the d(^{18}O, ^{16}N) reaction and was selected by the recoil mass separator JAERI-RMS.

In research of heavy element nuclear chemistry, successive anion-exchange experiments of element 104, rutherfordium, were conducted. A new isotope ^{241}Bk produced in the ^{239}Pu(^{6}Li,4*n*) reaction was identified with the gas-jet coupled JAERI-ISOL.

In research of nuclear theory, it was found as a result of Monte-Carlo Shell Model calculations that the shell gap at N=20 narrows as Z number decreases, and the narrowing was confirmed by anomalous electromagnetic moments of ^{30}Na. In addition, from the relativistic many-body theory, the pairing gap of Λ-hyperon in dense nuclear matter was found to decrease as the background nucleon density increased due to a reduction of the effective Λ-hyperon mass.

In research of solid state physics, a study of Li self-diffusion in $LiCoO_2$ and LiAl started using ^{8}Li RNB separated by the JAERI-RMS as a preliminary experiment for the JAERI-KEK joint RNB project. The α-particle measurements at different sample temperatures indicated that the technique was useful for the measurement of diffusion coefficients. On the other hand, sputtering yields of non-conductive oxides were measured applying a carbon foil collector method to investigate the electronic excitation effects on atomic displacement. The notable electronic excitation effect was observed and oxides with a large electronic sputtering yield had a tendency to have a large band gap.

Hiroshi Ikezoe
Deputy Director
Department of Materials Science

Contents

目　次

1. Accelerator Operation and Development

This is a blank page.

1.1 TANDEM ACCELERATOR AND BOOSTER OPERATION

TANDEM ACCELERATOR GROUP

Tandem Accelerator and Booster: There were two scheduled machine times in this fiscal year and the operations of the tandem accelerator and the booster for experiments were performed as scheduled. The operation time of the tandem accelerator was 4800 hours in 208 days. The super-conducting energy booster was operated steadily for 50 days for 15 experimental subjects. During these times, the helium refrigeration systems for the tandem booster were in operation for 98 days from April 15 in 2002, 114 days from September 18 in 2002. Few preliminary days was prepared at the end of the 2nd scheduled machine time, and these days were utilized to relieving the canceled schedule by unexpected maintenance's of the accelerator. The summary of the operation from April 1, 2002 to March 31, 2003 is as follows.

1) Time distribution in terms of terminal voltages (Tandem accelerator)

>16 MV	0 days	0 %
15-16	80	38.5
14-15	52	25.0
13-14	4	1.9
12-13	10	4.8
11-12	9	4.3
10-11	11	5.3
9 -10	12	5.8
8 - 9	2	1.0
<8	28	13.5

Booster operation for research program

^{48}Ca	~408 MeV	4 days
^{64,70}Zn	~275	3
^{76}Ge	~635	7
^{76,78,82}Se	~601	17
^{136}Xe	~655	7

The voltage dividing system for the tandem accelerator was exchanged to resistor network from the corona needles in the scheduled maintenance in the early 2002 to improve stability at low voltage operation and to reduce shorting rod operation. After this work, the tandem accelerator worked well at low voltage operation. But, the radial sparks between terminal and the pressure vessel surface increased few times even if the operation at the low voltage. We could not confirm the cause of sparks, but we found a broken resistor on the acceleration tube in the scheduled maintenance. It is not sure that the resistor related to the sparks or not.
Two maintenance time periods were scheduled. During these periods, the yearly governmental inspection of the gas handling system and the helium refrigeration system was scheduled. We performed the self-inspection

following the regulation to the high-pressure gas systems on early August, and passed the government inspections in September.

The KEK-JAERI joint project for the installation of the radioactive nuclear beam (RNB) accelerator carried out the construction of the expanding building. We also maintained the accelerator room, which proposes to the regulation area for installing the accelerator. KEK started carrying in accelerator components to JAERI, and also set the power supplies and cooling systems in the utility building. We started making proposal to change the previous licenses of governmental regulation for facility of the radiation and the nuclear fuel, which is needed before utilization of the RNB accelerator.

1.2 UTILIZATION OF TANDEM ACCELERATOR AND BOOSTER

T. YOSHIDA and S. KANDA

The utilization of the tandem accelerator facility was carried out for 208 days for various experiments in two scheduled machine time periods in the FY 2002. Collaboration research proposals for the FY 2002 were examined at late November in 2001, and 22 subjects were accepted by the program advisory committee. The collaboration programs accounted for approximately 88% of the whole machine time. Twenty-one ion species were utilized in the two experimental periods as follows. Inert gas ions like Ar, Kr, and Xe were accelerated steadily from a terminal ECR ion source for various experiments.

1) Time distribution in terms of projectiles

^{1}H	17 days	^{48}Ca	4 days
$^{6,7}Li$	19	$^{58,64}Ni$	17
$^{12,13}C$	15	^{63}Cu	1
$^{16,18}O$	20	^{64}Zn	9
^{19}F	5	^{74}Ge	7
^{27}Al	4	^{86}Kr	9
$^{35,37}Cl$	3	^{82}Se	14
$^{32,33}S$	14	^{90}Zr	1
^{40}Ar	3	^{127}I	2
^{48}Ti	2	^{136}Xe	35
		^{197}Au	7

The experimental terms allotted in the two periods were 106 days in April 15 to August 1, 123 days in September 18 to February 12 in 2003. The summary of allotted days to various fields of experimental subjects are as follows.

Research field	Allotted days	Total number of subjects
Nuclear physics	93	34
Atomic and Solidstate physics	67	55
Nuclear chemistry	48	29
Material research	8	8
Accelerator development	1	1

1.3 TREATMENT OF NEW ACCELERATOR TUBES BEFORE REPLACEMENT TO IMPROVE THE HIGH-VOLTAGE PERFORMANCE

S. TAKEUCHI, H. KABUMOTO, T. NAKANOYA and T. YOSHIDA

We have been planning to replace the accelerator tubes aged more than 20 years with compressed geometry type new tubes, in order to push up the terminal voltage from the presently operational range of 16 MV to the originally expected range of 20 MV. The replacement from the old tube system which contains useless aperture /heater-plate assemblies to the new tubes will increase the acceleration gaps by about 26 %. The increase seems to be very helpful to improve the terminal voltage. New tubes needed for the replacement have been purchased. However, we have to pay caution to the replacement plan. The conditioning after a replacement is usually very much time-consuming, while we want to re-start the operations for experiments as soon as possible. The new tubes as obtained are not always the best to use. For these reasons, we had an idea to clean the surfaces of alumina-ceramic insulating vacuum-walls and titanium electrodes by a high-pressure high-purity water jet, which has been proven to be very useful to clean super-conducting cavities. In addition to this motivation, the tube fabricator, NEC, noticed that bad ceramics had been used for the new tubes and resulted in strong discharge activities in a high voltage performance test, even below the rated voltage. We, therefore, studied the effect of high-pressure water jet rinsing on the tubes and their high voltage performances prior to the replacement.

We carried out various investigations into the ceramics used for the old and new tubes and found several results. The new ceramics are composed of finer grains and covered with more loosely bound micro-particles than the old ceramics. Such particles were easily removed by a high-pressure gaseous-jet or water-jet. Ultrasonic-wave rinsing was also effective to clean not only the ceramic surfaces but also the electrodes and the junctions between the electrodes and ceramics. The new ceramics contained a lot more gas than the old ceramics. The method of treatment was, then, settled to include ultrasonic-wave rinsing for 30 min, at 600 W and with some detergent, high-pressure water jet rinsing with de-ionized water mixed in an air-jet of 1 M Pa for about 25 min, drying at 50°C in a clean booth and baking at 200°C with pumping for two weeks.

With respect to high-voltage tests, a good feasibility was obtained in FY2001 by testing six old spare tubes in a 1-MV column-module of the tandem accelerator. A feasibility test with new tubes at a longer scale was desired so that a high voltage test with six cleaned new tubes were carried out at NEC on a commercial contract, in FY2002. The tubes were set in a 3 MV column structure in a SF_6-gas pressure-vessel. The high voltage testing was done over three days. The strip-chart records are shown in Fig. 1. The result was obvious. The voltage went up to the rated voltage of 3 MV in 4 hours, to 3.1 MV in the second day and 3.2 MV in the third day. There were only a few big discharges but no frequent micro-discharges at all. The fact that the voltage stability was improved more after the last moderate discharge in the third day indicates the condition reached perfect. On the other hand, the strip-chart during the test of the same new tubes before our cleaning treatment showed frequent full sparks and continuous micro-discharges at a level below the rated voltage.

It is concluded that the cleaning treatment with ultrasonic-wave rinsing and high-pressure water jet rinsing is very effective to remove loosely bound micro-particles from the surfaces and to reduce discharge activities drastically. In other words, loosely bound micro-particles on the ceramic surfaces were found to be the source of discharge activities.

The treatment of eighty new tubes has been carried out by January 2003 according to the cleaning prescription described above. The tandem accelerator was opened for the tube replacement in February. Old tubes were removed and the column was completely cleaned to be ready for the installation at the end of March. We expect to complete all the installation work including tube conditioning in June, 2003. We set a clean air environment during assembling the tubes.

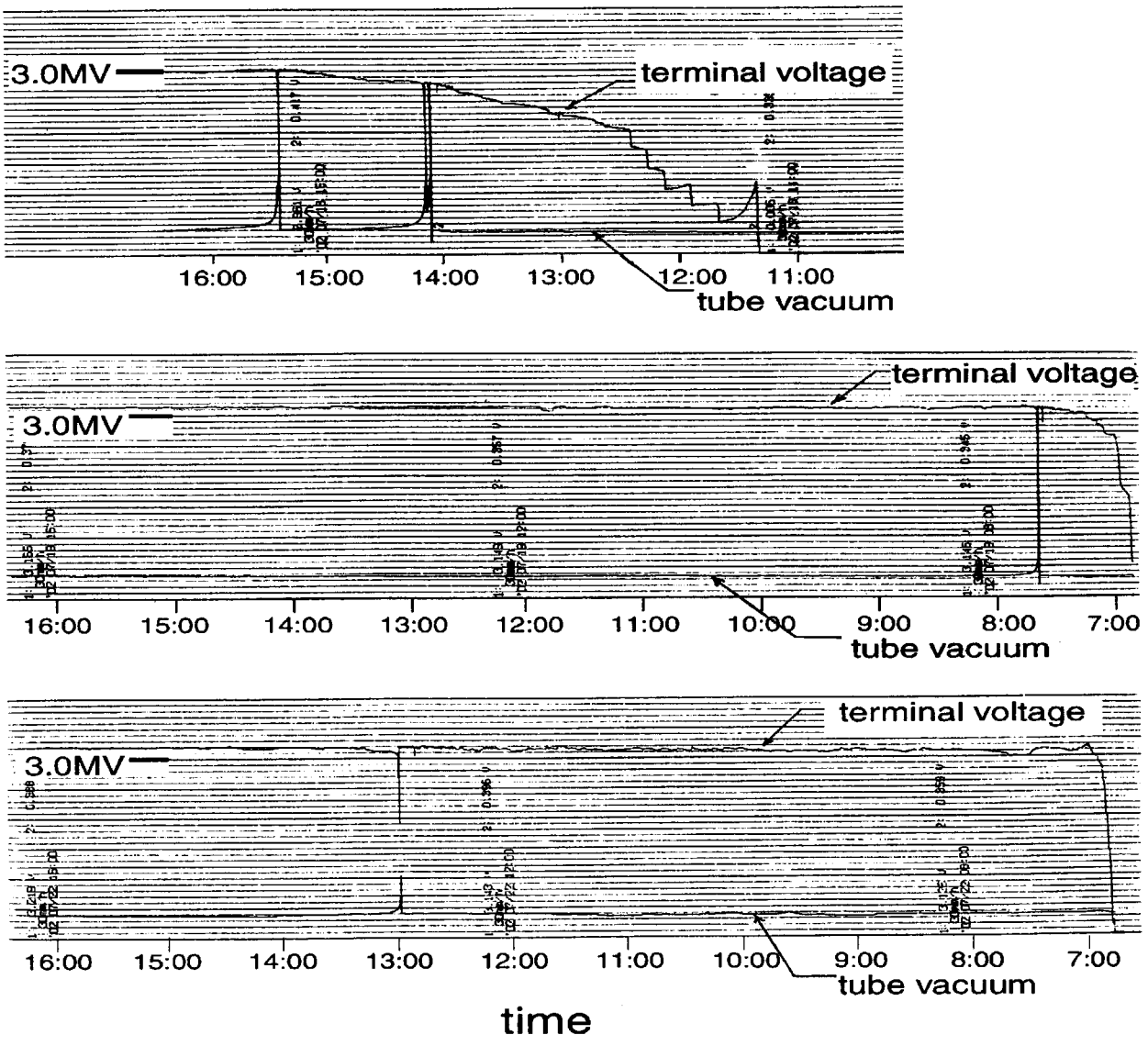

Fig. 1. Strip-chart record during the high voltage tensioning with six new accelerator tubes.

1.4 JAERI-KEK JOINT RNB PROJECT

S.TAKEUCHI and H. MIYATAKE[1]

JAERI-Tokai and KEK-IPNS(Institute of Particle and Nuclear Studies) have been constructing an ISOL-based radioactive nuclear beam (RNB) facility in the tandem accelerator laboratory since 2001. The RNB facility will have a linac system, which was once used at KEK-Tanashi for acceleration of RNB. For producing RNB, proton beams from the tandem accelerator are to be used as primary beams. A prospective RNB production target is a uranium-carbide which emits a number of neutron-rich fission products(FP). An existing ISOL system will be utilized for isotope separation. A charge breeder was developed by KEK at Tsukuba, which will be used to strip electrons from the RNB primary ions up to multiple charge states necessary for the acceleration all the way through the RNB acceleration system. An ECR ion source will be also implemented as an injector for intense stable ion beams (SNB). The first acceleration unit is a split-coaxial RFQ linac of 26MHz with acceleration energy of 0.18 MeV/u and the second unit is an IH(interdigital-H type) linac of 52 MHz with exit beam energy of 1.1 MeV/u[1,2]. Another linac with exit beam energy of 2 MeV/u needs to be built in future to inject the beams into the superconducting booster(of which frequency is 130 MHz) in order to get the beam energy beyond the Coulomb barrier energy for all beam and target species.

We expect that the RNB will be obtained with an intensity of 10^5 to 10^7 particles/s and will develop innovations in the studies on nuclear structures of unstable nuclei, formation processes of nuclear species in astro-physics, material science with RNB implantation and so on. For SNB from the ECR ion source and accelerated by linacs, there is a big prospect to multiply the present intensities from the tandem or booster by orders of 10 to 1000, or to the order of 1 pμA. Such an increase of SNB is useful for the studies of the synthesis of super heavy nuclei and chemical properties of transactinoide elements from the point of relativistic effect on orbital electrons or for the experiments which need a high beam fluence.

The layout plan is shown in Fig. 1. The existing linacs and experimental apparatus will be installed in an old target room next to the ISOL room. In FY2001, a utility building for accelerator power supplies and cooling systems was built near the RNB accelerator room. A series of safety studies against generating FP with protons and uranium-carbide and accelerations of radioactive isotopes were carried out and made it ready to take steps to get this RNB plan authorized by the government. R&D for RNB ion sources started. KEK built an 18GHz ECR type charge breeder and started experiments with it. In FY2002, the old target room was converted into the RNB acceleration room by extending the building and by furnishing with a ventilation system capable of handling non-enclosed radioactive isotopes. The linacs had some modifications including frequency adjustment at the factory in FY 2002 and will be moved to JAERI in FY2003. We expect some experiments to be carried out with 1 MeV/u RNB in FY 2004.

[1] Institute of Particle and Nuclear Studies, KEK

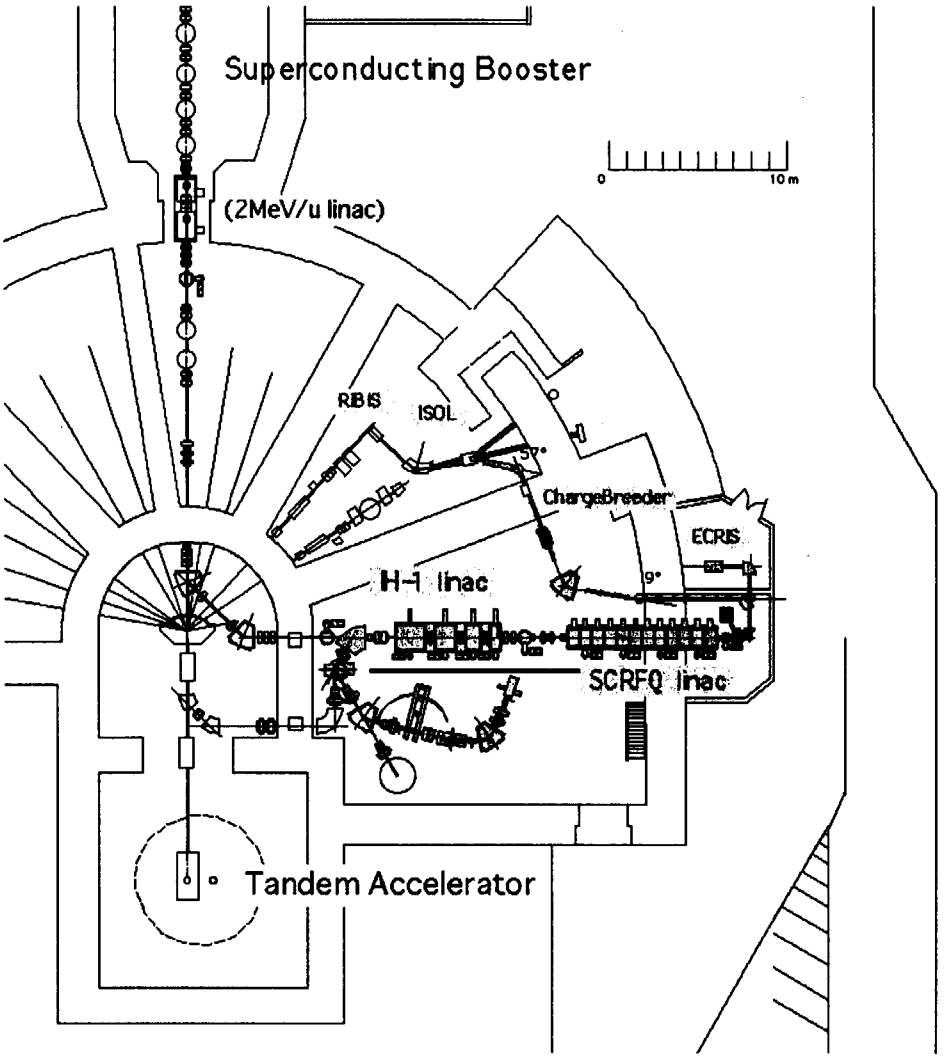

Fig. 1. Layout plan of the JAERI-KEK's RNB project.
(The first three year plan does not include the transport line and additional injector linac to the superconducting booster.)

References

[1] S. Arai *et al.*, Nucl. Instr. and Methods **A390**(1997)9-24.
[2] M. Tomizawa *et al.*, Proc. of the Heavy Ion Accelerator Technology:Eighth International Conference, AIP 1-56396-806-1/99, pp451-465.

1.5 CAVITY MODIFICATIONS AND LOW POWER TESTS OF THE KEK RFQ/IH LINAC

S. Arai[1], Y. Arakaki[1], K. Niki[1], M. Okada[1] and M. Tomizawa[1]

JAERI and KEK are constructing jointly a radioactive nuclear beam (RNB) facility since fiscal year 2001 at JAERI-Tokai tandem site [1]. In the first stage, RNBs from the ISOL are accelerated by a split coaxial RFQ (SCRFQ) and an interdigital-H (IH) linac up to the energies of 0.14 to 1.09 MeV/u. In the second stage, the beam from the SCRFQ and IH linac is accelerated by an IH2 linac up to 2-MeV/u, and further accelerated by the superconducting (SC) linac up to the energy above Coulomb barrier. The maximum beam energies are 5 Mev/u for q/A=1/7 ions and 8 MeV/u for q/A=1/4 ions.

We modified the existing SCRFQ and IH cavities to match their resonant frequencies to that of the SC linac. Since the resonant frequency of SC linac is 129.8 MHz, the frequency of SCRFQ has been changed from 25.5 to 25.96 MHz and that of IH from 51 to 51.92 MHz. As for the SCRFQ, resonant frequency and inter-vane voltage along beam axis were well tuned by changing locally inter-vane capacitance and stem (used for supporting the vanes) inductance. For changing the capacitance, C-tuners of the copper plates (Fig. 1) were attached on the back-plates of the vanes so that a plate confronted a stem with a distance of 25 mm. We adjusted the stem inductance by changing the area of the stem-flange windows with panels (Fig. 2). For tuning the frequency and field distribution, height of the C-tuners installed in the first, second and 12th modules was changed as shown in Table 1; the number of tuners is four per module. Height of the panels before and after tuning is summarized in Table 2.

Table1: Height of C-tuners installed in the first, second and 12th modules

	1st module	2nd module	12th module
Height of C-tuners before tuning (mm)	170	120	120
Height of C-tuners after tuning (mm)	170	70	95

Table2: Height of Panels attached on the stem flanges

Before tuning		After tuning	
Positions of the stem flanges	Height of panels	Positions of the stem flanges	Height of panels
Between 3rd and 4th modules	0 mm	Between 3rd and 4th modules	136.5 mm
Between 6th and 7th modules	125 mm	Between 6th and 7th modules	136.5 mm
Between 9th and 10th modules	0 mm	Between 9th and 10th modules	136.5 mm

Values of the capacitance and inductance to be changed were estimated by using an equivalent circuit analysis [2]. For the inter-vane voltage measurements, a Teflon perturbing object of a square plate, $30\times30\times8\,mm^3$, was moved along two vanes used as a guide. Figure 3 shows the measured longitudinal inter-vane voltage distribution of the SCRFQ.

As for the IH cavities, the resonant frequencies were tuned by increasing the gap lengths between drift-tubes, that is, by decreasing the capacitance. For increasing the gap length, the drift-tube length was shortened. All drift-tubes except end drift-tubes were replaced to the modified ones. Dimensions of the drift-tubes were finally determined by model tests after rough estimations by MAFIA calculations [3].

Accelerator Laboratory, KEK

Each cavity of IH Linac has a capacitive tuner and a inductive one. They change the frequency 100 or 150 kHz. Therefore, we tuned the frequency to the goal one with an accuracy better than ± 50 kHz . For the field measurements, a perturbing bead was moved along the beam axis. The bead is an aluminum sphere of 6.3 mm in diameter. Figure 4 shows the measured electric field distributions along beam axes of the IH cavities.

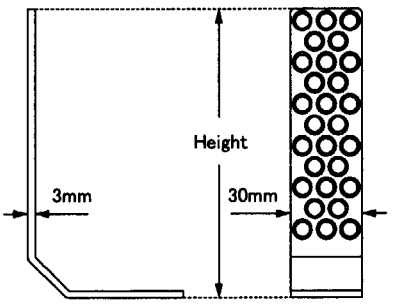

Figure 1: Shape of the C-tuner.

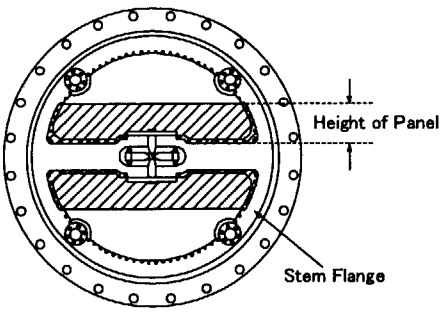

Figure 2: Panels attached on the stem flange.

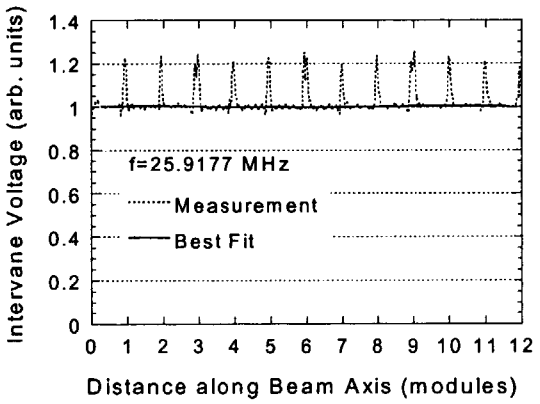

Figure 3: Longitudinal inter-vane voltage distribution.

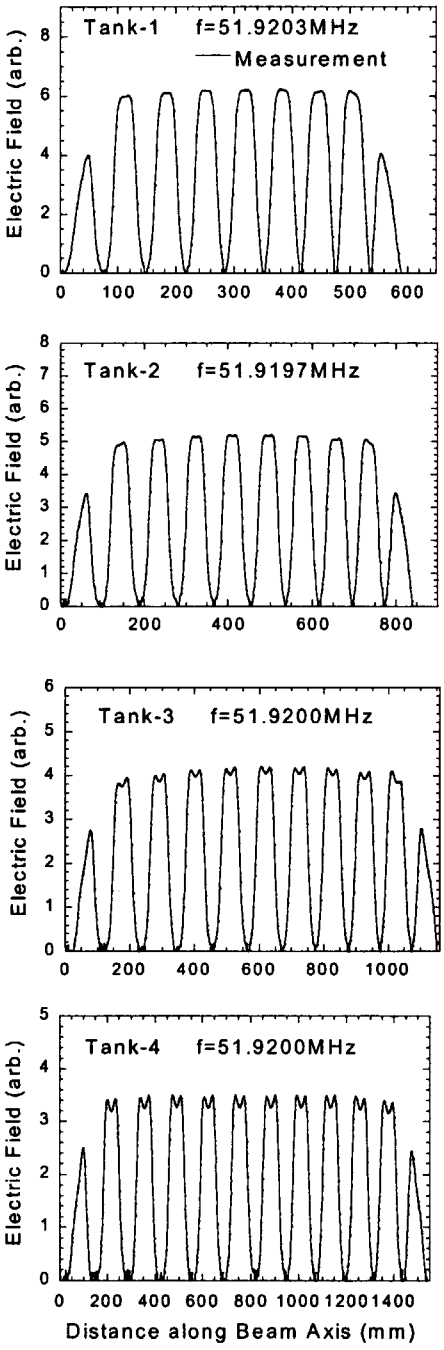

Figure 4: Electric field distributions.

References

[1] S. Arai et al., Proc. of EPAC 2002, Paris, France, 2002, p.861.

[2] S. Arai, KEK Report 2001-7, 2001.

[3] Y. Arakaki et al., Proc. of EPAC 2002, Paris, France, 2002, p.864.

1.6 ION SOURCE DEVELOPMENT FOR THE JAERI-KEK JOINT RNB PROJECT

S. ICHIKAWA, A. OSA, M. MATSUDA, S.C. JEONG[1)] and I. KATAYAMA[1)]

In accordance with the JAERI-KEK joint radioactive nuclear beam (RNB) project, two kinds of ion sources, surface ionization type and FEBIAD type, have been developed to produce heavy neutron-rich RNBs with proton-induced fission of ^{238}U at the JAERI-ISOL. In the present FEBIAD type ion source, a uranium-carbide target is directly attached to a plasma chamber, while in the surface ionization type one, a uranium-carbide target is located inside.

In the design of both integrated-target-ion source systems, the proton beam energy and intensity should be considered. The accelerator provides the proton beams with energy of 36 and 18 MeV. The beam intensities are expected to be 3 μA and 10 μA, respectively. The range of the proton beams at 36 MeV is 2-3 g/cm^2 for the UC target.

Fig. 1(a) shows an ion-source housing which consists of magnet coils, current feedthroughs, gas lines, cooling water connections, a vacuum valve and a base plate. Fig. 1(b) depicts a part of the FEBIAD type integrated-target-ion source which consists of the FEBIAD ion source and a target container with a heating device. The target of about 2.6-g ^{238}U impregnated on a graphite disk of 8 mm in diameter is usable in the target container made of tantalum, which attached to the graphite holder. The entrance window is made of a 0.1 mm thick tantalum foil. The center of the target is 25 mm apart from that of the anode as is seen from scale in the Fig. 1(b). The close distance gives a short effusion time for the atoms to move through the transfer region after diffusing out of the target material. The target is heated by the electron bombardment. The electrons emitted from a filament of the target heater are accelerated to the target container which is biased at about 300 V with respect to the filament.

In the proton-induced fission of ^{238}U, a large number of isotopes and elements are simultaneously produced. The present ISOL system is not capable of separating an isobar, and the molecular ion formation method in the ion source should be considered. To obtain chemically selective performance, the target container was connected to a gas transfer line as shown in Fig. 1(b). With a reactive gas injection into the target assembly, it is expected that gaseous volatile compounds would be formed. By using this setup, the fluoride, chloride, oxide and sulfide compounds will be also available.

A schematic drawing of the surface ionization type ion source, which is modified from the previous one [2], is shown in fig. 2. The target container and the ionizer are heated by electron bombardment from a tungsten filaments, which is at potential of typically -500 V relative to the ionizer as well as target container. With this arrangement, the ionizer and target container can be heated at 2700 K. So, present

[1] Institute of Particle and Nuclear Studies, KEK

surface ionization ion source is capable of effective ionization of alkali, alkaline earth and rare-earth atoms.

Each target/ion source unit is mounted on a base plate and set into a housing. A self-contained unit of the ion source is coupled to the acceleration chamber of the separator through a simple transport device. For the safety maintenance of the target/ion-source, a compact remote-handling system and a storage section are under design.

References

[1] S. Ichikawa, A. Osa, M. Matsuda, K. Tsukada, M. Asai, Y. Nagame, S.C. Jeong, I. Katayama, Nucl. Instrum. Method **B204** (2003) 372-376.

[2] S.Ichikawa, T. Sekine, H. Iimura, M. Oshima and N. Takahashi, Nucl. Instrum. Method **A274** (1989) 259-264.

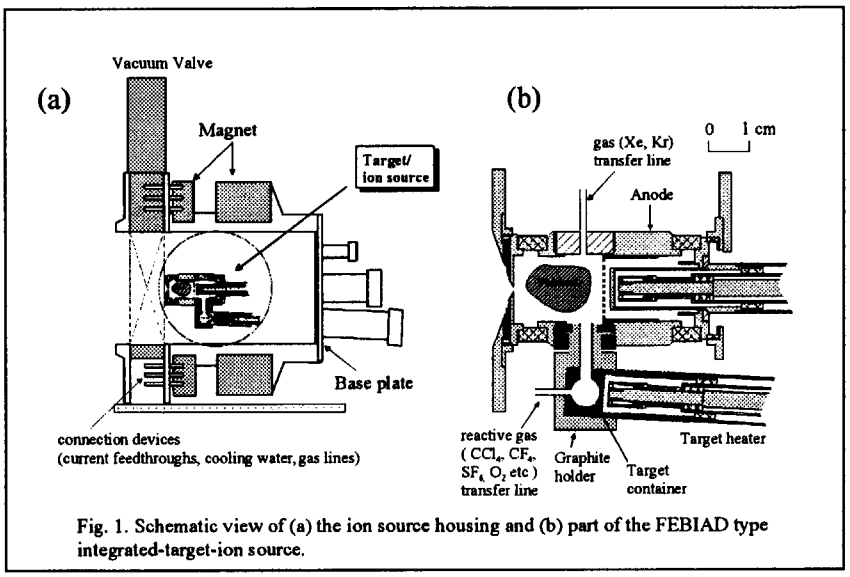

Fig. 1. Schematic view of (a) the ion source housing and (b) part of the FEBIAD type integrated-target-ion source.

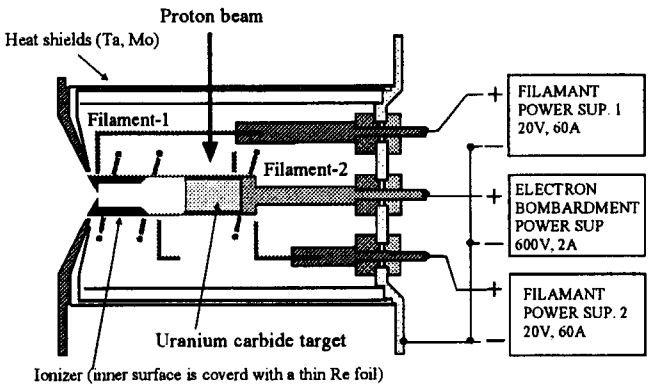

Fig. 2. Schematic drawing of the surface ionization type ion source.

1.7 18GHZ ECR CHARGE BREEDER

S.C. JEONG[1], M. OYAIZU[1], E. TOJYO[1], H. KAWAKAMI[1], H. ISHIYAMA[1],
H. MIYATAKE[1], K. ENOMOTO[1], Y. WATANABE[1], I. KATAYAMA[1], T. NOMURA[1],
M. MATSUDA, A. OSA and S. ICHIKAWA

The radioactive nuclear beam (RNB) facility, originally constructed at KEK-Tanashi, will be moved to Tandem Accelerator Facility at JAERI-Tokai under the collaboration between KEK-IPNS and JAERI-Tokai [1]. In the facility, the neutron-rich fission products of ^{238}U induced by protons of 30MeV[2] will be accelerated to the energies exceeding 5MeV/A. The accelerated energies depend on their mass to charge ratio (A/q), which should be less than 7. An UC_2-target of 2.6g is going to be implemented in a target-ion source module of JAERI on-line isotope separator (JAERI-ISOL)[3], presently operating with a surface ionization type or a FEBIAD ion source. Since the ions from the ISOL are singly charged, a charge breeding system is necessary for acceleration. The charge breeder (CB) converts singly charged radioactive ions from the ISOL to highly charged ions having $A/q<7$. We made an electron cyclotron resonance (ECR) ion source as the charge breeder for the facility, based on our previous studies [4,5] about the conditions necessary for an ECRCB with high efficiency of charge breeding. The ECR charge breeder (ECRCB) operating at the microwave frequency of 18GHz has been installed at KEK test bench. The source is currently operating for tests. Here, we report the result of the charge breeding experiments performed by externally injecting Xe^{1+} ions into the charge breeder.

Fig.1 shows the test bench used for test experiments. Singly charged (1+) ion beam of 12keV was produced by the 12GHz ECR ion source. After being analyzed by a 45° magnetic separator, the beam was characterized by a double slit located at the focal point of the separator. The emittance of the beam was fixed to about 50 π mm mrad, by using the slit. The continuous beam was injected into the 18GHz ECRCB for further ionization, after being properly shaped and decelerated by the following beam optical system. The optical system for the injection consists of an einzel lens doublet and two concentric cylindrical deceleration electrodes. The outer cylinder, 40mm in diameter, will be operating as a final stage of deceleration, whereas the inner cylinder, 20mm in diameter, stays on the ground potential. Therefore, the main deceleration will happen between two electrodes and further smooth potential drop could exist between the outer cylinder and the plasma chamber if necessary. The high voltage applied to the charge breeder is slightly lower than 12kV in order to compensate the difference in the plasma potentials of two ECR ion sources. The final energy of 1+ ions at the instant of injection can be tuned to be close to zero, by adjusting the

[1] Institute of Particle and Nuclear Studies, KEK

difference in the high voltages actually applied to two sources in an order of 10V according to the operational conditions of two sources. During the present experiment, the outer cylinder of the deceleration system stayed on the same potential as the charge breeder.

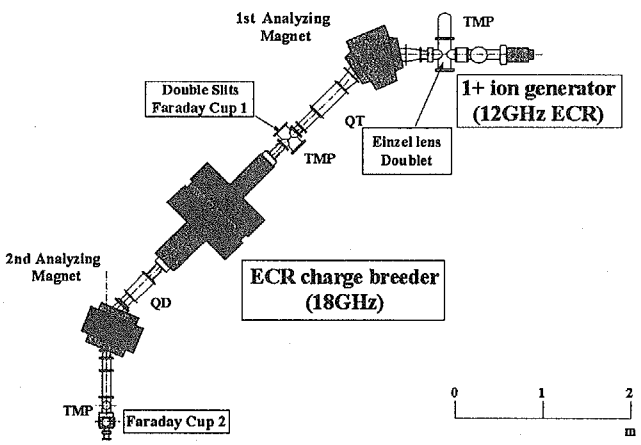

Fig.1 Layout of the test bench at KEK

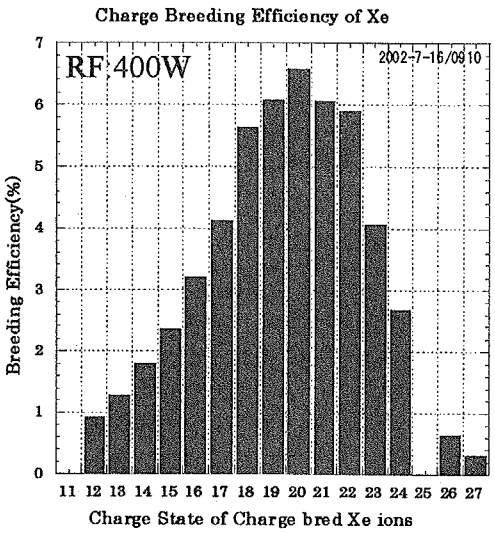

Fig.2 Charge state distribution of charge bred Xe ions

Under an operational condition of the ECRCB adjusted for Xe^{18+} before injection, the charge breeding efficiency for Xe^{1+} ions was measured. The Xe^{1+} ion with an intensity of about 500nA was injected into the ECRCB as discussed above. The ECR plasma consists sorely of residual gases, such as O and C ions. The charge-bred Xe ions are extracted again and their charge distribution was measured. In Fig.2 shown are the charge breeding efficiencies for Xe, resulting from the continuous injection of Xe^{1+} ions of 500nA. The global efficiency, sum of specific efficiencies for ions shown in the figure, was about 50%. The maximum observed at Xe^{20+} reaches about 6.5%.

References

[1] H. Miyatake et al., Nucl. Instrum. Meths. B204 (2003) 746
[2] H. Kawakami, KEK Report 2001-15.
[3] S. Ichikawa et al., Nucl. Instrm. Meths. B204 (2003) 372
[4] M. Oyaizu et. al., Rev. Sci. Instrum.73 (2002) 806.
[5] S.C. Jeong et. al., Rev. Sci. Instrum.73 (2002) 803.

This is a blank page.

2. Nuclear Structure

This is a blank page.

2.1 SEARCH FOR NEW HIGH-K ISOMERS IN THE $A \approx 180$ REGION

T. SHIZUMA, T. HAYAKAWA, S. MITARAI[1], T. MORIKAWA[1] and H. UTSUNOMIYA[2]

High-K isomers in the Hf-W-Os nuclei with $A \approx 180$ arise due to the presence of many high-j and high-Ω orbitals near the Fermi surface [1]. For these axially deformed nuclei, the projection of the total angular momentum onto the nuclear symmetry axis, K, is approximately conserved. Consequently, the K selection rule governs the decay of the K isomers so that transitions from high-K to low-K bands are strongly hindered. These transitions, in practice, can proceed by admixture of K values. In rotating nuclei, the Coriolis interaction changes the spin orientation to lead to a $\Delta K = \pm 1$ mixing. On the other hand, shape fluctuations towards γ deformation can couple states with K quantum numbers differing by two units ($\Delta K = \pm 2$ mixing). In this context, of special interest have been the surprisingly low hindrances for the very large ΔK transitions [2, 3, 4]. So far, different mechanisms including Fermi-aligned Coriolis K mixing [3, 5, 6, 7], γ-tunneling through the potential barrier [2, 4, 8, 9], and the statistical K mixing due to high level density [10] have been proposed for these transitions.

High-spin studies of neutron-rich nuclei in the $A \approx 180$ region have been limited due to inaccessibility using the fusion-evaporation reaction with stable isotopes for both the projectile and the target. In order to populate excited states of these nuclei, we employed deep inelastic reactions. The experiment was carried out by use of the JAERI tandem and booster accelerator. A natural rhenium foil with a thickness of 26 mg/cm^2 was bombarded by a 600 MeV ^{82}Se pulsed beam. The beam energy was selected as 40 % higher than the Coulomb barrier for the ^{82}Se + ^{187}Re system. Emitted γ rays were detected by four Ge-detector detectors both in beam-on and beam-off periods. Events were recorded on magnetic tapes when two or more Ge detectors were fired in coincidence.

Figure 1 shows γ-ray spectra taken in-beam (top) and off-beam (bottom). In the in-beam spectrum, the γ-ray peaks of ^{185,187}Re can been seen. On the other hand, the 213, 324 and 425 keV transitions associated with the known 4-s isomer in ^{178m}Hf appear in the off-beam spectrum. Further analysis of isomeric transitions is in progress.

References

[1] P.M. Walker and G.D. Dracoulis, Nature (London) **399**, 35 (1999).

[2] P. Chowdhury, *et al.*, Nucl. Phys. **A485**, 485 (1988);

[3] P.M. Walker, *et al.*, Phys. Rev. Lett. 65 (1990) 416; N.L. Gjørup, *et al.*, Nucl. Phys. **A582**, 369 (1995).

[4] B. Crowell, *et al.*, Phys. Rev. C **53**, 1173 (1996).

[5] P.M. Walker, *et al.*, Phys. Rev. Lett. **67**, 433 (1991).

[1]Kyushu University
[2]Konan University

[6] P.M. Walker, *et al.*, Phys. Lett. B **309**, 17 (1993).

[7] S. Frauendorf, in *Proceedings of the international conference on The Future of Nuclear Spectroscopy, Crete, 1993*, p.112 (1994).

[8] T. Bengtsson, *et al.*, Phys. Rev. Lett. **62**, 2448 (1989).

[9] K. Narimatsu, Y.R. Shimizu and T. Shizuma, Nucl. Phys. **A601**, 69 (1996).

[10] P.M. Walker, *et al.*, Phys. Lett. B **408**, 42 (1997).

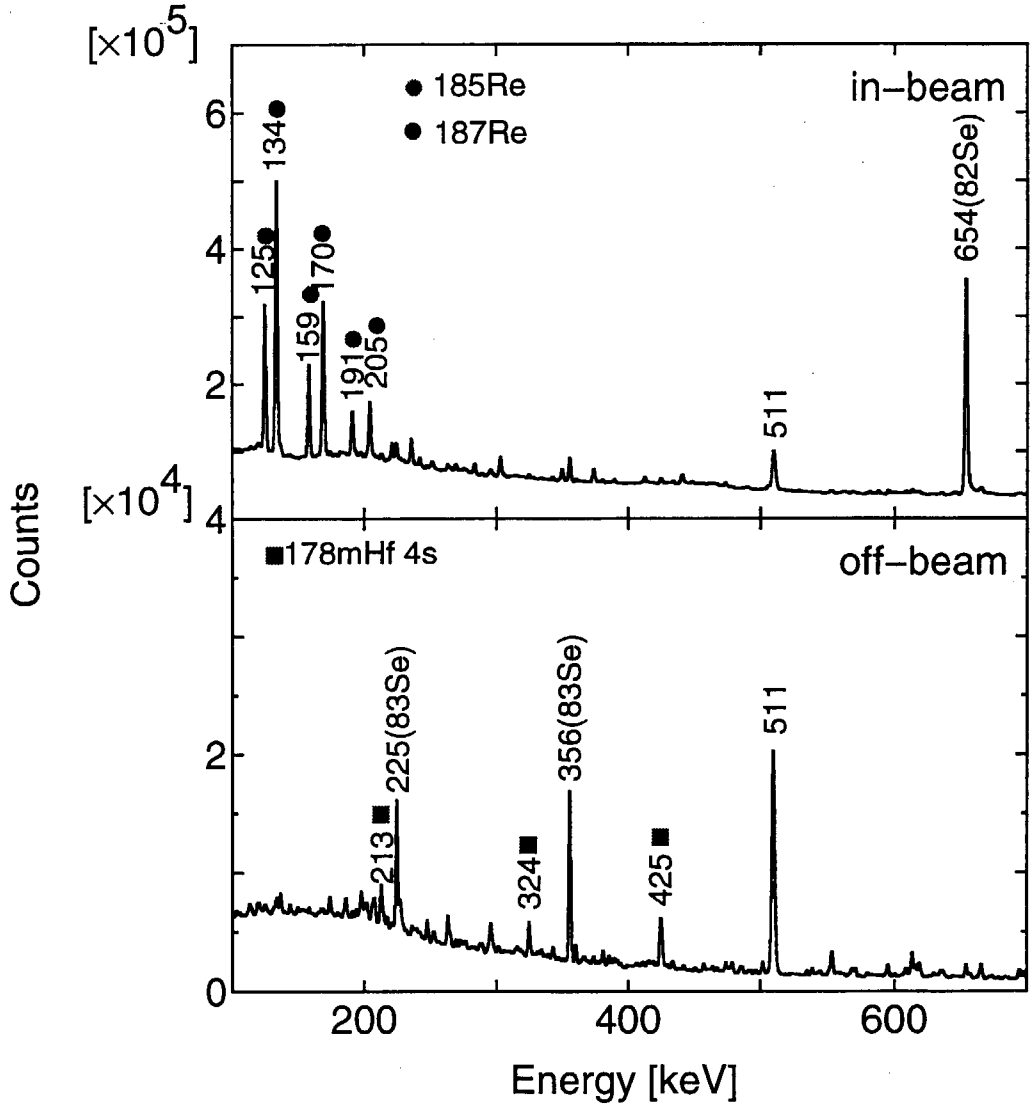

Figure 1: γ-ray spectra taken in-beam (top) and off-beam (bottom)

2.2 BAND STRUCTURE IN ^{152}Sm

Y. TOH, T. CZOSNYKA[1], M. OSHIMA, Y. HATSUKAWA, A. OSA,
M. KOIZUMI, J. KATAKURA, M. MATSUDA, N. SHINOHARA,
A. KIMURA, H. KUSAKARI[2] and M. SUGAWARA[3]

The low-lying excited 0^+ state in a wide range of deformed nuclei has been labeled as the β vibrational bandhead. Since the $K^\pi=2^+$ γ vibrational bandhead was observed as the low lying 2^+ state, it was naturally expected that the low-lying excited 0^+ state would be the β vibrational bandhead. The nucleus ^{152}Sm level scheme may at first seem suggestive of a traditional picture in which the low-lying excited 0^+ state is interpreted as a β vibrational bandhead and the low-lying 2_3^+ state as a γ vibrational bandhead. However, inspection of the level scheme reveals that the energy of excited states and B(E2) values is not consistent with pure rotational bands[1,2]. Moreover, the interband transitions cannot be fully explained even when mixing effects are taken into account[3].

The ^{58}Ni beam of 215MeV and about 1pnA from the tandem accelerator bombarded on a self-supporting ^{152}Sm target of 1.0mg/cm^2 thickness. The experimental setup, whose details are described elsewhere, consists of a gamma-ray detector array of 12 Ge detectors with BGO anti-Compton suppressors, GEMINI[4], and a newly developed position-sensitive particle detector system with 4 photomultiplier tubes in combination with 2 plastic and 2 Yap Ce scintillators[5]. The least-squares analysis code GOSIA [6] was used to extract the E2 matrix elements and the Q moments from the experimental data.

The property of the lowest excited $K^\pi=0^+$ band can be derived from the experimentally obtained Q moments. In the GOSIA χ^2 fitting analysis, unknown matrix elements of groundband states were used theoretical values. The Q moment of 2_2^+ ($K^\pi=0^+$ band) can be extracted from the previous experimental data. The preliminarily result made it difficult to interpret the 0_2^+ state as a β-vibrational bandhead.

References

[1] N.V. Zamfir *et al.*, Phys. Rev. C **60**(1999) R1553.
[2] B. R. Mottelson *et al.*, J. Phys. Soc. Jpn. **24**(1968) 87.
[3] L.L. Riedinger *et al.*, Phys. Rev. **179**(1969) 1214.
[4] K. Furuno *et al.*, Nucl. Instrum. Methods Phys. Res. **A421**(1999) 211.
[5] Y. Toh *et al.*, Rev. Sci. Instrum. (submitted).
[6] T. Czosnyka *et al.*, Nucl. Phys. **A458**(1986) 123.

[1]SLCJ, University of Warsaw
[2]Faculty of Education, Chiba University
[3]Chiba Institute of Technology

2.3 COULOMB EXCITATION EXPERIMENT OF ^{64,66}Zn

M. KOIZUMI, A. OSA, Y. TOH, M. OSHIMA, A. KIMURA, Y. HATSUKAWA, J. KATAKURA, M. MATSUDA, A. SEKI[1], T. CZOSNYKA[2], H. KUSAKARI[3], M. SUGAWARA[4] and T. MORIKAWA[5]

Having two extra protons outside the *Z=28* closed shell, stable even-even Zn nuclei are generally interpreted with collective vibrational models. For ^{64}Zn and ^{66}Zn, however, an enhancement of the *E2* transition probabilities was found between the states in the ground band, and between the states in the excited band based on the 2_2^+ state, while those of the inter-band transitions are weak. The low-lying states of those nuclei can be, therefore, interpreted as quasi-rotational bands [1,2]. Near the Zn isotopes, shape coexistences were found in Ge and Se isotopes [3-7]. Large triaxial deformations in the ground states of $^{72\text{-}76}$Ge and $^{74\text{-}78}$Se were pointed out in refs. [8,9]. Therefore, it would be important to experimentally confirm the *B(E2)* values and quadrupole moments of ^{64,66}Zn for understanding the low-lying structures.

Coulomb excitation is a useful technique for the measurements of $B(E2)$'s and quadrupole moments of low-lying levels. Because the excitation process is purely electromagnetic, those values can be derived model independently [10,11]. With a heavy ion bombardment, multiple Coulomb excitation enables us to study the nuclear structure up to about 2 MeV. Nowadays, an apparatus equipped with a 4π γ-ray detector array and position sensitive detectors, which covers the wide range of the scattering angle, has been proven to be useful to get necessary information of particle-γ correlation [3-7].

Multiple Coulomb excitation experiment of ^{64,66}Zn was carried out with an apparatus constructed at one of the beam lines of the Tandem-Booster accelerator facility of Tokai/JAERI. It consists of a gamma-ray detector array, GEMINI [12] and a position-sensitive particle detector system, LUNA [13]; the GEMINI was recently replaced with GEMINI-II, which can mount 17 Ge detectors with BGO anti-Compton suppressors, and 3 low-energy coaxial (LOAX) detectors. ^{64,66}Zn beams with energies of about 270 MeV, which do not exceed the Coulomb barriers, bombarded a ^{nat}Pb target with a thickness of about 1 mg/cm^2. Particle-γ coincidence events after the decay of Coulomb-excited nuclei were recorded. The experimental data were analyzed with the least-squares search code GOSIA [12, 13]. Then, we obtained some reduced *E*2 matrix elements between the low-lying states of ^{64,66}Zn. The resultant quadrupole moments of the 2_1^+ sates of ^{64}Zn and ^{66}Zn are $-0.01^{+0.09}_{-0.05}$ eb and $+0.32 \pm 0.10$ eb, respectively.

Deformation parameters of nuclear states can be derived from experimentally obtained reduced *E*2 matrix elements with the quadrupole sum rule [8,9]. In this approach, the deformation parameters (β_{rms}, δ_{eff}), which are analogous to the Bohr's deformation parameter (β, γ), were deduced from the experimentally obtained matrix elements. The (β_{rms}, δ_{eff}) of the ground state of the ^{64}Zn and ^{66}Zn are calculated to be (0.247 ± 0.007, $34^{\circ}{}^{+3}_{-5}$), and (0.23 ± 0.01, $46^{\circ}{}^{+11}_{-6}$),

[1] Ibaraki University
[2] Warsaw University
[3] Chiba University
[4] Chiba Institute of Technology
[5] Kyushu University

respectively, proving that the ground bands of those Zn are moderately triaxial deformed.

In order to investigate the deformation, the potential energy surface (PES) of ^{64}Zn and ^{66}Zn was calculated with the Nillson-Strutinsky model [16], in which a harmonic oscillator was used for the single particle energy calculation. The results of the calculation are given in figure 1. Both the PES's of ^{64}Zn and ^{66}Zn show a valley lying along the γ direction, while ^{64}Zn has a shallow potential minimum at $(\beta, \gamma) \sim (0.13, 0^{\circ})$. This structure points out to the possible interpretation of those nuclei as being γ-unstable. This interpretation does not contradict the result of the quadrupole sum rule mentioned above. In the quadrupole sum rule, the δ_{eff} and β_{rms} are averaged values over the large fluctuation, and contain both static and dynamic contributions. Consequently, the δ_{eff} would be around 30° and the β_{rms} would become larger than that given by the PES calculation.

It should be noted the asymmetric rotor model with $\gamma = 30^{\circ}$ and the O(6) limit of the interacting boson model reproduce the excitation energies and the *B(E2)* values in the ground band quite well. It seems that ^{64,66}Zn can be interpreted as triaxial or γ-unstable nuclei, or nuclei with a soft triaxial potential.

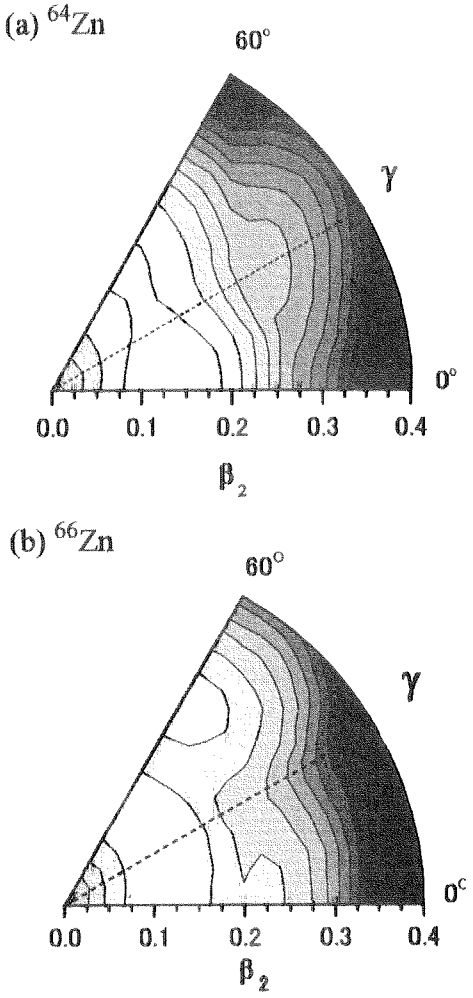

Fig. 1. Potential energy surfaces calculated with the Nillson-Strutinsky model [38]. The energy difference between the contour lines is 500 keV. The dashed line indicates $\gamma = 30^{\circ}$.

References

[1] D.N. Simister et al., J. Phys. G4 (1978) 1127.
[2] B. Crowell et al., Phys. Rev C 50 (1994) 1321.
[3] Y. Toh et al., J. Phys. G 27 (2001) 1475.
[4] Y. Toh et al., Eur. Phys. J. A 9 (2000) 353.
[5] B. Kotlinski et al., Nucl. Phys. A 519 (1990) 646.
[6] A.E. Kavka et al., Nucl. Phys. A 593 (1995) 177.
[7] M.Sugawara et al., Eur. Phys. J. A 16 (2003) 409.
[8] W. Andrejtsche and P. Petkov, Phys. Rev. C 48 (1993) 2531.
[9] W. Andrejtsche and P. Petkov, Phys. Lett. B 329 (1994) 1.
[10] K. Alder and A. Winther, Coulomb Excitation, Academic, NewYork, (1966).
[11] K. Alder and A. Winther, Electromagnetic Excitation, North Holland Publishing co., 1975.
[12] K. Furuno et al., Nucl. Instrum. Methods Phys. Res. A421 (1999) 211.
[13] Y. Toh et al., Rev. Sci. Instrum.73 (2002) 47.
[14] T. Czosnyka, D. Cline, L. Hasselgren, and C.Y. Wu, Nucl. Phys. A 458 (1986) 123.
[15] T. Czosnyka, C.Y. Wu, and D. Cline, Bull. Am Phy. Soc. 28 (1983) 745.
[16] T. Bengtsson et al., Computational Nuclear Physics vol. 1, ed. K. Langanke et al., (Springer-Verlag, Berlin, 1991) p. 51.

2.4 EXCITED STATES IN ^{70}Cu POPULATED BY DEEP-INELASTIC COLLISIONS

T. ISHII, M. ASAI, M. MATSUDA, P. KLEINHEINZ, HOU LONG[1], A. MAKISHIMA[2], T. KOHNO[3] and M. OGAWA[3]

Excited states in ^{70}Cu were populated by deep-inelastic collisions, ^{76}Ge(8 MeV/nucleon)+^{198}Pt, and the γ rays emitted by an isomer in ^{70}Cu were measured by the isomer-scope consisting of a tungsten block, Si ΔE-E detectors and Ge detectors [1,2]. The 20 μm Si-ΔE detectors with good thickness uniformity, made by ourselves, enabled us to identify the mass number of a copper nucleus emitting an unknown γ-ray cascade of 231-1083-1405 keV. A level scheme in ^{70}Cu is shown in Fig. 1. Although low-lying levels in ^{70}Cu are complex, this structure was revealed recently; the ground state is 6^- and the 3^- and 1^+ states are β-decaying isomers [3]. The isomer at 2720 keV found in our experiment is considered as the $(\pi p_{3/2}\nu p_{1/2}g^2_{9/2})10^+$ state, because this excitation energy is close to that of the $(\nu p_{1/2}g^2_{9/2})17/2^-$ isomer in the neighboring nucleus $^{69}_{28}$Ni$_{41}$. Furthermore, the $B(E2;10^+ \rightarrow 8^+)$ value of 60(9) e^2fm^4 is close to that of 63(3) e^2fm^4 between the $(\pi p_{3/2}\nu g^2_{9/2})19/2^-$ and $15/2^-$ states in ^{69}Cu [2]. Similar level structure is also known in analogous nuclei around ^{90}Zr. The $^{92}_{41}$Nb$_{51}$ nucleus has the $(\nu d_{5/2}\pi p_{1/2}g^2_{9/2})11^-$ isomer at 2203 keV and $^{91}_{41}$Nb$_{50}$ has the $(\pi p_{1/2}g^2_{9/2})17/2^-$ isomer at 2035 keV.

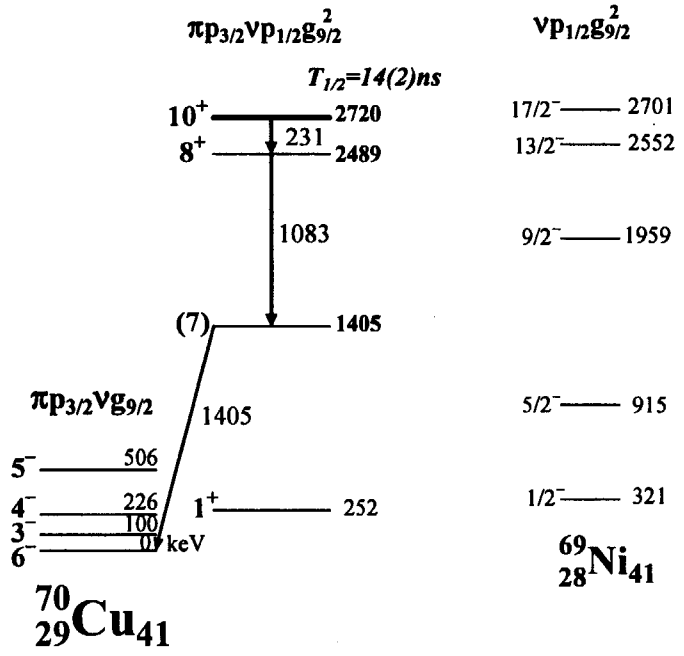

Fig. 1. A decay scheme of the 10^+ isomer in ^{70}Cu. The $\pi p_{3/2}\nu p_{1/2}g^2_{9/2}$ levels in ^{70}Cu are compared to the $\nu p_{1/2}g^2_{9/2}$ levels in ^{69}Ni.

References

[1] T. Ishii *et al.*, Nucl. Instrum. Methods Phys. Res. **A395** (1997) 210.
[2] T. Ishii *et al.*, Phys. Rev. Lett. **84** (2000) 39.
[3] L. Weissman *et al.*, Phys. Rev. C **65** (2002) 024315.

[1]On leave from China Atomic Energy Institute
[2]Department of Liberal Arts and Sciences, National Defense Medical College
[3]Tokyo Institute of Technology

2.5 ROTATIONAL BANDS OF ^{169}Re

X. H. ZHOU[1], M. SUGAWARA[2], M. OSHIMA, Y. TOH,
Y. H. ZHANG[1], Y. ZHENG[1], M. KOIZUMI, A. OSA,
T. HAYAKAWA, Y. HATSUKAWA, T. SHIZUMA

The very neutron deficient Re isotopes are expected to be rather soft with respect to β and γ deformations, and the polarizing effects of individual nucleons make the nuclear shapes strongly configuration- dependent [1-3]. For light odd-A Re isotopes, the proton Fermi surface is at the top of the $h_{11/2}$ and $d_{5/2}$ shells and below the down-sloping 1/2$^-$[541] and 1/2$^+$[660] Nilsson orbits of the $h_{9/2}$ and $i_{13/2}$ spherical parentages. A less deformed shape is favored with the 9/2$^-$[514] and 5/2$^+$[402] orbitals occupied, while the nucleus is driven towards large deformation when the $h_{9/2}$ and $i_{13/2}$ orbitals with Ω =1/2 are occupied by the unpaired proton. These shape differences depending on the proton configuration can be studied through the band properties such as band crossings, spin alignments and the signature dependence of level energies and transition probabilities.

The excited states in ^{169}Re were populated via the ^{144}Sm(^{28}Si, 1p2n)^{169}Re reaction. The ^{28}Si beam was provided by the tandem accelerator at the Japan Atomic Energy Research Institute(JAERI). The target is an isotopically enriched ^{144}Sm metallic foil of 1.3 mg/cm^2 thickness with a 7.0 mg/cm^2 Pb backing. A γ-ray detector array [4], GEMINI, comprising 12 HPGe's with BGO anti-Compton (AC) shields was used. In order to identify the in-beam γ-rays belonging to ^{169}Re and to determine the optimum beam energy, first, we measured the relative γ-ray yields at the beam energies of 140, 145, and 150 MeV. Then the γ-γ-t and X-γ-t coincidence measurements were performed at the optimum beam energy of 145 MeV. A total of 250×10^6 coincidence events were sorted into a symmetric matrix and a DCO matrix after accurate gain matching.

The level scheme of ^{169}Re, including three rotational bands, is proposed from the present work and shown in Fig. 1. Band 1 has a decoupled structure suggesting that the configuration includes proton from an Ω =1/2 orbital. From the knowledge in the neighboring odd-Z nuclei [1-3], band 1 is assumed to be based on the 1/2$^-$[541] Nilsson orbital. Band 2 was most strongly populated and extended up to (45/2$^-$). This band must be based on the 9/2$^-$[514] ground state and experiences a strong backbending at $\hbar\omega$=0.23 MeV with gain of 10.5 $\hbar$ in alignment, corresponding to the AB neutron crossing. Band 3 has the largest aligned angular momentum with a value of about 8.5 $\hbar$ even at low spins. In view of such a large alignment, band 3 must be based on a configuration of at least three quasiparticles. Properties of these three rotational bands are discussed in more detail in our paper [5] which has been published recently.

---

[1]Institute of Modern Physics, P. R. China
[2]Chiba Institute of Technology

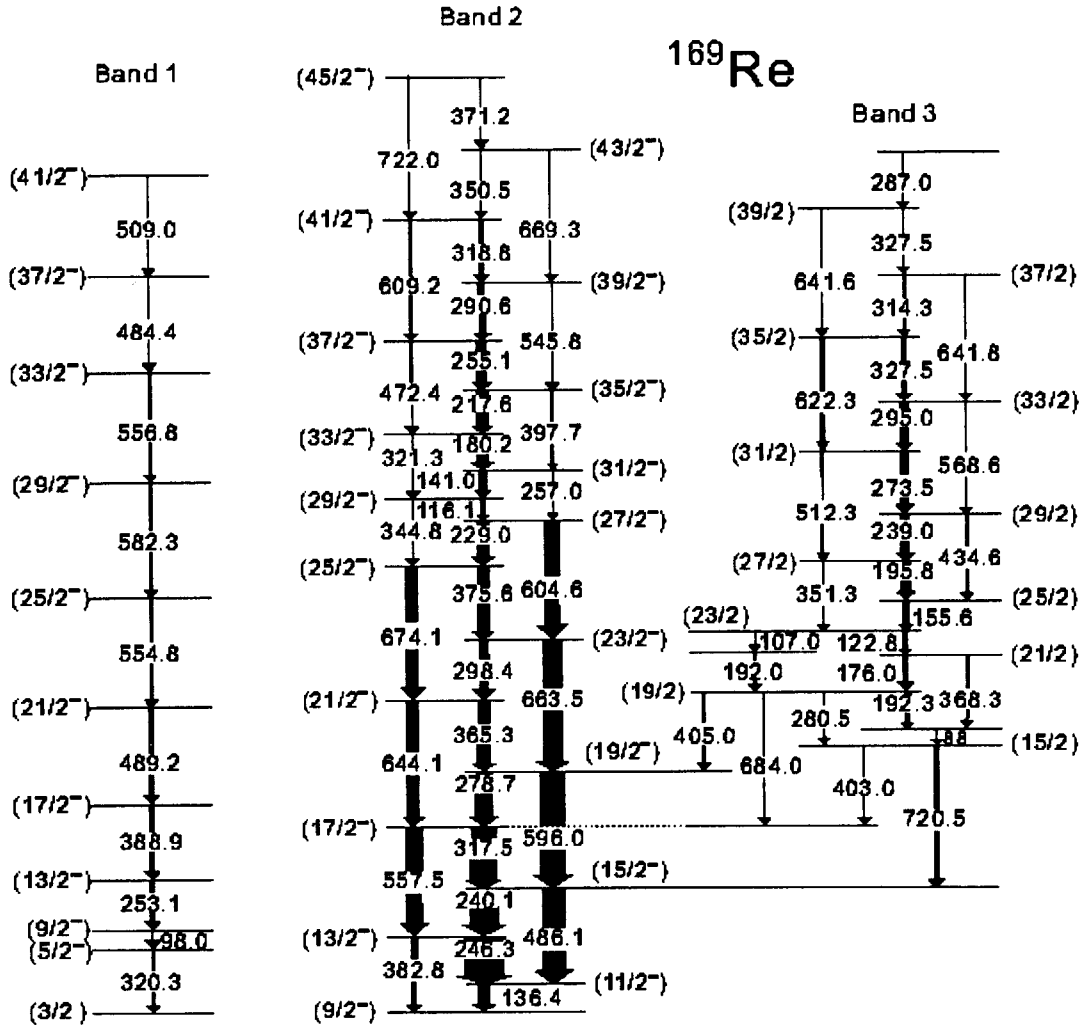

Fig.1 Proposed level scheme of ^{169}Re.

References

[1] R. A. Bark et al., Nucl. Phys. **A501**(1989) 157.
[2] H. Carlsson et al., Nucl. Phys. **A551** (1993) 295.
[3] L. Hildingsson et al., Nucl. Phys. **A513**(1990) 394.
[4] K. Furuno et al., Nucl. Instrum. Methods **A421**(1999)211.
[5] X. H. Zhou et al., Eur. Phys. J. **A15**(2002)285.

2.6 FIRST OBSERVATION OF ROTATIONAL BANDS IN ODD-ODD ^{172}Re

Y. H. ZHANG[1], M. OSHIMA, Y. TOH, X. H. ZHOU[1], M. KOIZUMI, A. OSA, A. KIMURA, Y. HATSUKAWA, T. MORIKAWA[2], M. NAKAMURA[2], M. SUGAWARA[3], H. KUSAKARI[4], T. KOMATSUBARA[5], K. FURUNO[5], H. L. WANG[1], P. LUO[1], C. S. WU[6] and F. R. XU[6]

During the past few years, efforts have been devoted to the studies of band structures of odd-odd nuclei in the A∼170 mass region; interesting high-spin spectroscopic information has been obtained in the odd-odd $^{176-180}$Ir and ^{182}Au [1, 2, 3, 4] using the JAERI Tandem-booster accelerator complex and the gamma ray detector array GEMINI [5]. As the progress of this research subject, we report here the first observation of three rotational bands in ^{172}Re. Prior to this work, the spin and parity of 5^+ were tentatively assigned to the ground state of ^{172}Re according to its intense β^+/EC feeding to the 4^+ and 6^+ rotational levels in ^{172}W [6]. The high-spin states in ^{172}Re have not been studied so far. The present work extends high-spin studies of odd-odd $A \sim 170$ nuclei to the lightest rhenium isotope investigated to date.

The experiment has been carried out at the Japan Atomic Energy Research Institute (JAERI). An enriched ^{149}Sm target of 2.1 mg/cm^2 thickness with a 5.5 mg/cm^2 Pb backing was bombarded by an ^{27}Al beam. The high-spin states in odd-odd ^{172}Re were populated via the ^{149}Sm(^{27}Al,4$n\gamma$)^{172}Re reaction. The in-beam γ rays were detected using a BGO-HPGe array GEMINI. The excitation function measurements were performed at beam energies of 130-, 135-, 140-, and 150-MeV, and a beam energy of 130 MeV was used for γ-γ coincidence measurements. About 250 million coincidence events were accumulated and sorted into a symmetric E_γ-E_γ matrix of 4k×4k size for off-line analysis. It should be noted that the relatively intense γ rays in this experiment were from the fusion-evaporation residues of ^{171,172,173}Re, ^{171,172}W, and ^{169}Ta corresponding to $5n, 4n, 3n, 4np, 3np$, and $\alpha 3n$ evaporation channels, respectively. Since the high-spin level schemes for ^{171,173}Re [7],^{171,172}W [8] and ^{169}Ta [9] had been well established, γ-ray assignment in ^{172}Re could be carried out using those information and the measurements of excitation functions and x-γ coincidence data.

From detailed analyses of the coincidence data, a partial level scheme of ^{172}Re has been established by the present work as shown in Fig. 1. The γ-transition energies in the level scheme are within an uncertainty of 0.5 keV. The ordering of the in-band transitions is established on the basis of γ-γ coincidence relationships, γ-ray energy sums and relative intensities. No linking transitions have been observed among the three bands observed. The relative spins within a band are proposed based on the measured *ADO* (γ-ray Angular Distribution from Oriented states) ratios [10] of emitting γ rays.

---

[1]Institute of Modern Physics, Chinese Academy of Sciences, Lanzhou, P. R. China
[2]Department of Physics, Kyushu University
[3]Chiba Institute of Technology
[4]Faculty of Education, Chiba University
[5]Institute of Physics and Tandem Accelerator Center, University of Tsukuba
[6]Department of Technical Physics and MOE Key Laboratory, Peking University, P. R. China

The absolute excitation energies of the bands presented in Fig. 1 are not known since neither inter-band connections nor connections from these bands to the ground states could be observed. This prevents us from firm spin and parity assignments using spectroscopic methods. The spin and parity given in Fig. 1 rely only on the band structure systematics in odd-odd nuclei of this mass region. According to the general classification scheme for the coupling modes of two non-identical valence nucleons [11], the three bands observed in ^{172}Re can be framed into compressed (band 1), semi-decoupled (band 2), and doubly decoupled (band 3) bands built on the $\pi h_{11/2}(9/2^-[514]) \otimes \nu i_{13/2}$, $\pi h_{9/2}(1/2^-[541]) \otimes \nu i_{13/2}$, and $\pi h_{9/2}(1/2^-[541]) \otimes \nu 1/2^-[521]$ configurations, respectively. Our configuration assignments are further supported by the analyses of alignments, in-band decay properties, and signature splittings. The signature inversion in the $\pi h_{9/2} \otimes \nu i_{13/2}$ and $\pi h_{11/2} \otimes \nu i_{13/2}$ bands has been established by the observation of signature crossing at $I \sim 18.5\ \hbar$, extending our knowledge on signature inversion to the lightest neutron deficient odd-odd rhenium isotope. These will be further discussed in a coming paper.

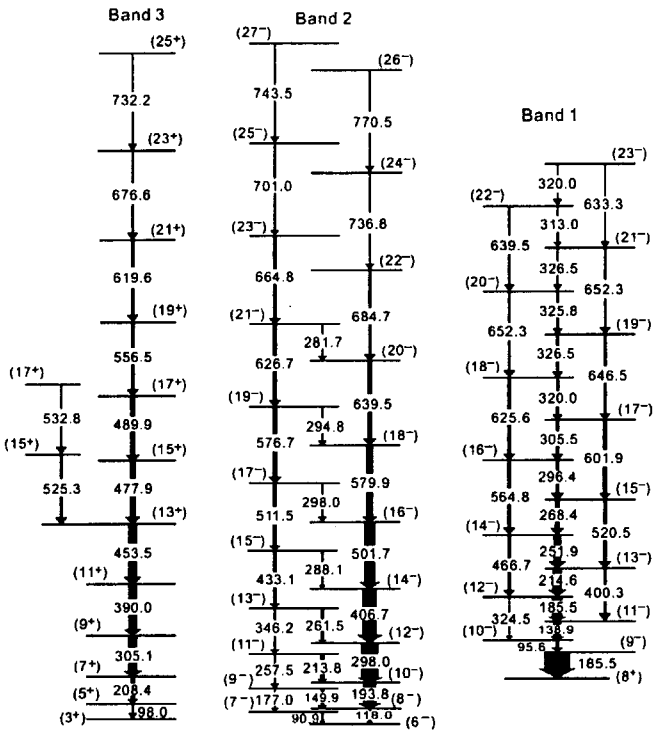

Figure 1: Partial level scheme of ^{172}Re deduced from the present work.

References

[1] Y. H. Zhang et al., Eur. Phys. J. **A 13** (2002) 429.
[2] Y. H. Zhang et al., Eur. Phys. J. **A 8** (2000) 439.
[3] Y. H. Zhang et al., Phys. Rev. C **65**, (2002) 014302.
[4] Y. H. Zhang et al., Eur. Phys. J. **A 14**, (2002) 271.
[5] K. Furuno et al., Nucl. Instrum. Methods in Phys. Res. A **421** (1999) 211.
[6] B. Singh, Nucl. Data Sheets **75** (1995) 199.
[7] R. A. Bark et al., Nucl. Phys. **A 501**, (1989) 157.
[8] J. Espino et al., Nucl. Phys. **A 567** (1994) 377.
[9] S. G. Li et al., Nucl. Phys. **A 555** (1993) 435.
[10] M. Piiparinen et al., Nucl. Phys. **A 605** (1996) 191.
[11] A. J. Kreiner et al., Phys. Rev. C **36**, (1987) 2309; Phys. Rev. C **37** (1988) 1338.

2.7 EC DECAY OF THE NEW ISOTOPE ^{241}Bk

M. ASAI, K. TSUKADA, S. ICHIKAWA, M. SAKAMA[1], H. HABA[2], Y. NAGAME, I. NISHINAKA, K. AKIYAMA, A. TOYOSHIMA, T. KANEKO, Y. OURA[3], Y. KOJIMA[4] and M. SHIBATA[5]

The decay of neutron-deficient Bk nuclei has been studied scarcely because of experimental difficulties. These nuclei predominantly decay via the electron capture (EC), and their production cross sections are around the order of microbarn. Thus, to measure γ rays following their EC decays, an isolation of the nuclei of interest from a large amount of other reaction products is indispensable. In the present work, we have identified a new neutron-deficient isotope ^{241}Bk and studied its EC decay using an on-line isotope separator (ISOL) [1].

The nucleus ^{241}Bk was produced by the ^{239}Pu(^{6}Li, $4n$) reaction at the JAERI tandem accelerator facility. A stack of twenty-one ^{239}Pu targets with an effective thickness of about 100 μg/cm^2 each was bombarded with a ^{6}Li beam of 200 pnA intensity. The beam energy was 34–42 MeV on targets. Reaction products recoiling out of the targets were stopped in He gas loaded with PbI_2 clusters, and transported into an ion source of the ISOL with a gas-jet stream. Ions accelerated with 30 kV were mass-separated with a resolution of $M/\Delta M \sim 800$, and implanted into an aluminum-coated Mylar tape in a tape transport system. The implanted source was periodically transported to a measuring position equipped with a short coaxial Ge detector (ORTEC LOAX) and a 35% n-type Ge detector (ORTEC GAMMA-X) at 400 s intervals. Gamma-ray singles and γ-γ coincidence events were recorded event by event together with time information.

Figure 1 shows a γ-ray spectrum in coincidence with Cm K X rays observed at the mass-241 fraction. Three γ lines were clearly observed in the spectrum, which are attributable to the EC decay of ^{241}Bk. Coincidence relationships among these γ rays are not clear owing to less statistics. Relative intensities of 152, 211, and 262 keV γ rays were deduced to be 6(2), 6(2), and 10(3), respectively, from the singles spectrum. The half-life of 4.6±0.4 min was derived from the decay curves of Cm $K_{\alpha 1}$, $K_{\alpha 2}$, and L_α X rays.

Alpha-decay studies of $^{243-249}$Es [2] suggested that the ground state of ^{239,241}Bk would have the $\pi 7/2^+[633]$ configuration, not the $\pi 3/2^-[521]$ one like ^{243,245}Bk. EC transitions from the $\pi 3/2^-[521]$ ground state to low-energy odd-Cm levels would have large log ft values because there are no Nilsson states whose asymptotic quantum numbers satisfy the selection rule of the allowed transition [3]. On the other hand, EC transitions from the $\pi 7/2^+[633]$ ground state can populate many positive parity states, especially the unoccupied $\nu 7/2^+[624]$ state strongly; the log ft value of the $\pi 7/2^+[633] \rightarrow \nu 7/2^+[624]$ transition is expected to be about 5.0~5.5 [1]. This small log ft value can reasonably explain the 4.6 min half-life; the partial

[1]Department of Radiologic Science and Engineering, The University of Tokushima
[2]Radioisotope Technology Division, Cyclotron Center, RIKEN
[3]Department of Chemistry, Tokyo Metropolitan University
[4]Graduate School of Engineering, Hiroshima University
[5]Facility for Nuclear Materials, Nagoya University

half-life of this transition becomes 4.4–14 min by using log ft=5.0–5.5, Q_{EC}=2400 keV [4], and the $\nu 7/2^+[624]$ energy of ~420 keV.

The observed three γ transitions are also consistent with the large population of the $\nu 7/2^+[624]$ state. In N=145 isotones, the ground state of ^{237}U and ^{239}Pu is the $\nu 1/2^+[631]$ state, and the $\nu 5/2^+[622]$ and $\nu 7/2^+[624]$ states lie in low energy as shown in Fig. 2. The ground state of ^{241}Cm is also the $\nu 1/2^+[631]$ state. If the EC decay of ^{241}Bk populates the $\nu 7/2^+[624]$ state strongly, the γ transition from the $\nu 7/2^+[624]$ state to the $\nu 5/2^+[622]$ one and the transitions from the $\nu 5/2^+[622]$ state to the $3/2^+$ and $5/2^+$ ones in the $\nu 1/2^+[631]$ band should be observed strongly like the decay patterns in ^{237}U and ^{239}Pu [3]. Taking into account the energies and intensities of the observed three γ transitions, we propose a partial decay scheme of ^{241}Bk as shown in Fig. 2.

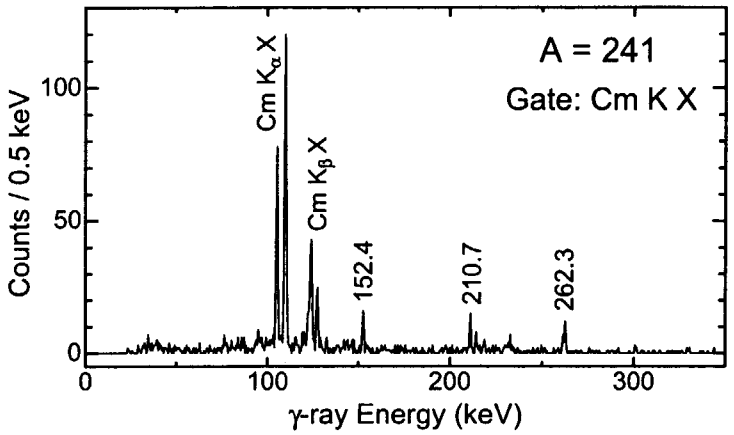

Fig. 1. Gamma-ray spectrum in coincidence with Cm K X rays observed at the mass-241 fraction.

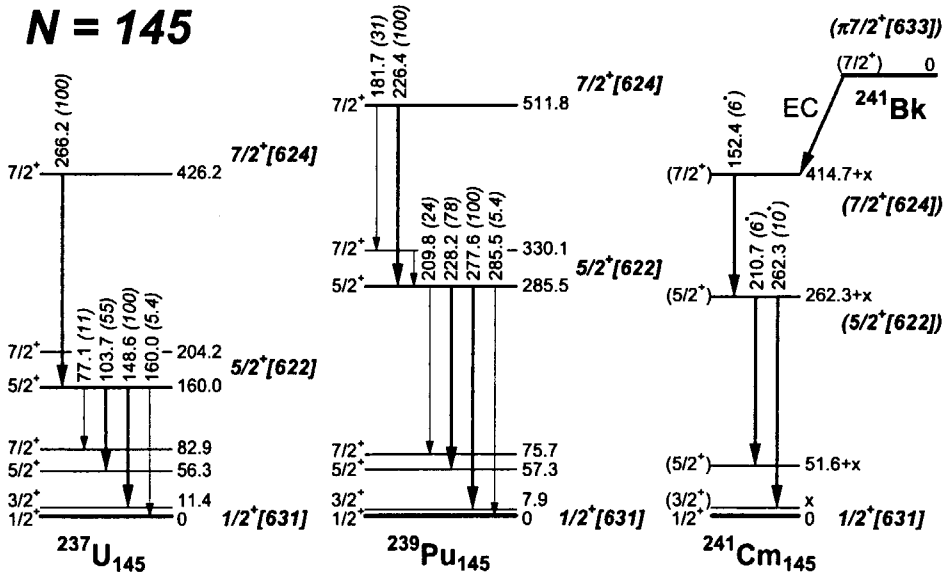

Fig. 2. The $\nu 1/2^+[631]$, $\nu 5/2^+[622]$, and $\nu 7/2^+[624]$ states in the N=145 isotones ^{237}U and ^{239}Pu, and γ transitions between these states [3]. Relative intensities of γ transitions are given in parentheses. A proposed decay scheme of ^{241}Bk is also shown.

References

[1] M. Asai, K. Tsukada, S. Ichikawa, M. Sakama, H. Haba, Y. Nagame, I. Nishinaka, K. Akiyama, A. Toyoshima, T. Kaneko, Y. Oura, Y. Kojima and M. Shibata, Eur. Phys. J. A **16** (2003) 17.

[2] Y. Hatsukawa, T. Ohtsuki, K. Sueki, H. Nakahara, I. Kohno, M. Magara, N. Shinohara, H. L. Hall, R. A. Henderson, C. M. Gannet, J. A. Leyba, R. B. Chadwick, K. E. Gregorich, D. Lee, M. J. Nurmia and D. C. Hoffman, Nucl. Phys. A **500** (1989) 90.

[3] *Table of Isotopes*, 8th ed., edited by R. B. Firestone and V. S. Shirley (John Wiley & Sons, New York, 1996).

[4] G. Audi, O. Bersilon, J. Blachot and A. H. Wapstra, Nucl. Phys. A **624** (1997) 1.

2.8 Q_β MEASUREMENTS OF NEUTRON-RICH RARE EARTH NUCLEI PRODUCED WITH PROTON INDUCED FISSION OF ^{238}U

M. SHIBATA[1], O. SUEMATSU[1], K. KAWADE[1], M. ASAI, S. ICHIKAWA, Y. NAGAME, A. OSA, K. TSUKADA, Y. KOJIMA[2] and A. TANIGUCHI[3]

Atomic masses are essential physical quantities in nuclear physics related to the stability of nuclei and nuclear structure and for nucleosynthesis in nuclear astrophysics. The theoretical prediction of half-lives strongly depends on the assumed beta-decay energies (Q_β-values). However, in the region far off the stability, both experimentally determined atomic masses and Q_β-values are scarce, and therefore the predicted half-lives disagree each other. The experimental values enable us to check the reliability of the model for the half-life prediction. The Q_β measurement is one of the precise methods for atomic mass determination. In the present experiment, we measured Q_β-values of ^{159}Pm and ^{161}Sm, which had been identified and their half-lives had been proposed by our group [1,2]. The Q_β measurement was made with a total absorption detector, which are composed of large volume twin BGO scintillators [3,4], coupled with the on-line mass separator JAERI-ISOL [5] installed at the tandem accelerator facility at the JAERI.

The nuclei of interest were produced with the ^{238}U(p,*f*) reaction by 16 MeV protons and separated by the JAERI-ISOL. The Q_βs were measured with event-by-event mode including timing information to determine the half-lives. The measuring and analyzing procedures were described in elsewhere [3,4,6].

A total absorption spectrum of ^{161}Sm measured for 30 hours are shown in Fig.1. The Q_β was deduced to be 4.92 MeV for the first time with the uncertainty of 0.10 MeV, approximately. The half-life was also deduced to be 4.3 s by a time spectrum near the end-points. The present half-life is in agreement with the previous result (4.8(8) s) derived from the decay of the Eu Kx-ray and the 263.7 keV γ-rays [1]. In ^{159}Pm, the present half-life was deduced to be 1.5 s, approximately. This value is also in agreement with the previous value of 1.47(15) s [7]. In Table 1, the deduced Q_β values for five nuclei using the JAERI-ISOL are summarized. The systematics by Audi *et al.* [8] are in agreement with the experimental values within the uncertainties.

In order to check some theoretical models, it is interesting to compare the experimental half-lives with the predicted ones. In Fig. 2, the comparison of half-life for ^{161}Sm between experimental one and theoretical ones proposed by the Gross Theory (GT) [11] and the pn-QRPA model [10] are shown. The GT predicts the half-lives better, while, pn-QRPA model predicts longer half-lives if the present Q_β-values are adopted. Similar behavior is also observed in ^{159}Pm and ^{166}Tb, and most of the theoretical models predict longer half-lives. The experimental Q_βs restrict in the prediction of the half-lives by theoretical models. They are considered to contribute to the refinements of the theoretical model in this region.

[1]Department of Energy Engineering and Science, Nagoya University
[2]Graduate School of Engineering, Hiroshima University
[3]Research Reactor Institute, Kyoto University

Using the total absorption detector, the Q_βs and also half-lives of the short-lived neutron-rich rare earth nuclei produced with the $^{238}U(p,f)$ reaction were measured at one time. In this region, the systematics by Audi *et al.* still predicts the Q_βs well and the present results propose a direction of the improvements of the nuclear models concerning atomic masses and half-lives. The measurements for other nuclei to A~170 will be continued systematically.

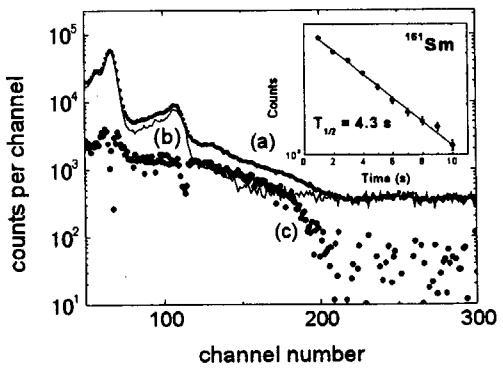

Fig.1 Measured total absorption spectrum (a), background spectrum (b), background-subtracted spectrum (c) of ^{161}Sm, and deduced half-life (inset).

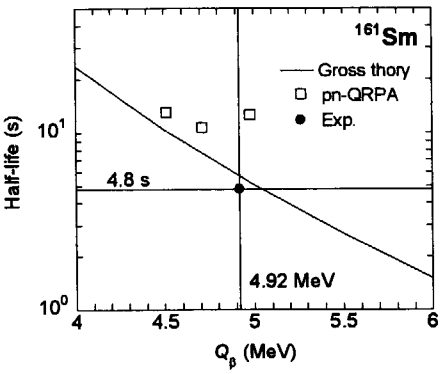

Fig.2 Comparison of experimental Q_β and half-life of ^{161}Sm with some theoretical predictions.

Table 1. Comparison of the deduced Q_βs with the systematics and theoretical ones.

Nuclei	Half-life [7] (s)	Q_β-value (MeV)				
		Present*	Systematics	Theoretical		
			Audi *et al.*[8]	KUTY[9]	FRDM[10]	FRLDM[10]
^{158}Pm	4.8(5)	6.12	6.243(408)	6.27	6.58	6.63
^{159}Pm	1.47(15)	5.66	5.524(585)	5.08	5.60	5.66
^{159}Sm	11.37(15)	3.84	3.834(298)	3.45	3.53	3.62
^{161}Sm	4.8(8)	4.92	4.797(585)	4.43	4.57	4.65
^{166}Tb	25.6(22)	4.83	4.887(298)	4.86	4.96	4.97

* Uncertainties are evaluated to be 0.10 MeV.

References

[1] S. Ichikawa *et al.*, Phys. Rev. **C58**, 1329 (1998).
[2] S. Ichikawa *et al.*, Proc. of Experimental Nuclear Physics in Europe, Sevilla, Spain, 1999, pp.103-106.
[3] M. Shibata *et al.*, Nucl. Instr. and Meth. Phys. Res. **A459**, 581 (2001).
[4] M. Shibata *et al.*, J. Phys. Soc. Jpn. **71**, 1401 (2002).
[5] S. Ichikawa *et al.*, Nucl. Instr. and Meth. Phys. Res. **A374**, 330 (1996).
[6] M. Shibata *et al.*, JAERI-Review 2002-029, p.26.
[7] M. Asai *et al.*, Proc. of 3rd Int. Conf. on Fission and Properties of Neutron-Rich Nuclei, Sanibel Island, Florida, USA.4-9, 11, 2002, to be published.
[8] G. Audi and A. H. Wapstra, Nucl. Phys. **A595**, 409 (1995).
[9] H. Koura *et al.*, RIKEN-AF-NP-394.
[10] P. Möller *et al.*, At. Data Nucl. Data Tables **59**, 185 (1995).
[11] T. Tachibana, private communication.

2.9 MEAN-SQUARE NUCLEAR CHARGE RADIUS OF ^{135}La BY LASER SPECTROSCOPY

H. IIMURA, Y. ISHIDA[1], M. KOIZUMI, N. SHINOHARA, M. OBA, M. MIYABE, T. HORIGUCHI[2] and H.A. SCHUESSLER[3]

The La isotopes (Z=57) are in a region of rapid transition from nuclei with nearly spherical shape (the singly magic ^{139}La) to nuclei that are soft towards deformation, presenting a good opportunity to test nuclear models. We have measured the hyperfine structure and the isotope shift (IS) of the 538.2-nm transition in accelerator-produced ^{135}La (19.5 h). The change in mean-square charge radius (MSCR) of this nucleus has been determined from the IS and compared with theoretical predictions.

The IS is composed of the normal mass shift (NMS), the specific mass shift (SMS) and the field shift (FS):

$$\delta\nu_{IS} = \delta\nu_{NMS} + \delta\nu_{SMS} + \delta\nu_{FS}.$$

The NMS is calculated from the masses of an electron and an ion with mass number A. Since the SMS can not be theoretically evaluated precisely, we performed a King-plot analysis to estimate the contribution of the SMS. Using the SMS thus estimated, the FS was derived from the observed IS. The FS, which is induced by the finite nuclear charge distribution, is written as $\delta\nu_{FS} = F\lambda$, where F is the electronic factor. The nuclear parameter λ gives changes in the MSCR. By dividing the FS of the isotope pair ^{139}La-^{135}La by that of a reference pair ^{139}La-^{138}La, the relative λ value was obtained. Using the value of $\lambda^{138,139}$ given by Aufmuth *et al.* [1], we obtained $\lambda^{135,139}$. The change in MSCR has been determined from the nuclear parameter λ by taking into account the contribution of the moments higher than $\langle r^2\rangle$. The result is $\delta\langle r^2\rangle^{135,139} = 0.08$ (3) fm^2. The corresponding values for the isotonic Ba and Ce nuclei are comparable with the present result. Figure 1 shows experimental $\delta\langle r^2\rangle^{139,A}$, where the value of A=135 is the present one and the others are from Ref. [1].

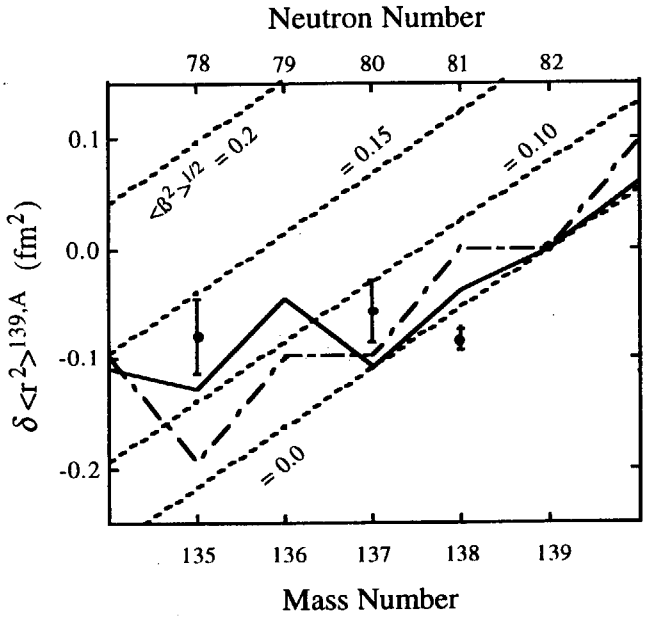

Fig. 1. Experimental changes of the MSCR $\delta\langle r^2\rangle^{139,A}$ for the La isotopes (solid circles).

For an interpretation of the result, the experimental $\delta\langle r^2\rangle^{139,A}$ values can be compared to the predictions of the droplet model. Isodeformation lines calculated by this model are indicated as dotted lines in Fig. 1, where the assumption was made that the singly magic ^{139}La has a deformation zero. It can be seen that the deformation of the odd-mass La nuclei gently increases when neutrons are removed in pairs from the magic number. Also, Fig. 1 includes the theoretical predictions by FRDM (solid line) [2] and HFBCS (dash-dotted line) [3]. The experimental value of $\delta\langle r^2\rangle^{135,139}$ is smaller than the predictions by these models.

References

[1] P. Aufmuth *et al.*, At. Data Nucl. Data Tables **37** (1987) 455 .
[2] P. Möller *et al.*, At. Data and Nucl. Data Tables **59** (1995) 185.
[3] S. Goriely *et al.*, At. Data and Nucl. Data Tables **77** (2001) 311.

[1]Institute of Physical and Chemical Research (RIKEN)
[2]Hiroshima International University
[3]Texas A&M University

3. Nuclear Reactions

This is a blank page.

3.1 EVAPORATION RESIDUE CROSS-SECTION MEASUREMENTS FOR THE REACTIONS $^{86}Kr+^{134,138}Ba$ AND $^{82}Se+^{140}Ce$

K.SATOU[1], H.IKEZOE, S.MITSUOKA, K.NISHIO, C. J. LIN and S. C. JEONG[2]

A fusion hindrance phenomenon is characteristic in fusion reactions of heavy systems where the charge product of projectile and target nuclei is greater than 1800. It means that a fusion barrier effectively becomes higher than the Bass barrier with increasing the charge product, and then reacting nuclei cannot always completely fuse though the energy of the projectile surmounts the Bass barrier. Investigating the phenomenon is important to understand the reaction mechanism between heavy ions. The main purpose of this study is to investigate the dependence of nuclear shell structure of colliding nuclei on the fusion reaction.

So far, we had measured the evaporation residue (ER) cross-sections for the reactions $^{82}Se+^{134,138}Ba$ [1] where the nucleus ^{138}Ba has a closed neutron shell N=82 while ^{134}Ba has a neutron number N=78, four neutron less than the closed shell. We showed that fusion is strongly dependent on nuclear shell structure of N=82. To investigate the dependence more detail, we measured the ER cross-sections for the reactions $^{86}Kr+^{134,138}Ba$ and $^{82}Se+^{140}Ce$, where ^{86}Kr has a closed neutron shell of N=50 and ^{140}Ce has one of N=82. The ^{86}Kr and ^{82}Se beams from the JAERI tandem booster accelerator irradiated the barium carbonate and cerium metal targets, respectively. The ERs emitted in the beam direction were separated in flight from the primary beams by the JAERI recoil mass separator. The energy and the position of incoming particles and their subsequent α-particle decays were measured event by event with the double sided position sensitive strip detector to determine the ER cross-sections. We extracted the fusion probabilities from the measured ER cross-sections. The details of the experimental procedure and the data analysis are described elsewhere [1-3].

The obtained fusion probabilities for the reactions $^{86}Kr+^{134}Ba$ and $^{86}Kr+^{138}Ba$ are shown in Fig.1. At the Bass fusion barrier energy region, the fusion probabilities for both the reaction systems are about 10^{-2}. These low fusion probabilities show clearly

[1]Department of Physics and Tandem Accelerator Center, Tsukuba University
[2]Institute of Particle and Nuclear Studies, KEK

the fusion hindrance because it should be 0.5 if the reaction system has no fusion hindrance. We fitted the obtained fusion probabilities using the procedure proposed by Quint el al. [4] to get the extra-extra push parameters (E_{xx}, σ_B), where E_{xx} is the extra-extra push energy and σ_B^2 is the variance of gaussian like fusion barrier distribution. The solid line indicates the fitted result. We obtained the extra-extra push parameters (E_{xx}, σ_B) = (16MeV, 6.4MeV) that are consistent with the value of Quint's systematics. Furthermore, in the reaction $^{86}Kr+^{138}Ba$, the fusion probability shows anomalous bump at the energy region of $E_{ex} \leqq 14$MeV.

It is concluded that fusion was hindered. At the energy region of $E_{ex} \geqq 20$MeV, the shell correction energy was damped, so the fusion probability shows no effect of shell correction energy. On the other hand, at the energy region of $E_{ex} \leqq 14$MeV, the shell effect can still remain, so that the fusion probability seems to be increased by the shell effect. As for the case of $^{82}Se+^{140}Ce$ experiment, the analysis is now proceeding.

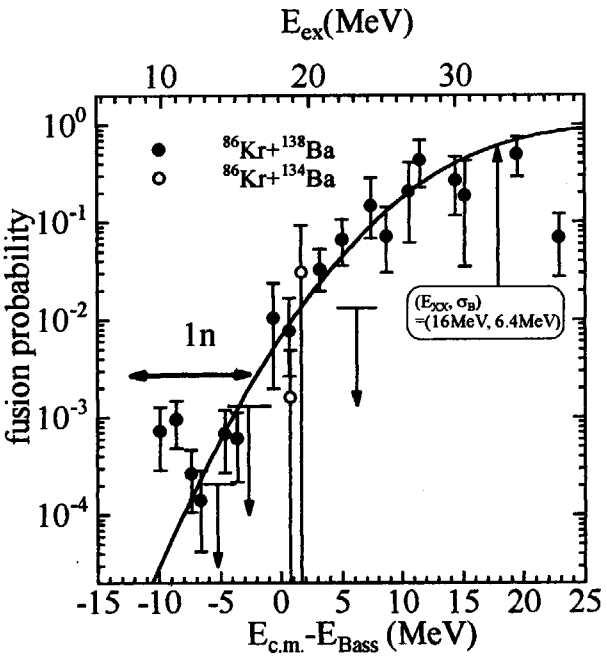

Fig.1
Fusion probability for the reaction $^{86}Kr+^{134}Ba$ and $^{86}Kr+^{138}Ba$ as a function of $E_{cm}-E_{Bass}$ (lower abscissa) and E_{ex} (upper abscissa), where E_{Bass} and E_{ex} represent the Bass fusion barrier and excitation energy, respectively. Solid arrows represent the upper limit for the reaction $^{86}Kr+^{134}Ba$.

References

[1] K. Satou, H. Ikezoe, S. Mitsuoka, K. Nishio, and S. C. Jeong, Phys. Rev. C 65 (2002) 054602.

[2] K. Nishio, H. Ikezoe, S. Mitsuoka, and J. Lu, Phys. Rev. C 62 (2000) 014602.

[3] S. Mitsuoka, H. Ikezoe, K. Nishio, and J. Lu, Phys. Rev. C 62 (2000) 054603.

[4] A. B. Quint, W. Reisdorf, K.-H. Schmidt, P. Armbruster, F. P. Hessberger, S. Hofmann, J. Keller, G. Münzenberg, H. Stelzer, H.-G. Clerc, W. Morawek, and C.-C. Sahm, Z. Phys. A 346 (1993) 119.

3.2 SUB-BARRIER FUSION OF ^{64}Ni+^{198}Pt AND ^{82}Se+^{176}Yb

S. MITSUOKA, H. IKEZOE, K. NISHIO, K. SATOU and C.J. LIN

We have investigated the mechanism of sub-barrier fusion between heavy projectiles and well deformed targets, in order to experimentally study the hugging fusion which were theoretically proposed as a new approach to the superheavy-element production. Our previous studies in the production of Th-U region [1-4] supported the original idea of hugging fusion that the compact touching configuration in the side collision is more favorable for complete fusion than the elongated configuration in the tip collision. In the next step to superheavy region, we studied the ^{82}Se+^{176}Yb and ^{64}Ni+^{198}Pt reactions to produce superheavies of ^{258}Rf (Z=104) and ^{262}Sg (Z=106), respectively.

Beams of ^{82}Se and ^{64}Ni from the JAERI tandem-booster accelerator were used to bombard well deformed targets of ^{176}Yb (oxide, 400μg/cm^2, 97.6% enriched) and ^{198}Pt (metal, 400μg/cm^2, 95.7% enriched), respectively, which were prepared by sputtering onto 1.1μm thick Al foil mounted on a rotating wheel. The beam energy was selected for the maximum cross section in 2 or 3 neutron-evaporation channel. The evaporation residues emitted from the target to the beam direction were separated in flight by the JAERI-RMS and implanted into a two-dimensional position sensitive SSD. The escaping α-particles and spontaneous fission fragments were detected by a side SSD box which totally covered 70% of 2π.

No evaporation residue was observed in the both reactions. The upper limits of the cross sections in the ^{82}Se+^{176}Yb reaction were 230pb and 40pb for 2n and 3n channels, respectively, and 160pb for 2n channel in ^{64}Ni+^{198}Pt. These values are smaller than the reported cross sections in the cold fusion reactions of ^{50}Ti+^{208}Pb and ^{54}Cr+^{208}Pb, which produced the same compound nuclei of ^{258}Rf and ^{262}Sg with in the present reactions of ^{82}Se+^{176}Yb and ^{64}Ni+^{198}Pt, respectively. This suggests the effect of nuclear deformation on the fusion enhancement would be smaller than the nuclear shell effect.

References

[1] S. Mitsuoka et al., Phys. Rev. C **62** (2000) 054603.
[2] K. Nishio et al., Phys. Rev. C **62** (2000) 014602.
[3] K. Nishio et al., Phys. Rev. C **63** (2001) 044610.
[4] S. Mitsuoka et al., Phys. Rev. C **65** (2002) 054608.

3.3 DIRECT MEASUREMENTS OF THE ASTROPHYSICAL REACTION RATES OF LIGHT NEUTRON-RICH NUCLEI

H. MIYATAKE[1], S.K. DAS[2], P.K. DAS[2], Y. FUCHI[1], T. FUKUDA[2], T. FURUKAWA[3], T. HASHIMOTO[4], S. ICHIKAWA, H. IKEZOE, T. ISHIKAWA[4], H. ISHIYAMA[1], H. IZUMI[3], S.C. JEONG[1], I. KATAYAMA[1], H. KAWAKAMI[1], T. KAWAMURA[4], M. MATSUDA, S. MITSUOKA, Y. MIZOI[5], K. NAKAI[4], K. NISHIO, T. NOMURA[1], T. SHIMODA[3], M. H. TANAKA[1], M. TERASAWA[6], Y. WATANABE[1], H. YANO[3] and N. YOSHIKAWA[1]

The (α, n) and (p, n) reactions of light neutron-rich radioactive nuclei play an important role in the heavy-element synthesis scenario such as the element synthesis in the hot bubble of the supernova explosion[1]. A systematic study for these astrophysical reaction rates with using low energy radioactive nuclear beams (RNB's) has been started at Tandem facility in Japan Atomic Energy Research Institute (JAERI)[2,3]. In this year, direct measurements of ^{8}Li(α, n)^{11}B and ^{16}N(p, n)^{16}O reaction cross sections have been performed successfully.

For the production of ^{8}Li- and ^{16}N-RNB, we utilized the transfer reaction of ^{7}Li and ^{18}O beam, respectively. The produced RNB was separated from the primary beam with the JAERI recoil mass separator. The typical intensities and purities of these RNB's are 5.0 kpps and 99%, and 4.7 kpps and 98.5%, respectively. For the exclusive measurement of the reaction cross section to each final state, a detector system consists of a Multi-Sampling and Tracking Proportional Chamber (MSTPC: Fig. 1)[4]

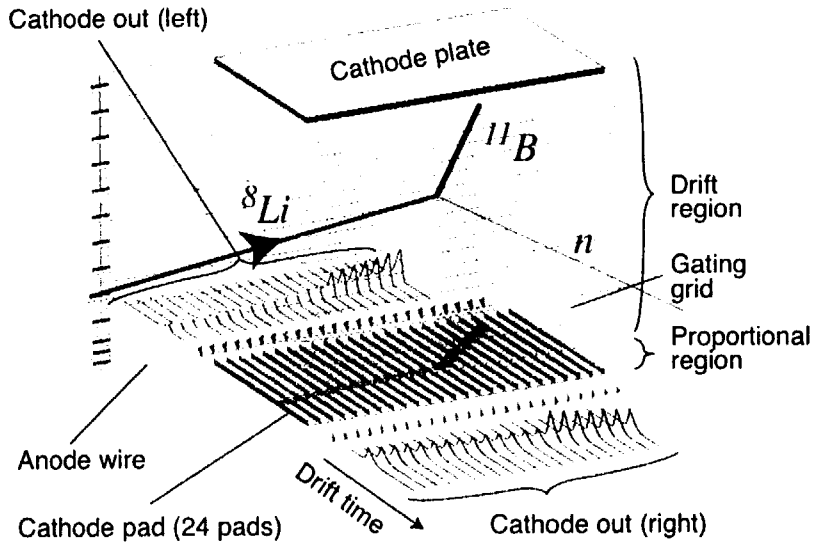

Fig.1 A schematic drawing of the MSTPC. The MSTPC consists of the drift and the proportional regions. The proportional region has 24 position sensitive proportional counters. The gating grid is placed between these two regions and controls the drifting electrons towards the proportional counters according to an external trigger signal.

1 Institute of Particle and Nuclear Studies, KEK
2 Osaka Electro-Communication University
3 Osaka University
4 Tokyo University of Sciences
5 RIKEN
6 University of Tokyo

and a large solid angle neutron detector array. The MSTPC, filled with He + CO_2(10%) or CH_4 gas, detects three-dimensional tracks of multiple charged particles and the energy losses along their trajectories. We can obtain the excitation function in a broad energy range with high detection efficiency. The gating grid system[5,6] was newly introduced to suppress the deterioration of the pulse heights from the MSTPC under the high injection rate of RNB.

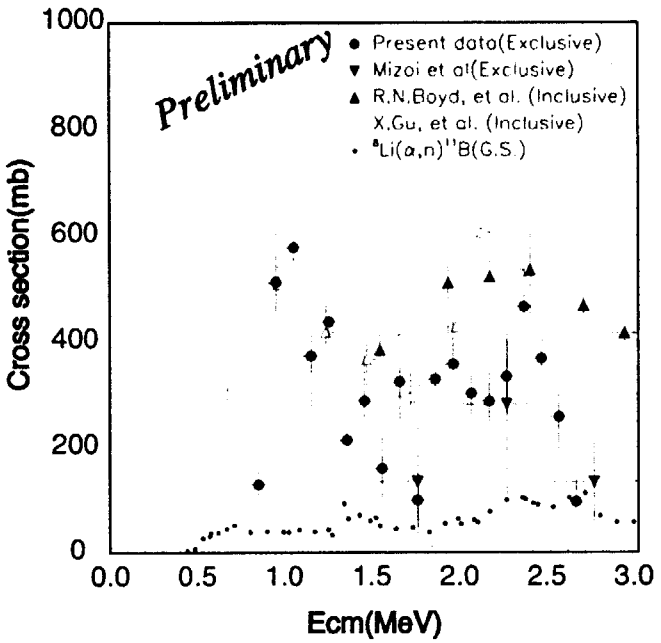

Fig. 2 The excitation fuction of the ^{8}Li(α, n) reaction.
The large black dot shows our experimental result and the black and white triangles correpond to the previous inclusive measurements. The small black dot was obtained from the inverse reaction. The black reverse triangle shows the previous exclusive measurement with the similar setup to ours.

The analyses are in progress. Figure 2 shows the preliminary result of the ^{8}Li(α, n) reaction cross section, indicated by large black dotts, in the energy region from 0.8 MeV to 2.7 MeV together with the previous data. There are some resonant like structures, although the obtained excitation function was constructed by only one seventh of the total events. Moreover there is a large discrepancy between our data and the previous one[7] in the higher energy region above 2 MeV. We will decompose the excitation function in terms of the corresponding Γ_α and Γ_n for each reaction channel at the further analysis. We will discuss again above characteristics in the preliminary result.

The most interesting energy region locates around the Gamow peak (~0.5 MeV) at the high temperature astrophysical circumstance. The expected cross section is about 100 mb. In the next experiment, we will measure it with a rather intense ^{8}Li-RNB to keep the similar level of the statistical error (~10%).

References

[1] M. Terasawa et al., Astrophy. J. **562** (2001) 470.
[2] H. Ishiyama et al., Nucl. Phys. **A718c** (2003) 481.
[3] T. Ishikawa et al., Nucl. Phys. **A718c** (2003) 484.
[4] Y. Mizoi et al., Nucl. Instrum. Method **A431** (1999) 112.
[5] P. Némethy et al., Nucl. Instrum. Method **212** (1983) 273.
[6] T. Kawamura, Master thesis, Tokyo University of Science (2003).
[7] R.N. Boyd et al., Phys. Rev. Lett. **B68** (1992) 1283.

3.4 HALF-LIFE OF ^{228}Pu AND α-DECAY OF ^{228}Np

K. NISHIO, H. IKEZOE, S. MITSUOKA, K. SATOU, C.J. LIN

The neutron deficient plutonium isotope ^{228}Pu was produced in the reaction ^{24}Mg+^{208}Pb [1], and the α-particle energy was reported to be 7810 keV. For the life-time, they did not report it. We have produced ^{228}Pu in the reaction of ^{34}S+^{198}Pt and the half-life was determined. In this reaction, we also produced ^{228}Np and its α-decay was firstly observed. The production cross sections for ^{228}Pu, ^{228}Np and ^{225}U were compared to a statistical model calculation.

The ^{34}S ions accelerated to $E_{\rm beam}$=170 and 172 MeV by the JAERI-tandem accelerator irradiated the ^{198}Pt target. The typical beam current was 40−50 pnA. The target with thickness 390μg/cm^2 was made by sputtering an enriched ^{198}Pt material (98%) on a 1.2μm thick aluminum foil. The beam energy corresponds to the center-of-mass energy ($E_{\rm c.m.}$) of 141 and 143 MeV, respectively, at the half-depth in the target layer. The evaporation residues emitted to the beam direction were separated in flight from the primary beams and other reaction products by the JAERI-RMS [2]. The ERs were then implanted into a silicon detector (73 × 55 mm^2, resolution=75 keV in FWHM) having two-dimensional position sensitivity. The identification of the nucleus is made by constructing an α-decay chain and observing the known α-particle energies (and also life-times) of descendants whose decay position agrees with that of the recoil implantation.

We observed two decay chains starting from ^{228}Pu as shown in Table.1. The first line is the kinetic energy (keV) and half-life cited from the literature. The detected life-time is shown in parenthesis where the symbol '<' means that the corresponding time interval is measured from the preceding α decay. The signal of pile up, '*pileup*', is caused by the α decays of itself and its daughter indicated by '←—'. The half-life of ^{228}Pu was determined to be $1.1^{+2.0}_{-0.5}$ s. The present results on the half-life and α-decay Q-value (Q_α=7948±36 keV) is plotted in Fig.1 together with the other data [3]. In this figure, the Geiger-Nuttall curves for elements Th, U, and Pu are drawn by referring the expression and constants in [4]. Our result of ^{228}Pu follows the systematics of the Pu isotopes. This means that the decay of ^{228}Pu is dominated by the α decay. The dominant α decay is supported by the theoretical calculation that the partial half-life for α decay ($T_{\alpha,1/2}$) 0.42 s [5] is two orders of magnitude shorter than that for EC-decay $T_{\rm EC,1/2}$ =44 s [6].

At the bombarding energy of $E_{\rm c.m.}$ =143 MeV, we observed five α-decay chains starting from ^{228}Np. The average E_α value of ^{228}Np was 7123 keV. The obtained half-life 56^{+45}_{-17} s agrees with 61.4 s [7].

Figure 2 shows the production cross sections determined in this experiment. The data are compared with the statistical model calculation. In the calculation, the partial wave cross section for the fusion ^{34}S+^{198}Pt was calculated by using the CCDEF code [8], which was then inputted to the HIVAP code [9] to calculate the surviving probability and the ER cross section of the specific channel. The calculation reproduces the experimental data.

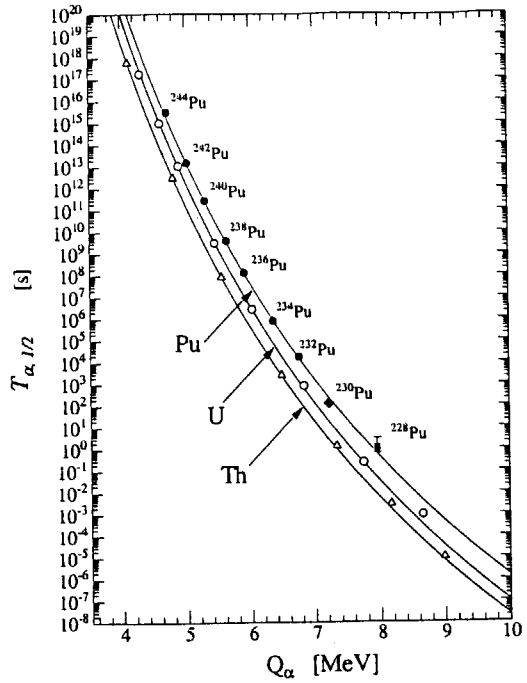

Fig.1. The present results on α-decay Q-value and half-life for ^{228}Pu (solid square with error bar) is plotted on the map of $T_{\alpha,1/2}$ versus Q_α together with the other nuclei (solid circle=Pu, open circle=U, open triangle=Th [3]). The $T_{\alpha,1/2}$-value for ^{230}Pu [10] is shown by the solid diamond. Geiger-Nuttall curve for even-even Pu, U, and Th isotopes [4] are shown by the solid curves.

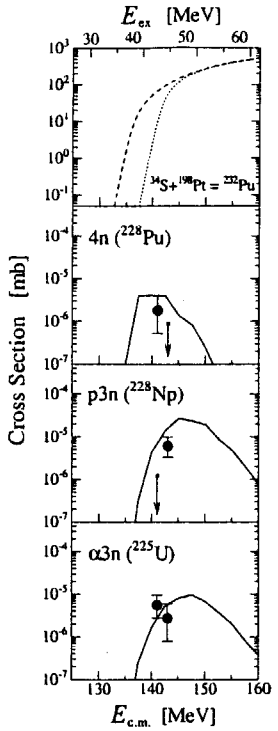

Fig.2. Evaporation residue cross sections for ^{228}Pu, ^{228}Np, and ^{225}U are shown together with the HIVAP calculation (solid curve). The vertical bar with arrow shows the upper limit of the cross section. The fusion cross section by the CCDEF code is shown by the dashed-curve and the fusion cross section of the one-dimensional barrier penetration model is shown by the dotted-curve.

Table 1 Alpha-decay character starting from the ^{228}Pu implantation.

^{228}Pu	^{224}U	^{220}Th	^{216}Ra	^{212}Rn
7810 [1]	8466 [0.9ms][3]	8790 [9.7μs][3]	9349 [0.18μs][3]	6264 [23.9min][3]
7807 (0.35s)	–	10817_{pileup} (<0.77ms)	⟵	6309 (34min)
7736 (2.76s)	8446 (3.2ms)	–	–	2960_{escape} (11min)

REFERENCES

[1] A.N. Andreyev, D.D. Bogdanov, V.I. Chepigin, A.P. Kabachenko, O.N. Malyshev, A.G. Popeko, R.N. Sagaidak, G.M. Ter-Akopian, M. Veselsky, and A.V. Yermin, Z. Phys. A **347** (1994) 225.

[2] H. Ikezoe, Y. Nagame, T. Ikuta, S. Hamada, I. Nishinaka and T. Ohtsuki, Nucl. Instrum. Meth. A **376** (1996) 420.

[3] R.B. Firestone, Table of Isotopes, edited by V.S. Shirley (Wiley, New York, 1996).

[4] J.O. Rasmussen, 'Alpha, Beta, and Gamma-ray spectroscopy', Vol.1, North-Holland, Amsterdam (1966) p. 701.

[5] H. Koura, J. Nucl. and Radiochem. Sci. **3** (2002) 201.

[6] T. Tachibana, M. Yamada, Proc. Inc. Conf. on exiotic nuclei and atomic masses, Arles, 1995 (Editions Frontueres, Gif-sur-Yvette, 1995) p. 763.

[7] S.A. Kreek, H.L. Hall, K.E. Gregorich, R.A. Henderson, J.D. Leyba, K.R. Czerwinski, B. Kadkhodayan, M.P. Neu, C.D. Kacher, T.M. Hamilton, M.R. Lane, E.R. Sylwester, A. Türler, D.M. Lee, M.J. Nurmia, and D.C. Hoffman, Phys. Rev. C **50** (1994) 2288.

[8] J.O. Fernández Niello, C.H. Dasso and S. Landowne, Comput. Phys. Commun. **54** (1989) 409.

[9] W. Reisdorf and M. Schädel, Z. Phys. A **343** (1992) 47.

[10] P. Cagarda, S. Antalic, D. Ackermann, F.P. Heβberger, S. Hofmann, B. Kindler, J. Kojouharova, B. Lommel, R. Mann, A.G. Popeko, Š. Šaro, J. Unsitalo, A.V. Yeremin, GSI Scientific Report 2001 (2002).

3.5 A FOCAL PLANE DETECTOR INSTALLED IN MAGNET SPECTROGRAPH *ENMA*

K. NISHIO, S.C. JEONG[1], C.J. LIN, S. MITSUOKA, K. SATOU, M. SAKAMA[2], H. IKEZOE

A one-dimensional position sensitive proportional counter was made and installed at the focal plane of the magnet spectrograph (ENMA) [1] in order to determine energy of protons associated with the (d,p) reaction. Special interest is to populate the excited state of the actinide nucleus in this reaction and to investigate the fission properties at sub-threshold energy region. In this energy region, the fission cross section in the (d,p) reaction shows fine structures as a result of resonance tunneling, whose structure reflect the shape of the double-humped fission barrier. Recent topics include search for the hyper-deformation (HD) minimum of the actinide nucleus [2]. In the HD-state, a calculation implies that the system forms a ^{132}Sn-like cluster [3] in the dumbbell shape, which should appear in the post scission quantities such as mass and total kinetic energy distribution.

The active length of the proportional counter is 900 mm to cover the momentum acceptance of 5%, and the position is determined by a conventional charge-division method. The detector consists of single anode wires and two cathode (ground) planes with the wire-cathode distance of 3.2 mm. The anode is made of the Ni-Cr wire of 15 μm-diameter (61 Ω/mm), and the cathode is made of the Al-coated Mylar film (2 μm). The Ar(95%) + CO_2(5%) mixed gas was filled with 700 Torr, and the voltage supplied to the anode was 1150 V. The position resolution was determined to be 0.7 mm (FWHM) by exposing the detector to the α-particles of ^{241}Am source. The active height of the detector was $\pm$10mm around the wire level, large enough to cover the vertical aberration. The sum of pulse heights from both ends is nearly proportional to the energy deposition ΔE, so that we can separate proton from deuteron with the help of an additional E-detector such as a plastic scintillator.

The detector was installed at the focal plane of ENMA and the elastically scattered protons from the ^{208}Pb-target was analyzed at 90°. At the proton beam energy of 12.5MeV, we obtained energy resolution of 8－9 keV (FWHM) at the solid angle of 6.2 msr and 9－10 keV at 13.7 msr.

REFERENCES

[1] Y. Sugiyama, N. Shikazono, H. Ikezoe, H. Ikegami, Nucl. Instrum. Meth. **169** (1980) 77.

[2] A. Krasznahorkay*et al.*, Phys. Rev. Lett. **80** (1998) 2073.

[3] S. Cwiok *et al.*, Phys. Lett. B **322** (1994) 304.

[1]Institute of Particle and Nuclear Studies, KEK
[2]Department of Radiologic Science and Engineering, School of Health Science, University of Tokushima

3.6 EXCITATION ENERGY DEPENDENCE OF ASYMMETRIC FISSION MODE IN PROTON-INDUCED FISSION OF URANIUM ISOTOPES

I. NISHINAKA, M. TANIKAWA[1], S. GOTO[2],
K. NISHIO, M. ASAI, K. TSUKADA, Y. NAGAME and H. KUDO[2]

How are shell effects responsible for mass division in fission at moderate excitation energy? Recently the excitation energy dependence of mass and E_k distributions has been studied in the 10 – 13 MeV proton-induced fission of ^{232}Th [1], where excitation energies of the compound nucleus ^{233}Pa are 15.2 – 18.2 MeV. It was found that, even in the asymmetric fission mode, the yields at A $\sim$ 140 with the deformed shell of N = 86 – 88 break down compared with those at A $\sim$ 132 with the spherical shell of Z = 50 and N = 82. Observed excitation energy dependence shows the opposite trend for thermal neutron fission and cold fission of ^{230}Th [2]. In view of fragment shell effects, observed excitation energy dependence at moderate excitation energy is anomalous and the reason is not known now. Similar excitation energy dependence of mass yields was also observed in the photofission of ^{232}Th [3]. The fissioning nuclei of ^{233}Pa [1] and ^{232}Th [3] have the same neutron number N = 142. Therefore, in view of nuclear structure of fissioning systems, we study how the asymmetric fission mode changes with excitation energy in the 10 – 13 MeV proton-induced fission of ^{233}U and ^{238}U, where the compound nuclei are ^{234}Np (N = 141) and ^{239}Np (N = 146), respectively.

Thin targets of ^{233}U and ^{238}U were irradiated with protons of energies 10, 11.5 and 13 MeV. Excitation energies of the compound nucleus are 14.2 – 17.2 MeV for ^{234}Np and 15.2 – 18.2 MeV for ^{239}Np. Velocities of fission fragment pairs were measured coincidentally by a double time-of-flight detection system with flight paths of 958 and 1104 mm. The number of events for each target and bombading energy was accumlated in the range of 9.5×10^4 – 1.5×10^5. Primary mass and E_k were derived from observed velocities, applying mass and momentum conservation and assuming isotropic neutron emission from fragments.

Figure 1 shows mass yields and the average E_k as a function of light fragment mass. Corresponding heavy fragment mass is shown in the scale on the top. Data are shown by open circles for 10 MeV and solid circles for 13 MeV. The yields for 10 MeV are normalized to the 200 % yields for 13 MeV in the light fragment mass range of A < 95, where the asymmeric fission mode is considered to be independent of excitation energy because no change in the shape of the mass yield curve and in the average E_k occures with excitation energy. Data for 11.5 MeV are not shown but located between those for 10 MeV and 13 MeV. Yields for symmetric mass division increase with incident beam energy, as well observed in the proton-induced fission of uranium isotopes [4,5,6]. The differences of mass

[1]School of Science, The University of Tokyo
[2]Faculty of Science, Niigata University

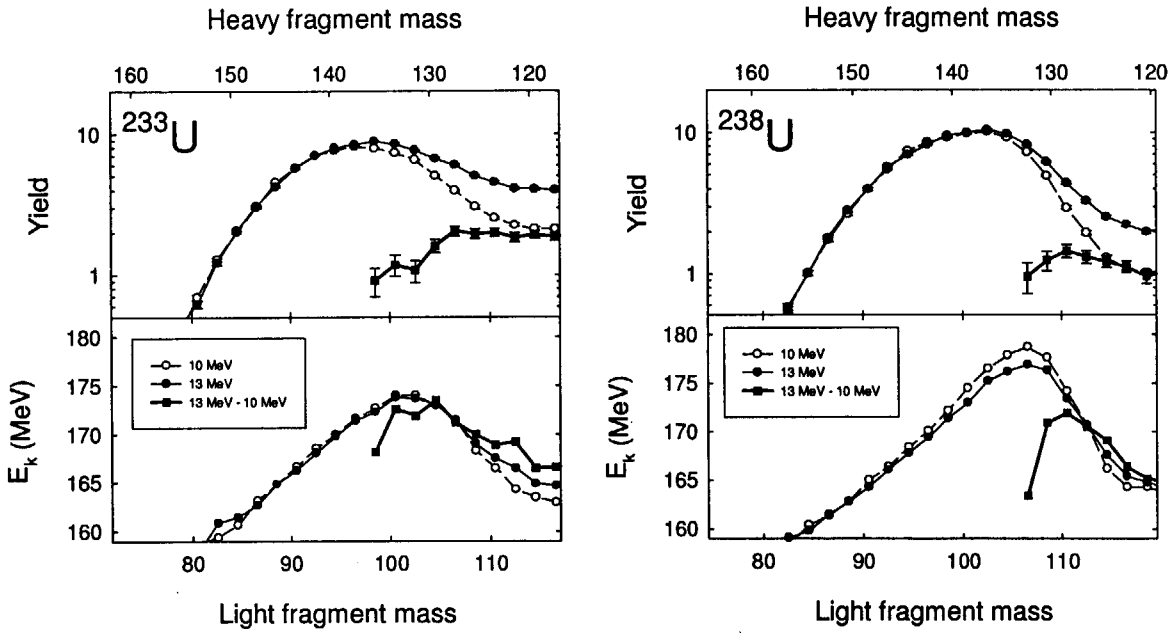

Fig. 1: Mass yields and average E_k as a function of fragment mass in the proton induced fission of ^{233}U and ^{238}U. The differences of mass yields between 13 MeV (solid circles) and 10 MeV (open circles) and the corresponding average E_k are shown by solid squares.

yields between 13 MeV (solid circles) and 10 MeV (open circles), and the corresponding average E_k were derived and are shown by solid squares in Fig. 1. For both targets the differences of mass yields show almost constant values in the heavy fragment mass region A < 130. The corresponding average E_k increases with mass asymmetry. If the symmetric fission mode is assumed to show liquid drop characteristics, that is, the Gaussian-shaped mass yield curve as well as parabolic mass dependence of the average E_k, the asymmetric fission mode with high E_k is found to contribute to the observed increments in the yield at A $\sim$ 130.

For the asymmetic fission mode, increments in the yield at A $\sim$ 130 with excitation energy were observed in the proton-induced fission of uranium isotopes ^{233}U and ^{238}U, as well as ^{232}Th [1]. It was found that observed excitation energy dependence was not related to the shell structures of fissioning nuclei. Observed excitation energy dependence shows a common feature of the asymmetric fission mode of light actinides at moderate excitation energies and the opposite trend for fission at lower excitation energies.

References

[1] I. Nishinaka et al., JAERI-Review **2002-029** (2002) p.38.

[2] P. Armbruster, Rep. Prog. Phys. **62** (1999) 465.

[3] M. Piessens et al., Nucl. Phys. **A556** (1993) 88.

[4] S. Baba, H. Umezawa and H. Baba, Nucl. Phys. **A175** (1971) 177.

[5] R. L. Ferguson et al., Phys. Rev. C **7** (1973) 2510.

[6] T. Ohtsuki et al., Phys. Rev. C **44** (1991) 1405.

This is a blank page.

4. Nuclear Chemistry

This is a blank page.

4.1 SEARCH FOR α-EMITTER ^{239}Cm BY MEANS OF GAS-JET COUPLED ISOL

N. SHINOHARA, M. ASAI, Y. HATSUKAWA, K. TSUKADA, A. OSA,
M. OSHIMA, H. HABA, S. ICHIKAWA, Y. NAGAME, YU. N. NOVIKOV[1],
A. V. POPOV[1], D. M. SELIVERSTOV[1], G. MÜNZENBERG[2]
and H. WOLLNIK[3]

In order to evaluate the masses of Super Heavy Elements, Q_α values of the "missing" α-emitters have to be experimentally determined. We started this program by searching for one of the "missing" α-emitters: ^{239}Cm. From the Q_α value of ^{239}Cm, the mass values of the nuclides starting from the ^{267}110 nuclide can be evaluated in principle [1]. In the previous work, we have measured the decay characteristics of the ^{239}Cm nuclide produced by the ^{232}Th(^{12}C,5n)^{239}Cm reaction. The decay data of ^{239}Cm and the masses of the α-decay nuclides starting from ^{259}Sg which is the α-decay grand-daughter of ^{267}110 have been evaluated. The detailed results will be reported in a separate paper [2].

In this study, the ^{237}Np(^{6}Li,4n) reaction was used for producing the ^{239}Cm nuclide at the JAERI tandem accelerator facility to obtain the more detailed information on the ^{239}Cm decay by means of an on-line isotope separator (ISOL). Reaction products recoiling out of the targets were stopped in He gas loaded with PbI_2 clusters, and transported into an ion source of the ISOL with a gas-jet stream. Atoms ionized in the surface ionization-type thermal ion source were accelerated and mass-separated. The separated ions were implanted into a Si PIN-photodiode detector and α measurements were carried out. X- and γ-ray measurements were also performed for the mass-separated nuclides.

Figure 1 shows an α spectrum measured with the Si PIN-photodiode detector for the mass-239 fraction separated by the gas-jet coupled ISOL. Alpha particles associated with the decay of ^{239}Am are clearly observed in the figure. In the X-ray measurements, Pu K_α X-ray from ^{239}Am was also observed strongly in the mass-239 fraction, and no X ray from ^{239}Cm was detected. The measured intensity of the X ray due to ^{239}Am was more than one hundred times larger than that of ^{239}Cm estimated from the measured X-ray spectrum. On the other hand, α branching

---

[1] Petersburg Nuclear Physics Institute, Gatchina, 188300, Russia
[2] Gesellschaft für Schwerionenforschung, 64291 Darmstadt, Germany
[3] Giessen University, 35392 Giessen, Germany

values of the ^{239}Cm and ^{239}Am decays are 0.006% [2] and 0.01% [3], respectively, and the total number of α particles from ^{239}Am given in Fig. 1 is 151 counts. Because the total number of α particles coming from ^{239}Cm is estimated to be less than unity by considering these experimental values, three α particles near the energy 6500 keV seen in Fig. 1 may be due to the α decay of ^{239}Cm even in its poor statistics. In other words, such an extremely-small α branching value (0.006%) of ^{239}Cm previously measured can be confirmed by this fact. Detailed analysis of the very weak α-emission from ^{239}Cm is now in progress.

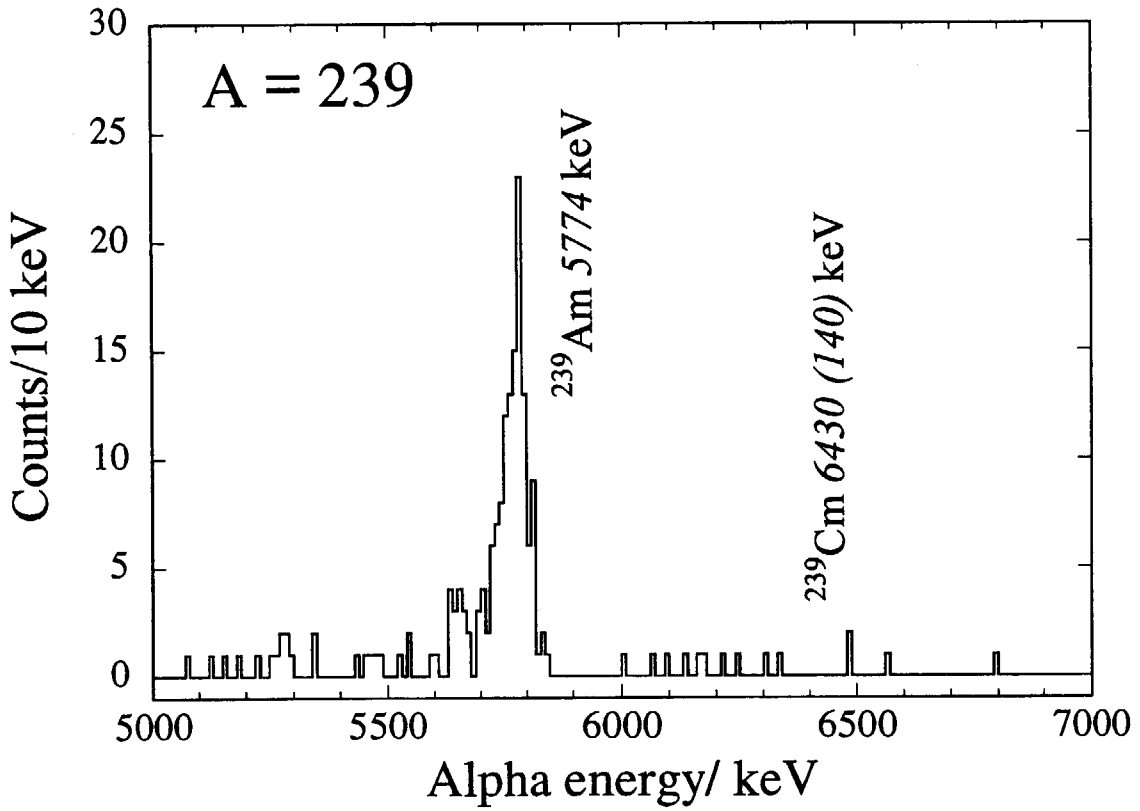

Fig. 1. Alpha spectrum of the mass-239 fraction separated by the gas-jet coupled ISOL. The α energy (6.43 MeV) from ^{239}Cm has been measured chemically in the previous work [2].

References

[1] N. Shinohara *et al.*, JAERI-Review 2002-029 (2002) 45.

[2] N. Shinohara *et al.*, to be published (2003).

[3] R.B. Firestone, Table of Isotopes, Eighth edition, vol. II (John Wiley and Sons, Inc, 1999).

4.2 ANION-EXCHANGE BEHAVIOR OF Rf IN HF SOLUTION

H. HABA,[1] K. TSUKADA, M. ASAI, A. TOYOSHIMA,[2] K. AKIYAMA, I. NISHINAKA, M. HIRATA, S. ICHIKAWA, Y. NAGAME, K. YASUDA, Y. MIYAMOTO, T. KANEKO, S. GOTO,[3] S. ONO,[3] T. HIRAI,[3] H. KUDO,[3] M. SHIGEKAWA,[2] A. SHINOHARA,[2] Y. OURA,[4] H. NAKAHARA,[4] K. SUEKI,[5] H. KIKUNAGA,[6] N. KINOSHITA,[6] N. TSURUGA,[6] A. YOKOYAMA,[6] M. SAKAMA,[7] M. SCHÄDEL [8] and J. V. KRATZ[9]

Increasingly strong relativistic effects on the valence electrons of transactinide elements can induce deviations in chemical properties from periodicities based on lighter homologues in the periodic table [1]. The first transactinide element, rutherfordium (Rf), is expected to be a group-4 member with a ground state electronic configuration of $[Rn]5f^{14}6d^{2}7s^{2}$, though the relativistic calculations have predicted the conflicting configurations such as $7s^{2}7p^{2}$ and $6d7s^{2}7p$ [1]. The nuclide ^{261}Rf which has a half-life of 78 s is commonly used for chemical studies of Rf. The production yield of ^{261}Rf is the order of one atom per minute, which forces us to perform rapid and repetitive chromatographic experiments with single atoms. Previously, we investigated anion-exchange behavior of Rf together with the group-4 elements Zr and Hf in 4.0–11.5 M HCl and 8.0 M HNO_3 solutions [2]. It was found that the adsorption trends of Rf in HCl and HNO_3 are very similar to those of Zr and Hf, indicating that Rf is typically the member of the group-4 elements. Reported in this paper is our recent result of the successive anion-exchange study of Rf in HF solutions. The fluoride complexing strength of Rf deduced from 2784-times anion-exchange experiments at 3.9–13.9 M was compared with those of Zr and Hf and also with the latest relativistic molecular density-functional calculation [3].

The isotope ^{261}Rf was produced in the ^{248}Cm(^{18}O,5*n*) reaction using the 94-MeV ^{18}O beam delivered from the JAERI tandem accelerator. The ^{248}Cm target of 610 μg cm^{-2} thickness was prepared by electrodeposition onto a 2.4 mg cm^{-2} thick Be foil. This target contained Gd of 36 μg cm^{-2} thickness to simultaneously produce ^{169}Hf and to monitor the behavior of Hf in the identical experimental condition with ^{261}Rf. The beam intensity was about 0.3 particle μA. The reaction products recoiling out of the target were transported by the He/KCl gas-jet system to the **A**utomated **I**on-exchange separation apparatus coupled with the **D**etection system for **A**lpha spectroscopy (**AIDA**) [2]. ^{261}Rf and ^{169}Hf deposited on the collection site of AIDA were dissolved with 240 μL of 13.9, 11.6, 7.7, 5.8, 4.8, and 3.9 M HF and fed into an anion-exchange column (MCI GEL CA08Y, 1.6 mm i.d.×7.0 mm) at a flow rate of 0.74 mL min^{-1}. The effluent was collected on a Ta dish as Fraction 1 and evaporated to dryness with hot He gas and a halogen heat lamp. The remaining Rf and Hf in the column were eluted with 210 μL of 4.0 M HCl. This effluent was collected on another Ta dish and evaporated to dryness as Fraction 2. Each pair of Ta dishes, Fractions 1 and 2, were automatically transferred to the α spectrometry station equipped with eight 600 mm^2 PIPS detectors. In order to investigate the behavior of Zr

[1] Cyclotron Center, RIKEN
[2] Department of Chemistry, Graduate School of Science, Osaka University
[3] Department of Chemistry, Faculty of Science, Niigata University
[4] Department of Chemistry, Graduate School of Science, Tokyo Metropolitan University
[5] Department of Chemistry, Tsukuba University
[6] Department of Chemistry, Faculty of Science, Kanazawa University
[7] Department of Radiologic Science and Engineering, School of Health Sciences, University of Tokushima
[8] Gesellschaft für Schwerionenforschung
[9] Institut für Kernchemie, Universität Mainz

and Hf, ^{85}Zr and ^{169}Hf were simultaneously produced by the ^{nat}Ge(^{18}O,*xn*) and ^{nat}Gd(^{18}O,*xn*) reactions, respectively. The anion-exchange experiments with ^{85}Zr and ^{169}Hf were performed at 7.7–17.4 M under the same experimental conditions as those with ^{261}Rf. The effluents collected in polyethylene tubes were assayed by γ-ray spectrometry with Ge detectors.

From ion-exchange experiments performed 849, 631, 322, 532, 179, and 271 times for the 13.9, 11.6, 7.7, 5.8, 4.8, and 3.9 M HF, respectively, a total of 183 α events from 78-s ^{261}Rf (8.28 MeV) and its daughter 25-s ^{257}No (8.22, 8.27, 8.32 MeV) were registered in the energy range of 8.00–8.36 MeV, including 15 time-correlated α pairs. From the activities A_1 and A_2 observed in Fractions 1 and 2, respectively, the percent adsorption (%*ads*) on CA08Y was evaluated according to the equation: $\%ads = 100A_2/(A_1 + A_2)$. The variation of the %*ads* is shown in Fig. 1 as a function of HF concentration, [HF]. The data for ^{261}Rf and ^{169}Hf obtained from the Cm/Gd target are shown by closed squares and closed circles, respectively, while those for ^{85}Zr and ^{169}Hf from the Ge/Gd target are by open squares and open circles, respectively. The Hf data from both targets agree well. The %*ads* values of Zr and Hf are consistent with each other and both decrease steeply with an increase of [HF] above 8 M. As HF is a weak acid, equilibrations among HF, H^+, F^-, and HF_2^- in the solution are established following the two chemical relations: $H^+ + F^- \leftrightarrow HF$ and $HF + F^- \leftrightarrow HF_2^-$ [4]. Above 1 M, $[HF_2^-]$ is more than one order of magnitude higher than $[F^-]$, and the decrease of %*ads* with [HF] is explained as displacement of the metal complexes in the binding sites of the resin with HF_2^-. Although the %*ads* of Rf shown in Fig. 1 also decreases with [HF], the values are apparently smaller than those of Zr and Hf, implying that the fluoride complexing strength of Rf is weaker than that of Zr and Hf. Recently, the relativistic molecular density-functional calculations of electronic structure of the hexafluoride complexes of Zr, Hf, and Rf were performed [3]. The free energy change for fluorination reactions $M(H_2O)_8^{4+} \leftrightarrow MF_6^{2-}$ showed that the fluoride complexation of Rf is weaker than that of Zr and Hf at pH < 0. This agrees with the present order of adsorption: Zr ≈ Hf > Rf, though chemical species of these elements should be confirmed in this system for quantitative discussion.

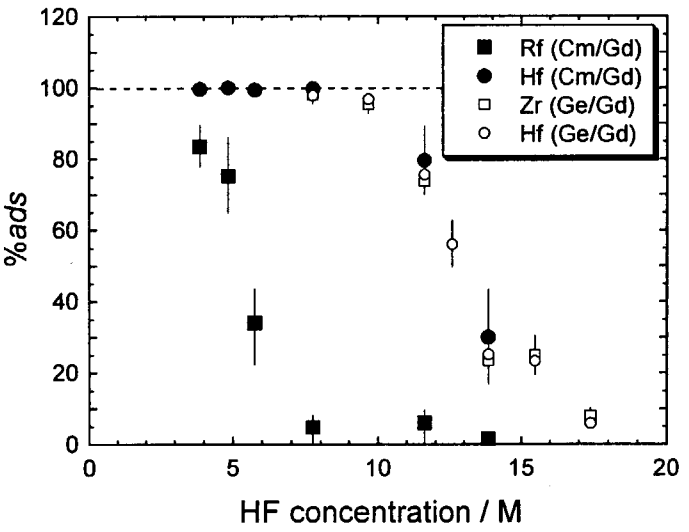

Fig. 1. Variation of the percent adsorption (%*ads*) of Zr, Hf, and Rf on CA08Y as a function of the HF concentration.

References

[1] J. V. Kratz, *Heavy Elements and Related New Phenomena, Vol. 1*, edited by W. Greiner and R. K. Gupta (World Scientific, Singapore, 1999), p. 129.
[2] H. Haba *et al.*, J. Nucl. Radiochem. Sci. **3**(2002)143.
[3] V. Pershina *et al.*, Radiochim. Acta **90**(2002)869.
[4] P. M. Plaisance and R. Guillaumont, Radiochim. Acta **12**(1969)32.

4.3 CHEMICAL BEHAVIOR OF DUBNIUM IN HF

K. TSUKADA, H. HABA,[1] M. ASAI, A. TOYOSHIMA,[2] K. AKIYAMA, I. NISHINAKA, K. HASHIMOTO, S. ICHIKAWA, Y. NAGAME, K. YASUDA, Y. MIYAMOTO, H. ISHIZU,[3] S. GOTO,[3] M. ITO,[3] J. SAITO,[3] H. KUDO,[3] W. SATO,[2] Y. TANI,[2] H. HASEGAWA,[2] A. SHINOHARA,[2] Y. OURA,[4] K. SUEKI,[5] H. KIKUNAGA,[6] N. TSURUGA[6] and A. YOKOYAMA[6]

Chemical behavior of fluoride complexes of element 105, dubnium (Db), has been investigated together with the group-5 homologues Nb and Ta, and pseudo-homologue Pa by anion-exchange chromatography.

^{262}Db and ^{169}Ta were produced in the ^{248}Cm(^{19}F, 5n) and ^{nat}Gd(^{19}F, xn) reactions [1], respectively, at the JAERI tandem accelerator. On-line anion exchange separations were performed at the 14 M HF solution using the Automated Ion exchange separation apparatus coupled with the Detection system for Alpha spectroscopy (AIDA) [2]. AIDA enables us to perform cyclic discontinuous column chromatographic separations of transactinide elements in the aqueous phase and automatic detection of α-particles within a typical cyclic time of 50-70 s. The reaction products recoiling out of the target were transported by the He/KCl gas-jet system to AIDA, and the products were dissolved and loaded onto a small column (MCI GEL CA08Y, 1.0 mm i.d. x 3.5 mm) with 110 μL of 14 M HF at a flow rate of 1.2 mL/min. The effluent was collected on a Ta dish as Fraction 1 and evaporated to dryness with hot He gas and a halogen heat lamp. Db and Ta remaining in the column was eluted with 200 μL of 6 M HNO_3/0.015M HF, and collected on another Ta dish and evaporated to dryness as Fraction 2. Each pair of Ta dishes, Fractions 1 and 2, was automatically transferred to the α spectrometry station equipped with eight 600 mm^2 PIPS detectors.

1702 times experiments were conducted with AIDA. In elutions with 14 M HF and 6 M HNO_3/0.015 M HF, 6 α singles (including one α–α-pairs of correlated mother-daughter decay) and 4 ones (including one correlation) from the α-decay of ^{262}Db were registered with the life time compatible with the 34 s. The K_d value of about 30 for Db at 14 M HF was evaluated. Figure 1 shows the K_d value of Nb, Ta, Pa, and Db as a function of the HF concentration. The K_d of Db is nearly equal to that of Pa, while that is smaller than those of Nb (150) and Ta (175); the order of adsorption is Pa≤Db<Nb=Ta. This result gives us interesting feature that the chemical behavior of Db is quite different from that of its homologues Nb and Ta.

[1] Cyclotron Center, RIKEN
[2] Department of Chemistry, Graduate School of Science, Osaka University
[3] Department of Chemistry, Faculty of Science, Niigata University
[4] Department of Chemistry, Graduate School of Science, Tokyo Metropolitan University
[5] Department of Chemistry, Tsukuba University
[6] Department of Chemistry, Faculty of Science, Kanazawa University

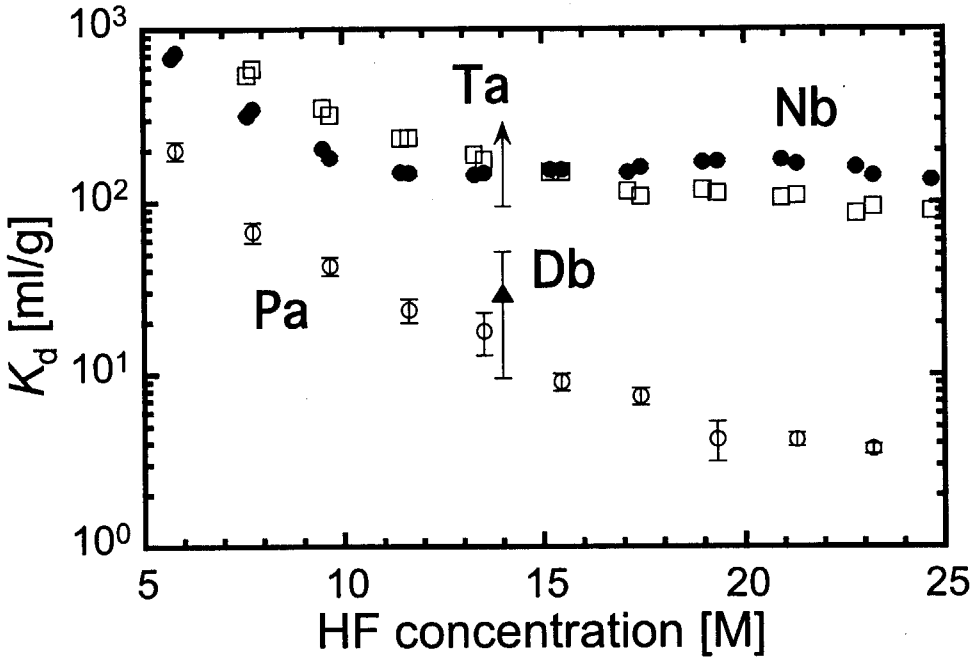

Fig.1 Distribution coefficients of Nb, Ta, Pa, and Db fluoride complexes on CA08Y as a function of the HF concentration. The data from the batch experiments for Nb, Ta, and Pa are shown by closed circles, open squares and open circles, while the on-line data for Db and Ta at 14 M HF are indicated by closed triangles and arrow (lower limit), respectively.

References

[1] Y. Nagame, M. Asai, H. Haba, S. Goto, K. Tsukada, I. Nishinaka, K. Nishio, S. Ichikawa, A. Toyoshima, K. Akiyama, H. Nakahara, M. Sakama, M. Schaedel, J.V. Kratz, H.W. Gaeggeler, and A. Tuerler, J. Nucl. Radiochem. Sci. **3** (2002) 85.

[2] K. Tsukada, I. Nishinaka, M. Asai, S. Goto, M. Sakama , H. Haba, S. Ichikawa, Y. Nagame, and M. Schaedel, JAERI-Review **29** (2002) 49.

[3] H. Haba, K. Tsukada, M. Asai, A. Toyoshima, K. Akiyama, I. Nishinaka, M. Hirata, S. Ichikawa, Y. Nagame, K. Yasuda, Y. Miyamoto, T. Kaneko, S. Goto, S. Ono, T. Hirai, H. Kudo, M. Shigekawa, A. Shinohara, Y. Oura, H. Nakahara, K. Sueki, H. Kikunaga, N. Kinoshita, N. Tsuruga, A. Yokoyama, M. Sakama, M. Schaedel, and J. V. Kratz, a separate paper of this JAERI-Review.

4.4 ISOTHERMAL GAS CHROMATOGRAPHY OF Rf AND ITS HOMOLOGUES, Zr AND Hf

T. KANEKO[1], K. TSUKADA, M. ASAI, K. AKIYAMA, H. HABA[2], A. TOYOSHIMA[3], S. ONO[1], T. HIRAI[1], H. ISHIZU[1], S. GOTO[1], S. ICHIKAWA, Y. NAGAME and H. KUDO[1]

Rutherfordium (Rf), the first transactinide element, is located in the group-4 elements in the periodic table. Isothermal gas chromatography is a promising method for the Rf chemistry in the gas phase. For the group-4 elements, it is well known that the chemical properties of Zr quite resemble with those of Hf and also for the chlorides of them. From extrapolations of the trends within the groups of the periodic table, $RfCl_4$ would be less volatile than $ZrCl_4$ and $HfCl_4$, whereas from relativistic calculations $RfCl_4$ is predicted to be more volatile than $HfCl_4$ and $ZrCl_4$ [1]. The volatilities of the Rf, Zr, and Hf chlorides were studied by Kadkhodayan *et al.* experimentally [2], and the order of the volatility was reported as $RfCl_4 \sim ZrCl_4 > HfCl_4$. However, the experiments were performed separately, the conditions might be different in each experiment.

In order to clarify the volatility of the Rf and its homologs chlorides, we conducted the isothermal gas chromatographic experiments of Rf together with the lighter homologues, Zr and Hf under the identical condition with a newly developed isothermal gas chromatographic apparatus. ^{261}Rf ($t_{1/2}$=78 s) used in this study is the longest-lived isotope and produced in the ^{248}Cm (^{18}O, 5n) reaction with the production rate of ~ 2 atoms per min, which forces us to perform rapid and repetitive chromatographic experiments with single atoms.

The experiments were performed at the JAERI Tandem accelerator. The schematic diagram of

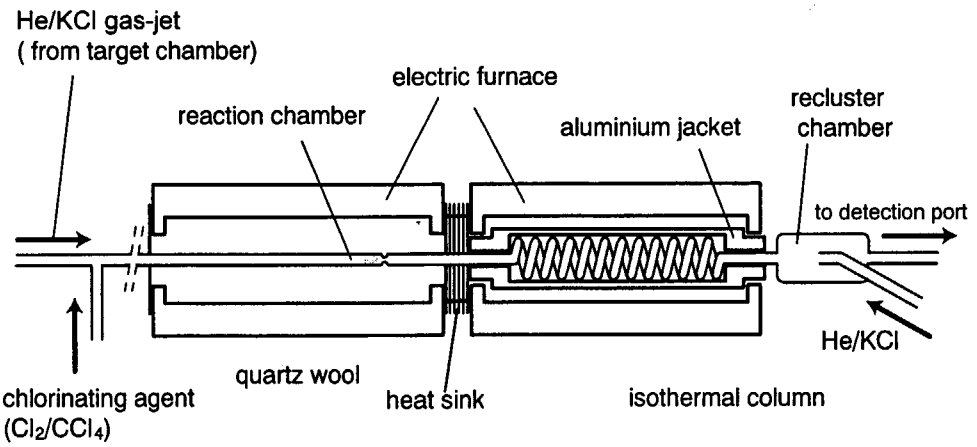

Fig.1 Schematic diagram of the on-line isothermal gas chromatographic apparatus.

[1] Department of Chemistry, Faculty of Science, Niigata University
[2] Cyclotron Center, RIKEN
[3] Department of Chemistry, Graduate School of Science, Osaka University

the isothermal gas chromatographic apparatus is shown in Fig. 1. The apparatus consists of a reaction chamber, an isothermal column, and a recluster chamber. They are made by quartz. The Zr and Hf isotopes, ^{85}Zr and ^{169}Hf, were produced via the ^{nat}Ge (^{18}O, xn) and ^{nat}Gd (^{18}O, xn) reactions, respectively, while the ^{261}Rf was produced via the ^{248}Cm (^{18}O, 5n) reaction. These isotopes were simultaneously produced. The reaction products were transported to the reaction chamber by means of the He/KCl gas-jet and converted to chlorides using the mixture of Cl_2 gas and CCl_4 vapor as chlorinating agents. The volatile compounds were transported to the isothermal column continuously. The volatile compounds that were eluted at the end of the isothermal column were transported to detection systems by another He/KCl gas-jet system.

Fig. 2 illustrates the relative yield curves for the ^{85}Zr, ^{169}Hf, and ^{261}Rf chlorides. It was found that the behaviors of the chlorides of Zr, Hf, and Rf were very similar among them. The similarity of the volatility of the Zr and Hf chlorides is consistent with the result obtained by the thermochemical methods. These results agree with the expectations from macro scale behavior for Zr and Hf, and indicate that Rf deviates from the trend expected based on the extrapolation of the Zr and Hf values.

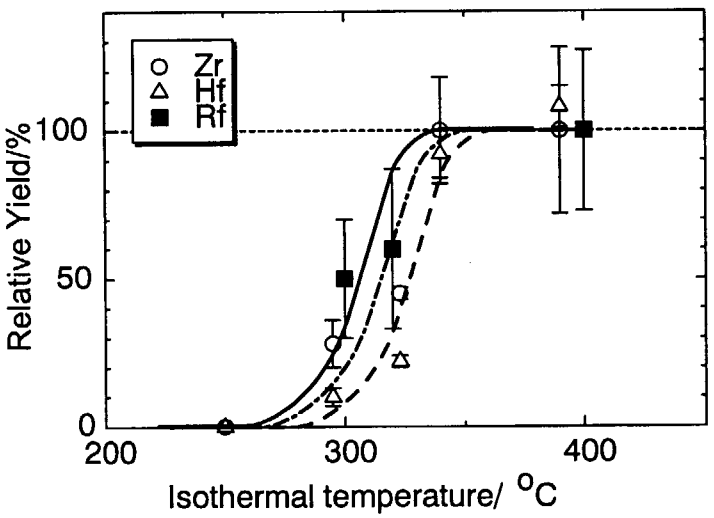

Fig. 2 Relative yield curve for ^{85}Zr-, ^{167}Hf-, and ^{261}Rf-chlorides. Cl_2/CCl_4 was used as chlorinating gas.

The present result indicates that the Rf chloride behaves like the Zr and Hf chlorides within the experimental accuracy as seen in Fig. 2.

References

[1] A. Türler *et al.*, PSI Annual Report 1994, Annex IIIA, 77 (1995).
[2] B. Kadkhodayan *et al.*, Radiochim. Acta, 72, 169 (1996).

4.5 AN ATTEMPT TO DETERMINE THE IONIC RADIUS OF TRIVALENT NOBELIUM BY CATION-EXCHANGE METHOD

A. TOYOSHIMA[1], K. TSUKADA, M. ASAI, K. AKIYAMA, I. NISHINAKA, T. KANEKO, S. ICHIKAWA, Y. NAGAME, H. HABA[2], M. SHIGEKAWA[1], Y. TANI[1], H. HASEGAWA[1] and A. SHINOHARA[1]

It was reported that the ionic radius of Lr^{3+} studied by a cation-exchange chromatography deviated from the trend of an actinide contraction, which was explained in terms of the influence of the relativistic effect or, possibly, the polarizability of the *f*-shell electronic orbital [1]. Although the ionic radius of No^{3+} is of key interest to discuss them in more detail, there are no available data due to the difficulty of the No^{3+} elution after and/or during the strong oxidation of No^{2+}. The purpose of the present study is to measure the ionic radius of No^{3+} by a cation-exchange chromatography with an α-hydroxyisobutyrate (α-HIB) eluent and a PbO_2 oxidant. In this method, a liner correlation between the logarithm of the distribution coefficients (K_d values) on the cation-exchange resin and the ionic radii of both lanthanides and actinides is utilized [2].

The experiment was performed at the JAERI Tandem accelerator. The short-lived nuclides ^{158}Tm, ^{155}Er, ^{150}Dy and ^{152m}Tb were produced in the ^{nat}Eu(^{12}C, *xn*), ^{nat}Sm(^{12}C, *xn*), ^{nat}Nd(^{12}C, *xn*) and ^{nat}Nd(^{12}C, *pxn*) reactions, respectively. The reaction products recoiling out from the target were transported by the He(KCl) gas-jet method to the collection site of the Automated Ion-exchange separation apparatus coupled with the Detection system for Alpha spectroscopy (AIDA) [3]. In addition to the above nuclides, ^{156}Ho was grown up from the disintegration of ^{156}Er during the collection. After the collection, these radionuclides were dissolved with 0.1 M α-HIB solution (pH=3.5) and passed through two successive columns at a flow rate of 1.1 mL/min: a PbO_2 column (1.6 mmϕ×10 cm) which were filled with 1:10 mixture of PbO_2 and slica gel powder (Disogel 15/30 μm, DAISO co. ltd.), and a cation-exchange column (MCI GEL CK08Y, 1.6 mmϕ×3 cm). After the elution with about 2000 μL of α-HIB, 200 μL of 6 M HNO_3 was pumped to wash the cation-exchange column. All effluents were collected in several polyethylene-tubes and were subjected to γ-ray measurements with Ge detectors. Typical elution curves of ^{158}Tm, ^{155}Er, ^{156}Ho, ^{150}Dy and ^{152m}Tb were shown in Fig. 1. The elution peak of No^{3+} is expected between Er^{3+} and Ho^{3+}, which have the similar ionic radii to Lr^{3+} and Md^{3+}, respectively [1]. Thus, the elution behavior of No^{3+} has been investigated at the range of 1100 - 1700 μL elution volume as indicated in Fig.1.

The elution behavior of ^{255}No produced in the ^{248}Cm(^{12}C, 5*n*) reaction was studied with AIDA together with ^{153}Er and ^{150}Dy simultaneously produced in the ^{nat}Sm(^{12}C, *xnyp*) reactions. The collection, dissolution and elution procedures were almost the same as those mentioned above. Six aliquots of 100 μL of α-HIB expected for the No^{3+} elution and two aliquots of 100 μL of 6 M HNO_3 for the No^{2+} elution were collected on separate Ta disks and evaporated to dryness by a halogen heat lamp and hot He and N_2

[1] Department of Chemistry, Graduate School of Science, Osaka University
[2] Cyclotron Center, RIKEN

gases in a few tens of seconds, and only the 7th Ta disk was finally flamed in order to get a higher resolution in α-spectrometry. These Ta disks were subjected to α-particle measurements with eight 600 mm^2 PIPS detectors. Figure 2 represents the elution curves obtained from α spectroscopy. The elution behavior of ^{153}Er and ^{150}Dy agrees with that of ^{155}Er and ^{150}Dy, respectively. Eight α-events of ^{255}No were observed in the No^{2+} fractions (0.1 M α-HIB) but not in the No^{3+} fractions (6 M HNO_3). There seem to be two possibilities that No^{2+} was not oxidized to No^{3+} in the PbO_2 column or that the oxidized No^{3+} was reduced before elution from the cation-exchange column. In the future, a modified oxidation condition such as higher temperature will be applied to the No oxidation.

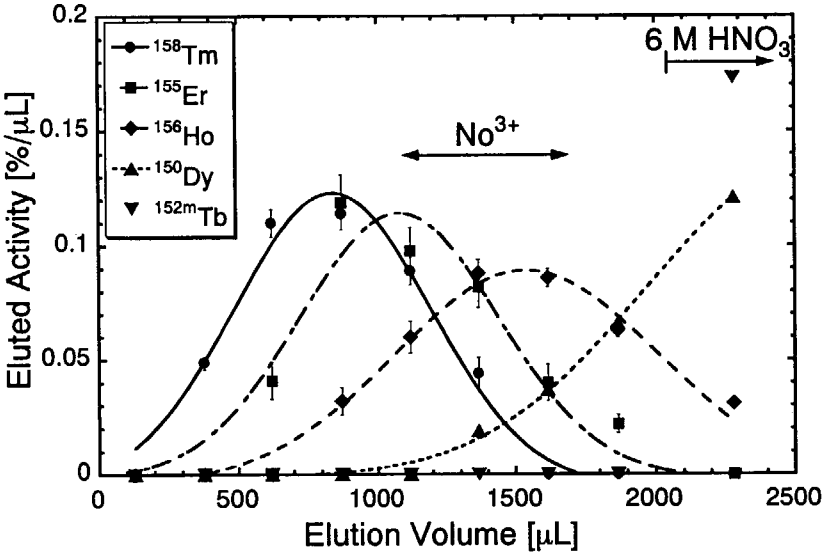

Fig.1. Typical elution curves of ^{158}Tm, ^{155}Er, ^{156}Ho, ^{150}Dy and ^{152m}Tb from in 0.1 M α-HIB solution (pH=3.7).

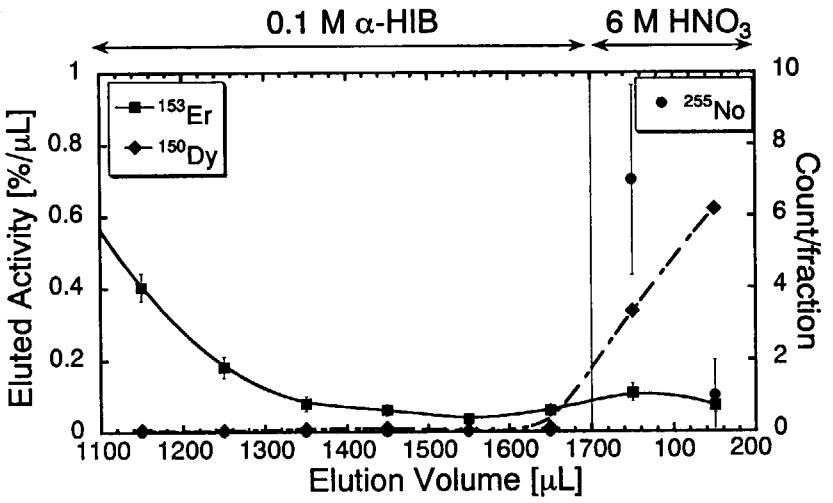

Fig.2. Elution curves of ^{153}Er, ^{150}Dy (left vertical axis) and ^{255}No (right vertical axis). Lines are guides to eye.

References

[1] W. Brüchle *et al.*, Inorg. Chim. Acta **146**(1988) 267.

[2] R. C. Gatti *et al.*, J. Inorg. Nucl, Chem. **11**(1959) 251.

[3] K. Tsukada *et al.*, JAERI-Review **29**(2002) 49.

4.6 HPLC ELUTION BEHAVIOR OF ACTINIUM METALLOFULLERENE

K. AKIYAMA, K. SUEKI[1], H. HABA[2], K. TSUKADA, M. ASAI, I. NISHINAKA, K. KIKUCHI[3], S. ICHIKAWA, Y. NAGAME, H. NAKAHARA[3] and M. KATADA[3]

It is well known that the chemical properties of Ac are similar to those of the rare earth elements, such as Y and La, and easily expected from the similarity of the chemical properties that the oxidation state of Ac in the fullerene cage is +3. Some physical properties of Ac, however, are little bit different from those of the rare earth elements. The ionic radius of Ac(III) is the largest among a series of the trivalent lanthanide and actinide, and close to those of the divalent lanthanide. It is interesting to study whether Ac(III) may induce the stabilization of the metallofullerenes. In this paper, we report the HPLC elution behavior of the Ac metallofullerene studied by the radiotracer technique.

The fullerenes encapsulating Ac atoms were synthesized by the arc discharge method. The anode for the discharge was made from a porous carbon rod (size: 10 mmϕ × 40 mm) which absorbed about 1 mL of the ethanol solution of $La(NO_3)_3$ mixed with the radiotracer of ^{225}Ac, and was sintered at 800°C under the He atmosphere. This anode was set in the chamber for the generation of fullerenes and discharged in the 400 Torr He with the direct current of 110 A. The soot containing Ac metallofullerenes was recovered from the chamber and dissolved in CS_2. The CS_2 solution was evaporated to dryness, re-dissolved to toluene, and filtered for removing the insoluble substance. The condensed solution was injected to a 5PBB (Pentabrombenzyle stationary phase) column and developed with the flow rate of 6 mL/min of toluene. The Ac fractions were collected and developed to a buckyclutscher (Tri-dinitrobenzyl stationary phase) column with the flow rate of 2 mL/min of hexane : toluene = 3 : 7 mixed solution. The effluent from the column was collected for every 1 min and monitored by the on-line UV absorption detector. The HPLC elution behavior of the Ac fullerenes was monitored by the α-ray detection

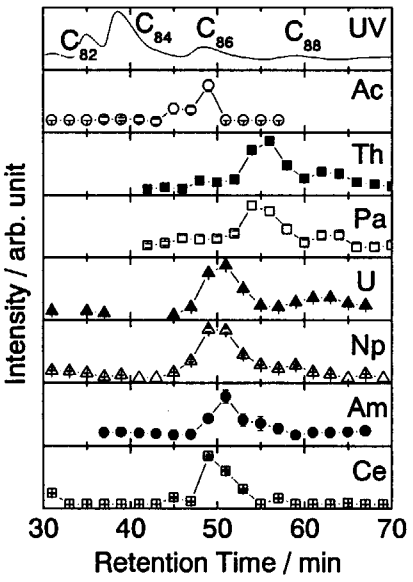

Figure 1. HPLC elution behavior on a 5PBB column of the Ac metallofullerene; The dominant elution peak of the Ac metallofullerene also consistent with those of the Ce, U, Np, and Am metallofullerene.

[1] Department of Chemistry, University of Tsukuba
[2] Cyclotron Center, The Institute of Physical and Chemical Research (RIKEN)
[3] Department of Chemistry, Tokyo Metropolitan University

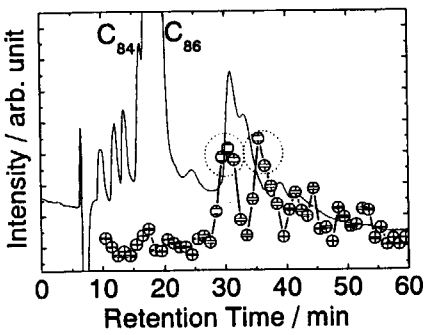

Figure 2. HPLC elution behavior of the Ac metallofullerene on a Buckyclutscher column: two intense elution peaks are marked by dotted circles.

of ^{225}Ac in each fraction.

Figure 1 shows the HPLC elution behavior of the Ac metallofullerene on a 5PBB column, which was obtained from the α-particle measurements of the eluant. For comparison, the HPLC chromatogram monitored by the UV absorption detector and the chromatogram of the metallofullerenes of Ce, Th, Pa, U, Np, and Am obtained from another experiment [1] are also plotted in this figure. As the results of the α-ray measurements for a series of HPLC fractions, the α-particle from ^{225}Ac and its daughters was intensively observed around the retention time of 50 min.

The HPLC elution behavior of the metallofullerenes has been well investigated [2], especially for the lanthanide metallofullerenes. The main product in the crude extracts of the lanthanide metallofullerenes is M@C_{82}. The dominant elution peak of the Ac metallofullerene also consistents with those of the Ce, U, Np, and Am metallofullerenes whose dominant elution peak in the chromatogram has been found to be M@C_{82} with a trivalent metal atom [3]. This result strongly suggests that the component of the dominant elution peak of the Ac metallofullerene is also this type of M@C_{82} metallofullerene. The M@C_{82} species encapsulating the lanthanides, except for Sm, Eu, Tm, and Yb, have only one stable structural isomer [3-5] in spite of the prediction for the existence of the stable 4 topologically different C_{82}^{3-} structures [6]. To investigate the existence of the M@C_{82} isomers, Ac@C_{82} fraction on the 5PBB column was collected and developed to a Buckyclutscher column which is generally used for the separation of the fullerene isomers from each other. The HPLC elution behavior of the Ac metallofullerene on this column is shown in the figure 2. In this chromatogram, at least two intense elution peaks are observed. This result strongly suggests the existence of the plural metallofullerene isomers. The further investigation for these metallofullerene isomers is in progress.

References

[1] K. Akiyama *et al.*, J. Am. Chem. Soc. **123** (2001) 181.
[2] D. Fuchs, *et al.*, J. Phys. Chem. **100** (1996) 725.
[3] T. Akasaka, *et al.*, Chem. Phys. Lett. **319** (2000) 153.
[4] K. Yamamoto, *et al.*, J. Phys. Chem. **98** (1994) 2008.
[5] S. Ohkubo, *et al.*, New Diamond Front. Carbon Technol. **11** (2001) 285.
[6] K. Kobayashi *et al.*, Chem. Phys. Lett. **282** (1998) 325.

4.7 MEASUREMENT OF IRIDIUM IN DEEP-SEA SEDIMENT USING MULTI-PARAMETER COINCIDENCE METHOD

Y. HATSUKAWA, Y. TOH, M. OSHIMA, M.HOSEIN,
A. KIMURA, T. NOGUCHI[1] and J. KAMATA[1]

Iridium concentrations in pelagic deep-sea sediment were measured by multi-parameter coincidence γ ray spectroscopy method. Relatively higher concentration iridium in the sediment samples was found.

The iridium concentration in the earth crust is quite low (about 10 ppt). On the other hand, extraterrestrial materials, meteorite, cosmic dust, contains high iridium (about 700 ppb). Iridium anomalies in geological samples have been considered as an evidence of the meteorite impact. In this study, iridium concentrations in pelagic deep-sea sediments collected from the eastern Philippine sea were measured by a multi-parameter coincidence γ ray spectroscopy method.

Sediment samples and an iridium standard were sealed in quartz tube, and irradiated in JRR-3 reactor for 48 hours. Gamma rays from each sample were measured with GEMINI for about 1 day. The γ–γ coincidence peak of 468-316 keV from ^{192}Ir ($T_{1/2}$ = 73.8 d) produced by the ^{191}Ir(n,γ) ^{192}Ir reaction was measured. The iridium content of the sediment samples were obtained from the comparison of ^{192}Ir intensities between the sediment samples and the iridium standard. The iridium contents of the deep-sea sediment samples obtained in this study are 130 - 248 ppt. These values are relatively high compared with the averaged value of the earth crust samples. It is thought that this high iridium concentration results from a huge contribution of cosmic dust which contains rich iridium. According to the results of this work, we found that the concentration of the iridium in deep-sea sediment is distributed uniformly in the boring core sample.

1) Department of Geological Science, Ibaraki University

4.8 GAMMA-RAY EMISSION PROBABILITY MEASUREMENT OF ^{149}Eu

H. MIYAHARA[1], K. KATOH[2],
S. ICHIKAWA, K. TSUKADA, I. NISHINAKA, M. ASAI and K. AKIYAMA

The γ-ray emission probability is one of the most important decay parameters for a radionuclide, and it is frequently used for determination of a disintegration rate from a γ-ray pulse height spectrum. Gamma-ray emission probabilities for a few hundreds nuclides with half-lives larger than minutes have been evaluated, but the values show still large uncertainties because of large spread of some absolute values with large uncertainties. To improve the certainties the γ-ray emission probabilities are to be determined from the γ-ray intensity and disintegration rate. Europium-149 decays with a half-life of 93.1 d by electron capture, and about 25% of EC go directly to the ground level [1]. The emission probabilities of the 277 and 328 keV γ-rays are evaluated to be 3.55±0.11% and 4.03±0.11%, respectively, by Szucs et al. [1]. It is, however, doubtful that the experiments used in the evaluation are reliable. The purpose of the present study is to establish γ-ray emission probabilities of ^{149}Eu by using a 4πβ-γ coincidence apparatus.

Preparing a sample source with high specific activity is important for precise measurement, but this requirement cannot be fulfilled because of the long half-life of ^{149}Eu. After the suitable proton energy was determined from a pre-experiment to avoid production of ^{148}Eu by the ^{149}Sm(p,2n) reaction, sources of ^{149}Eu were produced by about 9 MeV proton irradiation of enriched $^{149}Sm_2O_3$ (enrichment : 96.9%). The irradiated sample was scattered in dilute HCl solution and ^{149}Eu sources were prepared on thin metallized VYNS films stretched on brass mounts. The disintegration rate and γ-ray spectrum was measured using a 4πβ pressurized proportional counter, an HPGe γ-ray detector with relative efficiency of 23%, and a coincidence apparatus using a two-dimensional data-acquisition system [2]. The detection efficiencies of γ-rays were calibrated by measuring γ-ray spectra and disintegration rates of standard sources of ^{57}Co, ^{60}Co, ^{133}Ba, ^{134}Cs and ^{152}Eu. The γ-ray emission probabilities adopted for these nuclides were the evaluated values taken from an IAEA report [3]. A fourth-order polynomial function was fitted to the logarithms of the energy and efficiency by a method of least squares incorporating a covariance matrix. The γ-ray intensities of all measured spectra were corrected for cascade summing effect.

Coincidence efficiency functions to determine the disintegration rates of ^{149}Eu sources were

[1] Department of Radiological Technology, School of Health Sciences, Nagoya University

2 Department of Nuclear Engineering, Graduate School of Engineering, Nagoya University

deduced by setting the gate on the photopeak of the 328 keV γ-ray. The efficiency of the 4πβ counter was below 25% because of low specific activity of sample source, but the disintegration rate was successfully determined with an uncertainty of about 1%. The correction for impurities is important, because the γ-ray spectrum showed the existence of ^{148}Eu produced by the ^{149}Sm(p,2n) reaction. The disintegration rate was estimated from photopeak intensities of the 550 and 630 keV γ-rays, and the ratio of the disintegration rates between ^{148}Eu and ^{149}Eu ranged from 1.1% to 1.8%.

Two runs of irradiation were carried out using JAERI tandem accelerator, and the proton energy of each run was 8.9 and 9.2 MeV. Two sources were prepared at each run, and measurements were carried out at Nagoya University. The emission probabilities of the 277 and 328 keV γ-rays were calculated from the disintegration rate, γ-ray intensities and γ-ray detection efficiencies. The results are shown in Table 1 together with the published data and also relative γ-ray intensities calculated from those. The published values are smaller than the present ones by about 15%, and furthermore the present results show improved uncertainties. Figure 1 shows the decay scheme with recommended decay data that the γ-ray emission probabilities except the measured ones are calculated by multiplying the evaluated values [1] by 1.17. It is emphasized that EC branching ratio to the 0 and 22.5 keV levels are largely different from those of Szucs et al. [1].

References

[1] J.A. Szucs, M.W. Johns and B. Singh, *Nucl. Data Sheets* **46** (1985) 1.

[2] H. Miyahara, K. Ikeda and N. Marnada, *J. Nucl. Sci. and Technol.* **38** (2001) 270.

[3] IAEA, "*X-ray and gamma-ray standards for detector calibration*", IAEA-TECDOC-619, Vienna (1991).

Table 1. Measured and evaluated emission probabilities of the 277 and 328 keV γ-rays and relative intensities. The uncertainty of detection efficiency is not included in the uncertainty for each source.

γ-ray energy (keV)	γ-ray emission probability (%)								Relative γ-ray intensity	
	Run 1			Run 2			Mean	Szucs et al.		
	Source 1	Source 2	Mean	Source 1	Source 2	Mean			This work	Szucs et al.
277.1	4.14(3)	4.14(3)	4.14(4)	4.11(4)	4.13(5)	4.12(4)	4.13(3)	3.55(11)	86.9(5)	88.1(27)
327.5	4.76(4)	4.76(4)	4.76(4)	4.73(5)	4.76(6)	4.75(4)	4.75(3)	4.03(12)	100.0(6)	100(3)

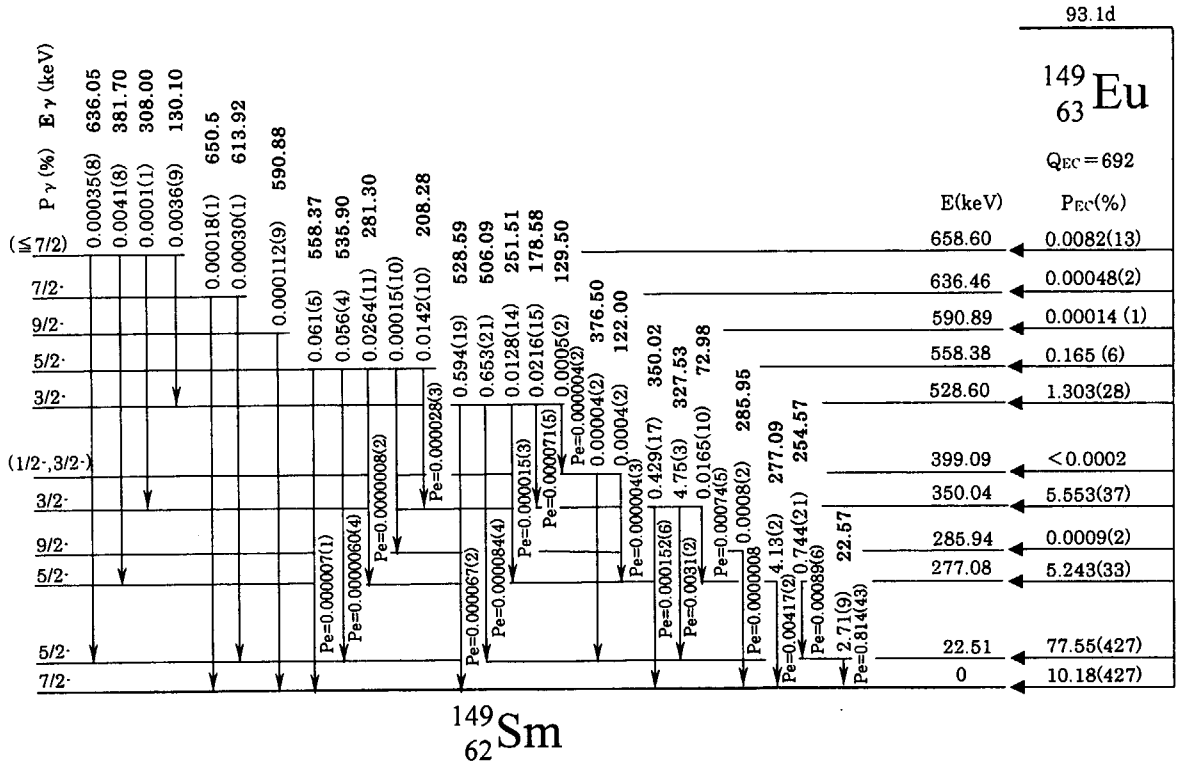

Fig. 1. Recommended decay scheme of ^{149}Eu.

5. Nuclear Theory

This is a blank page.

5.1 NARROWING N=20 SHELL GAP STUDIED BY ELECTROMAGNETIC MOMENTS OF Na ISOTOPES

Y. UTSUNO, T. OTSUKA[1], T. MIZUSAKI[2] and M. HONMA[3]

One of the most characteristic features in neutron-rich nuclei is that the magic number seen in stable nuclei can disappear, as studied most extensively in the $N=20$ region [1]. The origin of this disappearance is still somewhat ambiguous: it has been speculated that a certain proton number may favor the deformation associated with the breaking of the shell closure. Much interest has not been attracted in the possibility of the change of the shell gap itself, since well used one-body potentials like the harmonic-oscillator and the Woods-Saxon ones give a rather constant shell gap independently of the nucleon number. On the other hand, we recently pointed out that due to the spin-isospin dependence of the nucleon-nucleon interaction the width of the shell gap should vary as the proton (or neutron) number changes [2]. This is a property inherent in the two-body interaction.

The aim of the present study is to clarify the importance of the narrowing shell gap in the mechanism of the disappearance of the $N=20$ magic number. Electromagnetic moments of neutron-rich Na isotopes measured recently [3] provide much information about their ground-state properties, from which we can discuss the disappearance of the magic number. We performed large-scale shell-model calculations [4] based on the Monte Carlo shell model (MCSM) [5]. A large valence shell including lower parts of the pf orbits was adopted. A part of the numerical computation was carried out with the Helios parallel computer system in JAERI Tandem.

Figure 1 shows the quadrupole and magnetic moments compared between the experiment and the shell-model calculations. Up to $N=18$, the experimental moments are well reproduced by a standard sd-shell model calculation, implying that the $N=20$ magic number is preserved to large extent. Indeed, the MCSM calculation shows that the component of the ground-state wave function beyond the sd-shell configuration is only about 5% for $N=16$ and 17. At $N=18$, the sd-shell configuration decreases to about 60%, but its effect on the moments appears to be small. Experimental moments at $N=19$ are not reproduced by the sd-shell model at all, whereas they are very close to the MCSM value. This ground-state wave function turns out to be composed almost of the two-particle two-hole ($2p2h$) configuration excited from the $N=20$ closure.

We examine how the $2p2h$ dominance at $N=19$ is related to the width of the $N=20$ shell gap. In terms of the shell model, the width of the shell gap is defined by the so-called effective single-particle energy [4]. It varies as the nucleon number through the monopole interaction. In the present effective interaction, this gap is 3.5 MeV much narrower than that of stable nuclei ($\sim$6 MeV). We artificially enlarged the gap by means of the shift of the monopole interaction, obtaining the switch from the $2p2h$ dominance to the $0p0h$ one around the gap near 4 MeV for the $N=19$ isotope. Naturally, its moments deviate at the

[1]Department of Physics, University of Tokyo
[2]Institute of Natural Sciences, Senshu university
[3]Center for Mathematical Sciences, University of Aizu

same time.

To conclude, the experimental Na moments are not reproduced by a nuclear-structure model having a normal $N=20$ shell gap. The origin of the narrowing shell gap for small proton number can be the spin-isospin dependence of the nucleon-nucleon interaction [2], whose character has not been well incorporated in standard one-body potentials.

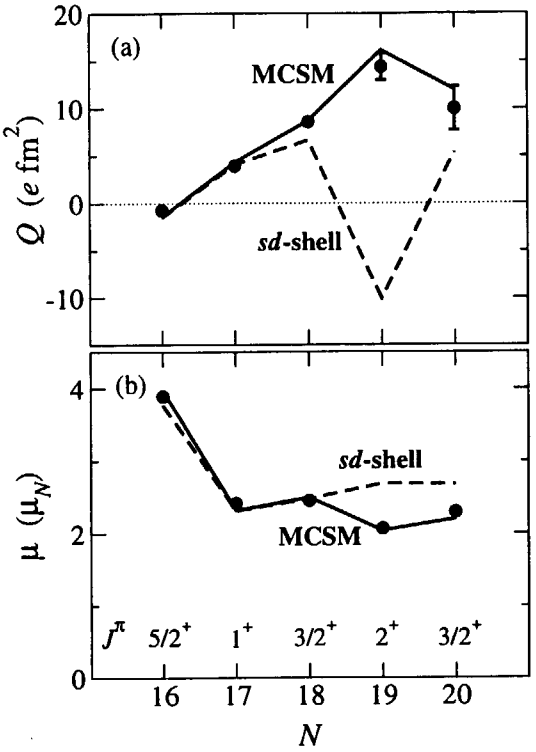

Fig. 1. (a) Quadrupole moments and (b) magnetic moments of Na isotopes compared between the experiment [3] and the shell-model calculations. The solid and dashed lines stand for the MCSM and the *sd*-shell model values.

References

[1] For instance, T. Motobayashi *et al.*, Phys. Lett. B **346** (1995) 9.

[2] T. Otsuka, R. Fujimoto, Y. Utsuno, B.A. Brown, M. Honma, and T. Mizusaki, Phys. Rev. Lett. **87** (2001) 082502.

[3] M. Keim, in *Proceedings of ENAM 98*, AIP Conf. Proc. **455** (1998) 50; M. Keim *et al.*, Euro. Phys. J. A **8** (2000) 8.

[4] Y. Utsuno, T. Otsuka, T. Mizusaki, and M. Honma, Phys. Rev. C **60** (1999) 054315.

[5] T. Otsuka, M. Honma, T. Mizusaki, N. Shimizu, and Y. Utsuno, Prog. Part. Nucl. Phys. **47** (2001) 319.

5.2 MOLECULAR DYNAMICS DESCRIPTION OF A FERMI-GAS

T. MARUYAMA, A. BONASERA[1] , M. PAPA[2] and S. CHIBA

There are several molecular dynamics models for nuclear many-body systems. One of the problems in calculating nuclear many-body systems is the treatment of Fermionic nature of nucleons. This is the reason why the quantum molecular dynamics (QMD) [1] was, in the beginning, used only for higher energy reactions. The Fermionic molecular dynamics (FMD) [2] and the antisymmetrized molecular dynamics (AMD) [3] treat explicitly the antisymmetrization of the wave function. In this way they have succeeded in describing the nuclear ground state and the reaction process with high accuracy. However the price is the CPU time which is proportional to the 4-th power of the particle number. Some QMD approaches have introduced a phenomenological potential (Pauli potential) which prevents nucleons of same spin and isospin from getting close in the phase-space [4, 5, 6]. This QMD with the Pauli potential has been able to reproduce a certain degree of Fermionic nature. However, the Pauli potential has brought a spurious potential energy, which should be renormalized into the effective interactions. Furthermore, the density-dependence of the kinetic energy of a Fermi-gas is not perfect. To compensate this shortcoming of the QMD with Pauli potential, the constrained molecular dynamics (CoMD) has been proposed [7]. This model brings into the system the Fermi motion in a stochastic way (rearrangement of momentum distribution to keep Pauli principle). This new model is feasible enough and can be used for low-energy phenomena. But the CoMD model still has several points to be cleared. One of them is the ambiguity in measuring the phase-space occupation which is used for the stochastic momentum rearrangement. Related to this ambiguity, the property of a Fermi-gas has never been checked with this model.

Our aim of this report is to make a definite way to measure the phase-space occupation in a molecular dynamics calculation by fitting the equation of state (EOS) of a Fermi-gas. First we briefly explain the framework of the CoMD model. In CoMD, we write the coordinate of each nucleon i as $\{\mathbf{R}_i, \mathbf{P}_i\}$. The time-evolution of the coordinate consists of two parts. One is the Newtonian equation of motion

$$\dot{\mathbf{R}}_i = \frac{\partial H}{\partial \mathbf{P}_i}, \quad \dot{\mathbf{P}}_i = -\frac{\partial H}{\partial \mathbf{R}_i}, \tag{1}$$

where the Hamiltonian H consists of kinetic energy and potential energy. The other part is the stochastic momentum rearrangement. This part is done as follows: At every time-step, we check the phase-space occupation $\bar{f}_i$of each particle. If $\bar{f}_i$ exceeds 1, e.g. Pauli principle is broken around particle i, then we define an ensemble of neighbors of i and carry out multiple *elastic* scattering among this ensemble (momentum rearrangement). If the new $\bar{f}_i$ in the final state of this scattering is reduced then we accept this final sate and continue the time-evolution. In Ref [7] $\bar{f}_i$ is calculated as

$$\overline{f}_i \;=\; \sum_j \delta_{\tau_i,\tau_j}\delta_{s_i,s_j} \int_{\Phi_i} f_j(\mathbf{r},\mathbf{p})\, d^3r\, d^3p, \tag{2}$$

[1] INFN-LNS, Via S. Sofia 44, Catania 95123, Italy.
[2] INFN-Sezione di Catania, Corso Italia 57, Catania 95129, Italy

where $f_j(\mathbf{r},\mathbf{p})$ is a Gaussian single-particle distribution function of particle j, τ and s are its isospin and spin, Φ_i is the phase-space around $(\mathbf{R_i},\mathbf{P_i})$ with a volume h^3. However, we do not have any strong reason to employ this prescription. If we prepare a many-particle system with given Fermi distribution of momenta, the density-dependence of the averaged $\bar{f}_i$ never satisfies the exact curve.

Here we look for another way of measuring the phase-space occupation. To avoid the density-dependence of calculated $\bar{f}_i$, the distance in momentum-space and coordinate-space between particles should affect oppositely to the calculated $\bar{f}_i$. We employ a power function of the distance in the coordinate- and momentum-space R_{ij} and P_{ij} as

$$\bar{f}_i = c\left[\sum_j (R_{ij})^{-\alpha}(P_{ij})^{-\alpha}\right]^{3/\alpha} \qquad (\alpha > 2). \tag{3}$$

By this power function, we can avoid the density-dependence in measuring the phase-space occupation. The parameters α and c are fixed by fitting the energy of a Fermi-gas by the kinetic energy of the simulated many-particle system. Figure 1 shows the density-dependence of the energy of a Fermi-gas. The solid line shows the exact one and the marks show our CoMD calculation for Fermi-gas (many-particle system without interaction). The parameters in Eq. (3) are $c = 0.2$ and $\alpha = 8$. We have found that c depends on α though the analytic relation is not clear. Now we are planning to apply this method of phase-space occupation to the CoMD simulation of nucleon system and quark systems with proper effective interactions.

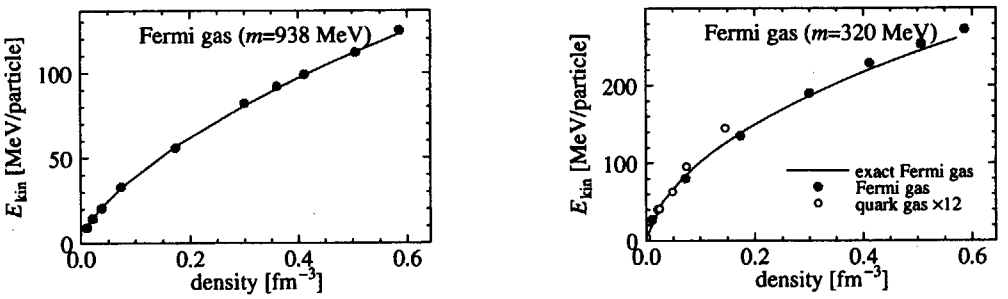

Figure 1: Kinetic energy per particle of Fermi-gas with mass $m = 938$ MeV and 320 MeV. In the right-hand side also shown are preliminary results with quark gas with two flavors.

References

[1] For review, see J. Aichelin, Phys. Rep. **202**, (1991) 233.

[2] H. Feldmeier and Jurgen Schnack, Rev. Mod. Phys **72**, (2000) 655.

[3] A. Ono, H. Horiuchi, T. Maruyama, and A. Ohnishi, Phys. Rev. Lett. **68**, (1992) 2898.

[4] L. Wilets, E. M. Henley, M. Kraft, and A. D. Mackellar, Nucl. Phys. A **282** (1977) 341.

[5] C. O. Dorso, S. Duarte and J. Randrup, Phys. Lett. B **188** (1987) 287.

[6] T. Maruyama, K. Niita, K. Oyamatsu, T. Maruyama, S. Chiba, and A. Iwamoto, Phys. Rev. C**57**, (1998) 655.

[7] M. Papa, T. Maruyama and A. Bonasera, Phys. Rev. C. **64** (2001) 024612.

5.3 ΛΛ PAIRING IN RELATIVISTIC MANY-BODY MODEL

T. TANIGAWA[1], M. MATSUZAKI[2], and S. CHIBA

There is growing interest in pairing correlation in hadronic matter due to a close relationship between properties of neutron stars and its interior superfluidity. Superfluidity inside neutron stars affects, for instance, heat capacity and neutrino emissivity. These quantities relate to the cooling processes of neutron stars. Nucleon pairing has been therefore investigated extensively so far. In addition, since many studies predict that various hyperons may appear in the inner core region of the stars, the ΛΛ pairing has been studied by two groups recently [1, 2]. The hyperon pairing affects the properties of neutron stars through, for example, suppression of the hyperon direct URCA processes. Their studies were done using nonrelativistic frameworks (with different approximations from each other). Meanwhile, recent investigations on baryonic composition of the stars are often performed using relativistic approaches such as a relativistic mean field (RMF) model.

Our aim of this study is to explore within a relativistic model an effect of Dirac effective mass [3] of Λ hyperons on the ΛΛ pairing correlations in binary mixed matter composed of Λ hyperons and nucleons. As is well known, in a particle-hole (*p-h*) channel, cancellation between large Lorentz scalar and vector fields provides a proper saturation mechanism of nuclear matter in the relativistic models. The former scalar fields are responsible for decrease of baryon masses; the decreased mass are called the Dirac effective mass. At the same time, such a covariant description may participate also in the pairing correlation in some means. This is an important issue of the study of the neutron star matter with complex composition of baryons using relativistic models. Therefore, we study the ${}^1S_0$ ΛΛ pairing in binary mixed matter of nucleons and Λ hyperons. We use the relativistic Hartree-Bogoliubov (RHB) model, in which density dependence of a relativistic one-boson-exchange interaction (we call it "RMF interaction") is automatically taken into account due to the covariant treatment. The Λ hyperons are immersed in pure neutron matter or symmetric nuclear matter that is treated as a background. Chemical equilibrium is neglected for the sake of simplicity. The density-dependence inherent in relativistic models may lead to a novel behavior of the pairing gap: Since pairs are formed in medium, medium effects on a particle-particle (*p-p*) channel interaction should be considered. In the RHB model, the mass decrease mentioned above may change the pairing gap to some extent in comparison with that obtained with the bare masses.

Figure 1 shows the resulting ${}^1S_0$ ΛΛ pairing gap at the Fermi surface in pure neutron matter of densities ρ_N at 0, ρ_0, $2.5\rho_0$, and $5\rho_0$, where ρ_0 is the saturation density of symmetric nuclear matter. Contrary to the results obtained by Balberg and Barnea [1], the ΛΛ pairing gap becomes suppressed as the neutron density increases. At $\rho_N = 2.5\rho_0$, where Λ hyperons already appear in some models of neutron stars [4], the maximal pairing gap is about 0.15 MeV. Note that results for background of symmetric nuclear matter are not presented in this report because they just present slight differences from those for background of pure neutron matter.

[1]Japan Society for the Promotion of Science and Advanced Science Research Center, JAERI
[2]Department of Physics, Fukuoka University of Education

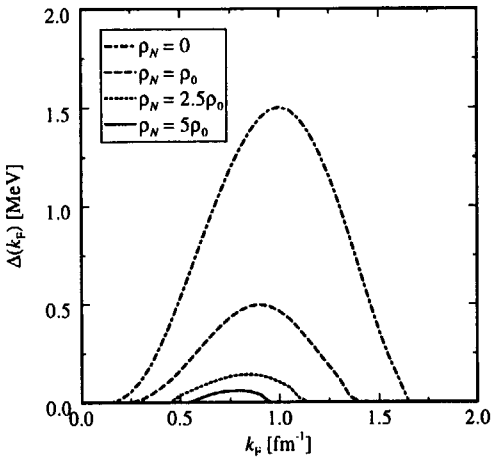

Figure 1: ΛΛ pairing gap at the Fermi surface of Λ hyperons, for pure neutron background densities $\rho_N = 0$, ρ_0, $2.5\rho_0$, and $5\rho_0$.

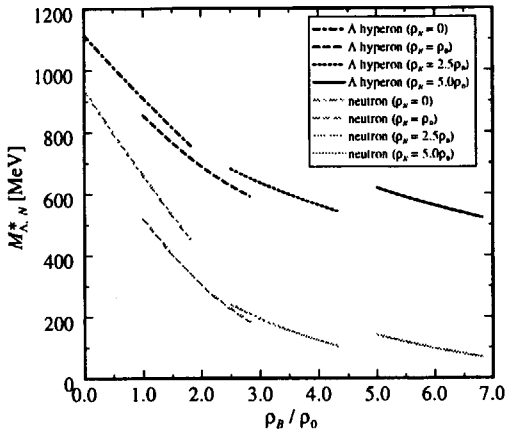

Figure 2: Effective masses of Λ hyperons and neutrons for pure neutron background densities $\rho_N = 0$, ρ_0, $2.5\rho_0$, and $5\rho_0$.

Figure 2 shows the density dependence of baryon effective masses, M^*_N and M^*_Λ, as functions of the total baryon density ρ_B. The background neutron densities are fixed here, so that variations in ρ_B correspond to those in the Fermi momentum of Λ hyperons. We obtain the values qualitatively similar to the ones shown in, for example, Fig. 4 of Ref. [4], regardless of discontinuous jumps in the curves that stem from the neglect of chemical equilibrium. This result shows that the in-medium property of the phenomenological ΛΛ interaction used in this study is justifiable.

To summarize, we have investigated the ΛΛ pairing in binary mixed matter of nucleons and Λ hyperons using the RHB model with the phenomenological RMF interaction both in the *p-h* and the *p-p* channels. The effect of the background nucleons has been naturally incorporated into the *p-p* interaction through the *self-consistent* Dirac effective mass of Λ hyperons in the Λ spinor. We have found that the value of the ΛΛ pairing gap becomes suppressed as the background nucleon density increases. This result is opposite to that reported in Ref. [1], in which the medium effect of different origin from the present study was introduced. Our result is traced back to the Lorentz covariant formulation inherent in the relativistic models. This automatically ensures another "medium effect" that the nonrelativistic models are lacking in. As for the hyperon pairing in neutron star matter, it is likely that complex composition of baryons affects relevant scalar boson fields, namely, the Dirac effective masses of the baryons. We must introduce other hyperons and a condition of the chemical equilibrium into the present model to construct a fully self-consistent model of the baryon pairing. Work in this direction is under progress.

References

[1] S. Balberg and N. Barnea, Phys. Rev. C **57** (1998) 409.

[2] T. Takatsuka and R. Tamagaki, Prog. Theor. Phys. **102** (1999) 1043.

[3] M. Jaminon and C. Mahaux, Phys. Rev. C **40** (1989) 354.

[4] J. Schaffner and I. N. Mishustin, Phys. Rev. C **53** (1996) 1416.

5.4 COSMIC CLOCK BY ^{190}Pt

T. HAYAKAWA[1,2], T. SHIZUMA, T. KAJINO[1,2]

Nuclear cosmochronometers provide an advance of the chronology of the Solar System and chemical evolutions of the Galaxy[1]. It is considered that the p-process nuclides were synthesized by photodisintegration reactions in supernova explosions[2,3]. A few p-process cosmic clocks whose half-lives are as long as the age of the Solar System are known[4]. We here propose a new chronometer of the p-process and present a calculated result of the mean age of the p-process which occured before the Solar-System formation using the Solar-System abundance. Since it is considered that the p-nuclei were produced from the progenitor s-nuclei rich seed in supernova explosions, there may be correlations in the abundances between p- and s-process isotopes. We calculated the ratio of the p-nuclei to the s-nuclei, which are two neutron-rich isotopes to the p-nuclei, for three isotopes of Os, Pt and Hg, and thereby we found that these ratios show good systematic values. The ground state of the ^{190}Pt nucleus, which is pure p-nucleus, is unstable against α-decay to ^{186}Os (half-life of 650 Gyr). With calculating the initial abundance of ^{190}Pt by using the systematic ratios of the p-nuclei to s-nuclei, we can use the ^{190}Pt-^{192}Pt system as a new cosmic clock of the p-process. Fig. 1 shows the calculation result using the average value of systematic ratios.

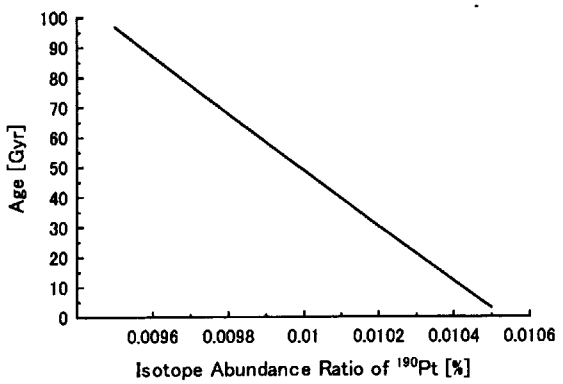

Fig. 1 The mean age of the p-process calculated by the clock of ^{190}Pt-^{192}Pt.

Taking the abundance of 0.01%, we obtained the result of 49 Gyr as the mean duration time of the p-process, which is much longer than the age of the Universe. We would like to stress that the age highly depends on the present abundance of ^{190}Pt. Replacing the abundance of 0.01% with 0.0104%, we obtained an age of 12 Gyr, which is shorter than the Galaxy age.

Reference

[1] W.A.Fowler, Rev. Mod. Phys. 55 (1957) 149.
[2] M.Arnould, Astron. Astrophys. 46 (1976) 117.
[3] S.E.Woosley and W.M.Howard, Astrophys. J. Suppl. 36 (1978) 285.
[4] J.Audouze and D.N.Schramm, Nature 237 (1972) 447.

[1]Japan Atmoic Energy Research Institute
[2]National Astronomical Observatory

5.5 MASS-MODEL DEPENDENCE OF R-PROCESS ABUNDANCE PATTERN IN A DYNAMICAL SNeII MODEL-CALCULATION

S. CHIBA, T. MARUYAMA, T. KAJINO[1] M. TERASAWA[2], H. KOURA[3],
T. TACHIBANA[4]G. J. MATHEWS[5] and K. OTSUKI[5]

Elements produced by the rapid neutron-capture process, the r-process, are important fingerprints of one of the most dramatic events in the universe[1], namely the type II supernovae (SNeII) or neutron star (NS) - NS mergers. Both kinds of events can provide environments with high neutron densities and high temperature, so heavy elements such as actinides and beyond are produced through highly unstable nuclei near the neutron drip-line via a chain of neutron capture reactions. Therefore, studies on the r-process give us unique and indispensable information from the astrophysical and nuclear/hadron physics points of view. For example, it is possible to determine the age of the progenitor events that produce the r-process nuclei since the r-processes occur in a time scale of around ms to 100ms. On the other hand, the r-process abundance pattern is sensitive to the physical condition of the site where it is cradled. This gives a critical information on, e.g., the equation-of-state of hadron/nuclear matter. Furthermore, the masses, structure and reaction mechanisms involving nuclei near the drip line can be inferred from the study of the r-process.

Actual r-process calculations associated with SNeII are usually carried out in two different approaches, namely a model-independent static approach and a dynamical one which follows the expansion of matter. Here we report our results on the r-process abundance pattern in the latter approach. We follow exactly the same method developed by Terasawa *et al.*[2]; the same nuclear- and weak-reaction rates, the same beta-decay rates, and the same SNeII expansion trajectory under the neutrino-driven wind were employed except for use of several different mass tables.

Figure 1 compares the solar r-process abundance pattern with those calculated by using various mass models; a table employed by Terasawa *et al.* (labeled as NAO), Terasawa's table partly replaced by Audi-Wapstra experimental one[3] where data are present in the latter (NAO+AWM95), Hilf et al.[4] (HGT), HGT table party replaced by Audi-Wapstra (HGT+AWM95), Koura et al.[5] (KUTY00), KUTY00 party replaced by Audi-Wapstra (KUTY00+AWM95), Finite-Range Droplet Model[6] table partly replaced by Audi-Wapstra (FRDM+AWM95), Hartree-Fock-BCS1[7] table party replaced by Audi-Wapstra (HFBCS1+AWM95) and Hartree-Fock-Bogoliubov[8] table party replaced by Audi-Wapstra (HFB2+AWM95). The calculated abundance data are normalized at the 3rd peak region (A $\sim$ 200). We can see interesting similalities and differences. Firstly, all the mass models can produce nuclei up to the actinide region, and 3 prominent peaks at A $\sim$ 80, 130 and 200 are present. Secondly, it is interesing to notice that inclusion of Audi-Wapstra data changes the abundance pattern drastically for NAO mass table, while such a change is milder for KUTY00 and HGT masses. The reason of such a drastic impact of the Audi-Wapstra table on NAO mass table is due to change of mass of a specific light nuclei. This is an important indication of using accurate nuclear data as much as possible.

[1]National Astronomical Observatory of Japan, [2]University of Tokyo, [3]RIKEN, [4] Waseda University, [5]University of Notre Dame

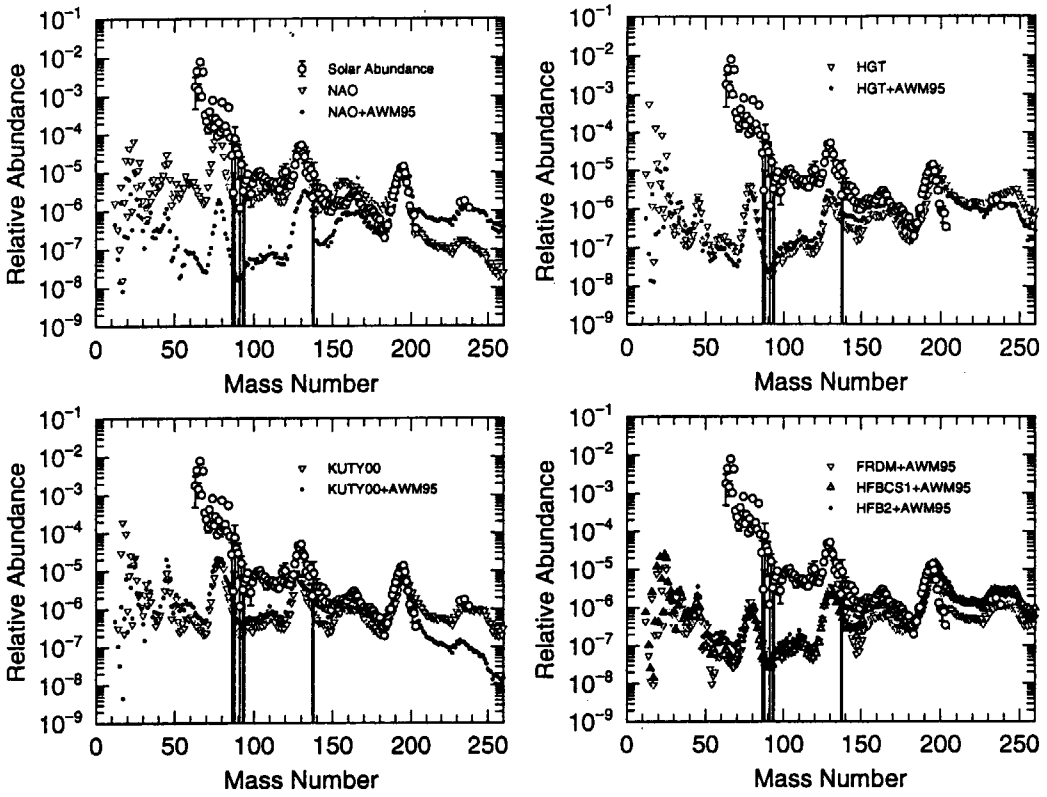

Figure 1: R-process abundance patterns calculated with various mass models compared to solar r-process abundance.

In Fig. 2, production ratios at 5 seconds after the temperature decreases from T_9=9 are shown for several pairs of nuclei relevant to nucleo-cosmochronology. Pairs of actinide/rare-earth nuclei have huge dispersions depending on mass models, while ratios such as rare-earth/rare-earth and actinide/actinide do not vary much. Therefore it will be useful to use nuclear pairs of same mass region to infer the age of the progenetor events[9].

References

[1] F.-K. Thielemann *et al.*, astro-ph/9802077(1998).
[2] M. Terasawa *et al.*, ApJ **562**(2001)470.
[3] G.Audi and A.H.Wapstra, Nucl. Phys. **A595**(1995)409.
[4] E.R. Hilf *et al.*, Proc. 3rd Int. Conf. on Nuclei far from Stability (Geneva: CERN), 76-13(1976)142.
[5] H. Koura *et al.*, Nucl. Phys. **A674**(2000)47.
[6] P. Möller *et al.*, At. Data Nucl. Data Tables 59(1995)185.
[7] S. Goriely *et al.*, At. Data and Nucl. Data Tables **77**(2001)311.
[8] M. Samyn *et al.*, Nucl. Phys. **A700**(2001)142.
[9] K. Otsuki *et al.*, New Astronomy (2003), in press.

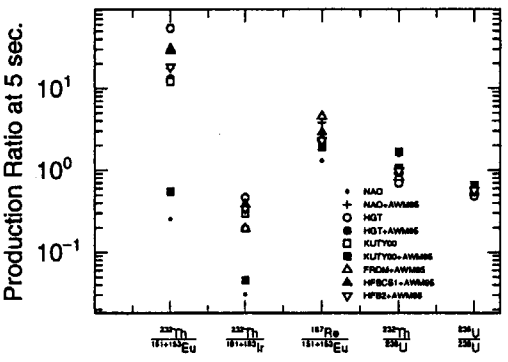

Figure 2: Ratios of several r-process nuclei at 5 seconds after T_9 = 9 calculated with various mass models.

This is a blank page.

6. Atomic Physics and Solid State Physics

This is a blank page.

6.1 HIGH-RESOLUTION ZERO-DEGREE-ELECTRON SPECTROSCOPY OF HIGHLY CHARGED OXYGEN IONS

K. KAWATSURA[1], K. TAKAHIRO[1], M. SATAKA, M. IMAI[2], K. KOMAKI[3] and H. SHIBATA[4]

High-resolution Coster-Kronig (C-K) and auger electron spectra from highly excited states in high-energy collisions of Si, S, Ar, Sc and Ti ions with He and C-foil targets have been widely investigated experimentally and theoretically by our group [1-8]. In the present, we have measured C-K and K Auger electrons produced in 32 MeV O^{q+} (q = 3,4) + He collisions [9,10]. The experiments were performed at the tandem accelerator facility of the JAERI in Tokai. The details of the experimental set up for zero-degree electron spectroscopy have been described before [1,2]. The primary O^{3+} and O^{4+} ion beams were produced by using the ECR ion source (ECRIS) installed at the high-energy terminal of the tandem accelerator.

Figure 1(a) and (b) show high-resolution ejected electron spectra produced by the collision of 32 MeV O^{4+} with a He target. Experimental results for 32 MeV O^{3+} + He collisions will be discussed but these electron spectra are not shown. In such a high-energy collision, the K Auger spectrum as shown in Fig. 1(b) is pure and simple. It is found that the peak positions of Auger transitions agree well with the results of 10 MeV O^{4+} + He collisions by Bruch *et al.* [11] and 10~28.5 MeV O^{4+} + He collisions by Lee *et al.* [12]. The intensities of Auger transitions depending on the fraction of incident metastable ions are different from each other. We have deduced a metastable fraction of incident O^{4+} ions of around 50 % for present experiment [9]. It is useful to know the metastable fraction of an incident beam from the ECRIS. Figure 1(a) shows the Coster-Kronig electrons from O^{4+} $1s^2 2pnl$ states which were produced by electron excitation process. The representative peaks are assigned to a series of $1s^2 2pnl - 1s^2 2s\varepsilon l$ (n = 6-11) C-K transitions. Vertical bars indicate line positions obtained by,

$$E_n = \Delta E \quad Q^2 R_y / n^2,$$

where E_n is the C-K electron energy, n is the principal quantum number, ΔE is the energy difference between the initial and final states of the ion core configuration, Q is the effective charge of the O^{5+} $1s^2 2p(^2P)$ ion core, and R_y is the Rydberg energy(13.606 eV). The present C-K spectrum [9,10] shows different l distributions from those produced by the low-energy collision of 60 keV O^{6+} with a He target [13-16], where the two-electron capture processes of He-like O^{6+} ions from the target He atom play a major role. These capture processes have also produced the Auger electrons from O^{4+} $1s^2 3lnl$ states. On the other hand, in the present case, the O^{4+} $1s^2 3lnl$ states could not be formed via electron excitation processes [9,10].

[1] Department of Chemistry and Materials Technology, Kyoto Institute of Technology
[2] Department of Nuclear Engineering, Kyoto University
[3] Institute of Physics, Graduate School of Arts and Sciences, University of Tokyo
[4] Research Center for Nuclear Science and Technology, University of Tokyo

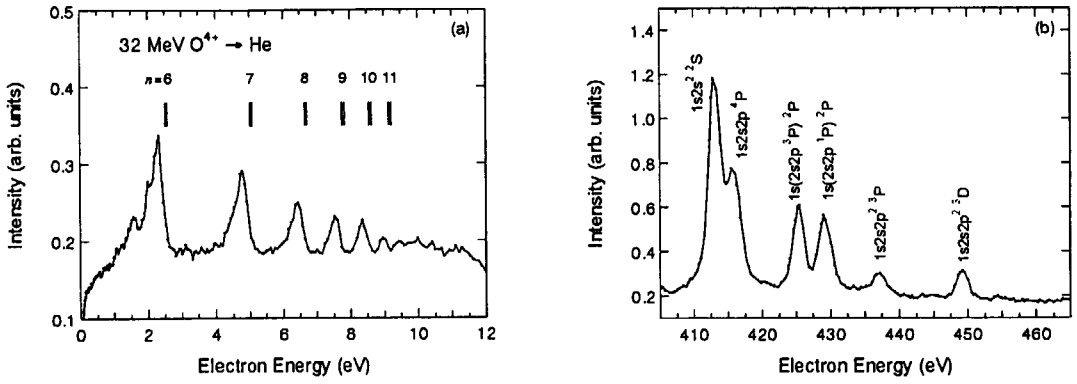

Fig. 1. Spectra of electrons ejected at 0° in collisions of 32 MeV O^{4+} on He. (a) Coster-Kronig electron spectrum and (b) K Auger electron spectrum. Energy scale refers to the projectile rest frame.

In summary, we have measured ejected electron spectra for 32 MeV O^{3+} and O^{4+} ions on a He target, though those from 32 MeV O^{3+} + He collisions are not shown. It is found that the $1s^2 2pnl$ states with relatively low angular momenta are excited in the O^{4+} ion collisions while the$1s^2 2s2pnl$ states with higher ones in the O^{3+} ion collisions. Angular momentum distribution for $1s^2 2pnl$ C-K transitions is also discussed and compared with the previous results for low energy collision system [13-16]. K Auger electron spectra produced in 32 MeV $O^{3+,4+}$ + He collisions qualitatively agree with the previous results [11,12]. However, higher-resolution measurements using a wide variety of charge states (q = 2-6) of O^{q+} ions on a He target are needed for more detailed analysis on excitation and ionization processes in high energy collision regime. This work was supported in part by the JAERI Tandem co-operation program.

References

[1] K. Kawatsura *et al.*, Nucl. Instr. and Meth. **B48** (1990) 103.
[2] K. Kawatsura *et al.*, Nucl. Instr. and Meth. **B53** (1991) 421.
[3] M. Sataka *et al.*, Phys. Rev. **A44** (1991) 7290.
[4] K. Kawatsura *et al.*, Nucl. Instr. and Meth. **B124** (1997) 381.
[5] M. Sataka *et al.*, J. Phys. **B35** (2002) 267.
[6] M. Sataka *et al.*, Phys. Rev. **A65** (2002) 052704.
[7] M. Imai *et al.*, Nucl. Instr. and Meth. **B193** (2002) 674.
[8] M. Imai *et al.*, Abstract of ICPEAC2003 (Stockholm, 2003) We194.
[9] K. Kawatsura *et al.*, Nucl. Instr. and Meth. **B205** (2003) 528.
[10] K. Kawatsura *et al.*, Abstract of ICPEAC2003 (Stockholm, 2003) Mo145.
[11] R. Bruch *et al.*, Phys. Rev. **A35** (1987) 4114.
[12] D.H. Lee *et al.*, Phys. Rev. **A46** (1992) 1374.
[13] N. Stolterfoht *et al.*, Phys. Rev. Lett., **57** (1986) 74.
[14] F.W Meyer *et al.*, Nucl. Instr. and Meth. **B 24/25** (1987) 106.
[15] N. Stolterfoht *et al.*, Nucl. Instr. and Meth. **B40/41** (1989) 28.
[16] Y. Kanai *et al.*, Nucl. Instr. and Meth. **B98** (1995) 81.

6.2 HEAVY-ION IRRADIATION EFFECT OF THE SUPERCONDUCTING PROPERTIES OF MULTI-LAYERED (Cu,C)$Ba_2Ca_{n-1}Cu_nO_{4+2n-\delta}$ SUPERCONDUCTOR

H.KITÔ[1], A.IYO[1], M.HIRAI[2], A.CRISAN[3], M.TOKUMOTO[1], S.OKAYASU, M.SASASE, M.SATAKA, H.IHARA[1] and Y.TANAKA[1]

To further enhance the critical current density (J_c) and irreversibility field (H_{irr}) of multi-layered ($Cu_{1-x}C_x$)$Ba_2Ca_{n-1}Cu_nO_{4+2n-\delta}$ (n=4; hereafter described as (Cu,C)-1234) superconductor, pinning centers were introduced by heavy-ion irradiation. This (Cu,C)-1234 phase has a layered structure composed of stacking of planes, BaO-MO-BaO-CuO_2-$(CaCuO_2)_2$ where M site is shared by Cu and CO_2 with nearly 1:1 ratio. The occupation of Cu at the M site in this plane is a characteristic common to (Cu,C)-12(n-1)n and Y-123 both of which have high critical temperature (T_c), and H_{irr}.

For the practical applications of high T_c oxide superconductors such as superconducting magnets, the J_c must be high enough in applied magnetic fields, which requests the introduction of effective pinning centers. One of the methods of introducing pinning centers is heavy-ion irradiation. Especially, Cu-based superconducting cuprates could be promising candidates for the application of the next generation because of high T_c, high J_c and high H_{irr} [1].

We research on dependence of a fluence for the J_c and the H_{irr} of the polycrystalline (Cu,C)-1234 by heavy-ion irradiation. The polycrystalline (Cu,C)-1234 sample was prepared by the solid state reaction method using the high-pressure apparatus (3.5 GPa, 1173 ~1373 K for 2 hours). Nominal composition was ($Cu_{0.5}C_{0.5}$)-1234. Lattice parameters are determined to be a = 0.3860 nm and c = 1.796 nm by X-ray powder diffraction.

Polycrystalline samples were cut and polished into thin discs less than 100 μm in thickness. The polycrystalline samples were irradiated with Au^{15+} ions (240 MeV energy) at various fluence (3.5×10^{10}, 6.5×10^{10}, 1×10^{11}, 2.5×10^{11} and 5×10^{11} ions/cm^2) at room temperature using a Tandem accelerator at JAERI. The ion energies were estimated from the range-energy relations proposed by Ziegler. For the heavy-iron irradiated (Cu,C)-1234 samples, the length of the ion tracks was determined by the stopping powers calculated using TRIM 2000 codes. The tracks of the Au^{15+} ion of 240 MeV were 12.2 μm for (Cu,C)-1234, this value being smaller than the thickness of the samples, so that all of the irradiated ions stop inside of the samples.

For the unirradiated and heavy-ion irradiated polycrystalline (Cu,C)-1234 samples, the intragrain J_c was determined from M-H curves using Bean's critical state model. Figure 1 show the heavy-ion irradiation dependence for the J_c at 5K, 20K and 77K of (Cu,C)-1234 [2]. With increase of the fluence, J_c shows a rapid increase and reaches a maximum value, 4.1×10^6 A/cm^2 (77 K and 1T) for the fluence of 1×10^{11}

[1]National Institute of Advanced Industrial Science and Technology (AIST) and CREST, Japan Science and Technology Corporation (JST)
[2]Tokyo University of Science [3]University of Bath

ions/cm^2 and above which it decreases slowly. The maximum value of H_{irr}(77K), determined by extrapolating J_c curves to a 10^3 A/cm^2 criterion, is about 14.5 T for the 2.5×10^{11} ions/cm^2. This value is comparable with that of Nd-123 with best pinning center engineering [3].

The α value in equation $H_{irr}(T)= H_{irr}(0)(1-T/T_c)^{\alpha}$ decreases from 2.97 for un-irradiated sample to 1.87 for the fluence of 1×10^{11} ions/cm^2 (see Figure 2). The exponent α of heavy-ion irradiated (Cu, C)-1234 is smaller than that of Hg-1223 [4], but slightly larger than α of Y-123 and Yb-123 for Au^{15+} ions irradiated sample [5, 6]. These results indicate the possibility of J_c (77K and 1T) enhancement and reaching a high H_{irr}(77K) at the fluence of the 1.5×10^{11} ions/cm^2. Heavy-ion irradiation was much effective to introduce strong pinning centers in (Cu,C)-1234 and to control or optimize J_c and H_{irr} values of (Cu,C)-1234. These results indicate the possibility of further enhancement of J_c and reaching a high H_{irr}.

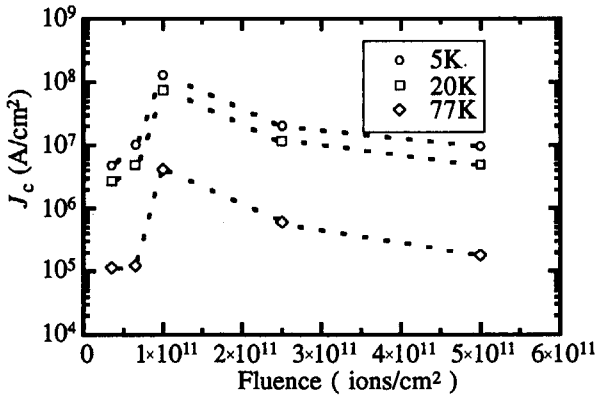

Fig. 1. The heavy-ion irradiation dependence for the critical current density J_c at 5K, 20K and 77K of (Cu,C)-1234.

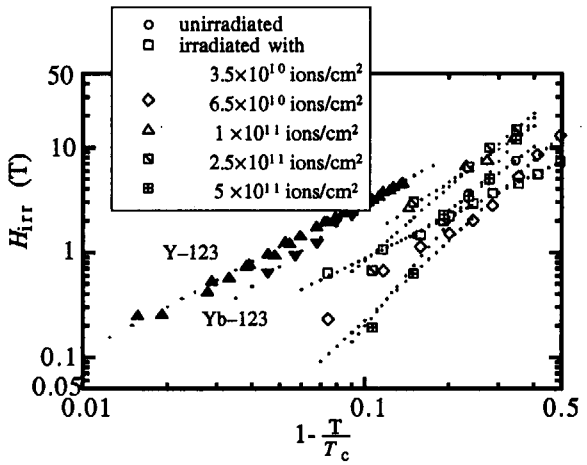

Fig. 2. H_{irr} versus $1-T/T_c$ of (Cu,C)-1234.

References

[1] H.Ihara: Kotaibuturi **35**(2000) 301 (in Japanese).

[2] H.Kitô, A.Iyo, M.Hirai, A.Crisan, M.Tokumoto, S.Okayasu, M.Sasase, M.Sataka, H.Ihara, Y.Tanaka: The 14th International Symposium on Superconductivity (ISS2002) PCP-13.

[3] N.Harish Kumar, Th Wolf and H.K pfer : Supercond. Sci. Technol. **13**(2000)1356.

[4] U.Welp, G.W.Crabtree, J.L.Wagner and D.G.Hinks: Physca **C218**(1993) 373.

[5] C.-Q.Jin, R.Puzniak, Z.-X.Zhao, X.-J. Wu, T.Tatsuski, T.Tamura, S.Adachi, K.Tanabe, H.Yamauchi and S.Tanaka : Phys. Rev. **B61**(2000)778.

[6] T.Nakane, Y.Yasukawa, E.S.Otabe, T.Matsushita, M.Karppinen and H.Yamauchi: Physca **C338**(2000) 25.

6.3 IRRADIATION EFFECTS ON MgB_2 SINTERED SAMPLES

S. OKAYASU, M. SATAKA, H. IKEDA[1] and R. YOSHIZAKI[1]

We investigated irradiation effects on sintered MgB_2 samples to improve the pinning properties of this new coming superconducting material for its practical applications.

Synthesis of MgB_2 was accomplished by a solid state reaction. Starting materials for the synthesis were high purity powders Mg and B. They were mixed and ground, then pressed into a small compound rod for sintering process. The rod was placed into a stainless tube, and the tube was put into a tube furnace. The sample was then sintered at 1193 K for 2 hours. Throughout the sintering process, high purity argon gas was flown in the furnace to avoid unexpected reactions such as MgO or BN. After the sintering, the sample was cut into small pieces. The superconducting properties were measured by a commercial SQUID magnetometer (MPMS, Quantum Design). We obtained the following results.

Electron irradiation reduces the bulk pinning properties of this material[1,2]. Electron irradiation usually introduces point-like defects into the interior of a crystal. For polycrystallines or sintered materials, however, grain boundaries are affected much more with the irradiation because combining energies within the boundaries are smaller than the binding energies knocking atoms out from inside crystals. Thus, electron irradiation acts on the degradation of coupling in the boundaries, instead of introducing pinning centers into the interior of the crystal. Considering the fact that the degradation of pinning with the irradiation coincides with the degradation of coupling within boundaries, pinning on the boundaries plays important roles for the bulk pinning of this material. In other word, it is very important to improve coupling within the boundaries for improvement of pinning for the bulk material.

A comparison of irradiation effects between neutron and high-energy boron-ion (45MeV) irradiation on MgB_2 bulk samples was investigated[3]. The irradiation doses were $8x10^{17}$ n/cm^2 (thermal neutron) and $2x10^{15}$ ion/cm^2 (B ion), respectively. Although the amount of defects were almost the same of the order (10^{-2} dpa) for both two cases, irradiation effects on superconducting properties of the material were completely different.

No change on the transition temperature Tc can be observed for the boron irradiated case, but a significant decrease for the neutron. This is because that leading process of defect formation is entirely different between the two cases. For the B-irradiation, nuclear collisions between bombarding ions and lattice atoms are dominant for the defect formation processes. Primary knock-on atoms flick out about 10 surrounding atoms and defect will be formed. In this situation, however, the flicked atoms remain near their original positions.

[1]Univ. of Tsukuba, Tsukuba, Ibaraki 305-8577, Japan

The overall crystal structure may not be damaged severely.

For the neutron case, on the other hand, the defect formation is mainly originated in the most probable nucleus reaction $^{10}B(n,\alpha)^{7}Li$. A ^{10}B atom captures a thermal neutron (cross section $3.8x10^{-25}$ m^2), and this process makes two high energetic particles, 1.7MeV-α and 1MeV-^{7}Li. It is worth emphasizing that the boron site is certainly affected with the reaction. As the result of this reaction, the boron atom in the crystal structure is replaced to a lithium atom, and band structure of MgB_2 will be affected seriously. M. Eisterer et al. compared irradiation effects between fast and thermal neutron [4]. Due to a low nuclear reaction cross section between a fast neutron and a boron atom or a magnesium atom, defect formation process of the former is similar to B-irradiated case, i. e. nuclear collisions. No decrease of Tc is observed for the fast neutron irradiation. The transition temperature decreases for the thermal neutron case only. It is obvious that the nuclear reaction above mentioned plays an important role for the deterioration of superconductivity of this material. Thus the following important conclusion is derived that the B-originated fermi surfaces are important for the appearance of the superconductivity on MgB_2. This result is consistent with calculations for the band structure of this material representing superconducting gaps derived from boron band [5].

Columnar defects introduced by heavy ion irradiation are well known as strong pinning centers to greatly improve pinning properties of high-Tc superconductors [2]. It is worth confirming the effectiveness of the heavy ion irradiation on the pinning properties for the new material. Heavy ion irradiation was accomplished at the TANDEM accelerator in JAERI with 200MeV Au ions and the ring cyclotron in RIKEN with 3.54GeV Xe ions. The irradiation dose was $1x10^{11}$ ions/cm^2 corresponding to the matching field B_ϕ= 2 tesla. For both cases, no enhancement of the critical current densities Jc in the lower field region can be observed in any temperature range. However, the irreversibility field B_{irr} shifts to the higher field region. For high-Tc superconductors, columnar defects improve both the magnitude of the Jc and the B_{irr}. For MgB_2, on the other hand, they improve only the latter. It is unlikely that the columnar defect formation will occur in MgB_2 due to the large number of carrier densities. There is no doubt, however, that the defects introduced by the irradiation act as pinning centers. The improvement of pinning process is still unclear, and further investigation is needed.

References

[1] Okayasu S. et.al., Physica **C 378-381** (2002) 462.
[2] Okayasu S. et.al., Physica **C 382** (2002) 104.
[3] Okayasu S. et. al., J. of Low Temp. phy. **131**(2003).
[4] M. Eisterer et al., Supercond. Sci. Technol. **15** (2002) L9.
[5] H.J. Choi et al., cond-mat/0111183.

6.4 LATTICE PARAMETER CHANGE DUE TO ELECTRONIC EXCITATION IN OXYGEN-DEFICIENT $EuBa_2Cu_3O_y$

N. ISHIKAWA, A. IWASE, Y. CHIMI, T. HASHIMOTO[1] and O. MICHIKAMI[1]

It is well-known that basically ion-tracks are easily produced along ion paths in an insulating solid, while in metals or other good conductors it is difficult to produce them [1,2]. Fleischer et al. [1] have pointed out that electrical resistivity is one of the appropriate parameters to judge the sensitivity of materials to irradiation-induced electronic excitation. The reason for the difficulty of producing tracks in good conductors is based on the belief that free electrons can rapidly and efficiently smear out the perturbation caused by ion irradiation. In order to test this qualitative explanation for the sensitivity to electronic excitation, we performed irradiation of oxide films of $EuBa_2Cu_3O_y$ (EBCO) having different oxygen content. In EBCO oxygen can be controlled in the range from y=7 to 6 by thermal annealing at temperature of about 500°C without changing the stoichiometry of other elements. The interesting feature of EBCO is that electrical resistivity can be varied over a wide range by changing its oxygen content. Electrical resistivity of EBCO films with oxygen content of y=7 is in the order of 10^{-4} Ωcm at room temperature and exhibits superconductivity at low temperature. When oxygen content decreases down to y=6, carrier density rapidly decreases, and as a result the material becomes insulating. It is expected that insulating EBCO with oxygen content of y=6 is much more sensitive to the irradiation-induced electronic excitation than conducting EBCO with oxygen content of y=7, if the electrical resistivity solely determines the electronic excitation effects as Fleischer pointed out. Based on this recognition, we have investigated the effect of electronic excitation on lattice parameter in EBCO with different oxygen content irradiated with energetic heavy ions (125MeV Br, 200MeV I and 200MeV Au) at room temperature.

Thin films of oxide superconductors EBCO about 300nm thick were prepared on MgO substrates by the dc magnetron sputtering method. The films were c-axis oriented; the c-axis direction corresponded to the direction of film thickness. As-sputtered films were expected to have an oxygen content of y=7, since superconducting transition temperature for these films was around 89K. The oxygen-deficient samples were prepared by annealing the as-sputtered samples at 550°C in the mixture gas of $Ar+O_2$(7%). By changing the annealing time, samples with oxygen content of y=6.6 and 6.1 were prepared. The oxygen content was determined from the c-axis lattice parameter which is sensitive to oxygen content [3-5]. The electrical resistivity of the samples was measured by a standard four-probe method. Both oxygen-deficient samples and as-sputtered samples were irradiated with 125MeV ^{79}Br, 200MeV ^{127}I and 200MeV ^{197}Au from the tandem accelerator at JAERI-Tokai.

The combination of the oxygen content of the samples and the irradiating ions are listed in Table 1. Resistivity at room temperature before irradiation is also shown in the table. All of the irradiations were performed from the direction of film thickness at room temperature under the pressure of $<10^{-6}$ Torr. As all ion ranges were much larger than the film thickness, a possibility of ion-implantation can be ruled out. X-ray (Cu Kα) diffraction pattern was measured before and after irradiation. Fluence dependence of c-axis lattice parameter was investigated by measuring the irradiation-induced shift of the (005) peak.

[1] Iwate University

The electrical resistivity at room temperature for y=6.1 is about 3000 times larger than that for y=7, while that for y=6.6 is about 3 times larger than for y=7. Figure 1(a) shows the c-axis lattice parameter as a function of fluence for y=7 and for y=6.1 when irradiated with 200MeV Au. In Fig.1(b), the comparison is also made for irradiation with 125MeV Br. A linear increase in c-axis lattice parameter as a function of fluence is observed for all the cases. It is already known that the linear increase is always observed when EBCO with oxygen content of y=7 is irradiated with various swift heavy ions [6,7]. The linear increase in c-axis lattice parameter shows that each irradiating ion produces defects along its ion path, and the defects contribute to elongation of the c-axis lattice parameter. Our previous study shows that the contribution of electronic excitation to the increase in c-axis lattice parameter per unit fluence can be scaled with the primary ionization rate, dJ/dx, which is defined as the number of ionized atoms per unit path length. Figure 2 shows the comparison between the electronic excitation effect for EBCO with oxygen content of y=7 and that for EBCO with oxygen content of y<7. The value of $(\Delta c/c_o)/\Phi$ is defined as a slope of $\Delta c/c_o$ against Φ, where $\Delta c/c_o$ is a change in c-axis lattice parameter normalized by the c-axis lattice parameter before irradiation, and Φ the fluence. The contribution of electronic excitation is represented by $((\Delta c/c_o)/\Phi)_{electronic}=(\Delta c/c_o)/\Phi-((\Delta c/c_o)/\Phi)_{elastic}$, where $((\Delta c/c_o)/\Phi)_{elastic}$ is the contribution of elastic displacements and is obtained by irradiation experiment using ~1MeV ions [6]. In the case of the present irradiations, we can find that $((\Delta c/c_o)/\Phi)_{electronic}$ is almost the same as $(\Delta c/c_o)/\Phi$ [6,7]. The electronic excitation effect for y=7 shows a power-law behavior as indicated by the dotted line [6,7]. The data for oxygen-deficient EBCO samples also lie on the dotted line, although the electrical resistivity for y=6.6 is about 3 times larger than that for y=7, and that for y=6.1 is about 3000 times larger than that for y=7. This result suggests that the electrical resistivity of the materials is not a major parameter that determines the electronic excitation effect, indicating that the electrical resistivity does not necessarily represent the efficiency of smearing out the perturbation caused by the irradiation. Generally, electrical resistivity is inversely proportional to both carrier density and mobility of carriers. There are literatures [8,9] showing that mobility of carriers at room temperature is almost constant and carrier density drastically changes when oxygen content is changed from y=7 to y=6.3. This suggests that the mobility of carriers may be important for the sensitivity to electronic excitation. Further investigation is necessary to know whether it is generally true that the mobility of carriers rather than density of carriers is an important parameter to determine the sensitivity to irradiation-induced ionization.

References

[1] R.L. Fleischer, P.B. Price, R.M. Walker(Eds)., Nuclear Tracks in Solids, Principles and Applications (University of California Press, 1975).
[2] A. Audouard, E. Balanzat, S. Bouffard, J.C. Jousset, A. Chamberod, A. Dunlop, D. Lesueur, G. Fuchs, R. Spohr, J. Vetter, and L. Thomé, Phys. Rev. Lett., **65** (1990) 875.
[3]Ch. Krüger, K. Conder, H. Schwer, and E. Kaldis, J. Solid State Chem. **134** (1997) 356.
[4] W.R. McKinnon, M.L. Post, L.S. Selwyn, G. Pleizier, J.M. Tarascon, P. Barboux, L.H. Greene, and G.W. Hull, Phys. Rev. **B38** (1988) 6543.
[5] J.D. Jorgensen, B. W. Veal, A.P. Paulikas, L.J. Nowicki, G.W. Crabtree, H. Claus, and W.K. Kwok, Phys. Rev. **B 41** (1990) 1863.
[6] N. Ishikawa, Y. Chimi, A. Iwase, H. Maeta, K. Tsuru, O. Michikami, T. Kambara, T. Mitamura, Y. Awaya and M. Terasawa, Nucl. Instrum. Methods **B 135**(1998) 184.
[7] N. Ishikawa, A. Iwase, Y. Chimi, O. Michikami, H. Wakana, T. Hashimoto, T. Kambara, C. Müller, R. Neumann, Nucl. Instrum. Methods **B 193** (2002) 278.
[8]B. Wuyts, V.V. Moshchalkov, and Y. Bruynseraede, Phys. Rev. **B53** (1996) 9418.
[9]H. Minami and H. Uwe, Physica C **282-287** (1997) 1193.

Table 1 Combination of the oxygen content of the samples and the irradiating ions. Resistivity at room temperature before irradiation is also shown.

Oxygen content	Resistivity at room temperature before irradiation	Irradiating ion
y=7	4×10^{-4} Ωcm	125MeV Br, 200MeV I, 200MeV Au
y=6.6	1.2×10^{-3} Ωcm	125MeV Br, 200MeV I
y=6.1	1.3 Ωcm	200MeV Au

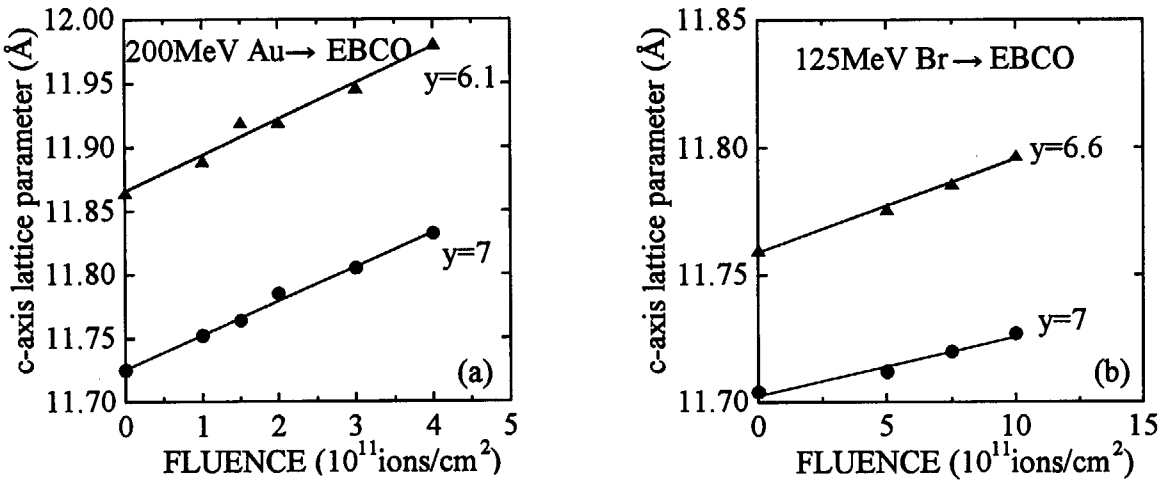

Fig.1 Fluence dependence of c-axis lattice parameter for the samples with oxygen content of y=7 and oxygen-deficient samples irradiated with (a) 200MeV Au and (b) 125MeV Br.

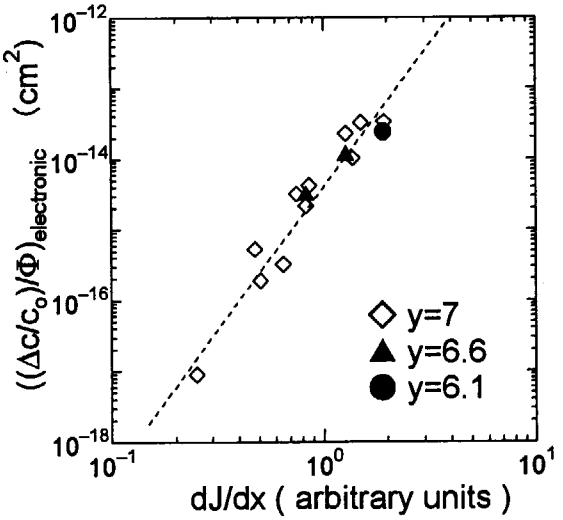

Fig.2 The contribution of electronic excitation to elongation of c-axis lattice parameter per unit fluence plotted as a function of the primary ionization rate for EBCO with various oxygen contents. The data obtained for EBCO with oxygen content of y=7 is quoted from ref. [7].

6.5 DEFECT STRUCTURES IN ION - IRRADIATED NICKEL AT LOW TEMPERATURE BY X-RAY DIFFUSE SCATTERING

N. MATSUMOTO, T. KATO, H. OHTSUKA, H.SUGAI, M. SATAKA and H. MAETA[1)]

Irradiation of materials with energetic heavy ions produces point defects such as vacancy-interstitial pairs and also displacement cascades containing high local concentrations of vacancy-interstitial pairs, and at ambient temperature theses vacancies and interstitials aggregated to form clusters such as dislocation loops. It is necessary to irradiate at low temperature that the defects can not migrate and measure physical properties of the defects such as at the low temperature. Especially, to study displacement cascades in the atomic energy materials is one of the most important problems [1]. Transmission electron microscopy (TEM) investigation of the production and thermal annealing of cascades have provided a considerable amount of information on this process. However, a few observations of TEM at low temperature have been carried out at 20K after the defect moved to change its original structure [2]. The cascade may be small size below the visibility limit of TEM. On the other hand, the x-ray diffuse scattering [3] is a powerful method to observe such a small defect studied nondestructively in bulk specimen at low temperature below 10K.

Close to the Bragg peaks the intensity of diffuse scattering (Huang diffuse scattering) is demonstrated by the long range part of the displacement field of the point defects and point like defect clusters . This Huang intensity has q-2 dependence, where the vector **q** is relative to **h** and scattering vector **k** is given by the sum of the reciprocal lattice vector **h,** (**k**= **h** + **q**). If the defects form cluster the distortion near the cluster such as dislocation loop or cascade may become large and the asymptotic or Stokes-Wilson scattering is observed farther away from the Bragg peak indicating q^{-4}-dependence. This scattering arises from local Bragg-like scattering from the strongly distorted region, for example, in the immediate vicinity of the dislocation loops. Therefore, the compressed region above and below such as an interstitial type loop (or cluster) gives to diffuse scattering at positive q ($q > 0$) and a vacancy type loop (luster) give rise to at negative($q < 0$) as a result of lattice relaxation into the volume of the missing plane [4]. From q-dependence of the diffuse scattering we can obtain the information of the point defects and large distorted defects (or clusters), indicating q^{-2} dependence and q^{-4} dependence, respectively. If the cascade will be present in the irradiated specimen, we will observe the diffuse scattering of the q-4 dependence from the irradiated specimen at low temperature.

High purity single crystal specimens of pure Ni were spark-cut from single crystals grown by the Czochoralski method. The size of all specimens is about $10 \times 5 \times 1$ mm^3. The specimens were irradiated below about 16K with 127 MeV iodine ions (I^{10+}) of fluence of 2.3×10^{13} ions/cm^2 by a tandem accelerator of JAERI. After the irradiation the specimens were transferred to the x-ray cryostat at below 35K. The measurements of the diffuse scattering near Bragg reflections have been performed with a four circle diffractometer using an 18 kW rotating x-ray anode with a wavelength of CuK α_1. The scattered intensities were always measured at 19K near the (200) reflection in the [100]

---

1)Hiroshima Kokusai Gakuin University

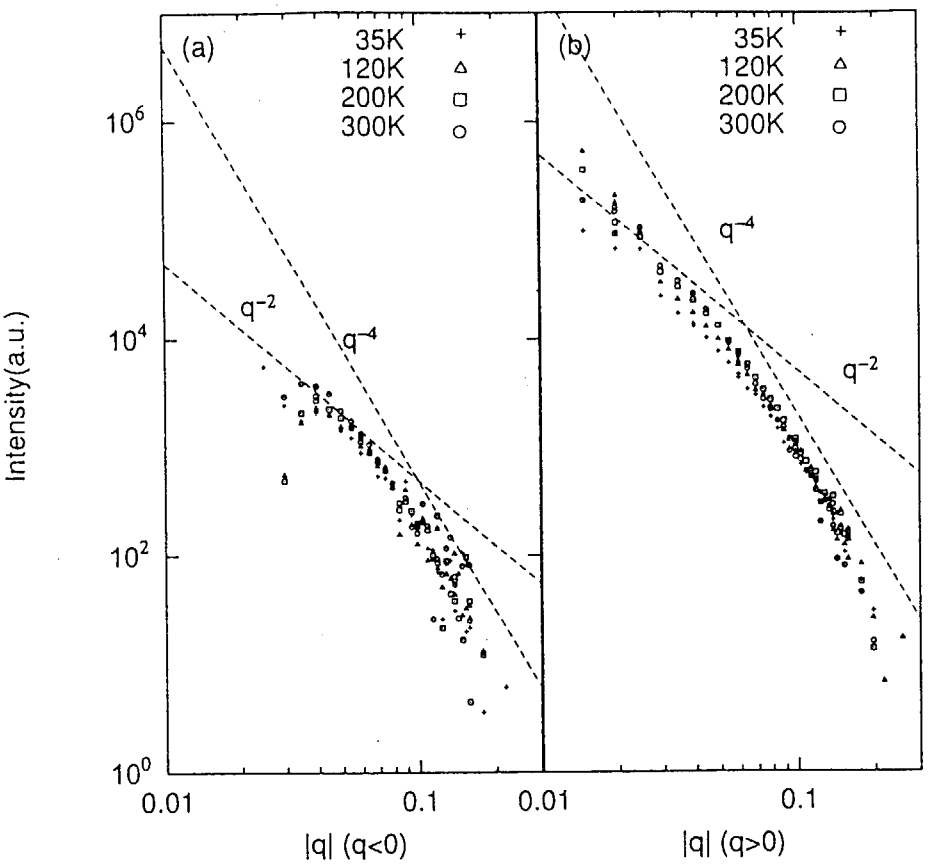

Fig.1 The q-dependence of diffuse scattering intensity I* in I^{10+} ions irradiated Ni at16K, measuring at 19K and isochronally annealings from 35K, 120K ,200K and 300K, respectively.

direction. The ions irradiated specimen was isochronally annealed from 35K, 120K, 200K and 300K. The diffuse scattering intensity was obtained by taking a difference between the intensity of the diffuse scatterings of the specimen before and after the irradiations. The intensities are plotted in Fig. 1 on a double logarithmic scale versus q. In the figure we can see both q^{-2} and q^{-4} dependences . At the q value where the q^{-2} dependence changes to q^{-4} the lattice is so heavily strained that the scattered x-ray wave comes out of phase [3]. We can roughly estimate average size of the clusters. From this figure one can roughly estimate the average size of clusters radius R_0 according to the relation $q_0 R_0 = 1$, where q_0 is the value at which the diffuse scattering intensity deviates from the q^{-4} dependence . We estimated the average size of cluster radius R_0 = 1.5 nm and 2.0 nm for interstitial type cluster and vacancy type clusters, respectively. Both interstitial and vacancy type clusters were observed at low temperature in ion irradiated Ni at low temperature, associated with the displacement cascades. The growth of the interstitial clusters below 200K and shrinkage of the clusters began below 300K. The vacancy clusters did not changes in size and density up to room temperature. More detailed analysis is now in progress.

References

[1] R.S.Averback : J.Nucl. Materials, **216**(1994) 49.

[2] Y.Shimomura, H.Fukushima and M.W.Guinan, J.Nucl.Mater. , **174**(1990) 210.

[3] P. Ehrhart, J. Nucl. Mat., **216** (1994) 170.

[4] P. Ehrhart, H. Trinkaus, B.C. Larson, Phys. Rev. ,**B 25** (1982) 834.

6.6 MEASUREMENT OF DIFFUSION CONSTANTS IN SOLIDS BY USING SHORT-LIVED RADIOTRACER OF ^{8}Li

S.C. JEONG[1], I. KATAYAMA[1], H. KAWAKAMI[1], H. ISHIYAMA[1], H. MIYATAKE[1], M. SATAKA, A. IWASE, S. OKAYASU, H. SUGAI, S. ICHIKAWA, K. NISHIO, Y. SUGIYAMA[2], M. YAHAGI[3], K. TAKADA[4] and M. WATANABE[4]

We have performed an experiment to measure the diffusion constants of Li in the sample of LiAl alloy, by using a α-emitting radiotracer of ^{8}Li ($T_{1/2}$=0.838s). The feasibility of the experimental method has been studied by simulation, showing that the time-dependent yields of the α-particles can be used as a measure of the diffusivity of the tracer in a non-destructive way [1]. The Li diffusion coefficients in LiAl have been measured in a wide range of temperature [2], and thus adopted it as an example of the sample in the experiment, providing good references for the experimental confirmation and calibration of the method.

The experimental set-up for the diffusion measurement is shown in Fig.1, installed nearly at the focal position of JAERI-RMS. The radioisotope of ^{8}Li was produced, by bombarding ^{7}Li of 24MeV on ^{9}Be target of 42μm in thickness. Separated by JAERI-RMS, the ^{8}Li beam of 14.6MeV with about 0.6MeV in FWHM was obtained with an intensity of 2500 particles/s by 30enA of ^{7}Li. The energy of ^{8}Li for implantation was further reduced to 4MeV by the energy degrader installed upstream, corresponding to the average implantation-depth of about 12μm from the front surface of the sample. One time sequence for the measurement consisted of the time-duration of 1.5s for implantation (beam-on) and of 4.5s for subsequent diffusion (beam-off). The beam-on and off operation was carried out by the beam shutter. The sample was set at 20°C (room temperature) before starting the measurement. The energies of α particles coming out of the sample were measured as a function of time by an annular solid-state detector (SSD). The sequence was repeated to obtain good statistics, where the time-zero is always at the beginning of the irradiation. We performed the measurement in the same way for the temperature of 150°C and 300°C, respectively.

[1] Institute of Particle and Nuclear Studies, KEK
[2] Nihon Advanced Technology
[3] Aomori University
[4] National Institute of Materials Science (NIMS)

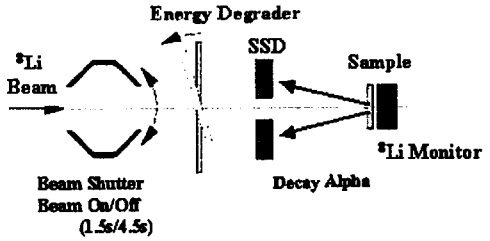

Fig.1 Experimental set-up

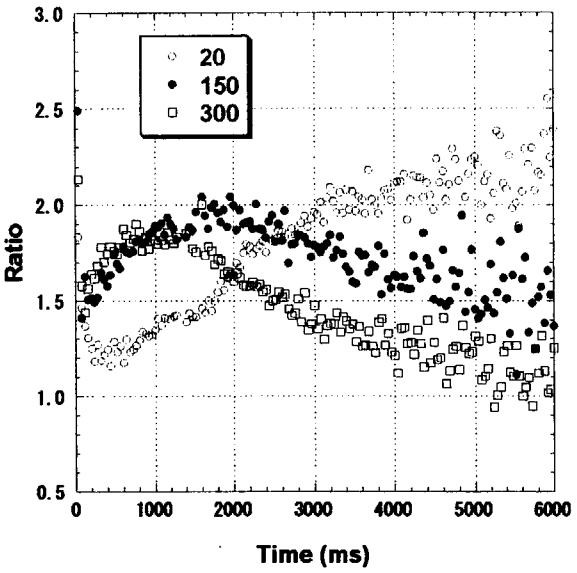

Fig.2 Normalized time spectra of α yields measured at the temperature of 20°C(○), 150°C(●) and 300°C(□), respectively. For the normalization, the growth-decay curve of the activity of ^{8}Li during the time sequence for the measurement was used.

The yield of α-particles with energies larger than 400keV showed different time-dependence according to the temperature of the sample. The observation implies that the time-dependence of α-yields is a good measure of the diffusivity of ^{8}Li in the sample, because the diffusivity depends on the temperature of the sample. By excluding the trivial time-dependence of the yields associated with the radioactivity of ^{8}Li during the measurements, we obtained the time spectra only depending on the temporal evolution of the profiles of diffusing ^{8}Li at a temperature of the sample. In Fig.2, the time spectra are represented by the ratios, yields of α- particles divided by those of ^{8}Li existing in the sample at the time of interest. If ^{8}Li does not diffuse at all, the spectra should be constant over time. By comparing the experimental time spectrum that is measured at a certain temperature, with results from the simulations, the diffusion coefficient could be finally obtained. The comparison is in progress.

References

[1] S.C. Jeong et al., Jpn. J. Appl. Phys., in press.

[2] J.C. Tarczon, W.P. Halpherin, S.C. Chen and O. Brittain: Mater. Sci. and Engineering A101 (1988) 99.

This is a blank page.

7. Radiation Effects in Materials

This is a blank page.

7.1 SURFACE DAMAGES IN Al_2O_3, $MgAl_2O_4$ AND MgO IRRADIATED WITH ENERGETIC IODINE IONS

T. ARUGA, Y. KATANO and T. OHMICHI

Oxide ceramics of aluminum and magnesium, such as Al_2O_3, $MgAl_2O_4$ and MgO, are currently considered to be important materials as insulators to be used in a fusion reactor and as candidates of inert matrices for transuranium element fuels. These are known to be stable against nuclear energy depositions as high as over 100 dpa (displacement per atom) at and above room temperature [1]. We have reported the amorphization of a polycrystalline Al_2O_3 irradiated with 85 MeV iodine ions at room temperature due to electronic energy depositions [2]. In the present report, we present the results of microstructural examinations made on $MgAl_2O_4$, MgO and also Al_2O_3 irradiated with 85 MeV iodine ions through a cross sectional transmission electron microscopy (XTEM) and the changes observed on the surface of these irradiated materials both after the irradiation and in a long term aging.

Polycrystalline samples of $MgAl_2O_4$, MgO and Al_2O_3, both having 99.9% purity, were used for this study. The samples were irradiated with 85 MeV I^{7+} iodine ions accelerated by Tandem Accelerator of JAERI-Tokai to doses of 0.12-1.2x10^{19}/m^2 at the ambient temperature with a particle flux of 1x10^{14}/m^2s. Experimental details and depth profiles of the energy deposition cross sections for 85MeV I-ions incident on $MgAl_2O_4$, MgO and Al_2O_3 are to be referred in ref. [2-4].

Structural changes in the polycrystalline $MgAl_2O_4$ sample irradiated with 85 MeV I^{7+} ions to a dose of 1.2x10^{19}/m^2, as observed in XTEM, is characterized by complete amorphization up to depths around 6 μm. Step heights are observed to have formed on the both surfaces of $MgAl_2O_4$ and Al_2O_3 samples irradiated to a dose of 1.2x10^{19}/m^2 along a border between the masked and the irradiated area, through an examination using a surface profilometer with a laser beam, as compared in Fig. 1. These indicate the expansion of the irradiated volume. However, in the case of $MgAl_2O_4$, the height of the step is observed to increase sharply from the irradiated area towards the edge at the border, forming a peak as tall as 1.5 μm; while the step height decreases gradually towards the edge at the border of Al_2O_3 sample. It is considered that susceptibility of $MgAl_2O_4$ to amorphization under a high density electronic excitation would be greater than Al_2O_3, as exemplified by the larger depth of almost completely amorphized region, about 6 μm, as compared with 5 μm, as observed in Al_2O_3 irradiated to the same dose [2]. That is, thin layers in the vicinity of the $MgAl_2O_4$ sample surface seem to be amorphized with smaller density of electronic excitations, therefore in the much earlier stage of irradiation than Al_2O_3; it is noted that the lateral expansion occurs in the amorphous phase under the swift ion beam[3]. No amorphization occurs for MgO samples even at the highest dose of 1.2x10^{19}/m^2, and grain structures remain and no amorphization takes place even near the ion-incident surface for the sample irradiated to this dose. Any step height are not observed either. Instead, a X-ray diffractometry revealed an enhancement of the diffraction peak for (200), (400) reflections, as compared with those before irradiation[4].

Unexpectedly, thin, glossy and silver-gray colored film is observed to have formed on the surface of

irradiated $MgAl_2O_4$ sample, in 3 yr aging after the irradiation or being kept in air after the irradiation. The result of an EDS (energy dispersive X-ray spectroscopy) analysis made on a piece of thin film from $MgAl_2O_4$ sample is compared with that measured on the $MgAl_2O_4$ sample before irradiation, in Fig. 2, which reveals that the film contains Al, Mg and Si. Silicon, which is one of impurities contained in the sample before irradiation (Fig.2(bottom)), is found to be enriched. Furthermore, thin, glossy and silver-gray colored film is also observed to have formed on the surface of irradiated MgO sample irradiated to the same dose, in 3 yr aging after the irradiation. It is considered that, oxygen atoms bonding with or associated with magnesium atoms would be lost preferentially during the irradiation, because such a film formation has not been observed until now on the surface of Al_2O_3 irradiated to the same dose.

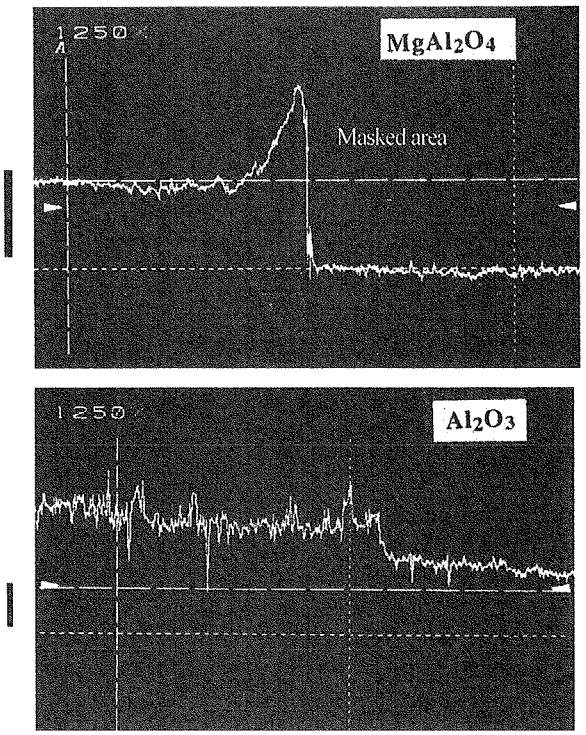

Fig. 1. Step heights formed on the both surfaces of $MgAl_2O_4$ (top) and Al_2O_3 (bottom) along a border of masked and irradiated area are compared, indicating an expansion of the irradiated volume. Scale bar each on the left is 1μm.

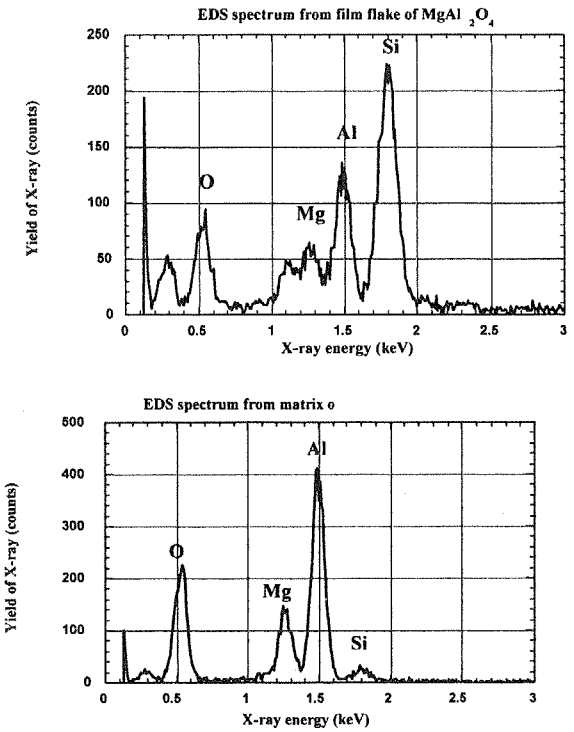

Fig. 2. The result of EDS (energy dispersive X-ray spectroscopy) analysis on a piece of thin film from $MgAl_2O_4$ sample revealing that the film contains Al, Mg and Si (top), and the result of analysis on the $MgAl_2O_4$ sample before irradiation (bottom).

References

[1] S. J. Zinkle and L. L. Snead, Nucl. Instrum. Methods B 116 (1996) 92.

[2] T. Aruga, Y. Katano, T. Ohmichi, S. Okayasu, Y. Kazumata, Nucl. Intrum. Methods B 166-167 (2000) 913.

[3] T. Aruga, Y. Katano, T. Ohmichi, S. Okayasu, Y. Kazumata, Nucl. Intrum. Methods B 197 (2002) 94.

[4] T. Aruga, Y. Katano T. Ohmichi, S. Jitsukawa, Surface and Coatings Tecchnology 158-159 (2002) 444.

7.2 ELECTRICAL EXCITATION EFFECTS ON RADIATION-INDUCED DISORDERING IN MAGNESIUM ALUMINATE SPINEL

M. SHIMADA[1], K. YASUDA[1], S. MATSUMURA[1], C. KINOSHITA[1],
Y. CHIMI, N. ISHIKAWA and A. IWASE

Magnesium aluminate spinel $MgO{\cdot}nAl_2O_3$ is a candidate material for insulators and radio frequency heating windows in a future fusion device, since it exhibits superior stability of electric insulation and swelling resistance under energetic particle irradiation[1,2]. The spinel structure has a considerable number of empty holes and vacant sites in the crystal lattice, and they are believed to be responsible for the excellent resistance to radiation damages, accommodating displaced ions. However the behavior of displaced ions under irradiation has not been conclusively confirmed by experiments. In this work, HARECXS (*high angular resolution electron channeling x-ray* spectroscopy[3, 4]) has been employed to investigate disordering behavior in $MgO{\cdot}nAl_2O_3$ induced by irradiation, and the disordering processes has been compared for irradiations with low energy ions (≤MeV) and swift heavy ions.

Specimens of $MgO{\cdot}nAl_2O_3$ (n =1.0, 2.4) were irradiated at 870 K with 1MeV Ne^+ ions up to fluence of 4.5 x 10^{20} Ne^+/m^2 and 500 keV He^+ ions up to fluence of 2.0 x 10^{21} He^+/m^2. The irradiated specimens were cut along the irradiated direction into several pieces and were then polished to be electron transparent. Electron transparent TEM specimens of $MgO{\cdot}nAl_2O_3$ (n = 1.1) were also prepared and subjected to irradiation at ambient temperature with 200 MeV Xe^{14+} ions up to fluence of 5 x 10^{15} Xe^{14+}/m^2. Electron microscopes of Philips EM420T at Argonne National Laboratory and Tecnai-20 at Kyushu University equipped with an EDX microanalyzer were operated at 120 kV and 200 kV in the experiments, respectively. HARECXS profiles were obtained by incident beam rocking between $-4\boldsymbol{g}$ and $+4\boldsymbol{g}$ ($\boldsymbol{g}$ = 400) Bragg conditions. The HARECXS profiles were simulated as a function of atomic configurations, based on the dynamical scattering theory[5] including the dechanneling and the delocalization effects on induced x-ray emission, to determine the atomic configurations quantitatively.

Structural disordering takes place with progress of displacement damage under irradiation with 1 MeV Ne^+ ions or 500 keV He^+ ions. It proceeds dominantly with positional exchange between Al^{3+} ions on octahedral (VI) sites and Mg^{2+} ions on tetrahedral (IV) sites in the stoichiometric spinel (n =1.0). On the other hand in nonstoichiometric spinel (n =2.4), Mg^{2+} ions are already distributed randomly on IV and VI sites before irradiation and positional change of Al^{3+} VI into IV sites is dominantly on disordering process. Displacement of O^{2-} ions is also recognized in heavily damaged areas. Irradiation with 500 keV He^+ ions has been found to induce lesser disordering than 1 MeV Ne^+ ions irradiation does at the same displacement damage. The lesser disordering tendency is ascribed to a higher ionizing rate under He^+ irradiation. The electronic excitation leads partly to ionization enhanced diffusion of ions[2]. Therefore one can consider that the reordering tendency is pronounced under 500 keV He^+ irradiation, suppressing the radiation-induced disordering.

---

[1]Kyushu University

Ion tracks with structural disordering were observed in plan-view of a specimen irradiated with 200 MeV Xe^{14+} ions. Fig. 1 shows HARECXS profiles of (a) unirradiated and (b) irradiated $MgO \cdot 1.1Al_2O_3$. HARECXS profiles also indicate that the disordering has taken place in some degree even at an extremely small amount of knocked-on displacements (less than 10^{-4} dpa). Highly enhanced electronic energy deposition more than 20 keV/nm induces local displacement of ions significantly, resulting in the disordering. The volume fraction of ion tracks was estimated to be around 1 % from the bright-field images at a fluence of 5 x 10^{15} Xe^{14+}/m^2. The rather large structural disordering shown in Fig. 1 (b), therefore, indicates that the structural disordering occurs not only inside the ion tracks but also at the surrounding regions. Further investigations are now on progress, including the determination of the structure of ion tracks.

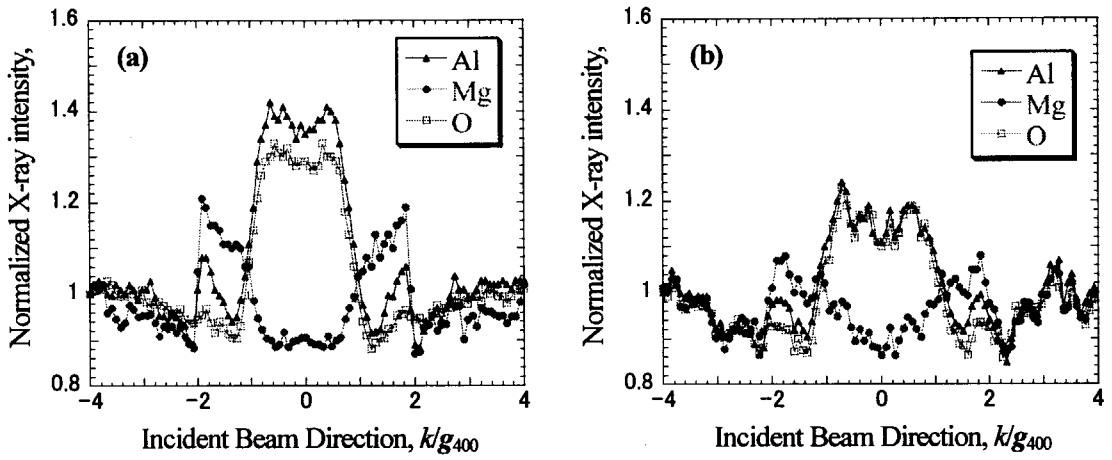

Fig. 1 HARECXS profiles of (a) unirradiated and (b) irradiated $MgO \cdot 1.1Al_2O_3$ at ambient temperature with 200 MeV Xe^{14+} up to fluence of 5 x 10^{15} Xe^{14+}/m^2.

References

[1] F.W. Jr. Clinard, G.F. Hurley, R.A. Youngman, L.W. Hobbs, J. Nucl. Mater. **133-134**(1985) 701.

[2] S.J. Zinkle, C. Kinoshita, J. Nucl. Mater. **251**(1997) 200.

[3] T. Soeda, M. Shimada, S. Matsumura, N.J. Zalusec, C. Kinoshita, *Proc. 4th Pacific Rim Int'l. Conf. Advanced materials and Processing (PRICM4)*, **2**(2001) 1423.

[4] S. Matsumura, T. Soeda, M. Shimada, N.J. Zalusec, *Proc. 15th Int'l. Cong. Electron Microscopy (ICEM)*, **1**(2002) 187.

[5] C.J. Rossouw, C.T. Forwood, M.A. Gibson, P.R. Miller, Micron **28**(1997) 125.

7.3 ATOMIC MIXING IN Bi-Al_2O_3 INTERFACE BY HIGH ENERGY ION IRRADIATION

A. IWASE[1], Y.CHIMI and N. MATSUNAMI[2]

It has been revealed recently that the high density electronic excitation due to swift heavy ions induces atomic displacements in materials. This report shows that the phenomenon can be applied to the effective mixing of different materials at their interface.

A bismuth thin film (about 800 Å thick) was deposited on an α-Al_2O_3 single crystal substrate by vacuum evaporation at room temperature in a vacuum below 7×10^{-6} Pa. The specimen was irradiated at liquid nitrogen temperature with 200-MeV ^{136}Xe ions up to the fluence of $1.4x10^{14}/cm^2$. After the irradiation, the mixing state of the Bi-Al_2O_3 interface was characterized by using Rutherford backscattering (RBS) spectroscopy. For comparison, the same irradiation and the RBS measurement were performed for Bi-Si system.

Figure 1 shows the RBS spectra of Bi-Al_2O_3 system near the Al edge and those for the Bi layer before and after the irradiation. The figure indicates that the mixing of Bi and Al atoms occurs at their interface. If atomic displacements are induced only through the elastic collisions, the Xe ion fluence of $1.4x10^{14}/cm^2$ corresponds to the defect concentration of 1%, which is too small to induce the atomic mixing. The present result suggests that the atomic mixing at the Bi-Al_2O_3 interface is induced by the high density electronic excitation. In the case Bi-Si system, however, atomic mixing was not observed even at the ion fluence up to $1x10^{15}/cm^2$. This result shows that the atomic displacements by electronic excitation strongly depend on materials; Al_2O_3 is much more sensitive to the electronic excitation than Si.

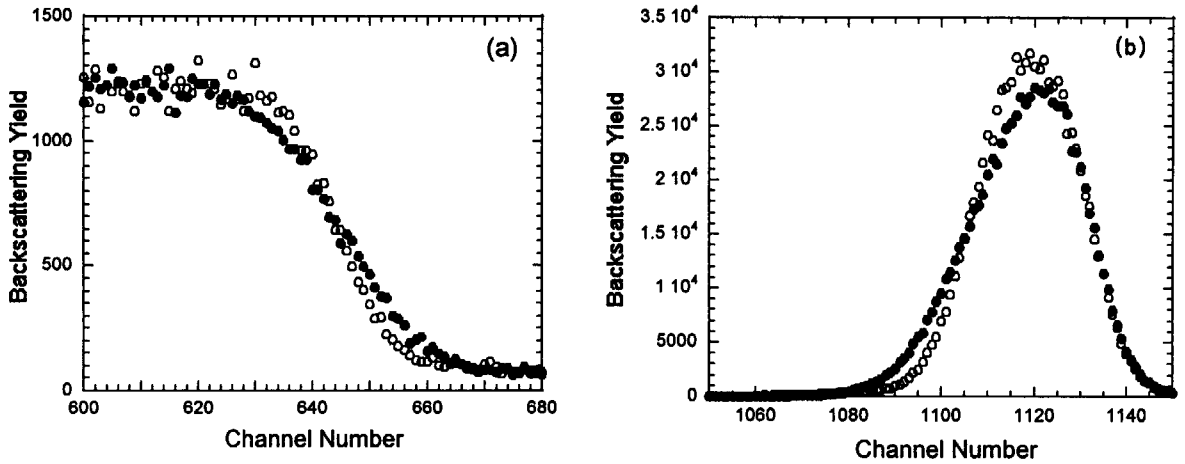

Fig.1 RBS spectra of Bi-Al_2O_3 system near the Al edge (a), and those for the Bi layer (b) before irradiation (open circles) and after irradiation (solid circles).

[1] Present address: Osaka Prefecture University

[2] Nagoya University

7.4 DISORDERING IN Li_2TiO_3 IRRADIATED WITH HIGH ENERGY IONS

T. NAKAZAWA, V. GRISMANOVS[1], D. YAMAKI, Y. KATANO, T. ARUGA

Lithium metatitanate (Li_2TiO_3) is regarded as one of the most suitable candidates for the solid tritium breeder material of D-T fusion reactors [1]. It is known that in an operating fusion reactor, the radiation damage in Li_2TiO_3 will be produced by fast neutrons, energetic tritons (2.7 MeV) and helium ions (2.1 MeV) generated by $^6Li(n, \alpha)^3H$ reaction. The damage caused by ionising radiation may result in the microstructure changes and hence may have an impact on the tritium release behaviour, and on thermal and mechanical properties of Li_2TiO_3. Thus, the study of microstructure changes and irradiation defects in Li_2TiO_3 is essential in order to evaluate its irradiation performance. Recently, the simultaneous exposure of Li_2TiO_3 to H^+ (0.25 MeV), He^+ (0.6 MeV) and O^{2+} (2.4 MeV) ions in the temperature range of 343 K to 873 K and at the fluence of $1.0x10^{21}$ ions/m^2 has been reported to cause the appearance of TiO_2 (anatase) phase in its surface layer [2]. In order to obtain further information on structural changes we irradiated Li_2TiO_3 with Xe and O ions, and performed X-ray diffraction.

The fused Li_2TiO_3 samples were irradiated at ambient temperature with the 80 MeV O and 160 MeV Xe ions, accelerated by the Tandem Accelerator of JAERI. Ion irradiations were carried out up to the maximum fluence of $1.4x10^{20}$ and $3.4x10^{18}$ ions/m^2 for 80 MeV O and 160 MeV Xe ions, respectively. The electronic (S_e) and nuclear (S_n) stopping powers are listed in Table 1 in which another irradiation conditions calculated with the SRIM2000 code [3] assuming the threshold energies of 40 eV for displacements of Li, Ti and O atoms. The XRD patterns of irradiated samples were obtained using a Cu-Kα line for the samples before and after irradiations. During XRD measurements, samples were masked with a gold foil of 10 μm in thickness leaving a hole 8 by 5 millimeters in order to remove diffractions from the unirradiated portion. The intensities of diffraction peaks from samples were normalized to that of a specified diffraction peak from the gold foil.

Table 1
Irradiation conditions of Li_2TiO_3

Ion	Xe	O
E (MeV)	160	80
Fluence (ions/m^2)	$3.3x10^{16}$, $3.4x10^{18}$	$4.6x10^{19}$, $1.4x10^{20}$
D (GGy)	0.03, 3.4	2.6, 8.0
R_p (μm)	10	50
S_n (keV/nm)	0.03	$2.0x10^{-4}$
S_e (keV/nm)	20.0	1.2

E: energy of ions, D: accumulated radiation dose, Rp: mean projected range, S_n: nuclear stopping power at near surface, S_e: electronic stopping power at near surface. R_p, S_n and S_e are calculated with the SRIM2000 code [5].

Li_2TiO_3 has the rock-salt structure in which the cations occupy octahedral sites in a cubic close-packed oxide ion array. The ordered structure has various cation ordering sequences associated with the different stoichiometries. The changes of ordered structure, that is, the disordering transformation has been observed by X-ray diffraction [4]. In disordered material, the disappearance of X-ray peaks corresponding to the cation-ordered superstructure implies that there is no long-range order in the cation arrangement.

[1]OECD Halden Reactor Project

The changes in XRD patterns of samples irradiated with the 80 MeV O and 160 MeV Xe ions are shown in the range of 19° to 25° for 2Θ in Figure 1. In the case of the O ion irradiations, the (110) and (021) peaks are observed to gradually decrease with fluences. The (020) and ($\bar{1}$11) peaks have disappeared with the irradiation to 4.6×10^{19} ions/m^2. On the other hand, these peaks have entirely disappeared with the Xe ion irradiation at small fluences of about 10^{16} ions/m^2, that is, at the accumulated radiation dose of 0.03 GGy. Such decrease in XRD intensities means that long-range disorder is caused with the irradiation. The disordering is thought to be due to the Li ion migration because the Li^+ ions lie on the (110) and (021) planes and are easy to migrate under ion irradiation [4, 5].

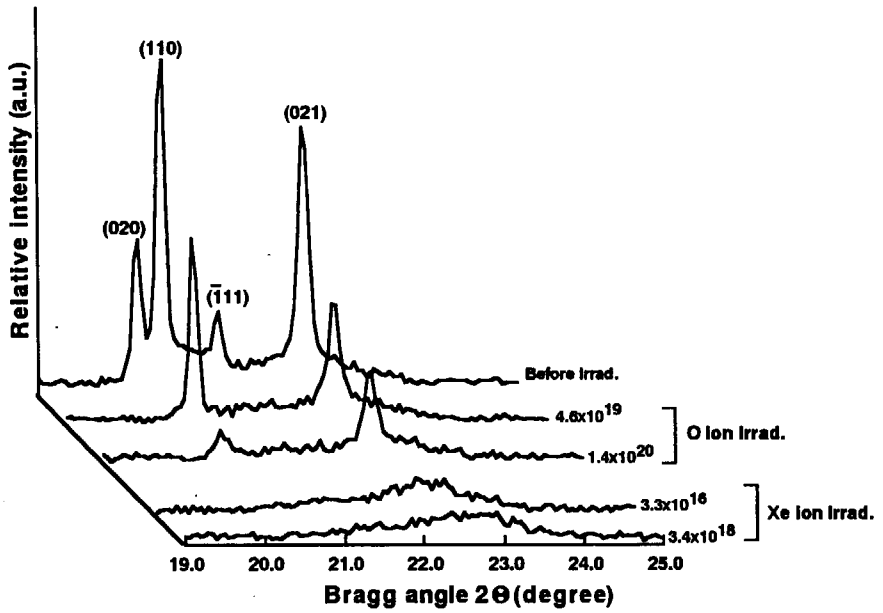

Fig. 1. X-ray diffraction patterns of Li_2TiO_3 irradiated with the 80 MeV O and 160 MeV Xe ions, and of Li_2TiO_3 before irradiation. Numerical values stand for ion fluences in units of ions/m^2. Figures in parentheses are diffraction indexes.

The degree of long-range disorder is thought to be related with the S_e. The XRD intensities of Li_2TiO_3 irradiated with the Xe ion are drastically reduced though fluences of Xe ion irradiation are much less than those of O ion irradiation. Accumulated electronic energy depositions with the Xe ion irradiation are also less than those with the O ion irradiation. Therefore, the ion fluence and the accumulated radiation dose cannot account for the reduction of XRD intensities. On the other hand, S_e for the Xe ion irradiation is a rather large value than that for the O ion irradiation (see Table 1). Thus, taking the above facts into account, the long-range disorder due to the irradiation is considered to strongly relate to S_e, and not to the ion fluence or the accumulated radiation dose. This fact indicates that the disordering transition in Li_2TiO_3 takes place on irradiation with ions with the larger electronic stopping power such as the Xe ion irradiation. Note that the nuclear stopping power merely produces the number of displacements per atom (dpa) $\ll$ 0.1 dpa, which is too small to destruct the lattice structure of Li_2TiO_3, in the near surface region for the present irradiations.

REFERENCES

[1] P. Gierszewski, Review of properties of lithium metatitanate, Report no. CFFTP G-9561, 1995.

[2] T. Nakazawa, V. Grismanovs, D. Yamaki, Y. Katano, T. Aruga and A. Iwamoto, 2000 Int. Conf. on Ion Implantation Technology Proc. (2000) 753.

[3] J.F. Ziegler, J.P. Biersack and U. Littmark, The Stopping and Range of Ions in Solids, Pergamon, Oxford, 1985.

[4] M. Castellanos and A.R. West, J. Mater. Sci. **14** (1979) 450.

[5] K. Noda, T. Nakazawa, Y. Ishii, K. Fukai, H. Matsui, D. Vollath and H. Watanabe, Mater. Trans., JIM **34** (1993) 1150.

7.5 RADIATION EFFECTS IN CeO_2 UNDER HIGH ENERGY ION IRRADIATION AS SIMULATIONS OF FISSION FIELD IN NUCLEAR FUELS

T. SONODA[1], M. KINOSHITA[1], N. ISHIKAWA, Y. CHIMI and A. IWASE

High burnup extension of LWR fuel is progressing to reduce the amount of total process flow in the nuclear fuel cycle and eventually to reduce the fuel cycle costs. In the periphery region of high burnup fuel pellets in LWRs, a crystallographic re-structuring is commonly observed, as named "rim structure" [1], which is characterized by the existence of highly dense small sub-grains whose size is approximately 200 nm, and the accumulation of small pores with average size around 1 μm. This structure shall be formed by the accumulation and mutual interactions of radiation damages, fission products (FPs) and electronic excitations deposited partially by nuclear fissions [2].

In order to separate the each processes, clarify the mutual interactions among them, and understand the formation mechanism of this restructuring, 70 – 210 MeV FP ions (Xe, I) irradiation examinations on CeO_2, as a simulation fluorite ceramics of UO_2, have been done at JAERI-Tandem facility. Microstructural evolutions in the specimen are observed in a 200 kV TEM (JEM-200CX) and 300kV FE-TEM (HF-3000) at CRIEPI. This paper mainly reports an electronic excitation effects on the microstructural evolution in CeO_2.

Fig. 1 shows typical micrographs of CeO_2 under irradiations with 210 MeV Xe ion (a), 100 MeV Xe ion (b), 80 MeV Xe ion (c), 70 MeV I ion (d) and 80 MeV I ion (e) at room temperature. This figure indicates that the irradiations of high energy FPs at room temperature cause the typical radiation damage, "ion tracks". Fig. 2 summarizes that the average diameters of ion tracks of (a) - (e) are ~ 9.3 nm, ~ 7.9 nm, ~ 5.7 nm, ~ 4.6 nm and ~ 5.1 nm, respectively. These results suggest that the affected area of electronic excitation by fissions in CeO_2 seems to be around 5 ~ 7 nm ϕ, because the fission energy of Median light FPs and Median heavy FPs are around 95 MeV and 67 MeV, respectively.

Fig. 3 shows the microstructural evolution in wedge-shaped TEM specimen under 210 MeV Xe ions irradiation. In this figure, the elliptical deformation of diffraction spots and faint "halo-pattern" become clear as the fluence becomes higher, $> 1 \times 10^{12}$ ions/cm^2. These figures and the results of the high-resolution micrographs indicate that the inner structure of ion tracks under room temperature shall be amorphous or grain-subdivided.

Fig. 4 shows the cross-section microstructure of CeO_2 irradiated 210 MeV Xe ions to a fluence of 1×10^{13} ions/cm^2, whose specimen is sampled by Focused Ion Beam (FIB) method. In the wedge-shaped specimen, the microstructure under irradiation with 210 MeV Xe ions to a fluence of $> 1 \times 10^{12}$ ions/cm^2 become disordered as shown in Fig. 3. Though in the surface area (a) of this FIB specimen, there is no evidence of disordering from the observation of SADP. On the contrary, at around 5μm depth from the surface, as shown in area (b), ion tracks are clearly observed. This phenomenon indicates the possibility that the radiation damages in the surface area (a) are annealed by the effects of bulk and/or high-energy electronic excitation.

[1] Nuclear Energy Systems Department, Komae Lab., Central Research Institute of Electric Power Industry (CRIEPI)

References

[1] J. O. Barner, M. E. Cunningham, M. D. Freshley, and D. D. Lanning, HBEP-61, 1990, Battelle Pacific Northwest Laboratories.

[2] T. Sonoda, M. Kinoshita, I.L.F. Ray, T. Wiss, H. Thiele, D. Pellottiero, V.V. Rondinella and Hj. Matzke, Nucl. Instr. and Meth. B, 191 (2002) 622-628.

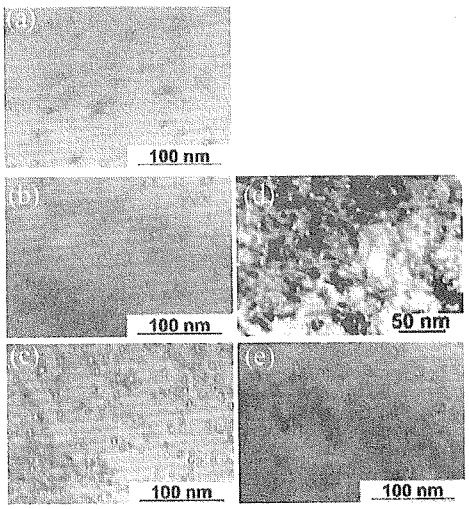

Fig. 1. Typical micrographs of CeO_2 under irradiation with 210 MeV Xe (a), 100 MeV Xe (b), 80 MeV Xe (c), 70 MeV I (d) and 80 MeV I (e).

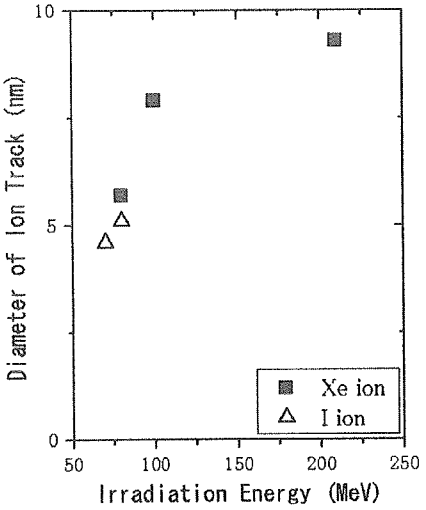

Fig. 2. Average diameter of ion tracks.

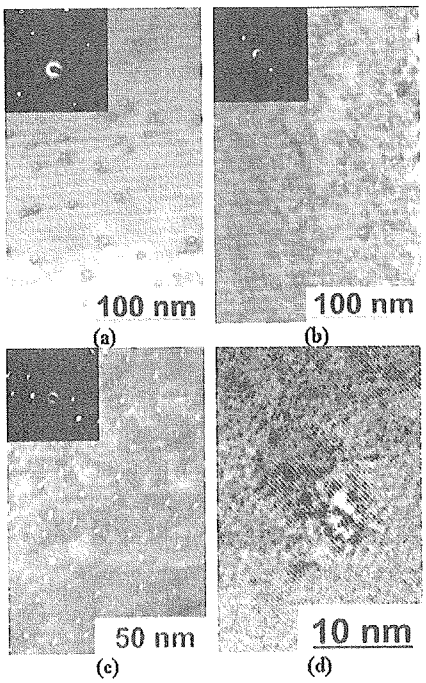

Fig. 3. Microstructural evolution of CeO_2 under irradiation with 210 MeV Xe to a fluence of 1×10^{11} ions/cm^2 (a), 1×10^{12} ions/cm^2 (b), and 5×10^{12} ions/cm^2 (c). (d) : High-resolution image of ion track.

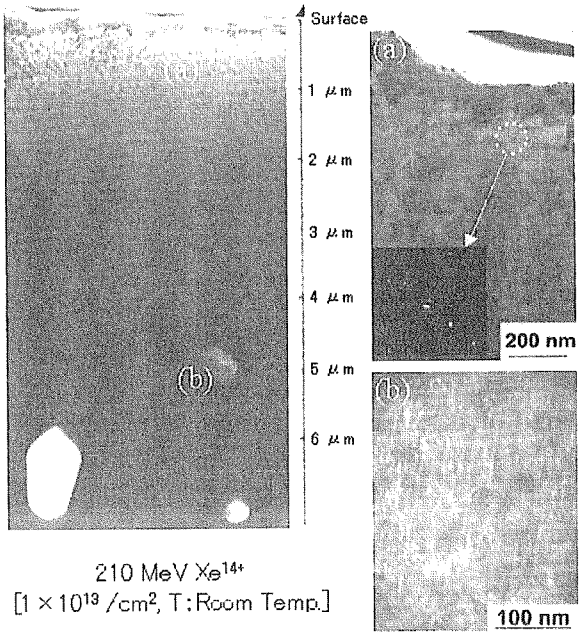

Fig. 4. Cross section microstructure of CeO_2 irradiated 210 MeV Xe to a fluence of 1×10^{13} ions/cm^2. (a) : Surface area (< 1 μm depth), (b) : ~ 5μm depth from the surface.

7.6 ELECTRONIC SPUTTERING OF INSULATING OXIDES BY HIGH ENERGY HEAVY IONS

N. MATSUNAMI[1], O. FUKUOKA[1], M. SATAKA, S. OKAYASU and A. IWASE[2]

We have measured sputtering yields of insulating oxides to investigate the effects of the electronic excitation on atomic displacement by high-energy heavy ions, applying a carbon (C)-film collector method [1-3]. Samples of amorphous (a)-SiO_2, crystalline (c)-SiO_2, $SrCe_{0.95}Yb_{0.05}O_{3-\delta}$ (SCO), $SrTiO_3$ (STO), CeO_2, Al_2O_3, MgO, TiO_2, ZnO and $MgAl_2O_4$ were irradiated with Xe, I, Ni, Ar and S ions with the energy of ~1 MeV/u. Sputtered atoms were collected in the C-films and analyzed by 1.8 MeV He Rutherford backscattering spectroscopy. From the linear part of the amount of atoms in the collector vs the ion dose (less than $10^{14}/cm^2$), the sputtering yield of each component was deduced, using the calibrated collection-efficiency of the C-films [2].

With the results of two additional oxides, i.e., c-SiO_2 and $MgAl_2O_4$, we come to the same conclusions as in the previous study [2]. Sputtering yields of each component are roughly proportional to the sample composition. The experimental sputtering yields Y (atoms per ion), i.e., sum of sputtering yield of each component, follow neither the mean charge of ions after transmission through the C-film or the nuclear stopping power [2]. The yields are larger by 30 - 2000 than the calculated yields based on the elastic collision cascades. Hence the electronic excitation effects are dominant in the sputtering of the oxides (electronic sputtering). The electronic sputtering yields increase super-linearly with the electronic stopping power Se: $Y=(BSe)^n$. The exponent n varies from 1.4 (Al_2O_3) to 4 (CeO_2). It appears that the values of B and n of c-SiO_2 agree with those of a-SiO_2. The parameters B and n of $MgAl_2O_4$ are 0.13 nm/keV and 1.8.

The representative sputtering yields taken at Se = 10 keV/nm (medium Se in this study) vs the band gap (Eg) are shown in Fig.1. Here, Eg of c-SiO_2 is taken as 8.9 eV [4] and that of $MgAl_2O_4$ is 5.1 - 7.8 eV [5,6]. Eg of CeO_2, which was assumed to be the same as that of SCO, is re-examined and determined as 3.4 eV by optical absorption measurement. The sputtering yield of $MgAl_2O_4$ at Se = 10 keV/nm is ~1.6 and in between MgO and Al_2O_3 ($MgAl_2O_4$ data is not shown in Fig. 1). As indicated by the dotted line in Fig. 1, the suggestion remains valid that the electronic sputtering yield at a given electronic stopping power has its maximum that depends on Eg^4 [2]. It is reasonable to assume that the relaxation time from the highly excited sates just after the ion impact to the lower excited states is very short and thus the available energy to the atomic displacement is due to the transition of electrons at lower excited states to the ground states (recombination) which is presumably determined by the band gap. Super-linear dependence of the electronic sputtering yields on the band gap indicates that the multiple excited states come into play. This recombination-induced atomic-displacement implies that the thermal spike model is not appropriate. The sputtering yields of Al_2O_3, MgO and $MgAl_2O_4$ are small, though their band gaps are large. No systematic trend has been revealed by the electron mobility (a possible candidate of the electron-phonon coupling) [2]. This subject, and the relation with the track formation and track volume are to be investigated.

[1] Center for Integrated Research in Science and Engineering, Nagoya University
[2] Research Institute for Advanced Science and Technology, Osaka Prefecture University

Another important subject is the charged fraction of the sputtered particles. We have measured the positive ion yields by ions transmitted through a C-film and by using a double-cylindrical Faraday-cup, which was negatively biased (typically -100V). A bias of 1.2 kV was applied to the C-film to minimize the effects due to electrons emitted from the C-film. According to preliminary results, the positive ion yields (per incident ion) is ~14 for 90 MeV Ni on SiO_2 film on Si, taking into account that the mean charge of Ni ions after C-film transmission is 19. The fraction of positive ions is roughly 10 %. The fraction will be much reduced, when the corrections due to the electron emission from the Faraday cup [7]. Hence, the charged fraction is very small and neutral components are dominant in the electronic sputtering. This result is not favor with the Coulomb explosion model.

The authors thank Dr. M. Tazawa for optical absorption measurements and Mr. T. Masuda for technical assistance of ion beam analysis.

References

[1] N. Matsunami, M. Sataka, A. Iwase, Nucl. Instrum. Meth. B193(2002)830.
[2] N. Matsunami, M. Sataka, A. Iwase, S. Okayasu, Nucl. Instrum. Meth. B(2003, in press).
[3] N. Matsunami, M. Sataka, A. Iwase, T. Inami, M. Kobiyama, J. Nucl. Mater. 302(2002)206.
[4] D.L. Griscom, J. Non-Crystalline Solids 24(1977)155.
[5] D. Jia, W. M. Yen, J. Luminescence (2003, in press).
[6] M. L. Bortz, R. H. French, D. J. Jones, R. V. Kasowski, F.S. Ohuchi, Phys. Scripta 41(1990)537.
[7] N. Matsunami, E. Hatanaka, J. Kondoh, H. Hosaka, K. Tsumori, H. Sakaue, H. Tawara, Phys. Scripta 65(2002)278.

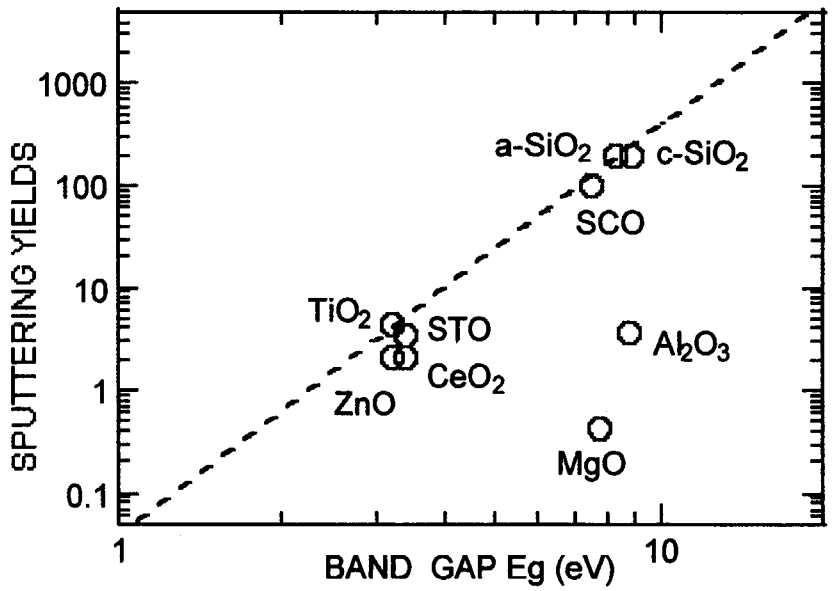

Fig. 1 Representative sputtering yields at electronic stopping power Se =10 keV/nm as a function of the band gap Eg. The dotted line shows Eg^4 dependence.

7.7 ELECTRONIC EXCITATION EFFECTS ON SECONDARY IONS EMISSION FROM CONDUCTIVE MATERIALS BOMBARDED BY HEAVY IONS

T. SEKIOKA[1], M. TERASAWA[1] and M. SATAKA

The interaction between swift heavy ions and solids has been an active research area. One of the important problems has been whether electronic excitations can induce the production of lattice defects in simple metals or not. In metals, it had been considered for a long time that on account of the great number of free conduction electrons and of their high mobility, inelastic interactions (electronic excitation) could not cause any radiation damage or annealing process. In recent years, there have been extensive studies on the electronic excitation effect in metals irradiated with high-energy heavy ions (1-10MeV/nucleon), where the electronic stopping power $S_e = -(dE/dx)_e$ dominates the nuclear stopping power (S_n) by a factor of about 100-1000 [1]. We have studied the secondary ion mass spectrometry from thin conductive solid targets irradiated with heavy ion beams from the JAERI-Tokai tandem accelerator in the energy region where the electronic stopping power is dominant.

An Au foil target of 2000Å thickness evaporated on C-foils of 8.5 $\mu g/cm^2$ was irradiated with high-energy Au ions from the tandem accelerator. The secondary ions ejected from the front surface of the target were collected by a time of flight (TOF) mass spectrometer by applying an acceleration voltage of –500V and detected by an electron multiplier. Secondary electrons from the back side of the target were detected by another electron multiplier and this signal was used as the start signal of the TOF. The projectiles were 240 MeV Au^{15+} and 320 MeV Au^{25+} ions. Immediately before the measurement of the secondary Au^+ ion yield from the Au target, we cleaned the target by infrared radiation heating. We maintained the temperature of the target about 500°C for two hours in the vacuum of 1.6×10^{-6} Pa. Without cleaning, we could find no Au^+ secondary ion peak in the TOF spectrum because the weak Au^+ peak is buried in the background mainly due to hydrocarbon contaminants.

Figure 1 shows the yields of the secondary ions of Au^+ from Au target normalized by the counts of secondary electron signal, together with the yield of the secondary ions of Cu^+ from Cu target as a function of the electronic stopping power. The values of the electronic stopping power are obtained from Ziegler's table by TRIM. The solid line in the figure

[1] Himeji Institute of Technology

represents the slope of S_e^2 and the dashed one represents the slope of S_e^4 for the eye guide. The yield of the Au^+ secondary ions from Au target is very small as compared with the yield of the Cu^+ secondary ion from Cu target, though Cu and Au have the same electronic structure ($^2S_{1/2}$). The tendency of the target mass dependence of the secondary ion yield agrees with the experimental results on the damage creation in metals by high electronic excitation effect by swift heavy ion irradiation [1]: the comparison of two metals with similar electronic and atomic properties shows that the lower target atomic number corresponds higher sensitivity to damage creation by S_e. The S_e dependence of the yield of the Au^+ secondary ions from Au target seems to be more sensitive than the one of the Cu^+ secondary ions from Cu target. To confirm these experimental results, it is important to study the secondary ions mass spectroscopy in a wide range of electronic stopping power with various combinations of projectiles and conductive targets.

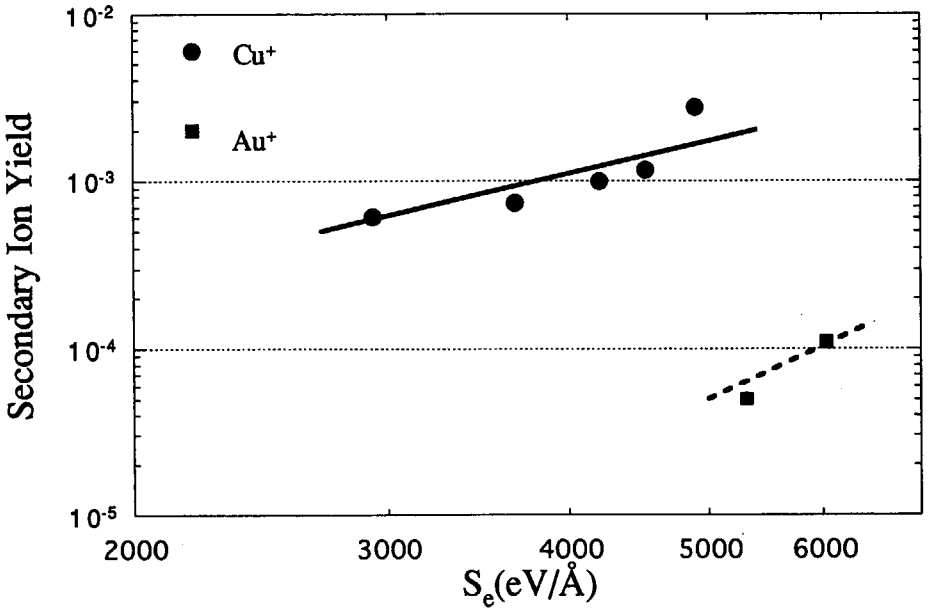

Fig. 1. The yields of the secondary ions of Cu^+ and Au^+ from Cu and Au target respectively normalized by the counts of secondary electrons, as a function of the electronic stopping power S_e. The values of the electronic stopping power are obtained by Ziegler's table (TRIM). The solid line in the figure represents the slope of S_e^2 and the dashed one represents the slope of S_e^4 for the eye guide.

Reference

[1] A. Dunlop and D. Lesueur, Radiat. Eff. Def. Solids 126 (1993) 123.

7.8 CHANGE IN ELECTRICAL PROPERTIES OF BISMUTH BY ENERGETIC ION IRRADIATION

Y. CHIMI, A. IWASE[1] and N. ISHIKAWA

Change in electrical properties, especially electrical resistivity, induced by energetic ion irradiation in semi-metallic bismuth is studied in relation to its structural change. Amorphous bismuth thin films are known to show a superconducting transition below ~6 K and a crystallization at 10–20 K [1]. We have tried to detect a sign of irradiation-induced amorphization in bismuth thin films as the change in electrical resistivity due to the superconducting transition and/or the re-crystallization of amorphous region.

A polycrystalline bismuth thin film (330 Å thick) was deposited on an α-Al_2O_3 single crystal substrate by vacuum evaporation at room temperature in a vacuum below 7×10^{-6} Pa with a mask for a conventional four-probe electrical resistivity measurement. The specimen was irradiated below 7.4 K with 200-MeV ^{197}Au ions. After irradiation, the resistivity was measured during heating up to 35 K and then cooling down to 6.9 K at a constant rate of 1 K/min for observation of annealing behavior.

Figure 1 shows the annealing behavior of the resistivity, ρ. In the heating process, ρ increases abruptly around 20 K, whereas ρ changes smoothly in the cooling process. For amorphous bismuth thin films of 300–500 Å thick deposited on cold substrates, a similar abrupt resistivity increase has been observed at 10–20 K, which is due to crystallization of the amorphous region [1,2]. Therefore, the present result implies that amorphous region in bismuth is induced by energetic ion irradiation. We are now planning to detect the superconducting transition below ~6 K by using another cryogenic system.

References

[1] W. Buckel, R. Hilsch, Z. Phys. 138 (1954) 109.
[2] T. Hamada, K. Yamakawa, F.E. Fujita, J. Phys. F: Metal Phys. 11 (1981) 657.

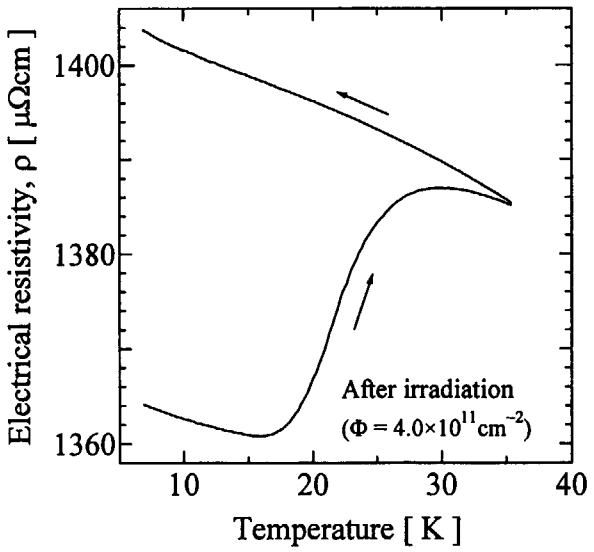

Fig. 1. Annealing behavior of electrical resistivity, ρ, of specimen after 200-MeV ^{197}Au ion irradiation.

[1] Present address: Osaka Prefecture University

7.9 EFFECT OF HIGH-ENERGY HEAVY ION IRRADIATION ON MAGNETIC PROPERTIES IN INVAR ALLOYS

F. ONO[1], S. KOMATUS[1], Y. HAMATANI[1], A. IWASE[2], Y. CHIMI, N. ISHIKAWA and T. KAMBARA[3]

Fe-Ni Inavr alloys around 35 at.%Ni are known to show various anomalies in physical properties [1]. Those anomalies have been understood as a result of the instability of the 3d-band ferromagnetism in fcc metals and alloys [2]. The Ni concentrations of those alloys are close to the boundary of the martensitic phase transition [3]. Irradiation of Fe-Ni Invar alloys with high-energy ions is expected to make a large effect on both the magnetic properties and lattice structure. Therefore, it seems one of the most effective ways for modification of physical properties of metals and alloys [4,5], and also for a search for new functional materials and their practical applications.

Specimens of Fe-30.2-33.9at.%Ni Invar alloys were in a form of thin discs of 5×5 mm^2 and the thickness of 100-200 μm. They were irradiated with 50-200 MeV Xe-ions to the dose up to 10^{14} ions/cm^2. AC-susceptibility measurements were made using a specially designed apparatus for rapid temperature variation. To detect any induced component along the beam direction, the measurements were performed by making the angle θ variable between the surface of the specimen and the direction of the external AC-field. The range of the Xe-ions was up to 7 μm, which was smaller than the thickness of the sample.

Observed AC-susceptibility versus temperature curves before and after the irradiations are shown in Fig. 1 and 2, respectively. In these figures all the curves were normalized to the value of θ =0 at T=300 K. In Fig.2 it is seen that the curves have two stages of magnetic transition. The first stage corresponds to the original Curie temperature that comes from the part where ion beams did not penetrate. The second stage is caused by the irradiation-induced ferromagnetism. The tailing effect, which was most clearly seen above the original Curie temperature when the external AC-magnetic field was applied along the direction of the ion beams, implies that the magnetically easy direction is parallel to the beam axis. These results show locally ferromagnetic parts exist at high temperatures. Those ferromagnetic needles were produced along the paths of high energy ions through high density electron excitations [6]. The present type of modification of introducing thin ferromagnetic needles in paramagnetic media has a possibility of applications for perpendicular high-density memory and giant magneto-resistance materials.

---

[1] Department of Physics, Okayama University
[2] now at Research Institute for Advanced Science and Technology, Osaka Prefecture University
[3] Atomic Physics Laboratory, The Institute of Physical and Chemical Research

To investigate the mechanism of the large modification of the ferromagnetism and the structure of the modified portion, measurements of the beam-energy dependence of AC-susceptibility-temperature curves are being made. It was found that the amount of the shift of the Curie temperature was not a function of the beam energy, but the intensity of the susceptibility of the modified portion increased with the beam energy. The high-density electronic excitation is responsible for the large modification of the ferromagnetism in Fe-Ni Invar alloys.

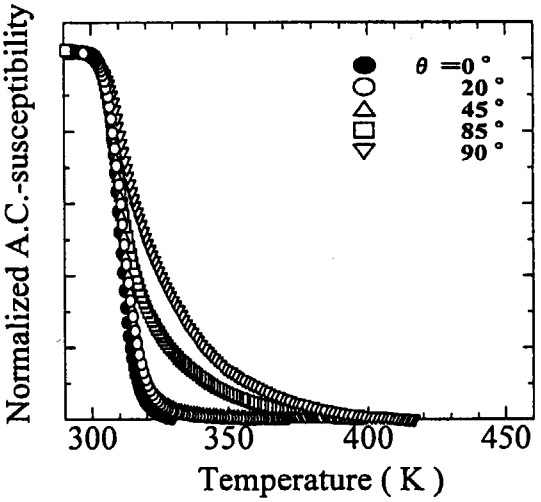

Fig. 1 AC-susceptibility-temperature curves in Fe-Ni Invar alloy before irradiation.

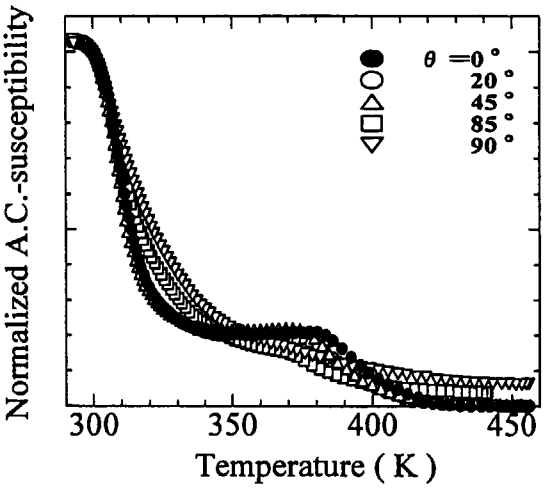

Fig.2 AC-susceptibility-temperature curves in Fe-Ni Invar alloy after irradiation

References

[1] For example, see "*The Invar Effect: A Centennial Symposium*" ed. by J. Wittenauer (The Minerals, Metals and Materials Society, 1997)

[2] T. Mizoguchi, J. Phys. Soc. Japan**25** (1968) 904.

[3] F. Ono, L. Bang and H. Maeta, in [1], p.197.

[4] A. Iwase, Y. Hamatani, Y. Mukumoto, N. Ishikawa, Y. Chimi, T. Kambara, C. Muller, R. Neumann and F. Ono, Nucl. Instrum. Methods Phys. Res. B, in press.

[5] F. Ono, Y. Hamatani, Y. Mukumoto, S. Komatsu, N. Ishikawa, Y. Chimi, A. Iwase, T. Kambara, C. Muller, R. Neumann, Nucl. Instrum. Methods Phys. Res. B **206** (2003) 295.

[6] N. Ishikawa, A. Iwase, Y. Chimi, O. Michikami, H. Wakana and T. Kambara, J. Phys. Soc. Japan **69** (2000) 3563.

7.10 RADIATION DEFECTS IN NANOCRYSTALLINE MATERIALS

H.OHTSUKA, H.SUGAI and K.HOJOU

'Nanocrystal is the radiation resistant material': this opinion has been verified through a series of our experiments. The aim of this study was to realize such materials taking advantage of intrinsic effects of the nanocrystal. We report herewith the present status of our study which has reached a milestone successfully. We took two complementary methods to show the radiation resistant properties. One is a microscopic and the other is a macroscopic approach.

In the microscopic approach we investigated formation of defect clusters within nano-particles by using a transmission electron microscope (TEM). In order to introduce defects into the nano-particles JAERI tandem accelerator was used. The studies were made putting an emphasis on the diffusion processes of point defects. Changing the specimen temperature we have observed changes in pattern of defect clusters. That implied that the cluster formation within nano-particles was determined by the diffusion. In addition to the observation we have developed a computer program which simulates the cluster formation. The result of the simulation agreed with the observation. This means that the cluster formation is one of the diffusion limited reaction [1]. Hence, we have concluded that nanocrystal has basically a radiation resistant property.

In the next step we have to see whether the nanocrystal of agglomerated state still shows the radiation resistant properties, or not. This test is indispensable for the practical use of the nanocrystal as a new material. Thus, the study changes to the macroscopic approach. Specimens which consist of agglomerated nano-particles were irradiated and resulting defects were diagnosed by a x-ray diffractometer (XRD). Typical XRD signals, which demonstrates features of the nanocrystal are shown in Fig.1 where changes in profiles after irradiation are presented. In this experiment nanocrystalline Cu was irradiated with 100 MeV Xe ions up to 1.5E15 ions/sq-cm. Figure (a) and (b) show 2θ -angle dependence of profile change; namely, broadening of profile appears asymmetric at high 2θ angles as shown (b) compared with (a), where the surfaces of reflection are (311) and (200), respectively. That seems to be due to some particular defect clusters but details are unknown. Clear temperature dependence can be seen in Fig. (b) and (c) where samples were at room temperature and 250 ℃, respectively. At high temperature irradiation no clear changes in the

profiles are observed as shown in (c). This means that the diffusion coefficient of the point defects increased due to temperature rise and thus the cluster formation became hard to take place. The size effect of the cluster formation is shown in Fig.(d) as compared with (b) where the average sizes of the nano-particles are 25 nm and 50 nm in diameter, respectively. Lowering the size of the constituent particles resulted in the reduction of the cluster formation, as can be seen in the smaller profile broadening in Fig.(d). These results give us, thus, directions how to avoid radiation damage at the use of nanocrystal.

Summarizing both the microscopic and the macroscopic investigation we have derived the conclusion as mentioned at the top of this text.

Generous supports of the Tandem group are gratefully acknowledged.

Reference

[1] H.Ohtsuka, K.Hojo, H.Maeta, H.Otsu, H.Sugai and H.Yamamoto, Eur. Phys. J.D. 16 (2001) 309.

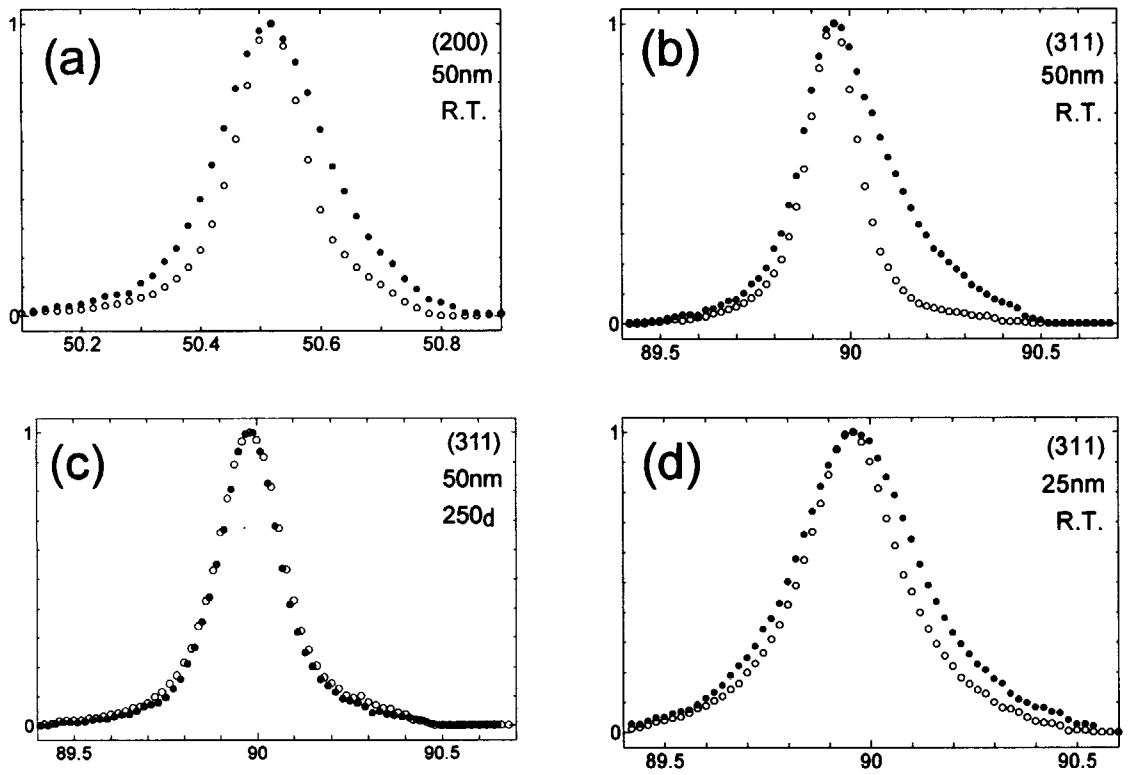

Fig.1 Profiles of XRD of $\theta - 2\theta$ scan. Close and open circles refer to before and after irradiation, respectively. Peak positions are adjusted so as to see the broadening of the profile. Key parameters are put in the insets; index of reflection, average particle size and temperature at the irradiation.

7.11 KRYPTON ION IRRADIATION BEHAVIORS OF 3.1eV PHOTO-LUMINESCENCE CENTER IN NON- IRRADIATED AREA OF SILICA GLASS

S.NASU[1], T. INAYOSHI[1], H.NANTO[1], K.OHHASHI[1] and A.IWASE

Silica glass is promising candidate materials for windows to introduce lights of laser fusion reactors [1], and to make plasma diagnostics of tokamak fusion reactors because of its excellent optical properties and stability. During operation of these fusion reactors, silica glass is subjected to irradiations of recoiled tritium and helium produced by the ^{6}Li (n,α)T reaction and fast neutrons, or intense light beams and silica glass will have some problems of transmission of lights. Therefore, a good understanding of radiation damages in silica glasses is necessary. In this work, we noticed the effect of 150 MeV Kr (+15) ions irradiation on the 3.1eV (400nm) photo-luminescence (PL) centers in silica glasses irradiated by 150 MeV Kr (+15) ions.

The specimen we used was GE-124 of commercially available silica glasses with mirror polished surfaces and its dimensions were 0.1 mm and 1.0 mm thick with an area of 10×10 mm^2. This silica glass has the intrinsic PL center at 3.1 eV (400 nm). Kr injection was done by Tandem Accelerator of Japan Atomic Energy Research Institute, Tokai Institute. The ion fluences were 1.0×10^{15} Kr/m^2 (500nA),1.0×10^{16} Kr/m^2 (500nA),1.0×10^{17} Kr/m^2 (95nA) and 2.0×10^{17} Kr/m^2 (90nA) for the 0.1 mm samples and 1.0×10^{17} Kr/m^2 (95nA) for the 1.0 mm thick sample. The calculated implanted range of Kr ions with 150 MeV is 19.80 μm in silica glass by TRIM code. Optical absorption (OA) spectra were measured with a double beam spectrum photometer (HITACHI,U-3300) and PL and PL excitation (PLE) spectra were obtained with a fluorescence spectrometer (Hitachi,F-3010) with a 150W Xe lamp as an excitation source. All the measurements were done at room temperature.

Figure 1 shows PL spectra of the 1.0 mm thick sample excited by 5.0 eV (250nm) corresponding to the maximum peak of PLE spectrum before and after irradiation. The intrinsic 3.1 eV (400nm) PL center (B2β center) decreased by about 60 % after 1.0×10^{17} Kr/m^2 irradiation, though the irradiation area is only about 2% of the whole sample. Furthermore, for the 0.1mm thick samples, where the percent of the irradiated area is about 20%, PL spectra showed about 40% (1.0×10^{15} Kr/m^2) to about 60% (1.0×10^{16} Kr/m^2) reduction or complete annihilation (1.0×10^{17} Kr/m^2, figure2) of the intrinsic 3.1 eV PL center. In general, this center is supposed to be one of the oxygen deficient centers, since this is observed in the samples prepared in the reduction atmosphere, and shows such strange behaviors as disappearance by irradiations of neutrons [2], or ions [3], or by decreasing temperatures [4]. For the 3.1 eV PL center to annihilate, some oxygen atoms should be supplied to the center, and the source of oxygen atoms should be elucidated.

Two well-known PL bands at 4.4 eV (280nm) and at 2.7eV (470nm) were also observed after Kr ion irradiation for both of the 1.0mm and 0.1mm thick samples as shown in figures 1 and 2,

[1] Kanazawa Institute of Technology, Ohgigaoka 7-1, Ishikawa, 921-8501 Japan

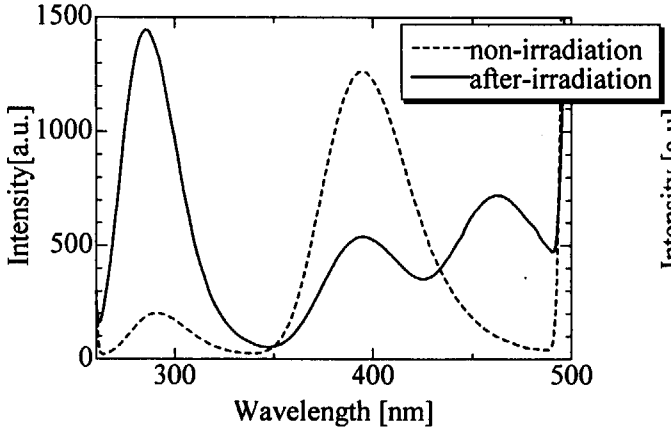

Fig.1. PL spectra of silica glass (GE124) before and after 150MV Kr ion irradiation

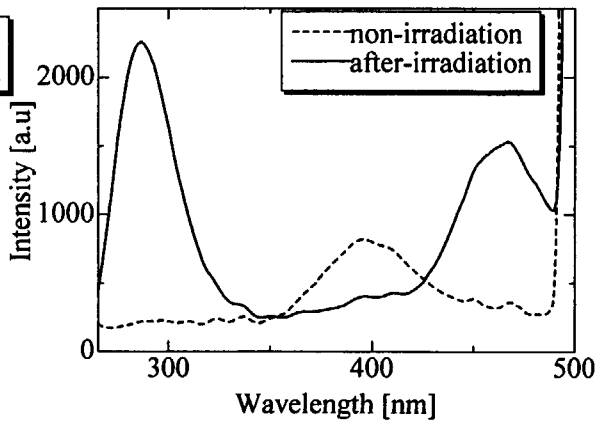

Fig.2. PL spectra of silica glass (GE124) before and after 150MV Kr ion irradiation

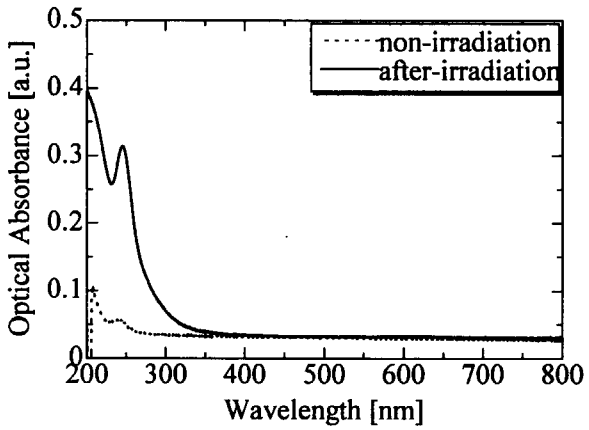

Fig.3. OA spectra of silica glass (GE124) before and after 150MV Kr ion irradiation

although a weak intrinsic 4.4 eV PL band was observed before irradiation for the 1.0mm thick sample. And a strong OA peak at 5.0 eV (250nm), which corresponds to the PLE of the 4.4eV and the 2.7eV PL bands, was observed as shown in figure 3. These two bands seem to be induced in the 19.8 μ m thick irradiation area of the penetration depth of 150 MeV Kr ions in silica glass.

In summary we examined the effect of Kr ion irradiation on the intrinsic 3.1 eV PL center in non-irradiated area of silica glass. After 150 MeV Kr ion irradiation, the intrinsic 3.1 eV PL center decreased or completely annihilated although the irradiation area is 2% or 20% of the whole sample and two well-known PL bands at 4.4 eVand at 2.7 eV were also observed..

References

[1] C.D.Orth, S.A.Payne and W.F.Krupke, *Nucl.Fusion*, **36**, 75-116 (1996)
[2] S.Nasu, T.Sutani, S.Ishida, A.Koshino, R.Yamamoto, H.Nanto, T.Tanifuji and Y.Morimoto, J.Light & Vis.Env.24(2000) 19-24
[3]Suk-Ho Choi,R.G.Elliman,S.Cheylan and J.P.D.Martin, Appl.Phys.Lett.76(2000) 2062-2064
[4] M.Leone, R.Boscaino, M.Cannas and F.M.Gelardi, J.Non-Cryst.Solids 167(1997)105-110

7.12 ION IRRADIATION EFFECTS ON TENSILE PROPERTIES AND MICROSTRUCTURES OF CARBON FIBERS

A. KURUMADA[1], Y. IMAMURA[1], T. OKU[2], M. ISHIHARA, S. BABA and J. AIHARA

Carbon/Carbon composite materials have good nuclear characteristics, high thermal conductivity and excellent mechanical properties at high temperatures. They have been taken as one of the candidate materials for plasma facing components of the next fusion experimental reactors and for the cladding tube of the control rod of the High Temperature engineering Test Reactor (HTTR). In order to apply them for their reactors, it need to study on the changes in material properties and microstructures due to irradiation damage and to develop the excellent C/C composite materials with the irradiation damage resistance. On the other hand, material properties of the C/C composite are well known to depend on those of carbon fibers since carbon fibers in the C/C composite are generally less crystalline than the carbon matrix part. In this study, high energy ions of carbon, nickel and argon are irradiated to carbon fibers with different microstructures and different properties, and the effects of ion irradiation damage on the tensile properties and the microstructures are evaluated.

Materials tested in this study were five kinds of carbon fibers with different microstructures and different properties, which were a pitch based fiber (K13C2U), two mesophase pitch based fibers (YS-15-60S and YS-70-60S), a polyacrylonitrile based fiber (M55JB) and a vapor growth carbon fiber (K1100X). Carbon ions ($^{12}C^{6+}$) of 100 MeV with 0.5 μA were irradiated to 1×10^{-5} or 3×10^{-5} dpa, nickel ions ($^{59}Ni^{13+}$) of 200 MeV with 0.4 μA were irradiated to 1×10^{-5} or 5×10^{-4} dpa by the TANDEM accelerator in Tokai, JAERI, and argon ions ($^{40}Ar^{8+}$) of 175 MeV with 1 μA were irradiated to 1×10^{-3} dpa by the AVF cyclotron in Takasaki, JAERI.

The cross-sectional area of the carbon fiber was observed by SEM, and the diameter and the sectional area were evaluated from the photographs. The tensile test of the carbon fiber was carried out in accordance with the JIS R 7601-1986 method. The single carbon fiber was straightly put on the center of a frame paper with a square hole using epoxy resin adhesive. The both ends of the frame paper were picked by clips, and the single carbon fiber was stretched after the both sides of the frame paper were burned off by an incense stick. The Young's modulus of the carbon fiber was the slope of the straight line within the limits from 25 to 50 % of the maximum load because the stress raiser phenomenon was appeared on the stress-strain curve.

[1] Faculty of Engineering, Ibaraki University

[2] Ibaraki Study Center, The University of the Air

The ranges of carbon, nickel and argon ions calculated by TRIM-98 code were 161, 25.5 and 38.4 μm for the carbon material of 2.2 g/cm^3, respectively. Therefore, irradiation damages in the carbon fibers were uniform across the cross section because the diameter of about 20 μm was enough smaller than the ranges.

The cross-sectional areas of carbon fibers increased with increasing ion irradiation damage except for the K1100X of a Vapor Growth Carbon Fiber (VGCF). One of the reasons was the swelling of carbon basal planes due to lattice defects in the graphite interlayer. In the case of the K1100X, however, the cross-sectional area was stable against ion irradiation damage. Figure 1 showed changes in tensile strengths of carbon fibers after ion irradiation. The tensile strengths decreased with increasing ion irradiation damage except for the K1100X of the VGCF and the YS-15-60S of a mesophase pitch based fiber [1,2]. The tendency of the decrease was the same as that of carbon fibers due to neutron irradiation [3]. One of the reasons of the decrease was thought that the microstructures of carbon fibers were damaged on the axial direction because ions were irradiated vertically to the longitudinal direction of carbon fibers. In the case of the K1100X and the YS-15-60S, however, the tensile strengths were almost constant or increased with increasing ion irradiation damage, so the K1100X and YS-15-60S carbon fibers were considered to have irradiation damage resistance. The Young's moduli of carbon fibers tended to decrease with increasing ion irradiation damage like that of the tensile strength. And within the limits of this study, carbon fibers with the random structure were considered to have comparatively more excellent irradiation damage resistance than those with the radial structure.

Therefore, the VGCF and the mesophase pitch based carbon fiber were effective to develop the excellent C/C composite materials with irradiation damage resistance.

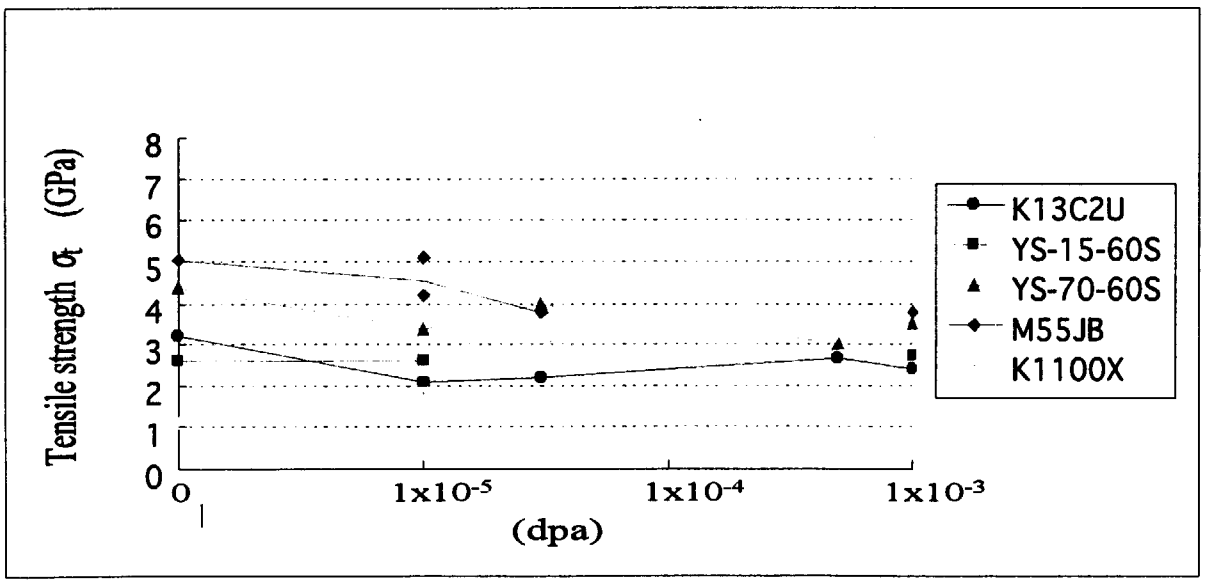

Fig. 1. Tensile strength of irradiated carbon fibers.

References

[1] T. Oku, A. Kurumada, B. McEnaney, T. D. Burchell, M. Ishihara, K. Hayashi, S. Baba and J. Aihara, Eurocarbon 2000, 1st World Conference on Carbon, Berlin, Germany (2000.7.9-13) Vol.II, 947-948.

[2] T. Oku, A. Kurumada, K. Kawamata and M. Inagaki, J. of Nuclear Materials, 303 (2002) 242-245.

[3] T. Oku, Y. Imamura, A. Kurumada, M. Inagaki and K. Kawamata, TANSO, No.190 (1999) 262-266.

7.13 A STUDY ABOUT THE STRUCTURE OF POWER MOSFETS WITH HIGH RADIATION TOLERANCE

H.SATO[1], T.HIRAO, H.SHINDO[1], S. KUBOYAMA[1]
T.KAMIYA, H. OHIRA[2], Y. NAGAI[2] and S. MATSUDA[1]

The single-event effects (SEE) due to cosmic rays become the most serious problem in applying a high voltage to the semiconductor devices used in space environments. The Single Event Burnout (SEB) is known as a possible catastrophic failure mode for power MOSFETs. The SEB is triggered when a high energy heavy ion passes through a power MOSFET under the off-state bias condition. The transient current, i_{ds}, generated by the heavy ion incidence turns on a parasitic bipolar transistor (BJT) in MOSFET, causes a short-circuit between the source, S, and the drain, D, due to carrier multiplication transistor action, and then destroys the device itself [1].

In our previous result, we pointed out that the Si crystal parameter affects the SEB tolerance greatly. In this paper, we have investigated experimentally that the SEB tolerance can be improved by optimizing the Si crystal parameter. The cross-sectional view of power MOSFET is shown in Fig. 1: S the source, G the gate, and D the drain.

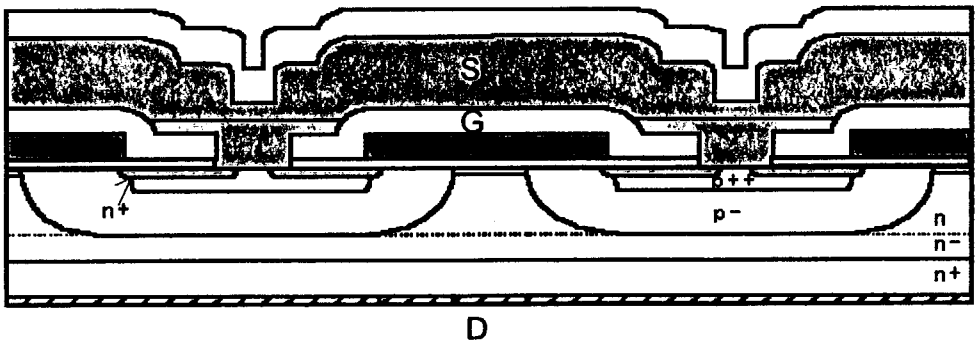

Fig.1 A schematic cross-sectional view of Power MOSFET

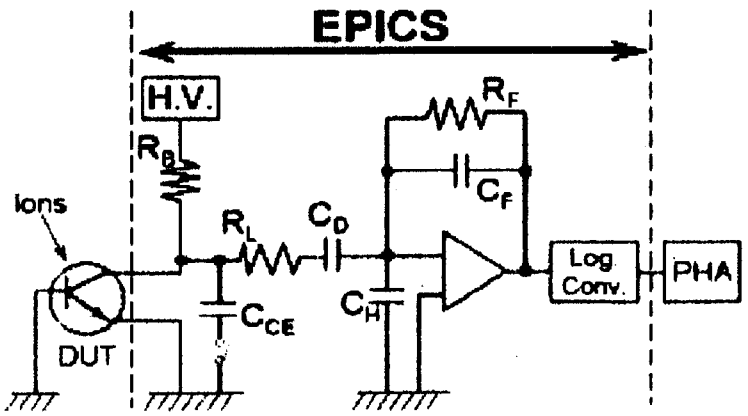

Fig.2 Block diagram of EPICS

[1] Technology Research Department, Office of Research and Development, National Space Development Agency of Japan

The SEB tests were carried out by using an Energetic Particle Induced Charge Spectroscopy (EPICS) system [2] as shown in Fig.2. EPICS is a specially designed with a pulse-height analyzer (PHA) system to characterize the generated charges, $\int i_{ds}dt$, in Device Under Test (DUT). In the high energy heavy ion irradiation test, we used Ni ions of LET=28.0[MeV/(mg/cm^2)] from the TANDEM accelerator at JAERI. The beam current was about 1.0nA. The primary ion beam was scattered by an Au thin foil to decrease intensity of ion beam irradiated directly over the Si die surface of MOSFET.

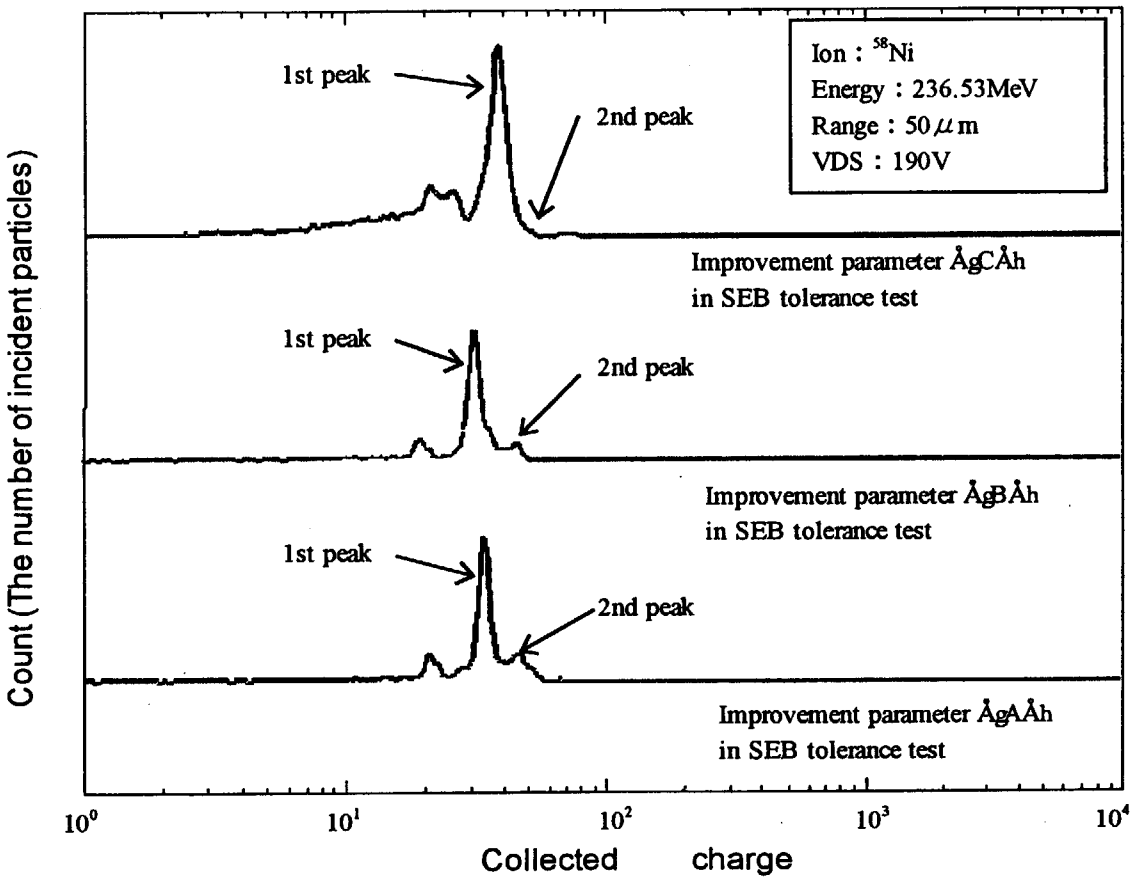

Fig.3 The observed result of SEB tolerance

Figure 3 shows the graph of the observed results of SEB tolerance as a function of 3 types of optimization parameters. The difference in a optimization parameter is a difference in the manufacture parameter of MOSFET. The SEB tolerance is improved greatly, especially the 2nd peak caused by the transistor action of BJT is lowered. For the device with the parameter "C", the 2nd peak cannot be observed. The generating mechanism of SEB relates to generating mechanism 2nd peak, that is, if the 2ndpeak are small, it can be said that it is hard to generate SEB. Thus we have successfully demonstrated a SEB free of MOSFET.

The power MOSFET having SEB free and low electrical on-state resistance, Ron, is necessary for developing the DC/DC converter with high efficiency. The power MOSFET under development will be used for the next generation DC/DC converter for space use.

References

[1] M.Allenspach et al, IEEE Trans. Nucl. Sci., Vol.NS-**43**, No.6(1996) 2927.
[2] S.Kuboyama et al, IEEE Trans. Nucl. Sci., Vol.NS-**39**, No.6(1992) 1698.

This is a blank page.

8. Publication in Journal and Proceedings, and Contribution to Scientific Meetings

This is a blank page.

ACCELERATOR OPERATION AND DEVELOPMENT

Journal/Proceedings

S. Arai, Y. Arakaki, K. Niki, M. Okada, Y. Takeda, M. Tomizawa, S. Takeuchi
Linac Complex in the JAERI-KEK Joint RNB Facility
Proc. of European Particle Accelerator Conf. 2002, Paris, France, 2002, p.861.

Y. Arakaki, S. Arai, K. Niki, M. Okada, Y. Takeda, M. Tomizawa
A Change of Resonant Frequency of IH-Linac for Radioactive Nuclear Beams
Proc. of European Particle Accelerator Conference 2002, Paris, France, 2002, p.864.

S. Ichikawa, A. Osa, M. Matsuda, K. Tsukada, M. Asai, Y. Nagame, S.C. Jeong, I. Katayama
Ion Source Development for the JAERI On-line Isotope Separator.
Nucl. Instrum. Methods **B204** (2003) 372-376.

S.C. Jeong, M. Oyaizu, E. Tojyo, H. Kawakami, H. Ishiyama, H. Miyatake, K. Enomoto,
Y. Watanabe, I. Katayama, T. Nomura, M. Matsuda, A. Osa, S. Ichikawa
The Development of an ECR Charge Breeder for KEK-JAERI Joint RNB Project
Nucl. Instrum. Methods **B 204** (2003) 420-427.

M. Matsuda, Y. Fujii, S. Takauchi, T. Yoshida
In-terminal ECR Ion Source Installation Project II
Proc. of the 15th Workshop on Tandem Accelerators and their Associated Technology, Tsuruga, 2002, pp62-64.

M. Okada, S. Arai, Y. Arakaki, K. Niki, Y. Takeda, M. Tomizawa
Design and Model Tests of a Rebuncher in the JAERI-KEK Joint RNB Linac System
Proc. of the 27th Linear Accelerator Meeting in Japan, Kyoto, Japan, 2002, p.63.

M. Oyaizu, S.C. Jeong, E. Tojyo, H. Kawakami, H. Ishiyama, H. Miyatake, K. Enomoto,
Y. Watanabe, I. Katayama, T. Nomura, M. Matsuda, A. Osa, S. Ichikawa
The 18GHz ECR Charge Breeder for KEK-JAERI RNB Joint Project
Proc. of the 15th Int. Workshop on ECR Ion Sources, Finland, 2002, pp130-133.

S. Takeuchi, T. Nakanoya, T. Yoshida
Study on Ceramics in Accelerator Tubes
Proc. of the 15th Workshop on Tandem Accelerators and their Associated Technology, Tsuruga, 2002, pp88-91.

S. Takeuchi, M. Matsuda, N. Ishizaki, H. Tayama, A. Iijima, T. Yoshida
Operational Status of Superconducting Resonators of the JAERI Tandem- Booster
Proc. of the 10th Workshop on RF Superconductivity, Tsukuba, 2001, pp591-593.

T. Yoshida, S. Kanda, S. Takeuchi, K. Horie, S. Hanashima, I. Ohuchi, Y. Tsukihasi, S. Abe, N. Ishizaki, H. Tayama, M. Matsuda, T. Nakanoya, H. Kabumoto
The Status of the JAERI Tandem Accelerator and the RNB Project
Proc. of the 15th Workshop of the Tandem Accelerator and their Associated Technology, Tsuruga, 2002, pp51-53.

Meetings

S. Ichikawa, A. Osa, M. Matsuda, K. Tsukada, M. Asai, Y. Nagame, S.C. Jeong, I. Katayama
Ion Source Development for the JAERI On-line Isotope Separator
14th Int. Conf. on Electromagnetic Isotope Separators and Techniques Related to their Applications, Victoria, B.C. Canada (May. 6-11, 2002)

M. Matsuda, Y. Fujii, S. Takauchi, T. Yoshida
In-terminal ECR Ion Source Installation Project II
The 15th Workshop on Tandem Accelerators and Associated Technology, Tsuruga, (Jun. 24-25, 2002)

M. Matsuda, T. Nakanoya
Development of Stable Nuclei Beam for RNB Project
Material Science Symposium "Heavy Ion Science in Tandem Energy Region", Tokai (Jan. 8-9, 2003)

S. Takeuchi,
Projected Gradients for the Drift-tube Cavities: Performance and Reliability, Operating Experience at JAERI
RIA Driver Workshop II, Argonne (May. 23, 2002)

S. Takeuchi, T. Nakanoya, T. Yoshida
Study on Ceramics in Accelerator Tubes
15th Workshop on Tandem Accelerators and their Associated Technology, Tsuruga (Jun. 24, 2002)

S. Takeuchi
The JAERI-KEK Joint RIB Project
17th Int. Conf. on the Application of Accelerators in Research and Industry CAARI 2002, Denton (Nov. 15, 2002)

S. Takeuchi
Improvement of the High-voltage Performances of Acceleration Tubes by Cleaning the Inner Walls with a High Pressure Water Jet
Seminar at Oak Ridge National Laboratory, Oak Ridge (Nov. 18, 2002)

S. Takeuchi
Development of Tandem Accelerator plus RNB Acceleration System
Symp. on Heavy Ion Science in the Tandem Accelerator Energy Region, Tokai (Jan. 8, 2003)

T. Yoshida, S. Kanda, S. Takeuchi, K. Horie, S. Hanashima, I. Ohuchi, Y. Tsukihasi,
S. Abe, N. Ishizaki, H. Tayama, M. Matsuda. T. Nakanoya, H. Kabumoto
The Status of the JAERI Tandem Accelerator and the RNB Project
15th Workshop of the Tandem Accelerator and their Associated Technology,
Tsuruga (Jun.24-25, 2002)

NUCLEAR STRUCTURE

Journal/Proceedings

M. Asai, K. Tsukada, S. Ichikawa, M. Sakama, H. Haba, Y. Nagame, I.Nishinaka,
K. Akiyama, A. Toyoshima, T. Kaneko, Y. Oura, Y. Kojima, M. Shibata
Identification of the New Isotope ^{241}Bk
Eur. Phys. J. **A 16** (2003) 17.

M. Asai, M. Sakama, K. Tsukada, S. Ichikawa, H. Haba, I. Nishinaka, Y.Nagame, S. Goto,
K. Akiyama, A. Toyoshima, Y. Kojima, Y. Oura, H. Nakahara, M. Shibata, K. Kawade
Decay Studies of Neutron-deficient Am, Cm, and Bk Nuclei using an On-line Isotope Separator
J. Nucl. Radiochem. Sci. **3** (2002) 187.

M. Asai, M. Sakama, K. Tsukada, S. Ichikawa, H. Haba, I. Nishinaka, Y.Nagame, S. Goto,
Y. Kojima, Y. Oura, H. Nakahara, M. Shibata, K. Kawade
Measurements of EC and Weak α–Decays of Neutron-deficient Transuranium Isotopes
J. Nucl. Sci. Technol. Suppl. **2** (2002) 474.

T. Hayakawa, Y. Toh, M. Oshima, M. Matsuda, Y. Hatsukawa,
J. Katakura, H. Iimura, T. Shizuma, S. Mitarai, M. Sugawara, H. Kusakari, Y.H. Zhang
Rotational Alignment of the $h_{11/2}$ Band in ^{157}Dy
Eur. Phys. J. **A15** (2002) 299-302.

T. Hayakawa, Y. Toh, M. Oshima, M. Matsuda, Y. Hatsukawa,
N. Shinohara, H. Iimura, T. Shizuma, Y.H. Zhang, M. Sugawara, H. Kusakari
Electric-dipole Transition Probabilities between Yrast Bands in ^{157}Gd
Phys. Lett. **B551** (2003) 79.

S. Ichikawa, M. Asai, A. Osa, K. Tsukada, H. Haba, S. Goto, Y. Nagame,
M. Shibata, Y. Kojima, M. Sakama, T. Tachibana
Systematic Studies of β-decay Half-lives of New Neutron-rich Lanthanide Isotopes
Proc. of the 3rd Int. Conf. on Exotic Nuclei and Atomic Masses
ENAM2001,Hämeenlinna, Finland (Springer, Berlin, 2003) p. 117.

H. Iimura, M. Oba, Y. Ishida, M. Koizumi, T. Shibata, N. Shinohara, T. Horiguchi,
H. A. Schuessler
Hyperfine Structure and Isotope Shift Measurements of Long-Lived La Isotopes by Collinear Laser Spectroscopy
Proc. of the 3rd Int. Conf. on Exotic Nuclei and Atomic Masses, Springer (2003) p.86.

H. Iimura, H. Ohba, T. Shibata, H. Miyatake
Velocity Distributions of Neodymium Atoms in Laser Ablation Plume
Proc. 3rd Symp. on Advanced Photon Research, JAERI-Conf **2002-008** (2002) p.84.

T. Ishii, M. Asai, A. Makishima, I. Hossain, P. Kleinheinz, M. Ogawa, M. Matsuda, S. Ichikawa
Gamma-ray Spectroscopy of the Neutron-rich Ni Region through Heavy-ion Deep-inelastic Collisions
Eur. Phys. J. A **13** (2002) 15.

Z. Liu, Y. H. Zhang, X. H. Zhou, M. L. Liu, W. J. Luo, Q. Y. Pan, Z. G. Gan, T. Hayakawa,
M. Oshima, Y. Toh, T. Shizima, Y. Hatsukawa, A. Osa, T. Ishii, M. Sugawara
New Yrast Excited States of the N=84 Nucleus ^{142}Ce Observed in Deep Inelastic Reactions
Eur. Phys. J. **A 13** (2002) 277.

A.Osa, T. Czosnyka, Y. Utsuno, T. Mizusaki, Y. Toh, M. Oshima, T. Hayakawa, Y. Hatsukawa,
J. Katakura, M. Koizumi, M. Matsuda, T. Shizuma, M. Sugawara, T. Morikawa, H. Kusakari
First Measurement of a Quadrupole Moment in the 2_1^+ State of ^{84}Kr
Phys. Lett. **B546** (2002) 48.

M. Sakama, K. Tsukada, M. Asai, S. Ichikawa, H. Haba, S. Goto, I. Nishinaka, Y. Nagame,
Y. Oura, Y. Kojima, A. Osa, M. Shibata, K. Kawade, M. Ebihara, H. Nakahara
Nuclear Decay Properties of the Neutron-deficient Actinides
J. Nucl. Sci. Technol. Suppl. **3** (2002) 34.

T. Shizuma, P.D. Stevenson, P.M. Walker,Y. Toh, T. Hayakawa, M. Oshima, K. Furuno,
T. Komatsubara
High-K Negative Parity States in ^{184}Os
Phys. Rev. **C 65** (2002) 064310.

T. Shizuma, Y.R. Shimizu, T. Hayakawa
Tunneling in High-K Isomeric Decays
J. Nucl. Sci. and Tech. **39** (2002) 1137.

T. Shizuma, Y. Toh, M. Oshima, M. Sugawara, M. Matsuda, T. Hayakawa, M. Koizumi, A. Osa, Y.H. Zhang, Z. Liu
Inelastic Excitation of ^{187}Re
Eur. Phys. J. **A17** (2003) 159.

M. Sugawara, Y. Toh, T. Czosnyka, M. Oshima, T. Hayakawa, H. Kusakari, Y. Hatsukawa, J. Katakura, N. Shinohara, M. Matsuda, T. Morikawa, A. Seki, F. Sakata
Multiple Coulomb Excitation of a ^{70}Ge Beam and the Int. of the 0^+_2 State as a Deformed Intruder
Eur. Phys. J. **A16** (2003) 409.

M. Sugawara, S. Mitarai, H. Kusakari, M. Oshima, T. Hayakawa, Y. Toh, Y. Hatsukawa, J. Katakura, H. Iimura, Y.H. Zhang, M. Sugie, Y. Satoh
Rotational Bands of ^{159}Dy
Nucl. Phys. **A699** (2002) 450.

Y. Toh, M. Oshima, T. Hayakawa, Y. Hatsukawa, J. Katakura, M. Matsuda, H. Iimura, H. Kusakari, D. Nishimiya, M. Sugawara, Y.H. Zhang
A Position-sensitive Particle Detector for Coulomb Excitation Experiment
Rev. Sci. Instrm. **73(1)** (2002) 47.

Y. Toh, T. Czosnyka, M. Oshima, T. Hayakawa, M. Sugawara, H. Kusakari, Y. Hatsukawa, M. Matsuda, J. Katakura, N.Shinohara
Shape Coexistence in Even-even Ge Isotopes
AIP Conf. Proc. **610** (2002) 793.

Y. Toh, T. Czosnyka, M. Oshima, T. Hayakawa, Y. Hatsukawa, M. Matsuda, J. Katakura, N. Shinohara, M. Sugawara, H. Kusakari
Shape Coexistence in Even-even Ge Isotopes - Complete Spectroscopy with Coulomb Excitation
J. Nucl. Sci. and Tech. Suppl. **2**, No.2, (2002) 497.

Y. H. Zhang, T. Hayakawa, M. Oshima, J. Katakura, Y. Hatsukawa, M. Matsuda, H. Kusakari, M. Sugawara, T. Komatsubara, K. Furuno
Configuration-dependent Band Structures in Odd-odd ^{180}Ir
Phys. Rev. **C 65** (2002) 014302.

Y. H. Zhang, M. Oshima, Y. Toh, M. Koizumi, A. Osa, T. Shizuma, T. Hayakawa M. Sugawara, H. Kusakari, T. Morikawa, S. X. Wen, L. H. Zhou
Rotational Bands and Signature Inversion Phenomena in $\pi h_{9/2} \times \nu i_{13/2}$ and $\pi i_{13/2} \times \nu i_{13/2}$configurations in ^{176}Ir
Eur. Phys. J. **A13** (2002) 429.

Y. H. Zhang, F. R. Xu, J. J. He, Z. Liu, X. H. Zhou, Z. G. Gan, T. Hayakawa, M. Oshima, T. Toh, T. Shizuma, J. Katakura, Y. Hatsukawa, M. Matsuda, H. Kusakari, M. Sugawara, K. Furuno, T. Komatsubara, T. Une, S. X. Wen, Z. M. Wang.
Signature Inversion Phenomena in Odd-odd ^{182}Au
Eur. Phys. J. **A14** (2002) 271.

X. H. Zhou, M. Oshima, Y. Toh, Y. H. Zhang, Y. Zheng, M. Koizumi, A. Osa, T. Hayakawa, Y. Hatsukawa, T. Shizuma, M. Sugawara
Rotational Bands in ^{169}Re
Eur. Phys. J. **A15** (2002) 285.

M. Zielinska, T. Czosnyka, J. Choinski, J. Iwanicki, P. Napiorkowski, J Srebrny, Y. Toh, M. Oshima, A. Osa, Y. Utsuno, Y. Hatsukawa, J. Katakura, M. Koizumi, M. Matsuda, T. Shizuma, M. Sugawara, T. Morikawa, H. Kusakari, A.D. Effimov, V.M.Mikhailov
Electromagnetic Structure of ^{98}Mo
Nucl. Phys. **A712** (2002) 3.

Meeting

M. Asai, K. Tsukada, S. Ichikawa, Y. Nagame, M. Sakama, Y. Oura, Y. Kojima, M. Shibata
Decay Spectroscopy for Am, Cm, and Bk Nuclei
Fall Meeting of the Physical Society of Japan, Tokyo (Sep. 13-16, 2002)

M. Asai, K. Tsukada, S. Ichikawa, Y. Nagame, I. Nishinaka, K. Akiyama,
A. Toyoshima, A. Osa, H. Haba, M. Sakama, Y. Oura, Y. Kojima, M. Shibata, K. Sueki
Ionization and On-line Mass-separation of Berkelium and Nobelium Isotopes
2002 Annual Meeting of the Japan Society of Nuclear and Radiochemical Sciences,
Sapporo (Sep. 23-25, 2002)

M. Asai, S. Ichikawa, K. Tsukada, A. Osa, I. Nishinaka, Y. Nagame, Y. Kojima, M. Shibata
Gamma-ray Spectroscopy for Neutron-rich A ~160-170 Nuclei: the β^- *Decay of* ^{159}Pm, $^{160\text{-}162}Sm$, ^{162}Eu, $^{164\text{-}166}Gd$ *and* $^{166\text{-}168}Tb$
The 3rd Int. Conf. on Fission and Properties of Neutron-rich Nuclei,
Sanibel Island, USA (Nov. 4-9, 2002)

M. Asai, T. Ishii, A. Makishima, M. Ogawa, M. Matsuda
Nanosecond Isomers in Neutron-rich N ~19 Nuclei
The 3rd Int. Conf. on Fission and Properties of Neutron-rich Nuclei,
Sanibel Island, USA (Nov. 4-9, 2002)

M. Asai, K. Tsukada, S. Ichikawa, Y. Nagame, T. Ishii, I. Nishinaka, K. Akiyama,
A. Osa, M. Sakama, Y. Oura, K. Sueki, M. Shibata
Conversion Electron Measurement for the α*- Decay of* ^{257}No
Annual Meeting of the Physical Society of Japan, Sendai (Mar. 28-31, 2003)

H. Iimura, M. Oba, M. Koizumi, N. Shinohara, T. Shibata, M. Miyabe, Y. Ishida,
T. Horiguchi, H. A. Schuessler
Isotope Shift Measurements of $^{135,137}La$ *by Collinear Laser Spectroscopy*
Fall Meeting of the Physical Society of Japan, Tokyo (Sep. 16, 2002)

T. Ishii, M. Asai, M. Matsuda, P. Kleinheinz, Hou Long, J. Hori, A. Makishima, T. Kohno,
M. Ogawa, K. Ogawa, H. Nakada
Nano-second Isomers in Neutron-rich Nuclei around ^{68}Ni
Third Int. Conf. on Fission and Properties of Neutron-rich Nuclei, Sanibel Island, Florida (Nov. 3-9, 2002)

M. Koizumi, A. Osa, Y. Toh, M. Oshima, Y. Hayakawa, Y. Hatsukawa, J. Katakura, M. Matsuda, T. Shizuma, Y. Utsuno, A. Kimura, A. Seki, A. Sugawara, T. Morikawa, H. Kusakari, T. Czosnyka

Multiple Coulomb Excitation of ^{66}Zn

Fall Meeting of the Physical Society of Japan, Tokyo (Sep. 16,2002)

M.Shibata, O. Suematsu, K. Kawade, M. Asai, S. Ichikawa, Y. Nagame, A. Osa, K. Tsukada, Y. Kojima

Q_β Measurement of Neutron-Rich Rare-Earth Nuclei produced with Proton Induced Fission of ^{238}U

3rd Int. Conf. on Fission and Properties of Neutron-Rich Nuclei, Florida, USA (Nov.4-9, 2002)

T. Shizuma

Nuclear Isomers and the Photo Nuclear Excitation

The 4th Symp. on Advanced Photon Research, Kizu (Nov. 2002)

T. Shizuma

Isomer Research in the A=180 Region by Photo-nuclear Reactions

The 2nd Workshop on "Nuclear isomers and FEL application"
Advanced Photon Reserach Center, Kizu (Mar. 2003)

T. Shizuma

Proposal for Isomer Experiments on ^{176}Lu and ^{180}Ta using Intense MeV-photons from the Superconducting Wigler

Workshop on "Generation of High Energy Synchrotron Radiation by Superconducting Wigler and its Application", Harima (Mar. 2003)

T. Shizuma

High-K Isomers at the A=180 Region and the K-mixing

Annual Meeting of the Physical Society of Japan, Sendai (Mar. 2003)

Y. Toh, M. Oshima, A. Osa, M. Koizumi, Y. Hatsukawa, N. Shinohara, A. Kimura, H. Kusakari, M. Sugawara, K. Furuno, H. Kimura,
A New Detector Array GEMINI-II
Annual Meeting of the Japan Physical Society of Japan, Sendai (Mar. 28, 2002)

Y. H. Zhang, T. Morikawa, M. Oshima, Y. Tho, M. Koizumi, A. Osa,T. Shizuma, T. Hayakawa, Y. Hatsukawa, H. Kusakari, M. Sugawara,S. X. Wen, L. H. Zhu
Rotational Bands in Odd-odd ^{176}Ir and Signature Inversion Phenomena
Fall Meeting of the Physical Society of Japan, Tokyo (Sep. 15, 2002)

X. H. Zhou, M. Sugawara, M. Oshima, Y. Toh, Y. H. Zhang, Y. Zheng, M. Koizumi, A. Osa, T. Hayakawa, Y. Hatsukawa, T. Shizuma
Configuration-dependent Bands in ^{169}Re
Fall Meeting of the Physical Society of Japan, Tokyo (Sep. 15, 2002)

NUCLEAR REACTIONS

Journal/Proceedings

H. Fujita, M. Hijiya, Y. Inotani, T. Mukae, K. Koga, M. Koga, F. Nakamura, S. Kato, T. Sugimitsu, N. Ikeda, S. Morinobu, Y. Sugiyama, Y. Tomita, H. Ikezoe, Y. Yamanouti, K. Ideno, S. Hamada, T. Ikuta
Intermediate Structures in $^{12}C(^{16}O, ^{12}C[2^+])^{16}O$ studied with the γ-ray Recoil Method
Phys. Rev. **C66** (2002) 024609.

S. Goto, D. Kaji, I. Nishinaka, Y. Nagame, S. Ichikawa, K. Tsukada, M. Asai,H. Haba, S. Mitsuoka, K. Nishio, M. Sakama, Y. L. Zhao, K. Sueki, M. Tanikawa, K. Takamiya, H. Kudo, H. Nakahara
Systematic Studies of Asymmetric Mass Distributions in Proton-induced Fission of Actinides
J. Nucl. Radiochem. Sci. **3** (2002) 63.

S. Goto, D. Kaji, I. Nishinaka, Y. Nagame, S. Ichikawa, K. Tsukada, M. Asai, S. Mitsuoka, K. Nishio, M. Sakama, Y. L. Zhao, K. Sueki, M. Tanikawa, K. Takamiya, H. Kudo, H. Nakahara
Characteristics of the Asymmetric Mass Distribution in Proton-Induced Fission of Actinides
J. Radioanal. Nucl. Chem. **255** (2003) 73.

H. Ikezoe, S. Mitsuoka, K. Nishio, K. Satou, I. Nishinaka
Dependence of Heavy-ion Fusion Reaction on Nuclear Deformation and Nuclear Shell Structure
AIP Conf. Proc. **610** (2002) p.604.

T. Ishikawa, H. Ishiyama, T. Hashimoto, T. Kawamura, H. Miyatake, M.H. Tanaka, Y. Fuchi, N. Yoshikawa, S.C. Jeong, Y. Watanabe, H. Kawakami, I. Katayama, T. Nomura, S. Mitsuoka, K. Nishio, M. Matsuda, S. Ichikawa, H. Ikezoe, T. Furukawa, H. Yano, H. Izumi, Y. Mizoi, M. Terasawa, T Fukuda, K, Nakai, T. Shimoda,
Measurement of the $^{16}N(\alpha, n)$ Reaction Cross Section
Nucl. Phys. **A718** (2003) 484c.

H. Ishiyama, T. Hashimoto, T. Kawamura, T. Ishikawa, H. Miyatake, M.H. Tanaka, Y. Fuchi, N. Yoshikawa, S.C. Jeong, Y. Watanabe, H. Kawakami, I. Katayama, T. Nomura, S. Mitsuoka, K. Nishio, M. Matsuda, S. Ichikawa, H. Ikezoe, T. Furukawa, H. Yano, H. Izumi, Y. Mizoi, M. Terasawa, T Fukuda, K, Nakai, T. Shimoda,
Direct Measurements of (α, n) and (p, n) Reaction Cross Sections using Light Neutron-rich Radioactive Nuclear Beams
Nucl. Phys. **A718** (2003) 481c.

C. L. Jiang, H. Esbensen, K. E. Rehm, B. B. Back, R. V. F. Janssens, J. A.Caggiano, P. Collon, J. Green, A. M. Heinz, D. J. Henderson, I. Nishinaka,T. O. Pennington, D. Seweryniak
Unexpected Behavior of Heavy-Ion Fusion Cross Sections at Extreme Sub-barrier Energies
Phys. Rev. Lett. **89** (2002) 052701.

Y. Nagame, M. Asai, H. Haba, S. Goto, K. Tsukada, I. Nishinaka, K. Nishio, S. Ichikawa, A. Toyoshima, K. Akiyama, H. Nakahara, M. Sakama, M. Schadel, J. V. Kratz, H. W. Gaggeler, A. Turler
Production Cross Sections of ^{261}Rf and ^{262}Db in Bombardments of ^{248}Cm with ^{18}O and ^{19}F Ions
J. Nucl. Radiochem. Sci. **3** (2002) 85.

K. Nishio, H. Ikezoe, Y. Nagame, S. Mitsuoka, I. Nishinaka, L. Duan, K. Satou, S. Goto, M. Asai, H. Haba, K. Tsukada, S. Shinohara, S. Ichikawa
Fragment Mass Distribution of the $^{239}Pu(d,pf)$ Reaction via the Superdeformed β-vibrational Resonance
Phys. Rev. **C 67** (2003) 014604.

K. Nishio, H. Ikezoe, S. Mitsuoka, K. Satou
Effects of Nuclear Deformation on the Fusion Probability in the Reactions of $^{76}Ge+^{150}Nd$ and $^{82}Se+^{nat}Ce$ near the Coulomb Barrier
J. Nucl. Sci. Technol. Suppl. **2** (2002) 599-602.

K. Nishio, H. Ikezoe, S. Mitsuoka, K. Satou, S.C. Jeong
Effects of Nuclear Deformation on the Fusion Probability in the Reactions of $^{76}Ge+^{150}Nd$ and $^{82}Se+^{nat}Ce$ near the Coulomb Barrier
J. Nucl. Sci. Technol. Suppl. **3** (2002) 26-29.

Y. L. Zhao, I. Nishinaka, Y. Nagame, K. Tsukada, K. Sueki, M. Tanikawa, S. Goto, H. Nakahara
Fission Characteristics of Individual Deformation Paths in Heavy Elements
J. Nucl. Radiochem. Sci. **3** (2002) 103.

Y. L. Zhao, I. Nishinaka, Y. Nagame, K. Tsukada, K. Sueki, S. Goto, M. Tanikawa, H. Nakahara
Primary Fragment Mass-Yield Distributions for Asymmetric Fission Path of Heavy Nuclei
J. Radioanal. Nucl. Chem. **255** (2003) 67.

Meetings

S. Goto, D. Kaji, H. Kudo, I. Nishinaka, Y. Nagame, S. Ichikawa, K. Tsukada, M. Asai, H. Haba , M. Tanikawa
Systematic Study of Asymmetric Mass Division in Proton-induced Fission of Actinides
Annual Meeting of the Japan Society of Nuclear and Radiochemical Sciences, Sapporo (Sep.,25, 2002)

T. Hashimoto, T. Ishikawa, T. Kawamura, T. Furukawa, H. Yano, H. Ishiyama, H. Miyatake, M.H. Tanaka, Y. Watanabe, Y. Fuchi, S.C. Jeong, N. Yoshikawa, Y. Matsyama, I. Katayama, T. Nomura, M. Mitsuoka, K. Nishio, M. Matsuda, S. Ichikawa, H. Ikezoe, H. Izumi, T. Shimoda, T. Fukuda, Y. Mizoi, M, Terasawa, K. Nakai
Measurement of the $^{8}Li(\alpha, n)^{11}B$ Reaction for Astrophysical Interest
Annual Meeting of the Physical Society of Japan, Sendai (Mar. 28, 2003)

S. Mitsuoka, H.I kezoe, K. Nishio, K.S atou, C. J. Lin
Effects of Nuclear Deformation on Fusion Probability in the Reactions of $^{64}Ni+^{198}Pt$ and $^{82}Se+^{176}Yb$ near the Coulomb Barrier
Annual Meeting of the Physical Society of Japan, Sendai (Mar. 28, 2003)

A. Nishinaka, M. Tanikawa, S. Goto, Y. Nagame, K. Nishio, A. Yokoyama, M.Asai, H. Haba, S. Ichikawa, K. Tsukada, K. Akiyama, A. Toyoshima, H. Kudo
Anomalous Excitation Energy Dependence of Shell Effects in Asymmetric Actinide Fission
Annual Meeting of the Japan Society of Nuclear and Radiochemical Sciences, Sapporo, (Sep. 25,

2002)

K. Nishio, H. Ikezoe, Y. Nagame, S. Mitsuoka, I. Nishinaka,L. Duan, K. Satou, S. Goto, M. Asai, H. Haba, K. Tsukada, N. Shinohara, S. Ichikawa
Fragment Mass Distribution of *the ^{239}Pu(d,pf) Reaction via the Superdeformed* β*-vibrational Resonance*
Annual Meeting of the Physical Socierty of Japan, Sendai (Mar. 28, 2003)

K. Nishio, H. Ikezoe, S. Mitsuoka, L. Duan, K. Satou
Experiment on the Fusion Reaction ^{136}Xe + ^{124}Sn
Fall Meeting of the Physical Socierty of Japan, Tokyo (Sep. 16, 2003)

K. Nishio, H. Ikezoe, Y. Nagame, S. Mitsuoka, I. Nishinaka, L. Duan, K. Satou, S. Goto, M. Asai, H. Haba, K. Tsukada, N. Shinohara, S. Ichikawa
Fragment Mass Distribution of the ^{239}Pu(d,pf) reaction via the Superdeformed β*-vibrational Resonance*
Fall Meeting of the Atomic Energy Socierty of Japan, Iwaki (Sep. 16, 2002)

K. Satou, H. Ikezoe, S. Mitsuoka, K. Nishio, C.J. Lin
Fusion Reaction Measurements for the Reactions ^{86}Kr+^{134,138}Ba
The meeting for the Heavy Ion Science using Tandem Accelerator, Tokai (Jan. 8, 2003).

K. Satou, H. Ikezoe, S. Mitsuoka, K. Nishio, C.J. Lin, S.C. Jeong
Shell Effect on the Heavy Ion Fusion Reaction
The meeting for the Studies of Nuclear Physics and Chemistry about Super Heavy Element, Tokai (Feb. 27, 2003)

K. Satou, H. Ikezoe, S. Mitsuoka, K. Nishio, C.J. Lin
Fusion Reaction Measurements for the Reactions ^{86}Kr+^{134,138}Ba
Annual Meeting of Physical Society of Japan, Sendai (Mar. 28, 2003)

NUCLEAR CHEMISTRY

Journal/proceedings

K. Akiyama, K. Sueki, H. Haba, K. Tsukada, M. Asai, T. Yaita, Y. Nagame, K. Kikuchi, M. Katada, H. Nakahara,
Production and Characterization of Actinide Metallofullerenes.
J. Radioanal. Nucl. Chem. **255** (2003) 155.

H. Haba, K. Tsukada, M. Asai, S. Goto, A. Toyoshima, I. Nishinaka, K. Akiyama, M. Hirata, S. Ichikawa, Y. Nagame, Y. Shoji, M. Shigekawa, T. Koike, M. Iwasaki, A. Shinohara, T. Kaneko, T. Maruyama, S. Ono, H. Kudo, Y. Oura, K. Sueki, H. Nakahara, M. Sakama, A. Yokoyama, J. V. Kratz, M. Schädel, W. Brüchle
Anion-exchange Behavior of Rf in HCl and HNO_3 Solutions
J. Nucl. Radiochem. Sci. **3** (2002)143.

Y. Hatsukawa, M. Oshima, T. Hayakawa, Y. Toh, N. Shinohara,
Application of the Multiparameter Coincidence Method to Neutron Activation Analysis
Nucl. Instrum. Methods **A482** (2002) 301-304.

Y. Hatsukawa, Y. Toh, M. Oshima, T. Hayakawa, N. Shinohara, K. Kushita, T. Ueno, K. Toyoda
New Technique fir the Determination of Trace Elements using Multiparameter Coincidence Spectrometory
J. Radioanal. Nucl. Chem. **255** (2003) 111-113.

T. Kaneko, S. Ono, S. Goto, H. Haba, M. Asai, K. Tsukada, Y. Nagame, H. Kudo
Isothermal Gas Chromatography of Chlorides of Zr and Hf as Rf Homologs
J. Radioanal. Nucl. Chem. **255** (2003) 381.

K Katoh, H. Miyahara, N. Marnada, N.Ueda, K. Ikeda, K. Fujiki, H. Haba, I. Nishinaka, K. Tsukada, Y. Nagame, M. Asai, S. Ichikawa
Production of ^{147}Eu for Gamma-ray Emission Probability Measurement
J. Nucl. Sci. Technol. **39** (2002) 329.

T. Maruyama, D. Kaji, T. Kaneko, S. Goto, K. Tsukada, H. Haba, M. Asai, S. Ichikawa, Y. Nagame, H. Kudo
Rapid Chemical Separation for Bk
J. Nucl. Radiochem. Sci. **3** (2002) 155.

T. Maruyama, D. Kaji, T. Kaneko, S. Goto, K. Tsukada, H. Haba,M. Asai, S. Ichikawa, Y. Nagame, H. Kudo
Chemical Separation of the Unknown Isotope ^{252}Bk
J. Radioanal. Nucl. Chem. **255** (2003) 253.

Y. Nagame, M. Asai, H. Haba, K. Tsukada, S. Goto, M. Sakama, I. Nishinaka, A. Toyoshima, K. Akiyama, S. Ichikawa
Status and Prospects of Heavy Element Nuclear Chemistry Research at JAERI
J. Nucl. Radiochem. Sci. **3** (2002) 129.

M. Oshima, Y. Toh, Y. Hatsukawa, T. Hayakawa, N. Shinohara
A High-sensitivity and Non-destructive Trace Element Analysis based on Multiple Gamma-ray Detection
J. Nucl. Sci. and Technol. **39** (2002) 292.

M. Oshima, Y. Toh, T. Hayakawa, Y. Hatsukawa, N. Shinohara
Development of a New Method of Neutron Activation Analysis with Multiple Gamma-ray Detection -a High-sensitivity and Non-destructive Trace Element Analysis
J. Nucl. Sci. and Technol., Suppl. **2**, No. 2 (2002) 1369.

N. Shinohara, Y.Hatsukawa, M. Oshima, Y. Toh, J. Katakura, O. Iwamoto, K. Nishio, H. Haba, Y. Nagame, K. Tsukada, I. Nishinaka
Measurement of Mass Yield Distribution in Proton-induced Fission of Minor Actinides
J. Nucl. Sci. Technol., Suppl. **2** (2002) 266-268.

K. Sueki, K. Akiyama, Y. L. Zhao, I. Ito, Y. Ohkubo, K. Kikuchi, M. Katada, H. Nakahara,
Systematic Study of Lanthanoid Endohedral Metallofullerenes: Production Yields, HPLC Retention Time and Reactor Irradiation Effects
J. Radioanal. Nucl. Chem. **255** (2003) 159.

Y. Toh, Y. Hatsukawa, M. Oshima, N. Shinohara, T. Hayakawa, K. Kushita, T. Ueno
Isotopic Ratio of $^{129}I/^{127}I$ in Seaweed measured by Neutron Activation Analysis with γ-γ Coincidence
Health Phys. **83** (2002) 110.

A. Toyoshima, K. Tsukada, H. Haba, M. Asai, S. Goto, K. Akiyama, I. Nishinaka, S. Ichikawa, Y. Nagame, A. Shinohara
Anion Exchange Behavior of Nobelium
J. Radioanal. Nucl. Chem. **255** (2003) 485.

Meetings

K. Akiyama, K. Sueki, K. Tsukada, H. Haba, M. Asai, S. Ichikawa, K. Kikuchi, T. Ohtsuki, Y. Nagame, M. Katada, H. Nakahara
Structural Study of Th Metallofullerenes
Annual Meeting of the Japan Society of Nuclear and Radiochemical Siences,
Sapporo (Sep. 23-25, 2002)

K. Akiyama, K. Sueki, K. Tsukada, H. Haba, A. Toyoshima, M. Asai, S. Ichikawa, K. Kikuchi, Y. Nagame, M. Katada, H. Nakahara
HPLC Behavior of Actinoids Metallofullerenes
Annual Meeting of the Japan Society of Nuclear and Radiochemical Siences,
Sapporo (Sep. 23-25, 2002)

K. Akiyama, K. Sueki, Y. Miyake, T. Kodama, K. Tsukada, T. Ohtsuki, K. Kikuchi, T. Yaita, Y. Nagame, M. Katada, H. Nakahara
Structure and Properties of Th Fullerene: $Th@C_{84}$
The 23rd Fullerene, Nanotubes General Symposium, Matsushima (Jul. 17-19, 2002)

H. Haba, K. Tsukada, M. Asai, I. Nishinaka, S. Goto, A. Toyoshima, K. Akiyama, M. Hirata, S. Ichikawa, Y. Nagame, Y. Shoji, M. Shigekawa, T. Koike, M. Iwasaki, A. Shinohara, T. Kaneko, T. Maruyama, S. Ono, H. Kudo, Y. Oura, K. Sueki, H. Nakahara, M. Sakama, A. Yokoyama, J. V. Kratz, M. Schädel
Chloride Complexation of Rutherfordium

14th Radiochemical Conference, Marianske Lazne, Czech Republic (Apr. 15, 2002)

H. Haba, K. Tsukada, M. Asai, K. Akiyama, A. Toyoshima, I. Nishinaka, S. Ichikawa, Y. Nagame
Anion Exchange Behavior of Zr and Hf in Hydrofluoric Acid -Model Experiments for Chemical Characterization of Element 104, Rutherfordium-
The 46th Symp. on Radiochemistry, Sapporo (Sep. 23, 2002)

H. Haba, K. Tsukada, M. Asai, K. Akiyama, A. Toyoshima, I. Nishinaka, S. Ichikawa, Y. Nagame
Anion Exchange Behavior of Nb, Ta, and Pa in Hydrofluoric Acid Solutions -Model Experiments for Chemical Characterization of Element 105, Dubnium-
The 83rd Spring Meeting of the Chemical Society of Japan, Shinjuku (Mar. 18, 2003)

Y. Hatsukawa, Y. Toh, M. Oshima, N. Shinohara
Application of Multidimensional Spectrum Analysis for Neutron Activation Method
The 5th Symp. on Iodine Utilization, Chiba (Oct. 18, 2002)

Y. Hatsukawa, Y. Toh, M. Oshima, N. Shinohara
New Technique for Determination of Long-lived Radioisotopes, Iodine-129, Using Multiparameter Coincidence Spectrometry
Int. Symp. on Transfer of Radionuclides in Biosphere -Prediction and Assessment-, Mito (Dec. 18-19, 2002)

T. Hirai, M. Hirata, Y. Nagame, H. Kudo
Electronic Structure of Fluoride Complexes of Rutherfordium and the 4th Row Elements
Annual Meeting of the Japan Society of Nuclear and Radiochemical Sciences, Sapporo (Sep. 23-25, 2002)

T. Kaneko, K. Tsukada, K. Akiyama, M. Asai, H. Haba, A. Toyoshima, S. Ono, T. Hirai, S. Goto, S. Ichikawa, Y. Nagame, H. Kudo
On-line Isothermal Gas Chlomatographic Behavior of Chlorides of Group IV Elements as a Model Experiment of Rf (Z=104)
Annual Meeting of the Japan Society of Nuclear and Radiochemical Sciences,

Sapporo (Sep. 23-25, 2002)

K. Katoh, H. Miyahara., K. Fujiki, S. Ichikawa, I. Nishinaka, K. Tsukada, M. Asai, H. Haba
Measurement of γ-ray Emission Probability for ^{149}Eu
Fall Meeting of the Atomic Energy Society of Japan, Iwaki (Sep. 14-16, 2002)

Y. Nagame, H. Haba, K. Tsukada, M. Asai, K. Akiyama, M. Hirata, I. Nishinaka, S. Ichikawa, H. Nakahara, S. Goto, T. Kaneko, H. Kudo, A. Toyoshima, A. Shinohara, M. Schadel, J. V. Kratz, H. Gaggeler, A. Turler
Transactinide Nuclear Chemistry at JAERI
14th Radiochemical Conference, Marianske Lazne, Czech Republic (Apr. 14-19, 2002)

Y. Nagame, H. Haba, K. Tsukada, M. Asai, A. Toyoshima, K. Akiyama, T. Kaneko, T. Hirai, S. Goto, M. Hirata, I. Nishinaka, S. Ichikawa
Few Atom Chemistry of the Transactinide Element, Rutherfordium (Rf)
The Int. Conf. on Applications of High Precision Atomic and Nuclear Methods, Neptune, Rumania (Sep. 2-5, 2002)

A. Toyoshima, K. Tsukada, M. Shigekawa, H. Haba, M. Asai, K. Akiyama, I. Nishinaka, S. Ichikawa, Y. Nagame, Y. Tani, H. Hasegawa, T. Kaneko, T. Hirai, A. Shinohara
Study of Cation Exchange Behavior of Nobelium(III)
Annual Meeting of the Japan Society of Nuclear and Radiochemical Sciences, Sapporo (Sep. 23-25, 2002)

A. Toyoshima, K. Tsukada, H. Haba, M. Asai, K. Akiyama, I. Nishinaka, S. Ichikawa, Y. Nagame, M. Shigekawa, S. Goto, T. Kaneko, S. Ono, H. Kudo, Y. Oura, K. Sueki, M. Sakama, H. Kikunaga, N. Kinoshita, N. Tsuruga, A. Yokoyama, A. Shinohara
Anion-exchange Behavior of Rf, Zr and Hf in HF Solution
The 83rd Spring Meeting of the Chemical Society of Japan, Shinjuku (Mar. 18-21, 2003)

K. Tsukada, H. Haba, M. Asai, A. Toyoshima, K. Akiyama, I. Nishinaka, S. Ichikawa, Y. Nagame, H. Nakahara, K. Yasuda, Y. Miyamoto, T. Kaneko, T. Hirai, S. Ono, S. Goto, H. Kudo, M. Shigekawa, A. Shinohara, K. Sueki, Y. Oura, M. Sakama, N. Tsuruga, N. Kinoshita, T. Murae, H. Kikunaga, A. Yokoyama

Anion-exchange Behavior of Rutherfordium in HF Media

2002 Annual Meeting of the Japan Society of Nuclear and Radiochemical Sciences, Sapporo (Sep. 23-25, 2002)

K. Tsukada, H. Haba, M. Asai, K. Akiyama, A. Toyoshima, T. Yaita, Y. Nagame

Aqueous Chemistry of Rf in HCl Solution

The 83rd Spring Meeting of the Chemical Society of Japan, Shinjuku (Mar. 18-21, 2003)

NUCLEAR THEORY

Journal/Proceedings

S. Chikazumi, T. Maruyama, K. Niita, A. Iwamoto, S. Chiba
Multifragmentation of Expanding Nuclear Mater
The Science and Culture Series - Advanced Scientific Culture Nucleus-nucleus Collisions, ed. G.C. Bonsignori, M. Buruno, A. Ventura, D. Vretenar, World Scientific (2002) p. 331.

Y. Hirata, A. Ohnishi, Y. Nara, T. Kido, T. Maruyama, N. Otuka, K. Niita, H. Takada, S. Chiba
Sideward Peak of Intermediate Mass Fragments in High Energy Proton Induced Reactions
Nucl. Phys. **A 707** (2002) 193.

T. Maruyama, A. Bonasera, M. Papa, S. Chiba
Formation and Decay of Super Heavy Systems
Prog. Theor. Phys. Suppl. **146** (2002) 587.

T. Maruyama, A. Bonasera, M. Papa, S. Chiba,
Formation and Decay of Super Heavy Composite Systems
AIP Conf. Proc. **644** (2002) 40.

T. Maruyama, A. Bonasera, M. Papa, S. Chiba
Lifetime of Heavy Composite Systems formed by Fusion between Heavy Nuclei
J. Nucl. Radiochem. Sci. **3** (2002) 77.

T. Maruyama, A. Bonasera, M. Papa, S. Chiba
Formation and Decay of Super Heavy Systems
Eur. Phys. J. **A 14** (2002)191.

M. Papa, A. Bonasera, T. Maruyama,
Dynamics and Exotic Cluster Production in the System Sn+Ni at 35 MeV/A
AIP Conf. Proc. **644** (2002) 206.

E. S. Sukhovitskij, S. Chiba, J.-Y. Lee, Y.-O. Lee, J. Chang, T. Maruyama, O. Iwamoto
Nuclear Level Structure, B(E2) γ-transitions and Nucleon Interaction Data for ^{56}Fe by a Unified Soft-rotator Model and Coupled-Channels Framework
J. Nucl. Sci. Technol. **39** (2002)816.

E.S. Soukhovitskij, S. Chiba
Soft-Rotator Model and Coupled-Channels Approach for Consistent Description of the Nuclear Collective Levels and Their Excitation by Nucleons
J. Nucl. Sci. Technol. Suppl. **2** (200)697.

E.S. Soukhovitskij, S. Chiba
Analysis of Nucleon Interaction with ^{238}U up to 150 MeV Incident Energies Using Coupled-Channels Approach with Saturated Coupling Scheme Based on Soft-Rotator Nuclear Model Hamiltonian
J. Nucl. Sci. Technol. Suppl. **2** (2002)144.

E.S. Soukhovitskij, S. Chiba, J.-Y. Lee, B.-t. Kim, S.-W. Hong
Analysis of Nucleon Scattering Data of ^{52}Cr with a Coupling Scheme Built with the Soft-rotator Model
J. Nucl. Sci. Technol. **40** (2003)69.

T. Tanigawa, M. Matsuzaki, S. Chiba
ΛΛ Pairing in NΛ Composite Matter
KEK Proc. **2002-29** (2003) 217.

Y. Utsuno, T. Otsuka, T. Mizusaki, M. Honma
Monte Carlo Shell Model Calculation for Unstable Nuclei around N=20
Nucl. Phys. **A704** (2002) 50c.

Y. Utsuno, T. Otsuka, T. Mizusaki, M. Honma
Vanishing of the N=20 Magic Number studied by the Monte Carlo Shell Model
J. Nucl. Sci. Technol. Suppl. **2** (2002) 818.

Y. Utsuno, T. Otsuka, T. Mizusaki, M. Honma
Electromagnetic Moments of Exotic Na Isotopes and their Relation to the N=20 Shell Gap
Prog. Theo. Phys. Suppl. **146** (2002) 488.

Y. Utsuno, T. Otsuka, T. Mizusaki, M. Honma, R. Fujimoto
Shell Formation and Disappearance in Exotic Nuclei around N=20
Proc. of the Fourth Italy-Japan Symp. on "Perspectives in Heavy Ion Physics" (World Scientific, Singapore, 2002).

Meeting

T. Hayakawa
Photon-induced Nucleosynthesis of Heavy Elements : A Frontier in Nuclear Astrophysics
Workshop on Science and Technology of LEPS in the Medium High Energy Region, Harima (Mar. 4, 2003)

T. Hayakawa
Universality of the Emprical Scaling Lows
Workshop of Nuclear Astrophysics -Strategy of the Study for Nuclear Astrophysics-, Wako (Mar. 13, 2003)

T. Hayakawa
Photonuclear Reactions and p-Process
Annual Meeting of Japan Physical Society, Sendai (Mar. 30, 2003)

T. Maruyama, A. Bonasera, M. Papa, S. Chiba
Formation and Decay of Super Heavy Composite Systems
Catania Relativistic Ion Studies, Catania (Jul.10-14, 2002)

T. Maruyama, A. Bonasera, M. Papa, S. Chiba
Dynamics of Superheavy Composite Systems
Nuclear Physics and Nuclear Chemistry of Superheavy Elements, Tokai (Feb. 27-28, 2003)

T. Maruyama, A. Bonasera, M. Papa, S. Chiba
Molecular Dynamics Description of a Fermi-gas
Annual Meeting of Japan Physical Society, Sendai (Mar. 28-31, 2003)

T. Tanigawa, M. Matsuzaki, S. Chiba
ΛΛ Pairing in NΛ Composite Matter
Fall Meeting of the Physical Society of Japan, Tokyo (Sep. 13-16, 2002)

T. Tanigawa, M. Matsuzaki, S. Chiba
Possibility of ΛΛ Pairing in NΛ Composite Matter
The XVI Int. Conf. on Particles and Nuclei, Osaka (Sep. 30-Oct. 4, 2002)

T. Tanigawa, M. Matsuzaki, S. Chiba
Possibility of ΛΛ Pairing in Dense NΛ Matter
XXI Symp. on Relativistic Astrophysics, Florence, Italy (Dec. 9-13, 2002)

T. Tanigawa, M. Matsuzaki, S. Chiba
ΛΛ Pairing in Relativistic Many-body Model
The 5th Symp. on Science of Hadrons under Extreme Conditions, Tokai (Mar. 18-20, 2003)

Y. Utsuno, T. Otsuka, T. Mizusaki, M. Honma
Axial Asymmetry in Neutron-rich Mg Isotopes
Fall Meeting of the Physical Society of Japan, Tokyo (Sep. 16, 2002).

Y. Utsuno, T. Otsuka, T. Mizusaki, M. Honma
Disappearance of the N=20 Magic Structure studied by Nuclear Moments of Na Isotopes
Fall Meeting of the Division Nuclear Physics of the American Physical Society, East Lansing, Michigan (Oct. 11, 2002).

ATOMIC PHYSICS AND SOLID STATE PHYSICS

Journal/Proceedings

M. Imai, M. Sataka, S. Kitazawa, K. Komaki, K. Kawatsura, H. Shibata, H. Tawara, T. Azuma, Y. Kanai, Y. Yamazaki
Auger Momentum Distributions of Rydberg States Electrons of Be-like Sulfur Produced through Foil Penetration
Nucl. Instrum. Methods **B193** (2002) 674.

M. Imai, M. Sataka, K. Kawatsura, K. Takahiro, K. Komaki, H. Shibata, H. Tawara,
Angular Momentum Distribution of Be-like Sulfur Rydberg States Produced through Foil Penetration
Atomic Collision Research in Japan **28** (2002) 25.

N. Ishikawa, A. Iwase, Y. Chimi, O. Michikami, H. Wakana, T. Hashimoto, T. Kambara, C. Müller, R. Neumann
S_e-Scaling of Lattice Parameter Change in High Ion-Velocity Region ($v>=2.6x10^9$ cm/s) in Ion-Irradiated $EuBa_2Cu_3O_y$
Nucl. Instrum. Methods **B 193** (2002) 278.

N. Ishikawa, A. Iwase, Y. Chimi, O. Michikami, H. Wakana, T. Hashimoto
Lattice Parameter Change Due to Electronic Excitation in Oxygen-Deficient $EuBa_2Cu_3O_y$
Nucl. Instrum. Methods **B 191** (2002) 606.

K. Kawatsura, K. Takahiro, M. Imai, M. Sataka, K. Komaki, H. Shibata
Ejected Electron Spectra from Highly Excited States in Collision of 2 MeV/u O^{q+} with He
Atomic Collision Research in Japan **28** (2002) 31.

H. Kitô, A. Iyo, M. Hirai, A. Crisan, M. Tokumoto, S. Okayasu, M. Sasase, H. Ihara
Superconducting Properties of the Heavy-ions and Neutron irradiated $(Cu,C)Ba_2Ca_{n-1}Cu_nO_{4+2n-\delta}$ (n =3,4 and 5)
Physica **C378- 381** (2002) 329.

S. Okayasu, H. Ikeda, R. Yoshizaki
Electron Irradiation Effects on MgB_2 Bulk Samples
Physica **C 378-381** (2002) 462.

S. Okayasu, M. Sasase, K. Hojou, H. Ikeda, R. Yoshizaki, T. Kambara, H. Sato, Y. Hamatani, A. Maeda
Irradiation Effects on MgB2 Bulk Sample and Formation of Columnar Defects on High-Tc Superconductor
Physica **C 382** (2002) 104.

S. Okayasu, M. Sataka, H. Ikeda, R. Yoshizaki
A Comparison of Two Irradiations on MgB_2 Bulk Samples
J. Low Temp. Phys. **131** (2003).

M. Sataka, M. Imai, K. Kawatsura, K. Komaki, H. Tawara, A. Vasilyev, U.I. Safronova
Comprehensive Theoretical and Experimental Analysis of Coster-Kronig Electron Spectra from 64 MeV S^{12+} Ions Excited through He Gas and C-foil Targets
Phys. Rev. **A65** (2002) 052704.

Meetings

K. Kawatsura, K. Takahiro, M. Imai, M. Sataka, K. Komaki, H. Shibata
Electron Spectra from Highly Excited States in High-energy Collisions of O^{q+} with He
11th Int. Conf. on the Physics of Highly Charged Ions, Caen (Sept. 1-6, 2002)

H. Kitô, A. Iyo, A. Crisan, M. Hirai, M. Tokumoto, S. Okayasu, M. Sasase, H. Ihara, Y. Tanaka
Heavy-ion Irradiation Dependence of the Superconducting Properties of $(Cu,C)Ba_2Ca_3Cu_4O_{10.5-\delta}$
The 23rd Int. Conf. on Low Temperature Physics, Hiroshima (Aug. 22, 2002)

H. Kitô, A. Iyo, M. Hirai, A. Crisan, M. Tokumoto, S. Okayasu, M. Sasase, M. Sataka, H. Ihara, Y. Tanaka
Heavy-ions Irradiation Dependence of Superconducting Properties for the Cu-based $(Cu,C)Ba_2Ca_{n-1}Cu_nO_{4+2n-\delta}$ $(n=4)$
The 14th Int. Symp. on Superconductivity, Yokohama (Nov. 12, 2002)

H. Kitô, M. Hirai, A. Iyo, M. Tokumoto, S. Okayasu, M. Sasase, M. Sataka, H. Ihara, Y. Tanaka
Effect of the Heavy-ion Irradiation of the High T_c Superconductor $(Cu,C)Ba_2Ca_4Cu_5O_{12-\delta}$
Fall Meeting of the Physical Society of Japan, Kasugai (Sep. 6, 2002)

H. Kitô, M. Hirai, A. Iyo, S. Okayasu, S. Sayaka, H. Ihara, Y. Tanaka
Effect of the Heavy-ion Irradiation of the High T_c Superconductor $TlBa_2Ca_4Cu_5O_{12.5-\delta}$
Annual Meeting of the Physical Society of Japan, Sendai (Mar. 28, 2003)

N. Matsumoto, T. Kato, M.S ataka, H. Ohtsuka H. Sugai, H. Maeta
Defect Structures in Ion irradiated Nickel at Low Temperature by X-ray Diffuse Scattering
The 13th Int. Conf. on Ion Beam Modification of Materials, Kobe (Sep.2, 2002)

H. Sato, N. Ishikawa, A. Iwase, Y. Chimi, O. Michikami, T. Hashimoto
Electronic Excitation Effects in Oxygen-Controlled $EuBa_2Cu_3O_{7-\delta}$ irradiated with High Energy Ions
Fall Meeting of the Physical Society of Japan, Tokyo (Sep.17, 2002)

H. Sato, N. Ishikawa, A. Iwase, Y. Chimi, O. Michikami, T. Hashimoto
Structural Change by High-Energy Irradiation and Post-Annealing in $EuBa_2Cu_3O_y$
Int. Symp. on Superconductivity (ISS 2001), Kobe (Sep. 26, 2001)

RADIATION EFFECTS IN MATERIALS

Journal/Proceedings

T. Aruga, Y. Katano, T. Ohmichi, S. Okayasu, Y. Kazumata, S. Jitsukawa
Depth-dependent and Surface in $MgAl_2O_4$ and MgO Irradiated with Energetic Iodine Ions
Nucl. Intrum. Methods **B 197** (2002) 94.

T. Aruga, Y. Katano, T. Ohmichi, S.Jitsukawa
The Interpretation of Surface Damages in Al_2O_3, $MgAl_2O_4$ and MgO Irradiated with Energetic Iodine Ions
Surface and Coatings Tecchnology **158-159** (2002) 444.

Y. Chimi, A. Iwase, N. Ishikawa, T. Kambara
Defect Production Induced by Electronic Excitation in Iron
Nucl. Instrum. Method **B 193** (2002) 248.

N. Fujii, R. Zach, T. Kanomata, H. Nishihara, F. Ono, M. Ishizuka, S. Endo
Effect of Pressure on the Magnetic Properties of MnRh1-xCoxAs
J. Alloy. Compounds **345** (2002) 59-67.

N. Fujii, R. Zach, M. Ishizuka, T. Kanomata, F. Ono, S. Endo
Pressure Dependence of the Magnetic Properties of MnRhX(X=P,As)
J. Phys. Cond. Matter. **14** (2002) 11135-11138.

A. Iwase, T. Hasegawa, T. Tobita, Y. Chimi, N. Ishikawa, M. Suzuki, T. Kambara, S. Ishino
Hardening of Fe-Cu Alloys by Swift Heavy Ion Irradiation
Nucl. Instrum. Methods **B195** (2002) 309-314.

C. Kawabata, N. Hayashi, F. Ono
Critical Temperature Tc versus Charging Energy Ec in MgB2 and C60/CHBr3
Physica **C 378-381** (2002) 220-224.

A. Kurumada, Y. Imamura
Effects of Irradiation damage on Mechanical and Thermal Properties of Carbon Composite Materials and Ceramics
Oarai Research Reports, Institute for Materials Research, Tohoku University (2002) 25-31.

M. Matsushita, T. Nishimura, S. Endo, M. Ishizuka, K. Kindo, F. Ono
Anomalous Magnetic Moments in Fe-Pt and Fe-Pd Invar Alloys under High Pressure
J. Phys. Cond. Matter. **14** (2002) 10753-10757.

N. Matsunami, M. Sataka, A. Iwase, T. Inami, M. Kobiyama
Sputtering of Nano-crystalline Gold by High Energy Heavy Ions
J. Nucl. Mater. **302** (2002) 206.

N. Matsunami, M. Sataka, A. Iwase
Electronic Sputtering of Oxides by High Energy Heavy Ion Impact
Nucl. Instrum. Methods **B193** (2002) 830.

K. Morita, S. Ishino, T. Tobita, Y. Chimi, N. Ishikawa, A. Iwase
Use of High Energy Ions for the Mechanistic Study of Irradiation Embrittlement in Pressure Vessel Steels Using Fe-Cu Model Alloys
J. Nucl. Mater. **304** (2002) 153-160.

T. Nakazawa, V. Grismanovs, D. Yamaki, Y. Katano, T. Aruga
Disordering in Li_2TiO_3 irradiated with High Energy Ions
Nucl. Instrum. Methods **B 206** (2003) 166-170.

T. Oku, A. Kurumada, K. Kawamata, M. Inagaki
Effects of Argon Ion Irradiation on the Microstructures and Physical Properties of Carbon Fibers
J. Nucl. Mater. **303** (2002) 242-245.

F. Ono, Y. Hamatani, Y. Mukumoto, S. Komatsu, N. Ishikawa, Y. Chimi, A. Iwase, T. Kambara, C. Muller, R. Neumann
Modification of Fe-Ni Invar Alloys by High-energy Ion Beams

Nucl. Instrum. Methods **B** (2003) 295-298.

T. Sekioka, M. Terasawa, M. Sataka, S. Kitazawa
Emission of Secondary Ions from a Foil bombarded with High Energy Heavy Ions
Phys. Scr. **T73** (1997) 335.

T. Sekioka, M. Terasawa, M. Sataka, S. Kitazawa, M. Niibe
Electronic Excitation Effects on Secondary Ion Emission from a Foil of Conducting Material bombarded by High Energy Heavy Ions
Nucl. Instrum. Methods **B 193** (2002) 751.

T. Sonoda, M. Kinoshita, I.L.F.Ray, T. Wiss, H. Thiele, D. Pellottiero, V.V. Rondinella, Hi. Matzke
TEM Observation on Irradiation - Induced Microstructural Evolution in High Burn-up UO_2 Disk Fuel,
Nucl. Instrum. Methods **B 191** (2002) 622-628.

S. Wei, R. Duraj, R. Zach, M. Matsushita, A. Takahashi, H. Inoue, F. Ono, H. Maeta, A. Iwase, S. Endo
The Effect of Pressure on the Curie Temperature in Fe-Ni Invar Alloys
J. Phys. Cond. Matter. **14** (2002) 11081-11084.

Meeting

Y. Chimi, A. Iwase, N. Ishikawa
Modification of Electrical Properties of Bismuth by Energetic Ion Irradiation
13th Int. Conf. on Ion Beam Modification of Materials, Kobe (Sep. 2, 2002)

Y. Chimi, A. Iwase, T. Iwata
Defect Production and Radiation Annealing in Platinum Irradiated with High-Energy Heavy Ions
5th Int. Symp. on Swift Heavy Ions in Matter, Taormina, Italy (May 22, 2002)

Y. Hamatani
Change in Magnetic Properties in Fe-Ni Invar Alloys by High-energy Ion Irradiation
Seminar of Materials Science, JAERI, Tokai (Mar. 5, 2002).

T. Inayoshi, K. Mori, S. Nasu, H. Nanto, K. Ohhashi, A. Iwase, S. Nagata
Disappearance of 400nm Photoluminescence of the Unirradiate of Regions in Silica Glass Range by Ion Irradiation.
Spring meeting of the Japan Society of Applied Physics, Kanagawa (Mar.28, 2003).

N. Ishikawa, A. Iwase, Y. Chimi, O. Michikami, T. Hashimoto, A. Dunlop, S. Della-Negra
Effect of Cluster Beam Irradiation in Oxide Superconductors Irradiated with 30MeV C_{60}
Fall Meeting of the Physical Society of Japan, Kasugai (Sep.6, 2002)

A. Iwase, Y. Hamatani, Y. Mukumoto, N. Ishikawa, Y. Chimi, T. Kambara, C. Mueller, R. Neumann, F. Ono
Anomalous Shift of Curie Temperature in Iron-Nickel Invar Alloys by High Energy Heavy Ion Irradiation
5th Int. Symp. on Swift Heavy Ions in Matter, Taormina, Italy (May 22-25, 2002)

A. Iwase, N. Ishikawa, Y. Chimi, T. Kambara
Primary Ionization as Parameter for Swift Heavy Ion Effects
Granzer-Workshop2002, Darmstadt, Germany (Dec. 2-3, 2002)

A. Kurumada, Y. Imamura, T. Oku, M. Ishihara, S. Baba, J. Aihara, Y. Hoshiya
Effects of Ion Irradiation on Mechanical Properties of Carbon Fibers
Symp. of Heavy Ion Science on TANDEM Field, Tokai (Jan.8-9, 2003)

N. Matsunami, M. Sataka, A. Iwase, S. Okayasu
Electronic Excitation induced Sputtering of Insulating and Semiconducting Oxides by High Energy Heavy Ions
Int. Conf. Swift Heavy Ions in Matter, Giardini Naxos, Taromina-Italy (May 22-25, 2002)

M. Matsushita, S. Endo, K. Miura, M. Ishizuka, F. Ono
Magnetic Phase Diagram in Fe-Pt Invar Alloys under High Pressure
Fall Meeting of the Physical Society of Japan, Kasugai (Sep. 25, 2002)

M. Matsushita, S. Endo, K. Miura, M. Ishizuka, F. Ono
Pressure-induced Magnetic Phase Transitions in Fe-Pt Invar Alloys
43th Annual Meeting of High Pressure Soc. Japan, Matsuyama (Nov. 28, 2002)

K. Miura, M. Ishizuka, T. Kanomata, H. Nishihara, S. Endo, F. Ono
Magnetic Properties of Weak Itinerant Ferromagnet FexCo1-xSi under High Pressure
43th Annual Meeting of High Pressure Soc. Japan, Matsuyama (Nov. 27, 2002)

Y. Miyoshi, M. Matsushita, F. Ono, N. Fujii, S. Endo, T. Kanomata, R. Zach
Measurements of AC-Susceptibility in MnRh0.8Co0.2As under High Pressure
Annual Meetings of Joint Physical Society and Applied Physics Soc of Cyugoku-Shikoku Branch, Kochi (Jul. 27, 2002)

T. Nakazawa, V. Grismanovs, D. Yamaki, Y. Katano, T. Aruga
Study on Disordering in Li_2TiO_3 irradiated with High Energy Ions
13th Int. Conf. on Ion Beam Modification of Materials, Kobe (Sep. 1-6, 2002)

S. Nasu, T. Inayoshi, E. Sugimata, K. Ohhashi, S. Yamamoto, A. Iwase, S.Nagata
H, He and Kr Ions Irradiation Effect of Silica Glass.
Fall Meeting of Atomic Energy Society of Japan, Sizuoka (Sep. 24, 2003)

H.Ohtsuka, H.Sugai, K.Hojo
Observation of Radiation Damages in Nano-particles
Annual Meeting of the Physical Society of Japan, Sendai (Mar. 2003)

F. Ono, M. Matsushita, S. Wei, R. Durj, R. Zach, D. Fruchart, A. Iwase, H. Maeta, S. Endo
Anomalous Pressure Effect on the Magnetic Properties in mechanically alloyed Fe-Ni Invar
1st Asian Conf. On High Pressure Research, Dunhuang, China (Aug. 22, 2002)

F. Ono, Y. Hamatani, Y. Mukumoto, S. Komatsu, N. Ishikawa, Y. Chimi, A. Iwase, T. Kambara, C. Muller, R. Neumann

Modification of Fe-Ni Invar Alloys by High-energy Ion Beams

The 13th Int. Conf. on Ion Beam Modification of Materials, Kobe (Sep.2, 2002)

F. Ono, S. Wei, A. Inoue, A. Takahashi, A. Iwase

Study on Particle Beam Irradiation Effects on High-Moment Magnetic Materials

Symp. of Research Center for Atomic Energy, Tokyo University, Tokyo (Oct. 7, 2002)

F. Ono

Modification of Magnetic Materials by High-energy Heavy Ions

2002 Colloquia of BESTEN, Tokai (Oct. 23, 2002)

T. Sonoda, M. Kinoshita, Y. Chimi, N. Ishikawa, A. Iwase, K. Yasuda

Radiation Effects in CeO_2 under Ion and Electron Irradiation as Simulations of Fission Field in Nuclear Fuels

Fall Meeting of Japan Institute of Metals, Osaka (Nov. 4, 2002)

T. Sonoda, M. Kinoshita, Y. Chimi, N. Ishikawa, A. Iwase, K. Yasuda

Radiation Effects in CeO_2 under High Energy Ion and Electron Irradiation as Simulations of Fission Field in Nuclear Fuels

Materials Science Symp. "Heavy Ion Science in Tandem Energy Region", Tokai (Jan. 08-09, 2003)

This is a blank page.

9. Personnel and Committees

This is a blank page.

(1) Personnel (FY 2002)

Department of Materials Science

Shoichi	Tachimori	Director
Yasutoshi	Komatsubara	Administrative Manager

Tandem Accelerator Group

Scientific Staff

Tadashi	Yoshida*
Suehiro	Takeuchi
Susumu	Hanashima
Makoto	Matsuda
Takamitsu	Nakanoya
Hiroshi	Kabumoto

Technical Staff

Susumu	Kanda
Isao	Ohuchi
Katsuzo	Horie
Yoshihiro	Tsukihashi
Shin-ichi	Abe
Nobuhiro	Ishizaki
Hidekazu	Tayama

Entrusted Operators

Akihiko	Iizima
Hisashi	Sakurayama
Manabu	Satoh
Hikaru	Nisugi
Takahiro	Yoshida

Entrusted Assistants

Teruo	Kozawa
Yasuharu	Sugiyama
Yoshio	Fujii

Research Group for Innovative Nuclear Science

Masumi	Oshima*
Hideki	Iimura
Tetsuya	Hirade
Yuichi	Hatsukawa

Akihiko	Osa	
Yutaka	Utsuno	
Yosuke	Toh	
Mitsuo	Koizumi	
Atsushi	Kimura	(Post Doc.)
Jun	Goto	(Post Doc.)
Haiming	Wang	(Visiting researcher)
Akiyuki	Seki	(Student)
Mahmudy Gharaie Mohamad Hosein		(Student)

Research Group for Solid State Phyics under Extreme Conditions

Kiichi	Hojou*	
Masao	Sataka	
Hideo	Ohtsuka	
Satoru	Okayasu	
Teruo	Kato	

Research Group for Radiation Effects and Analyses

Akihiro	Iwase*	
Norito	Ishikawa	
Yasuhiro	Chimi	
Takeo	Aruga	
Tetsuya	Nakazawa	
Daijyu	Yamaki	
Akira	Naito	
Atsushi	Hirose	(Student)
Seiji	Komatsu	(Student)

Advanced Science Research Center

Research Group for Fusion of Heavy Deformed Nuclei

Hiroshi	Ikezoe*	
Tetsuro	Ishii	
Shin-ichi	Mitsuoka	
Katsuhisa	Nishio	
Kenichirou	Satou	(Student)
Cheng-Jian	Lin	(JSPS fellow)

Research Group for Hadron Science

Satoshi	Chiba*	
Toshiki	Maruyama	

Masahiro	Fukushima	
Tomonori	Tanigawa	(JSPS Domestic Research Fellow)
Shinpei	Chikazumi	(Student)

Research Group for Nuclear Chemistry of Heavy Elements

Yuichiro	Nagame*	
Shin-ichi	Ichikawa	
Kazuaki	Tsukada	
Ichiro	Nishinaka	
Masato	Asai	
Kazuhiko	Akiyama	(Post Doc.)
Atsushi	Toyoshima	(Student)
Tetsuya	Kaneko	(Student)

Department of Environmental Sciences

R&D Group for Nonproliferation Technology

Nobuo	Shinohara*

Department of Health Physics

Radiation Control Division

Takayuki	Kawasaki
Hitoshi	Ogose
Hutao	Niino

Advanced Photon Research Center

Free Electron Laser Research Group

Takehito	Hayakawa
Toshiyuki	Shizuma

Takasaki Radiation Chemistry Research Establishment

Research Group for Severe Environment Materials

Toshio	Hirao

Oarai Research Establishment

High Temerature Irradiation Laboratory

Masahiro	Ishihara*
Shinichi	Baba
Jun	Aihara

* Head

(2) Tandem Consultative Committee

(Chairman)	Toru	Nomura	(Professor, Prime Scientist, High Energy Accelerator Research Organization (KEK))
(Vice Chairman)	Shoichi	Tachimori	(Director, Department of Materials Science)
	Hiroyasu	Ejiri	(Professor Emeritus of Osaka University)
	Kazuhiro	Yabana	(Associate Professor, Tsukuba University)
	Jun	Imasato	(Professor, High Energy Accelerator Research Organization (KEK))
	Kenji	Katori	(RI Beam Science Laboratory, RIKEN)
	Ken-ichiro	Komaki	(Professor, The University of Tokyo)
	Shigeru	Kubono	(Professor, The University of Tokyo)
	Hisaaki	Kudo	(Associate professor, Niigata University)
	Hiroshi	Kudo	(Professor, Tsukuba University)
	Tetsuo	Noro	(Professor, Kyushu University)
	Kenji	Morita	(Professor, Nagoya University)
	Seiichi	Shibata	(Professor, Kyoto University)
	Hiromi	Shibata	(Associate professor, The University of Tokyo)
(Secretary)	Masao	Sataka	(Research Group for Solid State Physics under Extreme Conditions)
(Secretary)	Suehiro	Takeuchi	(Tandem Accelerator Group)
(Secretary)	Tadashi	Yoshida	(Head, Tandem Accelerator Group)
(Secretary)	Yasutoshi	Komatsubara	(Administrative Manager, Department of Materials Science)

(3) Research Planning and Assessment Committee

(a) Sub-committee for Nuclear Physics and Nuclear Chemistry

(Chairman)	Seiichi	Shibata	(Professor, Kyoto University)
	Tetsuo	Noro	(Professor, Kyushu University)
	Shigeru	Kubono	(Professor, The University of Tokyo)
	Kazuhiro	Yabana	(Associate Professor, Tsukuba University)
	Eisuke	Minehara	(Head, Free Electron Laser Research Group)

	Nobuo	Shinohara	(R&D Group for Nonproliferation Technology)
	Suehiro	Takeuchi	(Tandem Accelerator Group)
(Secretary)	Susumu	Hanashima	(Tandem Accelerator Group)
(Secretary)	Tadashi	Yoshida	(Head, Tandem Accelerator Group)

(b) Sub-committee for Materials and Radiation Damage

(Chairman)	Kenji	Morita	(Professor, Nagoya University)
	Ken-ichiro	Komaki	(Professor, The University of Tokyo)
	Hiromi	Shibata	(Associate professor, The University of Tokyo)
	Hiroshi	Kudo	(Professor, Tsukuba University)
	Hiroshi	Naramoto	(Head, Research Group for Design of New Materials with Energy Beams)
	Takeo	Aruga	(Research Group for Radiation Effects and Analyses)
	Suehiro	Takeuchi	(Tandem Accelerator Group)
(Secretary)	Susumu	Hanashima	(Tandem Accelerator Group)
(Secretary)	Tadashi	Yoshida	(Head, Tandem Accelerator Group)

This is a blank page.

10. Cooperative Researches

This is a blank page.

	Title	Contact person Organization
1.	Precise Measurement of Gamma-Ray Emission Probability for Proton-Rich Nuclides	Hiroshi MIYAHARA Department of Radiological Technology, School of Health Science, Nagoya University
2.	Development of Target/Ion-Source System for the JAERI-KEK Joint RNB Project	Sun Chan JEONG Institute of Particle and Nuclear Studies, High Energy Accelerator Research Organization
3.	Synthesis of Actinide Metallo Fullerene	Motomi KATADA Department of Chemistry, Tokyo Metropolitan University
4.	Laser Spectroscopy of Radioactive Isotopes in the Light Rare Earth Elements	Takayoshi HORIGUCHI Hiroshima International University
5.	Excitation Energy Dependence on the Asymmetric Mass Division Mode in Actinide Fission	Hisaaki KUDO Department of Chemistry, Niigata University
6.	Nuclear Structure of the Neutron-Rich Ni Region by Deep-Inelastic Collisions	Masao OGAWA Research Laboratory for Nuclear Reactors, Tokyo Institute of Technology
7.	Study of Heavy-ion Fusion via Reverse Fission Process	Sun Chan JEONG Institute of Particle and Nuclear Studies, High Energy Accelerator Research Organization

8. Study on Nuclear Chemistry by Gas Phase Reaction of Transactinide	Hisaaki KUDO Department of Chemistry, Niigata University
9. Aqueous Chemistry of the Transactinide Elements, Rutherfordium and Dubnium	Atsushi SHINOHARA Department of Chemistry, Osaka University
10. Study of Superdeformed Nucleus by the Fission Experiment	Minoru SAKAMA Medical Department, Tokushima University
11. Nuclear Structure Study by Coulomb Excitation	Tsuneyasu MORIKAWA Department of Physics, University of Kyushu
12. Research on Nuclear Isomers in the Mass A=180 Region	Shiro MITARAI Department of Physics, University of Kyushu
13. Decay Study of Neutron-rich Nuclei far off the Stability produced with the Fission of Actinide Target	Michihiro SHIBATA Department of Engineering Nagoya University
14. Direct Measurement of the Astro-Physical Reaction Rate with Radioactive Nuclear Beams	Hiroari MIYATAKE Institute of Particle and Nuclear Studies, High Energy Accelerator Research Organization
15. Nuclear Structure of Heavy and Transactinide Nuclei	Yasuji OURA Department of Chemistry, Tokyo Metropolitan University
16. Study of Isomers and their Decay Mechanisms in Deformed or Spherical Nuclei	Masahiko SUGAWARA Department of Natural Science, Chiba Institute of Technology

17. Physics in Collective States of Deformed Rare Earth Nuclei	Hideshige KUSAKARI Faculty of Education, Chiba University
18. Effects of Electronic Excitation and Elastic Scattering by High Energy Kr Ions on Photo-luminescence from Triplet Defects in Silica Glasses	Shoichi NASU Kanazawa Institute of Technology
19. High-Energy Ion Beam Irradiation of Functional Electronic Materials	Takayuki TERAI Engineering Research Institute, School of Engineering, The University of Tokyo
20. Study on the Diffusion Processes in Solid Materials by Radioactive Nuclear Beams	Ichiro KATAYAMA Institute of Particle and Nuclear Studies, High Energy Accelerator Research Organization
21. Effect of Ion Irradiation for New Carbon Composite Materials and Fibers with High Thermal Conductivity	Akira KURUMADA Faculty of Engineering, Ibaraki University
22. Ion Irradiation Effect on a New Superconducting Material MgB_2	Hiroshi IKEDA Institute of Materials Science, Tsukuba University
23. Microstructural Study of Oxide Ceramics irradiated with High Density Electronic Excitation	Chiken KINOSHITA Department of Applied Quantum Physics and Nuclear Engineering, Kyushu University

24. Study on Interaction between Columnar Defects and Vortices in Oxide Superconductors	Takanobu KISU Department of Electrical and Electronic Systems Engineering, Kyushu University
25. Modification of Magnetic Materials by High-energy Heavy Ions through High-density Electronic Excitation	Fumihisa ONO Department of Physics, Okayama University
26. Study of Radiation Defects in Materials irradiated at Low Temperature with Heavy Ions by X-ray Diffuse Scattering	Hiroshi MAETA Hiroshima Kokusai Gakuin University
27. Electron Spectra induced by the Collision of highly charged Ions with Matter	Ken-ichiro KOMAKI Graduate School of Arts and Science, The University of Tokyo
28. Electronic Excitation Effects in Oxides by High Energy Heavy Ion	Noriaki MATSUNAMI School of Engineering, Nagoya University
29. Electron Excitation Effect on Sputtering induced by Heavy Ion Bombardment	Mititaka TERASAWA Faculty of Engineering, Himeji Institute of Technology
30. Radiation Effects of High Energy Fission Products in Light Water Reactor Fuels	Motoyasu KINOSHITA Nuclear Energy Systems Department, Central Research Institute of Electric Power Industry
31. Heavy-ions Irradiation Effect of Superconducting Properties of Multi-layered (Cu,C)$Ba_2Ca_{n-1}Cu_nO_{4+2n-\delta}$ Superconductor	Hijiri KITÔ National Institute of Advanced Industrial Science and Technology

32. Study of Single-Events induced by High Energy Ions

Sumio MATSUDA
Technology Research Department,
National Space Development Agency of Japan

This is a blank page.

国際単位系 (SI) と換算表

表 1　SI 基本単位および補助単位

量	名称	記号
長さ	メートル	m
質量	キログラム	kg
時間	秒	s
電流	アンペア	A
熱力学温度	ケルビン	K
物質量	モル	mol
光度	カンデラ	cd
平面角	ラジアン	rad
立体角	ステラジアン	sr

表 2　SI と併用される単位

名称	記号
分，時，日	min，h，d
度，分，秒	°，′，″
リットル	l，L
トン	t
電子ボルト	eV
原子質量単位	u

1 eV = 1.60218 × 10^{-19} J

1 u = 1.66054 × 10^{-27} kg

表 5　SI 接頭語

倍数	接頭語	記号
10^{18}	エクサ	E
10^{15}	ペタ	P
10^{12}	テラ	T
10^{9}	ギガ	G
10^{6}	メガ	M
10^{3}	キロ	k
10^{2}	ヘクト	h
10^{1}	デカ	da
10^{-1}	デシ	d
10^{-2}	センチ	c
10^{-3}	ミリ	m
10^{-6}	マイクロ	μ
10^{-9}	ナノ	n
10^{-12}	ピコ	p
10^{-15}	フェムト	f
10^{-18}	アト	a

表 3　固有の名称をもつ SI 組立単位

量	名称	記号	他の SI 単位による表現
周波数	ヘルツ	Hz	s^{-1}
力	ニュートン	N	$m \cdot kg/s^2$
圧力，応力	パスカル	Pa	N/m^2
エネルギー，仕事，熱量	ジュール	J	N·m
工率，放射束	ワット	W	J/s
電気量，電荷	クーロン	C	A·s
電位，電圧，起電力	ボルト	V	W/A
静電容量	ファラド	F	C/V
電気抵抗	オーム	Ω	V/A
コンダクタンス	ジーメンス	S	A/V
磁束	ウェーバ	Wb	V·s
磁束密度	テスラ	T	Wb/m^2
インダクタンス	ヘンリー	H	Wb/A
セルシウス温度	セルシウス度	℃	
光束	ルーメン	lm	cd·sr
照度	ルクス	lx	lm/m^2
放射能	ベクレル	Bq	s^{-1}
吸収線量	グレイ	Gy	J/kg
線量当量	シーベルト	Sv	J/kg

表 4　SI と共に暫定的に維持される単位

名称	記号
オングストローム	Å
バーン	b
バール	bar
ガル	Gal
キュリー	Ci
レントゲン	R
ラド	rad
レム	rem

1 Å = 0.1 nm = 10^{-10} m

1 b = 100 fm^2 = 10^{-28} m^2

1 bar = 0.1 MPa = 10^5 Pa

1 Gal = 1 cm/s^2 = 10^{-2} m/s^2

1 Ci = 3.7 × 10^{10} Bq

1 R = 2.58 × 10^{-4} C/kg

1 rad = 1 cGy = 10^{-2} Gy

1 rem = 1 cSv = 10^{-2} Sv

（注）

1. 表 1－5 は「国際単位系」第 5 版，国際度量衡局 1985 年刊行による。ただし，1 eV および 1 u の値は CODATA の 1986 年推奨値によった。
2. 表 4 には海里，ノット，アール，ヘクタールも含まれているが日常の単位なのでここでは省略した。
3. bar は，JIS では流体の圧力を表わす場合に限り表 2 のカテゴリーに分類されている。
4. EC 閣僚理事会指令では bar，barn および「血圧の単位」mmHg を表 2 のカテゴリーに入れている。

換　算　表

力	N(=10^5 dyn)	kgf	lbf
	1	0.101972	0.224809
	9.80665	1	2.20462
	4.44822	0.453592	1

粘度　1 Pa·s(N·s/m^2) = 10 P(ポアズ)(g/(cm·s))

動粘度　1 m^2/s = 10^4 St(ストークス)(cm^2/s)

圧力	MPa(=10 bar)	kgf/cm^2	atm	mmHg(Torr)	lbf/in^2(psi)
	1	10.1972	9.86923	7.50062 × 10^3	145.038
	0.0980665	1	0.967841	735.559	14.2233
	0.101325	1.03323	1	760	14.6959
	1.33322 × 10^{-4}	1.35951 × 10^{-3}	1.31579 × 10^{-3}	1	1.93368 × 10^{-2}
	6.89476 × 10^{-3}	7.03070 × 10^{-2}	6.80460 × 10^{-2}	51.7149	1

エネルギー・仕事・熱量	J(=10^7 erg)	kgf·m	kW·h	cal(計量法)	Btu	ft·lbf	eV
	1	0.101972	2.77778 × 10^{-7}	0.238889	9.47813 × 10^{-4}	0.737562	6.24150 × 10^{18}
	9.80665	1	2.72407 × 10^{-6}	2.34270	9.29487 × 10^{-3}	7.23301	6.12082 × 10^{19}
	3.6 × 10^6	3.67098 × 10^5	1	8.59999 × 10^5	3412.13	2.65522 × 10^6	2.24694 × 10^{25}
	4.18605	0.426858	1.16279 × 10^{-6}	1	3.96759 × 10^{-3}	3.08747	2.61272 × 10^{19}
	1055.06	107.586	2.93072 × 10^{-4}	252.042	1	778.172	6.58515 × 10^{21}
	1.35582	0.138255	3.76616 × 10^{-7}	0.323890	1.28506 × 10^{-3}	1	8.46233 × 10^{18}
	1.60218 × 10^{-19}	1.63377 × 10^{-20}	4.45050 × 10^{-26}	3.82743 × 10^{-20}	1.51857 × 10^{-22}	1.18171 × 10^{-19}	1

1 cal = 4.18605 J (計量法)

= 4.184 J (熱化学)

= 4.1855 J (15 °C)

= 4.1868 J (国際蒸気表)

仕事率　1 PS (仏馬力)

= 75 kgf·m/s

= 735.499 W

放射能	Bq	Ci
	1	2.70270 × 10^{-11}
	3.7 × 10^{10}	1

吸収線量	Gy	rad
	1	100
	0.01	1

照射線量	C/kg	R
	1	3876
	2.58 × 10^{-4}	1

線量当量	Sv	rem
	1	100
	0.01	1

（86 年 12 月 26 日現在）